Hawke's Bay - New Zealand

Global Climate Change &
Barrier-Beach Responses

Asset Management Group

Report to the Hawke's Bay Regional Council

HAWKE'S BAY, NEW ZEALAND: GLOBAL CLIMATE CHANGE AND BARRIER-BEACH RESPONSES

Prepared by

Paul D. Komar and Erica Harris

Consulting Oceanographers
3520 NW Elmwood Drive
Corvallis, Oregon 97330 USA
pdkomar@gmail.com

March 2014

TABLE OF CONTENTS

10   Summary and Discussion

EXECUTIVE SUMMARY

Projections by climatologists are that with continued global warming the average level of the sea will risen by about 1 metre by the end of the 21st century, a result of the more rapid melting of glaciers and increased ocean-water temperatures that produce its thermal expansion. There is also evidence that the intensities of storms and the heights of their generated waves are increasing, measured globally by satellites and locally by wave buoys, similarly attributed to global warming. The concern is that with these environmental changes the world's ocean shores will experience far greater impacts from erosion and flooding than occurred during the past 100 years.

The objective of this study is to investigate the Hawke's Bay ocean processes that are important to its erosion and flooding hazards — to undertake analyses of its waves, tides, and changing sea levels, and based on their projected magnitudes assess the future hazards to shore-front properties spanning the 21st century. This report is primarily concerned with the stretch of coast from Tangoio to Cape Kidnappers, that is to the Bay View and Haumoana Littoral Cells, that shore being most heavily developed within Hawke's Bay and with it being particularly susceptible to erosion and flooding.

This report begins with a general review of Earth's changing climate, including projections that have been made by climatologists for future rates of rise in globally-averaged sea levels, and an examination of evidence that storm intensities and ocean wave heights have been increasing. That global perspective is followed by a review specifically of the Hawke's Bay hazards, beginning with those associated with its tectonic setting, having been the origin of pre-historic major earthquakes and tsunami, but now responsible for ongoing changes in land elevations that are important to this coast's erosion hazards. The primary focus of the report is directed toward examinations of the Hawke's Bay ocean processes, its measured tides elevated by storm surges, the wave climate, and its nearshore processes of wave breaking and swash runup levels on the beaches. Analyses include assessments of the expected extremes of those individual ocean processes, and combinations of the processes, in particular the extreme high tides plus the swash runup of storm waves on the beaches, yielding total water levels during storm events that ultimately pose the greatest threat from erosion to the shores of Hawke's Bay.

Assessments of those potential extreme hazards require considerations of the expected responses of the barrier beaches as sea levels and storm-generated waves progressively increase through this century. This has included model analyses to determine whether the barrier beaches can be expected to adapt in their morphologies in such a manner that they continue to provide protection to this coast, or potentially might fail catastrophically, inundating the low-lying areas landward from the barrier gravel ridges. This report ends with a general consideration of the management responses that may be required and reasonably undertaken to improve the protection to properties and infrastructure along the coast of Hawke's Bay.

Based on our reviews of investigations that have been completed by other researchers, and the analyses we have undertaken of the ocean processes important to this coast's erosion and flooding, the principal findings of our study include the following:

- The coast of Hawke's Bay is located on the tectonically active Hikurangi Margin, where the oceanic Pacific plate collides with and is being subducted beneath the continental

Australian plate, pre-historically having generated strong earthquakes (magnitudes 8 to 9) on the subduction interface between the plates; historically, lower magnitude but still destructive earthquakes have resulted from the compression of the rocks within the upper Australian plate (e.g., the 1931 Hawke's Bay earthquake);

• Recent investigations by geologists and seismologists have found evidence in coastal sediments for occurrences of past extreme subduction earthquakes that resulted in subsidence of significant portions of this coast (including the Bay View and Haumoana Cell shorelines), which were then inundated by major tsunami generated by the quakes;

• This tectonic setting is important in producing changes in land elevations along this shore, the earthquakes within the body of the Australian plate having folded and faulted its rocks so that some areas (e.g., the Mahia Peninsula) have experienced a net uplift spanning thousands of years, whereas other stretches of this coast have experienced net subsidence;

• Hourly measurements of tides have been collected by the Port of Napier's gauge since 1989, but with a 3-year gap from 1995 to 1999 so that only 13 years of data were available for our analyses (Chapter 4), sufficient to define the distribution of water elevations affected by storm surges, but not providing a confident assessment of its potential extremes produced by severe but rare storm events;

• The Port's tide-gauge records have also been important in determining the Hawke's Bay trend of change in relative sea levels, affected by both the eustatic (global) increase in ocean levels plus the trend of change in local land elevations, our analysis having yielded a net increase of about 2 millimetres per year, but with this result being uncertain due to the short record of available measurements (Chapter 8);

• The present rate of rise in the Hawke's Bay measured sea levels has been projected into the future based on the results of investigations by climatologists that have predicted accelerated rates of global rise, the result of this projection being that the Hawke's Bay sea level will increase by approximately 1 metre by the end of this century (Chapter 8);

• The wave climate for Hawke's Bay is based on the hourly measurements collected by the Port of Napier's buoy located in 16-metres water depth offshore from its breakwater, this data set having included the years 2000 through 2010, applied to document the distributions of measured significant wave heights and periods, but with this limited data availability again reducing the confidence in the projections of future extreme waves generated by rare severe storm events (Chapter 5);

• With the Port's buoy being located in relatively shallow water, its hourly measured significant wave heights were transformed to their deep-water equivalents, initially calculated using available wave theory, but then empirically "corrected" so that its distribution of significant wave heights agrees with those from previous investigations that derived deep-water wave climates from hindcast analyses based on storm parameters; the result is a unified wave climate for Hawke's Bay based on all available data sets, showing that the mode of most frequent occurrence in the distribution of deep-water significant wave heights is 1.2 metre, with a maximum significant wave height of about 10 metres;

- A linear regression of the annual average deep-water significant wave heights, based on the Port's decade of measurements, yielded a trend of increase at a rate of 0.008 metre per year, amounting to approximately a 10-centimetres increase in 11 years, consistent with measurements by satellites off this coast, the increase being a response to enhanced storm intensities and representing a climate-controlled future hazard to the coast of Hawke's Bay (Chapter 5);

- The deep-water wave climate of significant wave heights and periods served as the basis for calculating the corresponding climates of nearshore processes, the distributions of wave breaker heights and swash runup levels on the Hawke's Bay beaches, the results being dependent on the shoreline site governed by the extent of wave refraction and energy losses as the waves traveled from deep water to that coastal site (Chapters 6 and 7);

- The principal product of these process analyses has been calculations of the hourly total water levels (*TWLs*) at the shore, the sum of the measured tides and calculated wave runup levels based on the measured waves, yielding distributions of *TWL* elevations with their extremes representing the present-day process hazards from erosion and flooding of back-shore properties (Chapter 7);

- The extremes in the *TWL* histograms based on the process analyses were compared with surveyed beach profiles from the Bay View and Haumoana Littoral Cells, a reasonable correspondence having been found with beach/backshore junction elevations on the profiles, which provide the best morphologic evidence for past occurrences of erosion during major storms and high tides; such comparisons also accounted for the history of overwash events in the Haumoana Cell where the crests of the barrier gravel ridges are sufficiently low that extreme water levels during storms have achieved still higher elevations (Chapter 7);

- A reasonable match was found between the evaluated *TWLs* affected by refraction and the alongcoast variations in the beach profile junction elevations where the active beach and backshore meet, both becoming progressively lower within the sheltered shores due to wave refraction having reduced the swash runup levels (Chapter 7);

- The analyses of the present-day hazards based on *TWL* extremes compared with beach profile morphologies served as the basis for projections of the enhanced future erosion and flooding hazards in the year 2100, those projections having first accounted for the 1-metre rise in sea levels, followed by the additional projected increasing storm intensities and swash runup levels; with these combined climate-controlled processes, the future elevated *TWL* is projected to be about 2 metres above the present-day levels on the exposed shores of the Bay View Cell, with a 1.5-metre increase on the Haumoana Cell's shoreline (Chapter 9);

- By the year 2100, the resulting erosional retreat of the barrier gravel ridge along the Bay View Cell's shoreline in response to those elevated water levels is estimated to be about 15 to 20 metres, while within the Haumoana Cell the erosion along its northern stretch of shore could be as much as 30 metres; Most destructive in the Haumoana Cell would be overwash events during the most extreme storms, with the *TWLs* predicted to significantly exceed the low elevations of the gravel ridge along its

southern shores, resulting in catastrophic impacts from erosion and flooding, potentially leading to the breaching of the barrier gravel ridge and flooding of low-lying inland areas;

- In recognition of the shortcomings in the *TWL* analyses due to the limited availability of measured tides and waves, presumably having under predicted the potential future impacts, Extreme Scenarios were developed based on projections of the individual processes and their joint probabilities of occurrence, representing something of a "worst case" storm and its potential impacts to Hawke's Bay coastal properties (Chapters 7 and 9); This Extreme Scenario yielded *TWL* elevations that are some 2 metres higher than the maximum *TWL* extremes based on analyses of the limited wave and tide measurements, and as such overwash of the barrier gravel ridge is projected to take place along the entire length of the Haumoana Cell's shore, and at least the southern half of the Bay View Cell's shore;

- With rising sea levels and increasing wave heights generated by more intense storms, the beach sediment budgets of the littoral cells are expected to be altered, important being the possible loss of the Tukituki River as a "credit" in the Haumoana Cell's sediment budget, due to its estuary being deepened by the rising water levels, but with the erosion of the barrier gravel ridges in both cells supplying significant volumes of gravel to the beaches; As a result of these potential changes in the sources of gravel supplying the beaches, with the loss of the Tukituki River as the primary source at the south end of the Haumoana Cell's shoreline, replaced by erosion of the gravel ridge along the northern stretch of that shore, in the long term there could be significant reversals in the patterns of longshore gravel transport by the waves, locally affecting the rates of backshore erosion versus accretion;

- Important to the stability of this coast, the volumes of gravel and widths of the beaches provide the primary buffer protection to the barrier gravel ridges and backshore properties from the assaulting forces of the storm-generated waves and high tides, with the present and future stabilities depending in large part on the sediment budgets of the littoral cells; this requires that efforts be directed toward shifting their balances from the "red" into the "black" by phasing out as soon as possible the commercial extraction of beach gravels, and exploring the possibility of measures taken in the rivers that would restore their capacities to again be significant sources of sand and gravel to the Hawke's Bay beaches.

With this study having been directed toward assessments of future erosion and flooding hazards along the Hawke's Bay coast, enhanced as a result of global warming, its results point to the need for additional investigations to fully define those hazards and to provide greater confidence in the results.   As well as needing longer records of measured waves and tides to define their extremes and the decadal trends of increasing wave heights and sea levels, focus needs to be directed toward how Earth's changing climate could alter the budgets of sediments supplying gravel and sand to the beaches. It is recommended that the following studies and data analyses be undertaken:

- It is important that the Port of Napier continues to collect quality measurements of waves and tides, and that every 5 years or so analyses be repeated to determine the distributions and extremes in those measured processes, supporting improved assessments of the erosion and flooding hazards, ultimately with a minimum of 25

years of measurements probably being needed before statistically satisfactory levels of confidence and projections into the future can be derived;

• With the Tukituki River being the primary source of gravel to the Haumoana Littoral Cell, a "credit" in its beach sediment budget that however might be lost with rising sea levels, consideration needs to be directed toward the consequences of climate change and human impacts on its sediment yields, the objective being management practices that would sustain or increase its supply of gravel and sand to the beaches;

• It is speculated in this report that with the probable decline of gravel supplied by the Tukituki River to the Haumoana Cell's beaches, but partially replaced by the erosion of the barrier gravel ridge along its northern shore, there could be significant changes in the patterns of longshore transport of the beach sediments by the waves, in part determining the resulting alongcoast variations in rates of property erosion versus accretion; numerical model analyses such as those undertaken previously to assess the impacts of beach sediment mining at Awatoto, could similarly be directed toward investigating the future climate-induced changes in this Cell's shorelines and property erosion, predicting with greater confidence assessments of the property impacts than offered by our speculation in this report.

ACKNOWLEDGEMENTS

1 The Coast of Hawke's Bay

1.1 INTRODUCTION

The climate-dependent ocean processes and resulting enhanced hazards from erosion and flooding are the focus of ongoing research along the world's coastlines. The objective of this investigation is to analyze the potential future impacts to the coast of Hawke's Bay, produced by Earth's changing climate. Those changes range from the few hours to days of a major storm, modifications of the weather and ocean processes that persist throughout the span of a year (for example, during La Niña or El Niño climate events), and progressive shifts in the climate that encompass decades to centuries. Of particular concern to society are the potential consequences of global warming, the rise in atmospheric and ocean-water temperatures, and the resulting melting of glaciers, which together are predicted to result in accelerated rates of rising sea levels. Assessments project that during the 21st century the increase in the global mean sea level could be on the order of 1 metre or more, far greater than the 0.2-metre rise that occurred during the 20th century. Furthermore, increased storm intensities and their generated wave heights have been documented along many coasts, also attributed by climatologists and oceanographers to global warming.

The shore of Hawke's Bay[1], Figure 1-1, extends along the east coast of New Zealand's North Island, from the Mahia Peninsula in the north to beyond Cape Kidnappers in the south. This coast has experienced significant changes during the past two centuries since European settlement, in part due to human-induced environmental impacts, but to a considerable extent having been caused by this region's tectonic activity that included a major earthquake in 1931 that altered land elevations along its shores. At the same time, episodes of extreme storm waves and progressively rising sea levels have impacted this coast, locally resulting in the erosion of its beaches and sea cliffs. These multiple factors important to the long-term evolution of the Hawke's Bay coast and to the hazards faced by ocean front properties from erosion and flooding have been reviewed in an earlier report and summary publication (Komar, 2005, 2010). The goal of the present study is to expand on the examinations of the consequences of Earth's changing climate, how it might affect the ocean processes of storms and sea levels, thereby impacting society's developments along the shores of Hawke's Bay.

The coast of Hawke's Bay is characterized by alternating stretches of rocky shores and embayments that contain its principal beaches (Figure 1-1). The rocky portions — the Mahia Peninsula, the high cliffs north of Tangoio, Bluff Hill within the city of Napier, and Cape Kidnappers at the south — all represent prominent headlands that limit or entirely prevent the passage of beach sediments around them, confining the sand and gravel to within the individual embayments. Coastal scientists commonly divide shorelines into what are termed

---

[1] This geographic and political region is referred to as *Hawke's Bay*, and in this report that name is also applied to its beaches and the shore, whereas *Hawke Bay* is the geographical term for the body of water and is used when discussing its waves and tides.

"littoral cells", representing stretches of shore containing a beach that is largely isolated from other beaches; the three Hawke's Bay embayments in Figure 1-1 are so designated, each named for a local community.
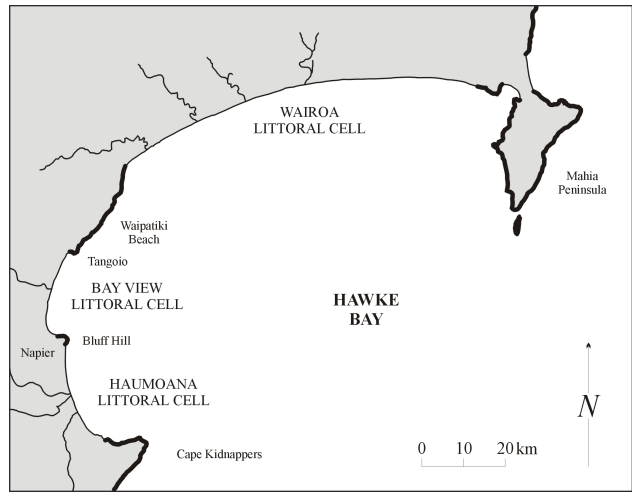
Figure 1-1: The coast of Hawke's Bay and its three littoral cells, stretches of beach separated by rocky shores and headlands.
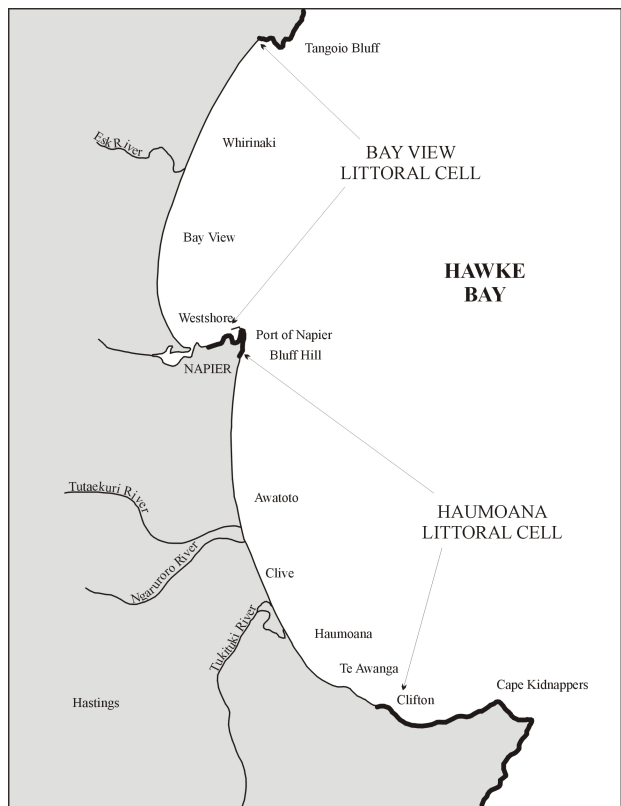
Figure 1-2: The Bay View and Haumoana Littoral Cells.

The focus of this report is limited to the stretch of coast from Tangoio to Cape Kidnappers, that is to the Bay View and Haumoana Littoral Cells shown in Figure 1-2. This stretch of shore is the most heavily developed in Hawke's Bay, including from north to south the communities of Whirinaki, Bay View, Napier, Awatoto, East Clive, Haumoana, Te Awanga and Clifton. Because of this development and with its shores locally having experienced beach and property erosion (the greatest having occurred at the south end of the Haumoana Cell), these littoral cells have been the primary focus of past investigations, the subject of nearly all of the considerable number of reports that have been written about the Hawke's Bay coast, reviewed in our previous reports (Komar, 2005, 2010).

1.2 THE HAWKE'S BAY BEACHES — MORPHOLOGY AND SEDIMENTS

The beaches of the Bay View and Haumoana Littoral Cells are composed of mixtures of gravel and sand, commonly found along the east coasts of New Zealand's North and South Islands, but comparatively rare elsewhere on the world's ocean shores. The pebbles and cobbles in the Hawke's Bay beaches are derived from the erosion of Mesozoic rocks found within the inland Front Range mountains, a greywacke that originated in the deep ocean as deposits of fine-grained silt but were later metamorphosed by heat and pressure during mountain building, yielding the most resistant rocks in the Front Range. A century ago four large rivers transported significant volumes of gravel to the ocean beaches, but over the years modifications of the rivers for flood management purposes reduced those volumes, and then in 1931 the tectonic uplift produced by the Hawke's Bay earthquake raised the lower reaches of the Tutaekuri, Ngaruroro and Esk Rivers, trapping the gravel so that now those rivers only deliver sand to the Bay's shores. In contrast, with its watershed having subsided at the time of the earthquake, only the Tukituki River now represents a significant source of gravel and sand to the ocean beaches, reaching the coast near the south end of the Haumoana Littoral Cell (Figure 1-2). The erosion of Cape Kidnappers, the headland that forms the southern boundary of that cell, also supplies some greywacke gravel to its shore. With both of those sources being located at the south end of the cell and with the waves arriving predominantly from the southeast (Chapter 5), there is a net northward longshore transport of the beach gravel and sand, carrying it to the beaches along the full length of this cell's shore. However, the volumes of gravel being transported progressively decrease with distance to the north, in part being lost as a result of the natural abrasion of the greywacke pebbles and cobbles, yielding particles of sand and silt that tend to be carried offshore by the waves. Particularly significant to the decreased volumes of sediments transported alongshore to the north has been the commercial mining of beach sediments at Awatoto, mid-way along the length of this cell, its operation having extracted large volumes of gravel and sand over the decades (Tonkin and Taylor, 2005).

The Bluff Hill headland in Napier forms the northern boundary of the Haumoana Littoral Cell, separating it from the Bay View Cell (Figure 1-2). There is strong evidence that the beach gravel has not been carried by the waves and currents past this headland, prior to the construction of the Port of Napier's breakwater in the late 19th century, or subsequent to its construction (Komar, 2005, 2010). However, since 1986 gravel and sand has been extracted from Pacific Beach, the Napier shore south of Bluff Hill, carried by truck to Westshore to nourish its recreational beach, this addition now representing the largest input of sediment into the Bay View Cell.

The Bay View Littoral Cell differs from the Haumoana Cell in there essentially being no natural sources of gravel to it beaches, the only river reaching its shore being the comparatively small Esk River, supplying minor quantities of sediment, mostly sand. Lacking significant natural sources of gravel, the Bay View Cell is in effect a pocket beach that over the long term has a net zero longshore transport, although there is evidence for seasonal and climate controlled reversals that account for cycles between periods of shoreline erosion versus accretion at the ends of that cell's shore, in the immediate proximity to the bounding headlands at Westshore in the south, and at Tangoio in the north (Komar, 2005, 2010). This quasi-equilibrium zero net transport of the beach sediments is explained by the orientation this cell's shoreline, facing directly toward the southeast and arrival of the dominant waves from that direction.

Examples of the Hawke's Bay mixed sand-and-gravel beaches are shown in Figures 1-3 and 1-4, respectively at Westshore within the Bay View Cell, and at the community of South Haumoana in the Haumoana Littoral Cell. Being located at the south end of the cell's shore, just north of Bluff Hill and the Port's breakwater, Westshore is partially sheltered from the largest storm waves that arrive from the southeast, the result being that it experiences lower waves than typical of this coast, and with its beach having a significantly higher content of sand. The beach at South Haumoana, Figure 1-4, is more typical in being dominated by the greywacke gravel, with sand being seen in this photograph only at the bottom of the beach, visible because the photo was taken during low tide and under calm-sea conditions on this otherwise exposed shore. The proliferation of sea walls seen in this photograph is evidence that at high tides and under storm-wave conditions, this seemingly extensive deposit of gravel is insufficient to protect the homes, and as will be reviewed later in this chapter, South Haumoana and the communities to its south have experienced significant problems with erosion, the greatest impacts along the Hawke's Bay shore.

Figure 1-3: The mixed sand-and-gravel beach at Westshore, located at the south end of the Bay View Littoral Cell. [Photo, 2005]

Figure 1-4: The gravel beach on the shore of South Haumoana, with sand evident only within the intertidal zone at the bottom of the beach, this photograph having been taken at low tide. [Photo, November 2013]

Although the greywacke gravel found in the Hawke's Bay rivers and beaches has the appearance of being highly resistant, it is actually susceptible to comparatively rapid rates of abrasion when transported by waves and currents. The result is that the angular particles derived from erosion and landslides in the mountains rapidly have their edges worn away when transported down the rivers, so that by the time they reach the beaches they are well rounded and smooth. This abrasion continues under the action of the waves on the beaches, the result being that the sizes of the gravel particles are progressively reduced, displaying size reductions and shape modifications as they are transported northward along the shore of the Haumoana Cell, away from their sources in the south. A number of research investigations have focused on the abrasion of these gravels, undertaken for purely scientific interest, but also because the resulting loss of gravel on these beaches is an important component (a "debit") in the sediment budgets for these littoral cells. The earliest of these investigations was undertaken by Marshall (1927), involving detailed laboratory experiments in a "tumbler" to measure the rates of particle abrasion, his results representing a fundamental contribution to our understanding of grain abrasion processes and the rates of gravel-size reductions. In a follow-up publication, Marshall (1929) applied the results of his experiments to interpretations of the abrasion of the gravel found in the Hawke's Bay beaches, and their resulting changes in grain sizes and shapes. His laboratory experiments had demonstrated that the abrasion of the greywacke gravel yields sand, which initially is quite coarse as it is the product of collisions between pebbles and cobbles. This coarse sand is able to temporarily remain on the beaches, accounting for their being mixed sand-and-gravel, but eventually that coarse sand is ground down into the silt and very fine particles of sand that originally were deposited in the ocean,

later to be compressed to form the greywacke rocks found in the Front Range. On the ocean beaches these very fine sediment particles released by the abrasion are quickly carried offshore by the waves, with some of the sand being deposited just seaward from the gravel beaches, as seen in Figure 1-4 from South Haumoana.

More recent investigations of particle abrasion on New Zealand's mixed sand-and-gravel beaches have been undertaken in the university theses by Hemmingson (2004), Tuthill (2008), and Kantor (2009). The laboratory and field experiments by Hemmingson and Tuthill focused on the processes and rates of greywacke gravel abrasion, their samples having been derived from both South Island beaches and from Hawke's Bay. The field study by Kantor (2009) is of particular interest in that it focused on the Haumoana Littoral Cell, having employed an innovative technique of tagging individual pebbles implanted with Radio Frequency Identification tags, so they could be followed for several months as they are transported by the waves northward along that shore, providing measurements of their transport rates and the extent of abrasion based on their decreasing weights.

1.3 BEACH SEDIMENT BUDGETS

Important to understanding the present-day and future problems with coastal erosion and property losses is the formulation of "beach sediment budgets", involving assessments of the sources ("credits") that supply sediment to the beach, versus its losses ("debits"), the "net balance" in the budget determining whether that beach experiences erosion or is accreting. A sediment budget for the Haumoana Littoral Cell is analyzed in Table 1-1, originally derived by Tonkin and Taylor (2005) with later modifications by Komar (2005). It needs to be recognized that all of the values listed for the credits and debits are estimates, subject to uncertainties and potential changes as additional information becomes available. In this budget it is seen that the Tukituki River and the erosion of Cape Kidnappers combine to contribute an estimated 46,000 m^3/year of gravel to this cell, while loses amount to a total of -91,000 m^3/year, the result being that the budget's balance is significantly "in the red" with a net annual loss of -45,000 m^3/year, indicating that on average the Haumoana Cell's shoreline has experienced erosion over the decades. This value for the balance in the budget is actually better established and has less uncertainty than the volumes of the individual credits and debits, it having been based on direct surveys of the beaches over the years as part of HBRC's monitoring program, providing a direct documentation of whether individual survey sites have experienced erosion or accretion, as well as collectively determining the net balance in the sediment budget for the entire littoral cell. Although the balance in the budget may therefore be known from the outset of the analysis, assessments of the credits and debits within the budget are informative in that they account for the correspond rates of shoreline change and sediment volumes, providing an explanation for the causes of the erosion problems and suggestions to be taken to solve those problems (Komar, 1998).

It is evident from this sediment budget for the Haumoana Cell that the most significant factor accounting for its negative balance has been the commercial mining of gravel and sand at Awatoto, mid-way along this cell's shoreline. With that extraction having averaged -47,800 m^3/year during the 30 years from 1973 to 2002, when good records were kept, nearly 1.5 million cubic metres of beach sediment had been removed. Based on the recognition of the negative consequences of this extraction on the Cell's sediment budget, it was decided that

this commercial mining operation would in time be phased out. According to Table 1-1, the elimination of sediment mining at Awatoto should essentially balance its budget, it would no longer be "in the red".

Table 1-1: The Sediment Budget for the Haumoana Littoral Cell.
[*From* Tonkin and Taylor (2005), modified by Komar (2005)]

Budget Components	Estimated Annual Rates (m³/year)
Sources ("Credits")	
Tukituki River	28,000
Cape Kidnappers Erosion	18,000
Total	46,000
Losses ("Debits")	
Awatoto Extraction	-47,800
Pacific Beach Extraction	-12,800
Gravel Abrasion	-30,400
Total	-91,000
Net Balance of Beach Sediments	-45,000

Beach gravel and sand has also been extracted from Pacific Beach in Napier, at the north end of the Haumoana Littoral Cell, serving as the source of sediment for nourishment of the recreational beach at Westshore, located just north of Bluff Hill at the south end of the Bay View Littoral Cell. Initiated in 1986, on average 12,800 m^3/year of gravel and sand has been extracted from Pacific Beach, representing a debit in the sediment budget for the Haumoana Littoral Cell, a "credit" in the Bay View Cell's budget.

While the sediment budget in Table 1-1 has provided an overview of the credits and debits in the Haumoana Cell, with its resulting balance being significantly in the red, to a degree it is misleading in that this cell's erosion has occurred almost entirely along the southern-most stretch of its shore, while there has been net accretion (although reduced) along its northern half. This difference was shown in the original analysis of this budget by Tonkin and Taylor (2005), having found that based on the beach profiles surveyed over the years, the stretch of shore south of the Tukituki River had eroded at an average rate of -48,800 m^3/year, while north of the river there had been a net accretion of 3,800 m^3/year; the combination of these rates yielded the -45,000 m^3/year net magnitude for the cell as a whole, the balance give in Table 1-1. This pattern of longshore variations in the rates for the multidecadal local erosion versus accretion has been further documented by Edmondson et al. (2011), having presented analysis results for the individually surveyed profile sites in the HBRC monitoring program. This pattern of shoreline erosion in the south versus accretion to the north is produced by there being a net northward longshore transport of the beach sediments, caused by the dominant waves arriving from the southeast, the gravel and sand supplied by the Tukituki River and erosion of Cape Kidnappers being rapidly carried to the north within this littoral cell.

Misconceptions have developed concerning the consequences of this northward net transport of sediments along the Haumoana Cell's shoreline, with beach erosion largely confined to the southern stretch of its shore, while accretion has occurred to the north. In particular, there have been misunderstandings concerning the impacts of the commercial mining of sediment from the beach at Awatoto. Since there continues to be net accretion at Awatoto and to its north in spite of this extraction, the assumption has been that the mining operation has not resulted in negative impacts beyond there being reduced rates of accumulation to the north. Furthermore, it has been assumed that the extraction could not have adversely affected the beaches to the south of Awatoto, it not having contributed to the erosion along the shores of East Clive, South Haumoana and Te Awanga. To a degree mistaken these views are mistaken, demonstrated by the numerical model analyses undertaken by Tonkin and Taylor (2005) to examine the shoreline changes that are a consequence of this beach mining operation at Awatoto.

The analyses by Tonkin and Taylor (2005) employed the UNIBEST model developed at the Delft Hydraulics Laboratory in the Netherlands, a model that has seen widespread acceptance in applications by coastal engineers and scientists. The model employs a formula that calculates the longshore transport rates of the beach gravel, depending on the wave heights, periods, and angles of wave approach to the shore, and also on the grain size of the beach sediments. UNIBEST first transforms the waves from the offshore deep water to the beach, accounting for their shoaling and refraction, and evaluates the wave energy losses due to bottom friction. It then calculates the profile of the longshore currents on the beach and the resulting longshore sediment transport rate. Analyses by Tonkin and Taylor (2005) were performed along the length of the Haumoana Cell's shoreline, providing determinations of the sediment transport into and out of each of 200 "cells" into which that shore had been divided; the difference between the input and exit of sediment from each cell determined its resulting shoreline change. The model also accounted for contributions from the sediment sources, the Tukituki River and erosion of Cape Kidnappers, and the losses of sediments being extracted from the beach at Awatoto and Pacific Beach in Napier. Model applications included runs where the Tukituki River supplied sediment at a range of rates, 28,000 and 13,000 m^3/year, accounting for its natural variability. Losses of gravel from abrasion were included, a uniform rate of loss of 0.5 m^3/year per metre of shoreline length having yielded the best results when calibrating the model. All of these credits and losses correspond to those in the sediment budget, Table 1-1, but application of the UNIBEST model represented a considerable advance in the analysis, it having determined the resulting changes of the shorelines, explaining the observed patterns of erosion versus accretion along the length of the Haumoana Cell's shore.

A systematic series of analyses were undertaken by Tonkin and Taylor (2005) to examine the effects of sediment extraction at Awatoto, beginning with the historic, pre-development conditions prior to beach sediment mining. The results are shown in Figure 1-5, the horizontal axis in the graph being the alongcoast distance southward from the Port's breakwater in Napier, with Clifton at a longshore distance of 20 kilometres; the vertical axis is the annual rate of shoreline change, positive values representing accretion, negative values being erosion. The pair of curves represent the range of sediment supplies by the Tukituki River. The model results show high rates of erosion and shoreline recession in the southern-most part of the cell, and accretion to the north, the cross-over point being located in proximity to the mouth of the Tukituki River. The highest rates of beach accretion are determined to have been in the area of Awatoto and to its immediate south near the mouth of the Ngaruroro River, the rate

of shoreline advance according to the model calculations having been on the order of 1.0 m/year prior to the inception of commercial sediment extraction. The location of this maximum zone of beach accretion was controlled by the alongshore variations in the orientations of the shoreline with respect to the refracted wave directions, such that the gradient in the decreasing rates of longshore sediment transport to the north were greatest along that stretch of shore, producing the highest rates of advancing shores.
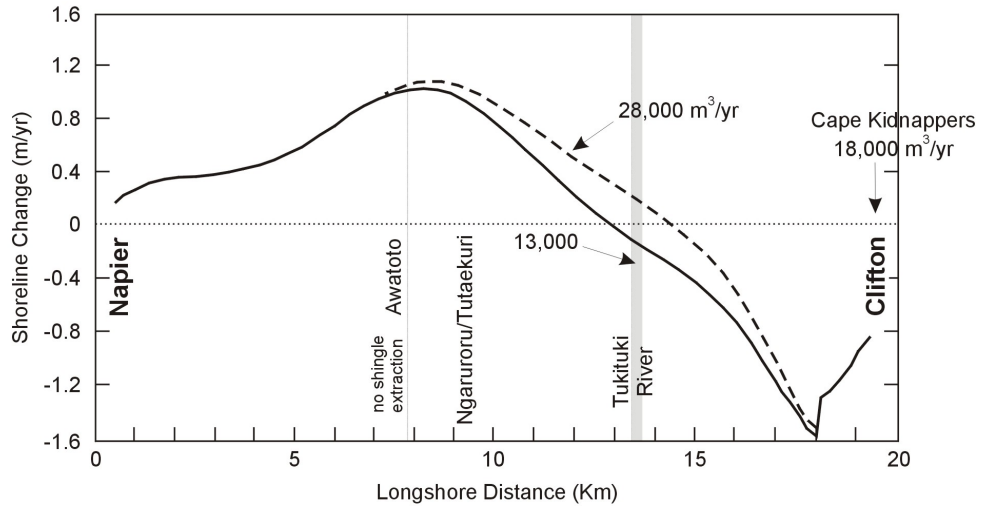
Figure 1-5: **The** UNIBEST model analysis of the patterns of shoreline erosion and accretion for the conditions prior to sediment extraction at Awatoto and Pacific Beach, for a range of volumes of sediments supplied by the Tukituki River. [*From* Tonkin and Taylor (2005)]
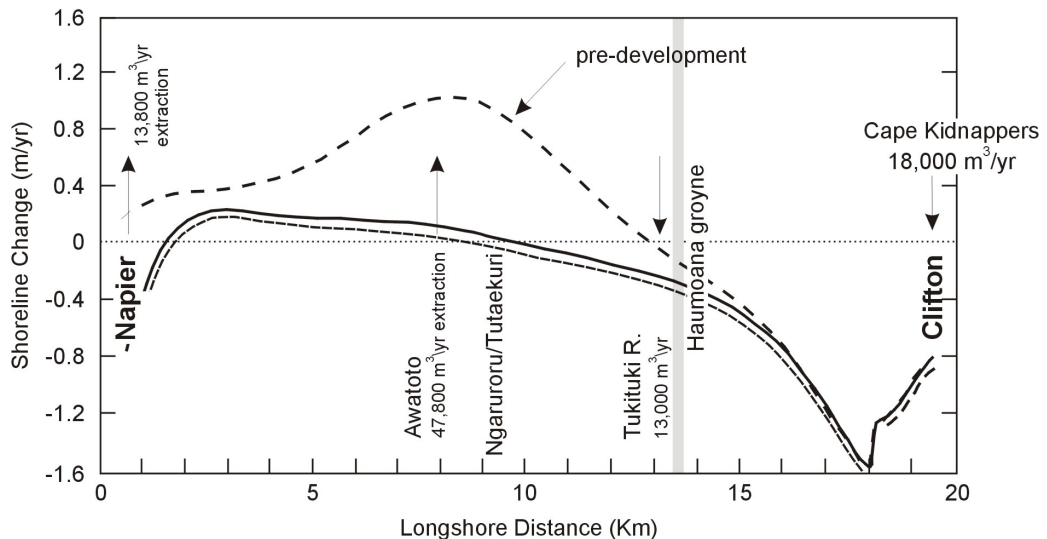
Figure 1-6: Model runs affected by beach sediment extraction at Awatoto and Pacific Beach in Napier, compared with the long-dashed line prior to extraction (Fig. 1-5). The short-dashed line includes the additional effects of gravel abrasion. [*From* Tonkin and Taylor (2005)]

The UNIBEST analysis in Figure 1-5 for the pre-development natural conditions served as the basis for a comparison with the computed shoreline changes that occurred later when sediment extraction at Awatoto and Pacific Beach altered the sediment budget, with the results graphed in Figure 1-6. The analysis is based on an average rate of sediment extraction of 47,800 m³/year at Awatoto, with extraction at Pacific Beach for the nourishment of Westshore having had a rate of 13,000 m³/year, conforming with the sediment budget in Table 1-1. It is seen that according to the UNIBEST analysis the extraction at Awatoto significantly reduced the rates of sediment accumulation along the central shoreline of the littoral cell, reduced from 1.0 m/year prior to extraction to about 0.2 m/year with mining having taken place at Awatoto. Of particular significance, it is seen that the effects of this extraction extend well to the south of Awatoto, with the point of transition between erosion to the south and accretion to the north having shifted to a more northerly location on this shore; a longer stretch of the cell's shoreline now experiences erosion in response to the mining operation. The results are sensitive to the volumes of sediment delivered by the Tukituki River to this cell; with a supply rate of 28,000 m³/year, the model results show that the beach experiencing erosion has shifted northward by about 500 metres due to the extraction at Awatoto, whereas with a reduced river supply of 13,000 m³/year the zone of shoreline erosion expanded by some 5,000 metres to the north (Tonkin and Taylor, 2005). Irrespective of which of these values is correct on average, the results demonstrate that during periods of reduced rainfall and flooding in the Tukituki River, when little or no sediment is delivered to the coast, there would be a considerably expanded stretch of shore that experiences beach erosion in consequence to the sediment mining at Awatoto.

These model results demonstrating the existence of adverse impacts to the shoreline south of Awatoto due to sediment mining might seem to be counter intuitive, it having affected the beach in the updrift direction to its south, as well as in the northward downdrift direction where impacts would more obviously be expected. It needs to be recognized that although there is a net longshore sediment transport to the north, under the natural conditions with waves from day to day arriving from a range of directions, there would at times be sediment movement to the south, while at other times it would be to the north, so impacts from the extraction could be expected in both directions relative to Awatoto. But even if the longshore transport was always to the north, not for a single day to the south, the "draw-down" effect of the sediment extraction at the mining site would locally alter the shoreline positions and orientations relative to the arriving waves, such that the extraction would induce an increase in the rate of transport arriving from the south, removing sediment at a greater rate from that stretch of shore. The inverse condition is more commonly seen and easily understood, where sediment is supplied to the shore by a river, building out a delta centered on the river's mouth. Even in the case where the delta is growing on a coast having a dominant direction of longshore transport, the sediment contribution from the river would still result in some growth of the delta in the updrift direction, although the overall shape of the delta would be skewed by the dominant transport. The greater the rate of longshore transport compared with that supplied by the river, the more asymmetrical the resulting delta, but with there still always being some degree of delta growth in the up-drift direction (Komar, 1973). Although the model analysis results by Tonkin and Taylor (2005), showing cell-wide impacts from sediment mining at Awatoto, might seem to be counter intuitive, they are correct, representing the inverse response compared with the growth of a delta when sediment is locally being added to the shore.

In their series of model runs Tonkin and Taylor (2005) also included the sediment extraction at North Beach in Napier. The result of the UNIBEST analysis in Figure 1-5 shows a localized inducement of shoreline recession, with the rate being on the order of -0.8 m/year, a result of the extraction exceeding the rate of sediment arrival from the south as the remnant longshore transport, having been reduced by losses of gravel from abrasion and its mining at Awatoto. While the analyses indicate that this induced erosion at Pacific Beach would be limited to the Napier shore, the results suggest that its effects need to be monitored, at least until the extraction at Awatoto has been terminated, after which greater volumes of sediment would reach North Beach.

1.4 EROSION PROBLEMS AND SUSCEPTIBILITIES FOR FUTURE IMPACTS

The concerns about this coast, its existing erosion problems and potential for increased impacts in the future due to rising sea levels, stem from its fragility with the backshore having low elevations fronted by relatively narrow mixed sand-and-gravel beaches. The photographs in Figures 1-7 and 1-8 are typical respectively of the shores in the Bay View and Haumoana Littoral Cells. The Bay View Cell on average experienced about 2-metres uplift at the time of the 1931 earthquake (Chapter 3), producing an elevated gravel ridge but with significantly lower elevations immediately inland, that prior to the uplift had been the submerged expanse of the Ahuriri Lagoon but is now the site of the region's main airport. Historic reports indicate that prior to its uplift this stretch of shore was frequently overtopped by high tides and storm waves, with the present-day developed area of Westshore adjacent to the Ahuriri Harbor having suffered the most during storms. Thanks to the 2-metre uplift over 80 years ago, the main ocean-front hazard along the shores of the Bay View Littoral Cell is now limited to wave attack and erosion of the seaward edge of its elevated gravel ridge, evident in the formation of the low wave-cut scarp along nearly the entire length of its shoreline (Figure 1-7). Although storm overtopping has not represented a significant hazard within the Bay View Cell since 1931, it is evident that a 1-metre rise in the level of the sea projected for this century, combined with more intense storms and their extreme waves, would renew the threat from erosion and flooding. The potential impacts would then affect a considerable numbers of homes that have been constructed over the decades atop this uplifted barrier-beach ridge, even though they have significant set-back distances from the present-day erosion scarp.

The shores of the Haumoana Littoral Cell are illustrated by the photographs in Figures 1-8 and 1-9, showing a greater degree of along-coast variations in the beach and backshore morphologies, and storm impacts to developed properties. Important is that the northern-most portion of this cell also experienced significant uplift during the 1931 earthquake, but to a progressively reduced degree alongshore toward the south, this trend continuing until south of East Clive subsidence of the land occurred (Chapter 3). The uplift of shore from downtown Napier to Awatoto amounted to 1.5 to 2 metres, transitioning rather abruptly to subsidence of the land by about 1 metre south of East Clive, rendering that shore particularly susceptible to future impacts from rising sea levels and storm-generated waves. This hazard is evident in Figure 1-8 showing the Haumoana shore just south of the mouth of the Tukituki River, where the barrier gravel ridge frequently experiences wave overtopping during combinations of high tides and storm waves. Impacts to homes and infrastructure have been extensive still further

to the south, Figure 1-9, in the communities of South Haumoana, Te Awanga and Clifton (Daykin, 2010). Although the earthquake and subsidence this shore at the south end of the Haumoana Littoral Cell occurred some 80 years ago, it may still represent a factor in the erosion impacts and flooding experienced there. However, as seen in the shoreline-change analyses undertake by Tonkin and Taylor (2005), with their results graphed in Figures 1-5 and 1-6, high rates of shoreline recession amounting to on the order of 1 metre/year have occurred to the south of the Tukituki River, which can be attributed primarily to the extreme negative balance (being "in the red") in that shore's sediment budget.

Figure 1-7: The Whrinaki beach and backshore in the Bay View Littoral Cell, where wave erosion has cut into the barrier gravel ridge that was raised by 2 metres during the 1931 Hawke's Bay earthquake. [Photo, September 2005]

Figure 1-8: The southern shore of the Haumoana Littoral Cell, where the barrier beach ridge experiences overwash during storm events. [Photo, September 2005]

Figure 1-9: Erosion and property damage in the community of South Haumoana, in part
attributed to the subsidence of this shore durng the 1931 earthquake, but with its
sediment budget "in the red" being the primary cause. [Photo, 2005]

1.5 SUMMARY AND CONTENTS OF THIS REPORT

Prior to the uplift this coast in 1931, produced by the Hawke's Bay earthquake, most of its beaches and backshore areas experienced chronic erosion and overwash flooding occurrences during storms, making it essentially impossible to develop. Even the downtown area of Napier was frequently inundated during the high water levels of storms. The character of this coast abruptly changed when the earthquake raised most of its shores by 1.5 to 2 metres, extending from Tangoio in the north to about the present-day communities of Awatoto and East Clive in the south. Elevated by that amount, those shores then exceeded the elevations of the tides plus the surge and wave runup of even major storms, their acquired stability permitting the development of homes and infrastructure found there today. Only the southernmost portion of this shore, extending along the present-day Haumoana, Te Awanga and Clifton, experienced subsided during the earthquake, increasing its hazards and in part accounting for its persistent problems with erosion and flooding. It is evident that any increase in the future levels of the sea and in the intensities storms, both being projected by climatologists to occur during the next 100 years, would result significantly enhanced threats to properties along the Hawke's Bay coast.

The objective of this investigation and report is therefore to undertake assessments of the potential consequences to the coast of Hawke's Bay as a result of Earth's evolving climate, including the potential impacts of a 1-metre rise in sea levels that have been projected by climatologists and oceanographers, combining with the expected enhanced storm intensities and the heights of their waves that reach its shores. Important questions involve the expected stability of the natural barrier beaches that consist of mobile gravel and sand, how

they might be expected to respond to these enhanced ocean forces, and whether the beach ridge will continue to represent the front line defense for shore-front homes and infrastructure. Considerations also need to be directed toward the possible mitigation measures for maintaining the integrity of this natural barrier, to ensure its continued protection for those coastal properties.

This report begins with a general review of Earth's changing climate, including the projections that have been made for future accelerated rates of rise in global-average sea levels (Chapter 2). That global perspective is followed by a review directed specifically to the Hawke's Bay hazards, including its tectonic setting, earthquakes, and land elevations along its shore (Chapter 3). The report then turns to the ocean processes, beginning with its measured tides elevated by storm surges (Chapter 4), the climate of wave heights and periods (Chapter 5), and the nearshore processes and extreme water levels of the tides plus the wave runup, compared with the morphologies and elevations of its beaches (Chapters 6 and 7). The primary focus of this investigation is therefore directed toward updated analyses of the processes and factors that have important roles in governing the erosion and flooding hazards of the Hawke's Bay coast. As such, the analyses include assessments of the expected extremes in those ocean processes, and combinations of the processes, particularly the extreme high tides plus the swash runup of storm waves on the beaches, events that pose the greatest threat to the shores of Hawke's Bay during this century. Assessments of those potentially extreme hazards also require considerations of the expected responses of the barrier beaches as sea levels and storm-generated wave heights progressively increase during this century, including model analyses to establish whether or not the barrier beaches could be expected to evolve and adapt in their morphologies in such a manner that they continue to provide protection to this coast. This report ends with a general consideration of the management responses required and could reasonably be undertaken to improve the protection to society's developments along the coast of Hawke's Bay.

1.6 REFERENCES

Daykin, N. (2010) *Haumoana Littoral Cell: Coastal Storm Analysis*: Asset Management Group Technical Report AM05/18, Hawke's Bay Regional Council.

Edmondson, E., N. Daykin, and Sara Bailey (2011) *Hawke's Bay Coastal Profile Monitoring 2011*: Asset Management Group Technical Report AM11/01, Hawke's Bay Regional Council, 219 pp.

Hemmingsen, M. A. (2004) *Reduction of Greywacke Sediments on the Canterbury Bight Coast, South Island, New Zealand*: Ph.D. Thesis, University of Canterbury, Christchurch, New Zealand.

Kantor, M.S. (2009) *Southern Hawke's Bay Gravel Transport Study*: Thesis, Master of Science in Environmental Science, The University of Auckland, 182 pp.

Komar, P. D. (1973) Computer models of delta growth due to sediment input from rivers and longshore transport: *Geological Society of America Bulletin*, v. 84, p. 2217-2226.

Komar, P.D. (1998) *Beach Processes and Sedimentation*: Prentice-Hall, Inc., Upper Saddle River, N.J., 2nd edition.

Komar, P. D. (2005) *Hawke's Bay, New Zealand: Environmental Change, Shoreline Erosion and Management Issues*: Report for the Hawke's Bay Regional Council, 244 pp.

Komar, P. D. (2010) Shoreline evolution and management of Hawke's Bay, New Zealand: Tectonics, coastal processes and human impacts: *Journal of Coastal Research*, v. 26, n. 1, p. 143-156.

Marshall, P. (1927) The wearing of beach gravels: *Transactions of the Royal Society of New Zealand*, v.58, p. 507-532.

Marshall, P. (1929) Beach gravels and sands: *Transactions of the Royal Society of New Zealand*, v. 60, p.324-365.

Tonkin and Taylor (2005) *Shoreline Modelling Report*: Report to the Hawke's Bay Regional Council.

Tuthill, Abraham (2008) *Rates of Gravel Abrasion on the Napier Coast, Hawke's Bay, NZ*: Dissertation in Science, The University of Auckland, 83 pp.

2   Earth's Changing Climate, Increasing Sea Levels and Wave Heights

2.1 INTRODUCTION

Major shifts in the climate of the Earth have taken place throughout its history, and are occurring today. In the context of changes in the distant past, particularly significant were the Ice Ages that began about two million years ago, during which there were major cycles in the growth and melting of glaciers, continuing up to nearly the present. Lowered sea levels occurred when water was first extracted from the oceans to form the glaciers, and then rose when the glaciers melted, the total change in ocean levels having been on the order of 125 metres.   One of the major concerns today is that greenhouse warming of the Earth is predicted to result in accelerated rates at which the level of the sea will rise, such that the global average level will be substantially higher by the year 2100 than it is today. Furthermore, it has been documented that storm intensities and their generated wave heights have increased over the decades, interpreted by most investigators as also having been caused by global warming, enhancing both extratropical storms at high latitudes and storms generated at low latitudes in the tropics (hurricanes, typhoons and cyclones). Recent global coverage by satellites in particular demonstrates that wave heights have increased throughout the world's oceans, including off the shores of New Zealand. The expectation is that with increased sea levels and ocean wave heights, problems with coastal erosion and flooding will become significantly greater and more widespread along the ocean's shores, achieving near-pandemic levels in their global impacts.

The objective of this chapter is to provide a global view of Earth's changing climate, with the primary focus being on evidence that exists for greenhouse warming and its consequences. Reviews will be presented of the recent research investigations that have documented the rates of global sea-level rise during the 20th century, with projections of future rates and the potential net increase that could take place during the 21st century. A review will also be presented of the climate controls on storm intensities and analysis results of wave-buoy and satellite measurements that have found wave-height increases throughout the world's oceans. Subsequent chapters will examine the past trends and future projections of sea levels and wave heights specifically on the coast of Hawke's Bay.

2.2 GLOBAL WARMING

There is a wealth of data that documents the increased temperatures of Earth's atmosphere and oceans, one evident consequence being the rapid melting of glaciers throughout the world. The records of directly measured atmospheric temperatures that span most of the Earth date back only to the late 19th century, measured on land by a large number of weather stations, with ships and more recently satellites providing temperature data over the oceans.

Those measurements have become crucial in documenting the increased temperatures that began in about 1880 to 1900, including the record-high temperatures that have occurred in recent years.   Hansen et al. (2006) analyzed these directly measured temperatures to determine global annual averages, with the results shown in Figure 2-1A.   The trends are graphed as global-mean anomalies, where the comparison is with the 1951-1980 baseline when temperatures had largely leveled off for about 30 years, attributed to industrial pollution, particularly the burning of high-sulfur coals that introduced aerosols into the atmosphere that reflected the radiation arriving from the sun back out into space. With the reduction of that pollution during the 1970s and 80s, temperatures again began to rise at a rapid rate. Based on the analyses by Hansen et al. (2006), Figure 2-1A, between about 1910 and 1940 there had been a significant trend of increasing temperatures, totaling about 0.4°C. After 1940 temperatures decreased slightly until 1970, after which there has been a dramatic and persistent increase, amounting to another 0.6°C increase by the end of the 20th century. When Hansen et al. (2006) undertook those analyses, the ten warmest years on record had all occurred within the 12-year period from 1997 through 2008; additional record temperatures have occurred since that time.

Figure 2-1B from Hansen et al. (2006) shows the global distribution of temperature changes that occurred during the first five years of the 21st century, 2001 through 2005. It is evident that global warming had not been uniform across the globe, but instead has been greatest in the high latitudes of the Northern Hemisphere where the increases have amounted to 2°C.   Direct evidence for those increased temperatures at high latitudes has been the dramatic melting of the summer ice that covers the Arctic Ocean, and in the accelerated rates of melting of the glaciers that cover Greenland (Howat et al., 2007; Slobbe et al., 2009).
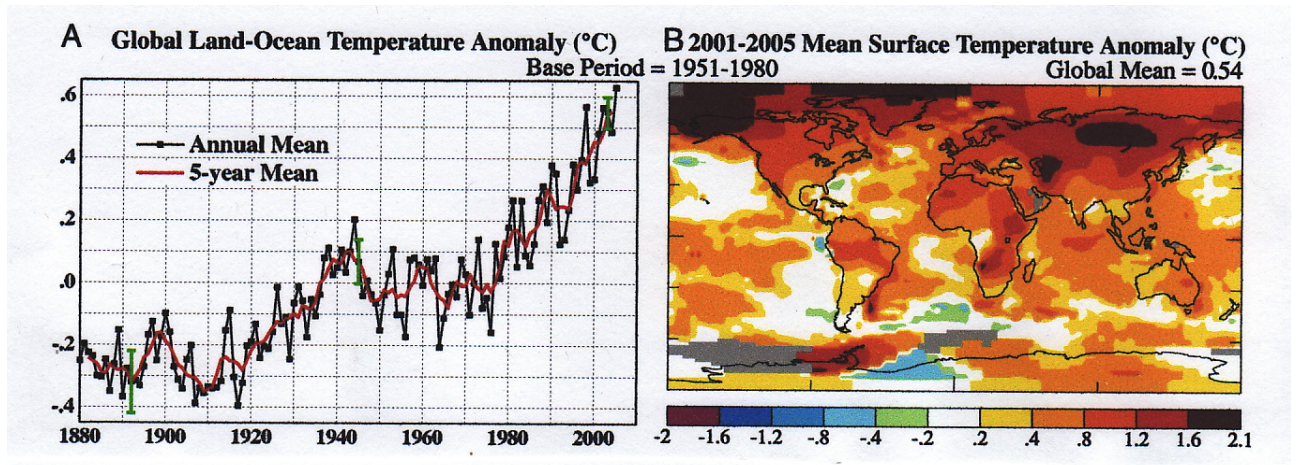
Figure 2-1: A. Changes in globally averaged temperatures measured since the 1880s, documenting an overall rise of nearly 1°C. B. The global distribution of temperature anomalies for the early 21st century (2001-2005). [*From* Hansen et al. (2006)]

The key to investigations of Earth's changing climate prior to the availability of direct measurements by weather stations has been what are termed "proxy indicators", archives of environmental records of past climate variations. One particularly important proxy is the record from tree rings, each annual growth ring providing evidence for the climate (temperature and precipitation) that year, at the location where the tree was growing.   Other proxies include

temperature assessments derived from ice cores collected from glaciers that cover Greenland and Antarctica, sediments in oceans and lakes that contain annual layers (varves) of accumulation, and corals that form annual growth layers of calcium carbonate. Mann et al. (1998, 1999) employed a "multiproxy" approach to investigate the long-term climate variations in the Northern Hemisphere spanning the past 1,000 years, while Mann and Jones (2003) extended the analyses back to the year 200 and included initial results from the Southern Hemisphere. The first step in their analyses was to empirically correlate the proxy environmental data that had been collected during the 20th century with the directly measured temperatures from weather stations. Based on that calibration, the more ancient proxy information could then be used back in time when direct temperature measurements were not available. The results from the proxy data analyzed by Mann et al. (1999) are graphed in Figure 2-2, showing an overall progressive cooling from the year 1000 to 1900, reverting to a dramatic increase during the 20th century and leading to the recent record-high temperatures (represented in the graph by that measured in 1998). Due to the marked shift in the temperature trend in about 1900, this graph with its kink is commonly referred to as the "hockey stick curve".
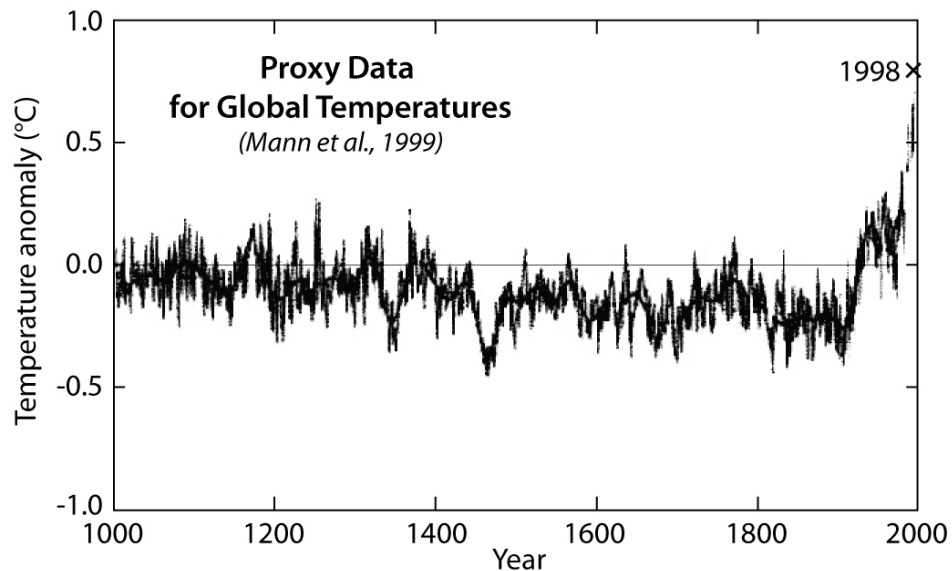
Figure 2-2: Millennial temperature variations based on proxy data, graphed as anomalies (°C) compared with the zero line that corresponds to the mean temperature during the 20th century. [*Modified from* Mann et al. (1999)]

Having extended the proxy-temperature analyses back another 800 years beyond that graphed in Figure 2-2, back to the year 200, Mann and Jones (2003) derived a proxy-temperature record that corresponds closely with historical records of climate changes. In particular, temperatures were elevated during what is called the Medieval Warm Period (800 to 1400), with cooler periods both before and afterwards, leading gradually into the Little Ice Age with its cooling evident in Figure 2-2, during which glaciers in Scandinavia and the Alps are known to have advanced. With significant warming having occurred during the 20th century, mountain glaciers throughout the world have melted at rapid rates [for example, the glaciers atop Mount Kilimanjaro in equatorial Africa (Thompson et al., 2009), the mountain glaciers of Alaska (Chen et al., 2006), and those in New Zealand (Salinger et al., 2008)].

Mann et al. (1998, 1999) undertook analyses to relate the temperature changes in Figure 2-2 to the potential environmental causes — the changes in solar radiation reaching the Earth during those 1,000 years, the occasional major volcanic eruption that injected aerosols into the atmosphere (temporarily acting to reduce global temperatures), occurrences of major El Niños that would temporally have raised temperatures, and the input of greenhouse gases into the atmosphere by humans, which increased during the Industrial Revolution and has been greatest since the late 19th century. Their statistical analyses showed a direct correlation between the increased temperatures and CO_2 measurements, providing strong evidence that the temperature increases since about 1900 have been caused by progressively higher concentrations of greenhouse gases. Prior to 1900 the changes in CO_2 levels in the atmosphere were less important, the variations in temperatures evident in Figure 2-2 having instead been affected mainly by solar irradiance and aerosols derived from volcanic eruptions. Hansen et al. (2006) similarly analyzed the changes in measured temperatures recorded during the 20th century by weather stations, having also concluded that only the increases in CO_2 and other greenhouse gases could account for the dramatically increased measured atmospheric temperatures.

As would be expected, the increasing temperatures of the atmosphere led to higher average temperatures of the ocean's surface waters (Levitus et al., 2000; Ishii et al., 2003). This increase has been demonstrated by direct measurements of the water temperatures, routinely collected over the decades by ships in transit, particularly during oceanographic expeditions beginning in the late 19th century. But significant now is the advent of data collection by satellites, beginning in the early 1990s, whose orbits within a few days cross the entire expanse of the oceans, collecting not only near-synoptic measurements of water temperatures but also sea-level elevations. Such measurements from satellites have demonstrated that global averages of both water temperatures and sea levels have on average been increasing. However, the data also show that the changes have not been uniform throughout the oceans, with some areas having cooled even though most are warmer. The resulting thermal expansion of the water in regions where the temperatures have increased has been a primary factor in locally raising sea levels, whereas levels have been dropping in regions where the water has become colder since the 1990s (Cazenave and Nerem, 2004; Cazenave and Llovel, 2010). For the first time this global documentation derived from satellites can account for the variations and net trends in rates of changing water temperatures and sea levels measured along the world's coastlines, important in understanding the erosion and flooding of those shores.

2.3 THE GLOBAL RISE IN SEA LEVEL

With increasing global temperatures since the late 19th century, there has been a nearly parallel increase in rising sea levels, documented mainly from tide-gauge records and more recently from satellites. The correspondence with Earth's changing temperatures is particularly evident in the longest sea-level records, derived from the earliest tide gauges located on relatively stable coasts. Several gauges in Europe became operational during the 1700s, with their records having been analyzed by Gornitz and Solow (1991). Figure 2-3 from that study represents a composite graph based on data from several of those long-term gauges, with the result being most directly similar to the nearly complete records from Amsterdam (the Netherlands) and Brest (France). It is seen in this record that there were minimal changes in annual mean sea levels from 1700 to about 1900, after which there had been a significant rise through the 20th century, continuing to the present.
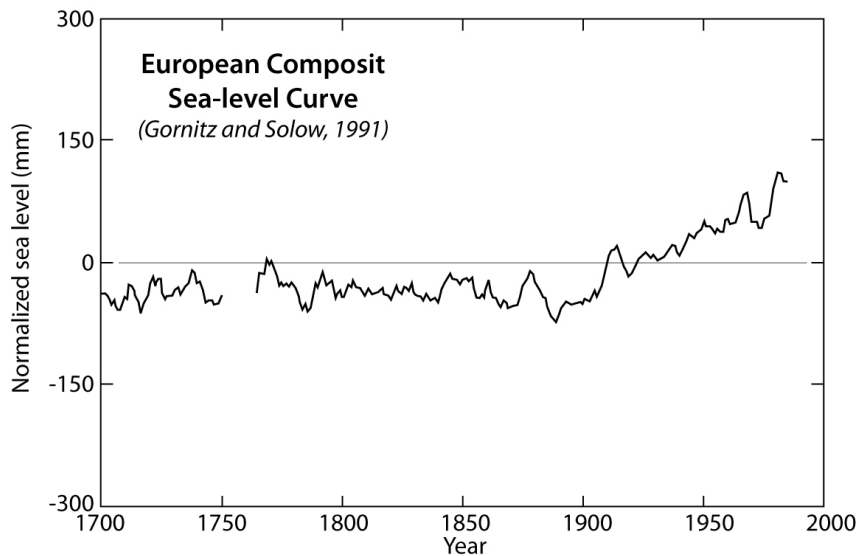
Figure 2-3: A composite sea-level curve based on the longest tide-gauge records available from northern Europe. [*Modified from* Gornitz and Solow (1991)]

There is a remarkable similarity between this curve for the changing sea levels and that in Figure 2-2 for the trend of increasing temperatures. To a significant degree this correspondence can be attributed to the sea-level rise having been caused by temperature increases of the ocean water in response to global warming, having produced a thermal expansion of the water as first demonstrated in the computations by Gornitz et al. (1982). The melting of continental glaciers clearly must also be an important factor in having brought about the measured rise in sea levels, with the extent of their melting on average paralleling the increased global temperatures. There has been considerable research directed toward surveying the changes in glacial masses, in an attempt to provide an accurate estimate of their melting and contribution to the global rise in sea levels [for example, the surveys of the West Antarctica Ice Sheet by Thomas et al. (2004)].

While the European composite curve in Figure 2-3 provides a reasonable depiction of the changes in annual mean sea levels spanning the past 300 years, recorded on relatively stable coasts, more widely such graphs show differences from one gauge location to another, generally minor but sometimes significant. This is because each gauge not only records the global (eustatic) rise in sea level, but also the existence of any land elevation changes at the coastal location of the gauge. As a result each gauge measures what is termed the "relative sea level", the sum of the rise in the actual water levels plus any changes in local land elevations. Many stretches of coast are naturally subsiding, so the rate of rise in the measured relative sea level is greater than the global average. In some locations humans have affected the local subsidence, increasing the rate by having pumped groundwater or having extracted oil; for example, those human-induced effects have respectively resulted in high rates of relative sea-level rise in Venice, Italy, and in Galveston, Texas. In the opposite direction, nearly all of Scandinavia is rising due to the rebound of that region after the glaciers melted, their weight during the Ice Age having depressed the land; the tide gauge in Stockholm, for example, shows a consistent drop in the relative sea level due to the land rebounding, rising faster than the global rise in sea level (Gornitz and Solow, 1991).

The coast's tectonic setting can also produce significant changes in land elevations, either subsidence or uplift. The tectonic effects on the trends in relative sea levels are illustrated in Figure 2-4 from our analyses of tide-gauge records along the coast of the U.S. Pacific Northwest, the states of Washington, Oregon and Northern California (Komar et al., 2011). This coast is affected by the collision and subduction of oceanic tectonic plates beneath the continental plate that encompasses all of North America. This tectonic setting is essentially the same as that of Hawke's Bay, which is being affected by the collision of the Pacific and Australian tectonic plates (Chapter 3). The plate collision along the U.S. Pacific Northwest is producing uplift of the land along that entire stretch of coast, but at different rates depending on the latitude, affecting the net trends of changing relative sea levels measured by tide gauges. Figure 2-4 shows the contrasting results from Neah Bay on the northern-most ocean shore of Washington, Yaquina Bay (Newport) on the mid-Oregon coast, and Crescent City to the south in California, close to the Oregon-California border. There is a high rate of tectonic uplift of the land along the northern Washington coast, faster than the eustatic rise in sea level, so the net trend of the relative sea level is negative (-1.85 mm/year), with that shore slowly emerging from the sea. Northern California is also an emergent coast, with the tide-gauge record from Crescent City similarly having a negative value (-0.78 mm/year). In contrast, although the mid-Oregon coast is also experiencing tectonic uplift, the rate of rise of that shore is slower, being less than the global rise in sea level. As evident in Figure 2-4, the result is a positive net change in the relative sea level (+2.21 mm/year, but with a large uncertainty due to the shortness of this record); the mid-Oregon coast is therefore submergent, the sea slowly transgressing over its shore.
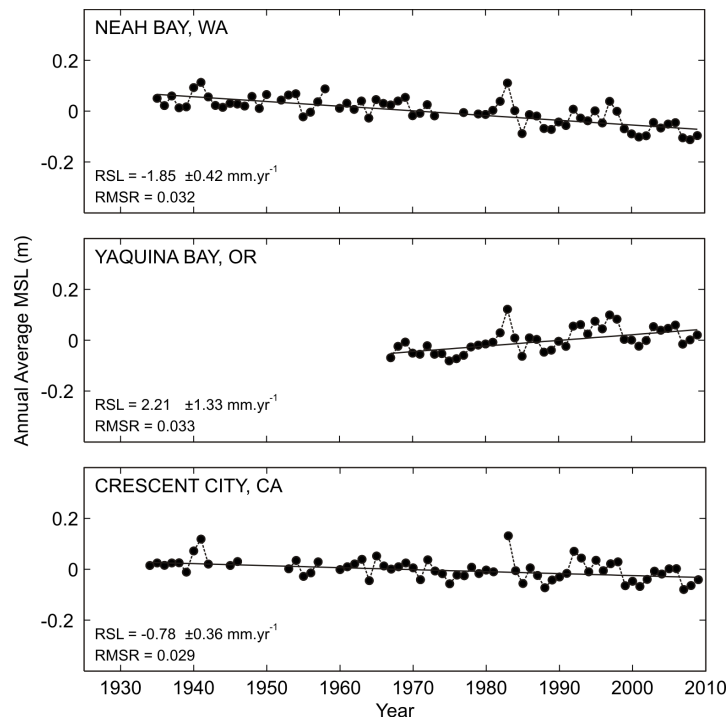
Figure 2-4: Trends of changing relative sea levels derived from tide-gauge records along the coast of the U.S. Pacific Northwest, affected by different rates of tectonic uplift. [*From* Komar et al. (2011)]

Over the years considerable interest has been directed toward assessments of the global average rate of sea-level rise and how it has been affected by Earth's changing climate, the focus now being directed toward whether global warming is producing an acceleration in the rate of rise. Assessments of the average rate of rise during the 20th century have been based primarily on measurements from tide gauges found throughout the world, the thought being that by averaging the results from different coastal settings the effects of land-elevation changes would largely be eliminated, leaving only the eustatic rise as the global average. A number of investigations have followed this approach, differing in details depending on which gauges are excluded because their records are too short and scattered to yield reasonable trends, or clearly are anomalous, the gauges in Scandinavia for example generally being omitted because of the glacial rebound and their falling relative sea levels. Overall the average rates of sea-level rise during the 20th century determined by those analyses have ranged from about 1 to 3 mm/year (Douglas, 2001; Pugh, 2004). The recent detailed analyses by Church and White (2006) and Holgate (2007) yielded almost identical rates, the latter study having obtained a mean rate of 1.74 ± 0.16 mm/year for the 20th century global rise in sea level, a net increase of 17 cm in 100 years.

While tide gauges along the world's coastlines have been the primary source of data used in assessments of mean sea levels and their trends of change, in recent years satellites now yield near-synoptic measurements of sea levels covering the entire oceans; recent reviews of that technology and the resulting analyses are provided by Cazenave and Nerem (2004) and Cazenave and Llovel (2010). The era of satellite measurements of sea levels began with the launch of the TOPEX/Poseidon satellites in 1992, which contained altimeters capable of measuring the level of the sea relative to the orbit height of the satellite, within an accuracy of 2 to 3 centimeters; the Jason mission beginning in 2001 continues this measurement series. The ground track of a satellite approximately repeats itself every 10 days, so the local eustatic mean sea level anywhere in the ocean can be computed by averaging the multiple measurements derived from having crossed each site. With the data series having now reached 20 years, it is possible to assess both the net trends and variations (spatial and temporal) in sea levels.

A combined analysis of the tide-gauge and satellite measurements of global average sea levels is shown in Figure 2-5 from the review by Cazenave and Llovel (2010), documenting the sea-level changes from 1800 to 2010 and including future projections to the year 2100. The thick black line represents the approximate average rise during the 19th century, based on a variety of geologic observations. The red line is based on the tide-gauge data analyzed by Church et al. (2004), while the green line is the satellite altimetry sea-level measurements since 1993, integrated as global averages. There is reasonably good agreement between the trends based on the tide-gauge and satellite measurements, indicating that for the past 15 to 20 years the mean rate of rise in the global sea level has been on the order of 3.3 ± 0.4 mm/year (Cazenave and Llovel, 2010). That rate is substantially greater than the 1.7 mm/year average rate for the span of the 20th century, with the concave curvature of the graph (red plus the green) in Figure 2-5 being suggestive of there having been an acceleration in the rate at which the level of the sea is rising. However, when detailed analyses of these measured sea levels are undertaken, multidecadal variations are found including periods of both accelerations and decelerations; there had been earlier decades when the rate of rise was on the order of 3 mm/year, only to later return to lower rates. It has also been suggested

that the post-1993 higher rate of sea level rise might represent a recovery from an earlier period of a reduced increase in the sea level, a result of there having been a degree of global cooling caused by aerosols derived from major volcanic eruptions, El Chichon in 1982 and Mount Pinatubo in 1991 (Church et al., 2005).
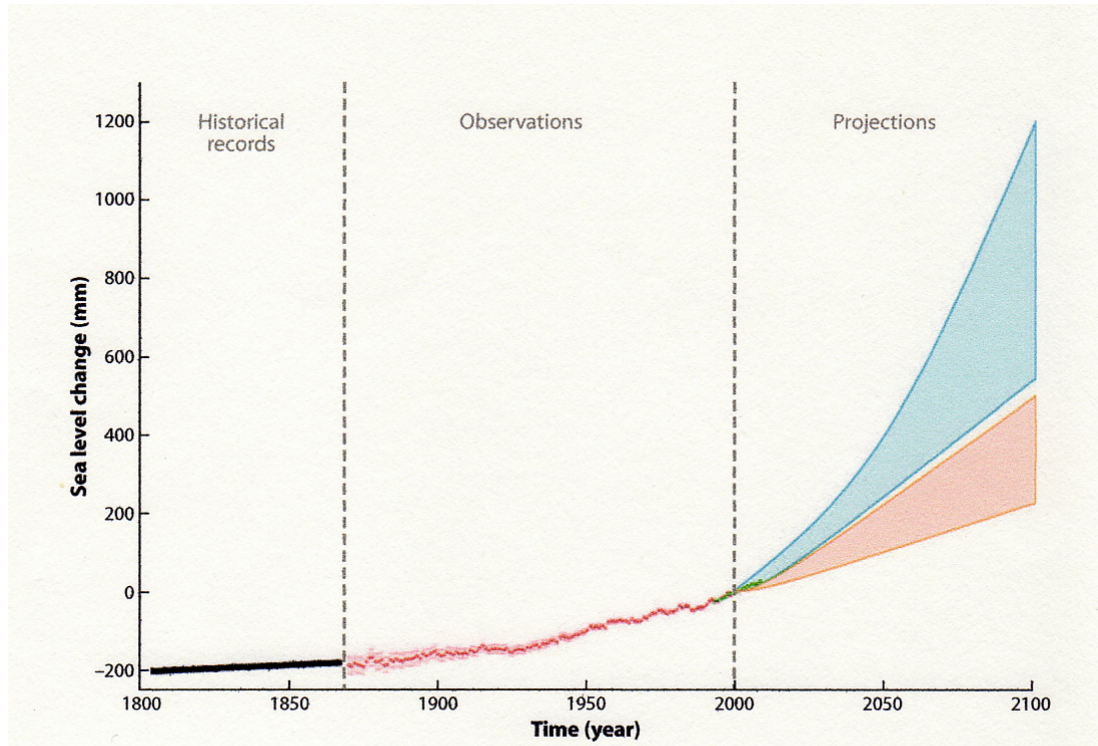
Figure 2-5: The increase in global mean sea levels from 1800 to the present, projected into the future to the year 2100 due to continued global warming. The red line is based on tide-gauge data, while the green line is from satellite measurements since 1993. The pink shaded projection is from the IPCC (2007) climate models, the light blue region being the range of recent projections determined by Rahmstorf (2007). [*From* Cazenave and Llovell (2010)]

Although the curvature of the graph in Figure 2-5, the portion based on the tide-gauge data and satellite altimetry measurements, is suggestive of there having been an overall acceleration in the rate of global rise in sea level during the 20th century, it may be premature to accept the post-1993 trend of 3.3 mm/year as having been caused entirely by global warming, setting the stage for future increases as society emits still more greenhouse gases into the atmosphere. On the other hand such projections are crucial, required in assessments of potential future hazards from erosion and flooding along the ocean shores. Such sea-level projections have been a primary objective of reports by the Intergovernmental Panel on Climate Change (IPCC), with their most recent report having appeared in 2007. The IPCC projections to the year 2100 are included in Figure 2-5, the pink-shaded region based on climate models and assumptions of the potential range of future greenhouse gas emissions, the result being a range of uncertainties in the future global mean sea levels (an increase of approximately 20 to 50 centimetres during the 21st century). The more extreme projections by Rahmstorf (2007) are also included in the diagram, the blue-shaded region showing sea-level increases of 50 to 120 centimetres by the year 2100. In contrast to the IPCC

projections that involved complex model analyses requiring a number of assumptions regarding climate responses to future increased greenhouse gases, Rahmstorf's approach is based simply on a semi-empirical correlation between the global sea-level rise and Earth's past changes in mean temperatures, representing the degree of global warming. There have been similar projections offered by other investigators, which have been summarized by Rahmstorf (2010); they also represent more extreme future sea levels than projected by IPCC (2007), and will be reviewed in Chapter 8 in the context of projections undertaken specifically for Hawke's Bay.

The consensus amongst climatologists is that future increases in sea levels produced by global warming will in all probability be greater than those projected by IPCC, and could represent an increase in the global mean sea level of more than 1 metre by the end of the 21st century.

The measurements of sea levels by satellites have become important in that they provide detailed documentations of the temporal and spatial changes in eustatic water levels, covering the entire oceans, not previously available from coastal tide gauges. This coverage now permits analyses of the local trends and variations in sea levels, including coastal sites of one's specific interest (e.g., Hawke's Bay). Furthermore, the satellite altimeter measurements determine the actual change in the level of the sea at each site, the eustatic component affected by local water temperatures and ocean currents; unlike the tide-gauge assessments of relative sea levels, the effects of land-elevation changes are not included.

The global variations in the local trends of satellite-measured eustatic sea levels are graphed in Figure 2-6, representing the net change in water levels from October 1992 to December 2012, approximately 20 years. The extent of the variations is apparent, with rising sea levels in the western Equatorial Pacific having been on the order of 10 mm/year, whereas sea levels in the eastern Pacific have been mostly dropping. Of interest in the context of the rise in sea levels along the coast of New Zealand, and specifically in Hawke Bay, the satellite data indicate a rate of rise on the order of 5 mm/year since 1993. These global patterns of contrasting change in sea levels, with some areas rising while others have lowered, are almost entirely due to changes in water temperatures during those 20 years, reflecting the water's thermal expansion or contraction. However, with the records representing only a relatively short period of time and it being recognized that there can be significant multidecadal variations in ocean water temperatures (for example, due to the El Niño/La Niña range of climate events), the local trends in sea levels graphed in Figure 2-6 cannot with certainty be accepted as indicative of long-term trends, and should not be accepted with confidence to necessarily represent a trend that could persist through the 21st century to the year 2100.

By averaging the satellite altimeter data throughout the oceans, the local variations evident in Figure 2-6 will tend to be eliminated, just as in studies that averaged the trends derived from tide gauges along the world's coasts undertaken to assess the global mean trend of sea-level rise. The resulting global mean sea levels from the satellite data are graphed in Figure 2-7, with the linear regression yielding a slope of 3.18 mm/year for the rate of rise, significantly greater than the 20th-century 1.74-mm/year rate derived by Church and White (2006) and Holgate (2007) based on tide-gauge data. If correct and sustained, the satellite data would therefore conform with the predictions of accelerated rates of sea-level rise caused by global warming.
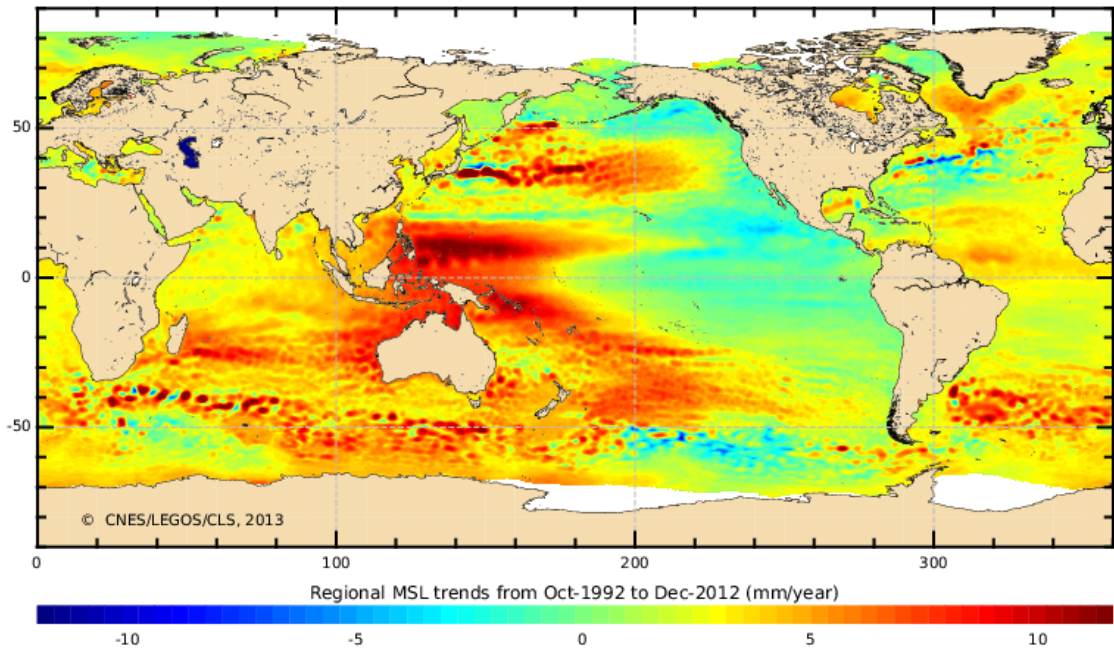
Figure 2-6: The net trends in the local sea levels from October 1992 to December 2012, derived from satellite altimeter measurements, showing substantial variations with some areas having experienced rapid rates of rise, while other regions have experienced a net decrease in sea levels. [*From* CLS/CNES/LEGOS, 2013]
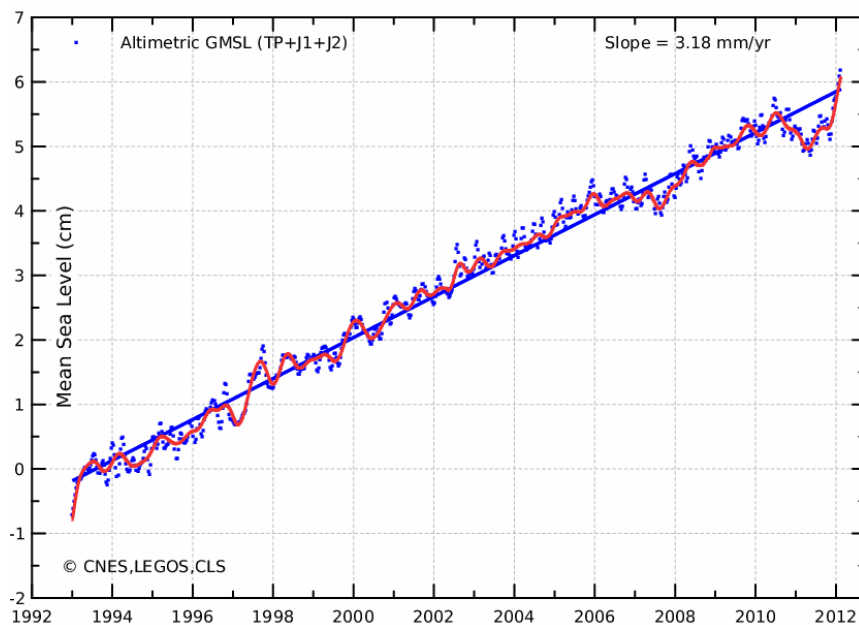
Figure 2-7: The rise in globally averaged eustatic sea levels measured by satellites since 1993. [*From* CLS/CNES/LEGOS, 2013]

Important to considerations of the erosion and flooding hazards for a specific coastal site is the development of a graph which is comparable to that in Figure 2-5 for the global average sea levels (Cazenave and Llovell, 2010), but one that accounts for the site's changes in land elevations as well as the eustatic sea levels, this being accomplished through the use of a local tide-gauge record that yields measurements of changes in relative sea levels. An example is shown in Figure 2-8, again from our analyses of the U.S. Pacific Northwest sea-level trends, including projections into the future (Komar et al., 2011, 2013). The examples included are the tide-gauge records for Yaquina Bay and Crescent City, the same as in Figure 2-4, but now with projections to the year 2100 having been added. As will be discussed in Chapter 8, these projections are based on the analyses by Rahmstorf (2007) and other recent investigations, collectively yielding a "consensus" projection for the future rise in the eustatic sea level, the assumption being that the rate of change in land elevations will continue and are accounted for by the regression slope of the tide-gauge records. The "consensus" projection curves are accordingly tangent to the tide-gauge regression lines, the upward curvature of the projections representing the accelerated rates of rising eustatic water levels. Of interest is the contrast between the submergent Yaquina Bay site on the mid-Oregon coast, compared with the present-day emergent Crescent City location on the coast of Northern California, the prediction being that in a few decades it too will become a submergent shore as a result of the increased eustatic sea levels (Komar et al., 2011, 2013).
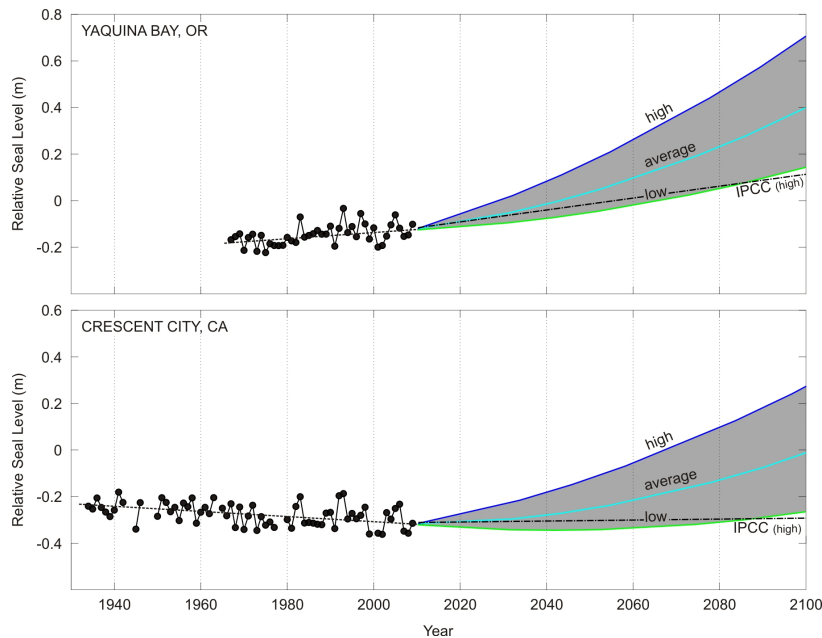
Figure 2-8: Projected relative sea levels beyond those measured by the Yaquina Bay (Newport) tide gauge on the central Oregon coast, and at Crescent City on the northern coast of California where the tectonic uplift of the land presently exceeds the eustatic rise in sea level but is projected to become a submergent coast in the future. [*From* Komar et al. (2013)]

The objective here has been to provide a general review of the global changes in sea levels and their dependence on Earth's changing climate. Later (Chapter 8) we will analyze the local trend in relative sea levels for Hawke's Bay, an assessment that will include the tectonic control on its changing land elevations, affected by both the large-scale consequences of

plate subduction along the Hikurangi Margin and episodic earthquakes such as that in 1931, which had a major effect on the elevations along its shore and the resulting along-coast variations in relative stability version erosion losses. Of interest will be the present-day trends in relative sea levels based on the Port of Napier's tide-gauge record, and projections through the 21st century that could result in increased coastal erosion and flooding hazards (Chapter 9).

2.4 INCREASING STORM INTENSITIES AND WAVE HEIGHTS

In addition to the increased rates of rising sea levels projected due to global warming, Earth's changing climate has also resulted in an intensification of storms that have generated more extreme waves, contributing to the enhanced coastal impacts. It is necessary to distinguish between two types of storms, tropical versus extratropical systems, since they differ in their modes of formation and dependence on the climate. Tropical storms — hurricanes in the Atlantic, typhoons in the northwest Pacific, and cyclones in the southwest Pacific — depend on warm water for their generation so their initial development occurs at low latitudes near the equator, although once formed they can migrate to higher latitudes. Requiring warm water, their season of occurrence is primarily the summer to early fall. In contrast, extratropical storms form during the winter at high latitudes, when a cold air mass moves down and collides with warm air at mid-latitudes. Changes in the global climate can be expected to produce an intensification of both types of storms, resulting in higher generated waves measured by ocean buoys and satellites.

Tropical cyclones have the clearest dependence on global warming since the "heat engine" responsible for their formation depends directly on elevated ocean-water temperatures (Emanual, 2005a), which have increased over the decades in parallel with global atmospheric temperatures. From the physics of tropical storm generation it is clear that their intensities would be expected to have increased due to the warmer water, and this has been demonstrated by Emanual (2005b) in analyses of wind speeds within hurricanes crossing the North Atlantic, and the reduction in their atmospheric pressures measured over the decades, with the increases in hurricane intensities having been most pronounced since about 1970. It follows that on average it can expected that there has been a parallel increase in the energies and heights of the waves generated by hurricanes in the North Atlantic, and this has been found in analyses of the hourly measurements of waves collected by buoys since the mid-1970s along the east coast of the United States (Komar and Allan, 2008). This was demonstrated by regressions of the annual averages of the measured significant wave heights[1] that are greater than 3 metres and occurred during the hurricane season, and also by the shift in histograms of hourly-measured significant wave heights over the decades, both the means and extremes in the histograms having become higher.

The documentation of increasing wave heights generated by extratropical storms at high latitudes is more clearly established as there are far more extratropical storms each year than tropical hurricanes, so the annual sample of generated waves is greater, yielding stronger statistical trends. Wave measurements in the North Atlantic have been collected since the

---

[1] The "significant wave height" is defined as the average of the highest one third of the waves, for example measured by a buoy, providing a commonly used assessment of the wave climate.

1960s using a recorder mounted on a lightship off the southwest coast of England, this being the longest record and the first to positively demonstrate an increasing trend in the annually-averaged significant wave heights (Carter and Draper, 1988; Bacon and Carter, 1991). We have similarly documented an increase in the Northeast Pacific, based on measurements from several buoys along the U.S. west coast (Allan and Komar, 2006; Komar et al., 2010; Ruggiero et al., 2010). The buoy data demonstrated that the multi-decadal trends of increasing wave heights depend on the latitude, with the greatest rate of increase having occurred off the coasts of Washington and Oregon (the U.S. Pacific Northwest), the increase having been less along the central California coast at lower latitudes, until on the shore of southern California there has not been a statistically significant long-term trend, the waves instead being most extreme during major El Niños due primarily to the southward shift of storm tracks during that climate event.
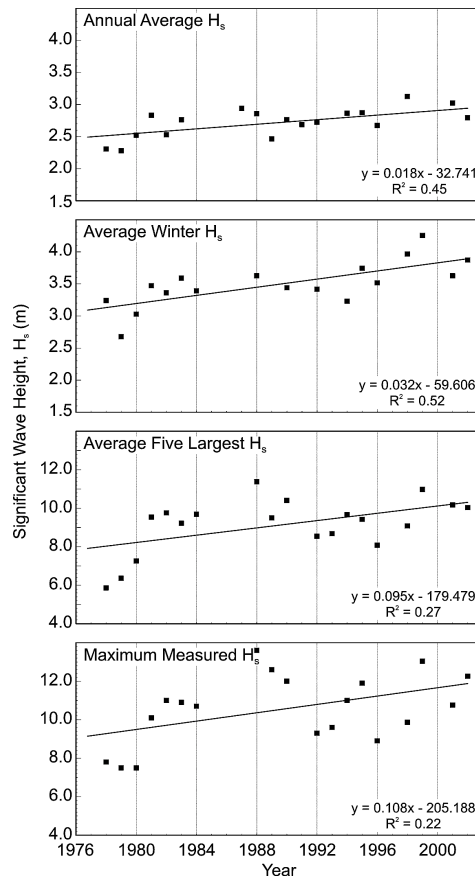
Figure 2-9: Increasing wave heights off the coast of the U.S. Pacific Northwest, representing progressively more extreme assessments. [*Modified from* Allan and Komar (2006)]

The increase in measured wave heights off the Pacific Northwest is evident in Figure 2-9, containing a series of graphs for the annual averages of the hourly-measured significant wave heights. The top-most graph is a plot of the annual averages for the entire year, with the regression yielding a rate of increase of 0.018 m/year, while the remaining series of graphs represent progressively more extreme storms and assessments of their wave heights. The second plot in the series of graphs is for the averages of the measured significant wave

2-13

heights during the "winter" (October through March), being most relevant to coastal impacts as erosion events occur during winter storms; the rate of increase has been 0.032 m/year (an increase of 0.8 metres in 25 years), substantially greater than for the annual averages. The third and fourth graphs are respectively the annual averages of the 5 highest recorded wave events experienced each winter, the rate of increase having jumped to 0.095 m/year, while the highest measured significant wave height each winter yielded a rate of increase of 0.108 m/year (2.7 metres in 25 years). Therefore, in this analysis of waves generated by extratropical storms in the North Pacific it was possible to demonstrate that the strongest storms and highest generated waves have increased with time, an increase that is also reflected in the statistically projected 25- through 100-year extreme significant wave heights that potentially could be generated by the most severe storms in the future (Ruggiero et al., 2010; Komar et al., 2010). Such projections are important in that it would be the waves of those extreme storms that potentially are most destructive in terms of their coastal impacts, with the erosion expected to increase in the future so long as those trends continue.

While the analyses of the trends of increasing wave heights generated by extratropical storms are statistically more certain than the trends from analyses of hurricane-generated waves, the reverse is true in understanding their respective climate controls. While warm water is recognized to be the "fuel" in the generation of hurricanes, and increasing water temperatures over the decades explain the increased hurricane intensities and the heights of their generated waves, water temperature is less of a factor in the formation of extratropical storms and their waves, obvious in the case of those that form over the land. In the North Atlantic, prior to the 1950s and availability of buoy data, wave observations from ships and hindcasts of the waves from the storm meteorology indicated that there may have been cycles in the annual average wave heights, with their climate controls being uncertain, and possibly with the wave heights at the beginning of the 20th century having been as high as measured recently by buoys (WASSA, 1998). The increase in measured wave heights off the southwest coast of England since the 1960s (Carter and Draper, 1988; Bacon and Carter, 1991) might therefore be part of a long-term cycle, one of uncertain origin, although greenhouse warming and increased water temperatures could still have had a role in recent decades.

Climatologists have also investigated the extratropical storms in the North Pacific, concluding that their intensities have increased at least since the 1950s (Graham and Diaz, 2001). However, the cause of that increase has not been confidently established. Graham and Diaz (2001) attributed it to global warming and the increased ocean-water temperatures, whereas Zhang et al. (2007) undertook analyses that attributed the greater storm intensities to increased concentrations of aerosols in the atmosphere derived from air pollution in Asia, having affected the cloud dynamics. While the increases in wave heights in the northeast Pacific have been firmly established from the buoy data (Allan and Komar, 2006; Ruggiero et al., 2010), uncertainties exist in their long-term projections, and will remain so until we acquire a more confident understanding of the climate controls on the storm intensities.

The traditional approaches to analyzing ocean-wave climates, including their multidecadal trends and climate controls, have involved either hindcasts from the storm parameters or direct measurements by buoys. Those approaches are obviously restricted in the extent of the region being covered, and in the case of hindcasts, by the accuracy of the measurements of winds and atmospheric pressures. The first global coverage for the wave assessments were based on visual observations from ships, and although the quality and consistency of those

measurements are obviously questionable, there have been investigations that yielded at least approximate patterns for the ocean-wide variations in wave heights and periods. This global coverage has vastly improved with the advent of satellites that provide assessments of the waves, as well as water temperatures and sea levels.

A variety of satellite-borne instruments has been important in acquiring measurements of wave heights and periods, and also of the surface-level winds that generate the waves — altimeters, scatterometers, and synthetic aperture radar. Almost continuous measurements on a global scale exist since the launch of GEOSAT in 1985, and this collective data has been analyzed by Young et al. (2011) for 2° by 2° regions covering the globe. For each of those small areas, multidecadal trends of both the wind speeds and wave heights have been derived, including the annual means and the 90th- and 99th-percentile extremes. The results for the 99th-percentile trends of the extreme wind speeds and wave heights are shown in Figure 2-10. The global values for the trends in the mean significant wave heights have remained close to zero, but it is evident that there have been statistically significant increases in the more extreme wave heights. Graphs for both the 90th- and 99th-percentiles show increases on the order of 1% per year. In the Northern Hemisphere the regions of increasing wave heights documented by the satellite data are in agreement with those found from the wave-buoy data discussed above, off the Atlantic coast of England and along the east and west coasts of the United States.
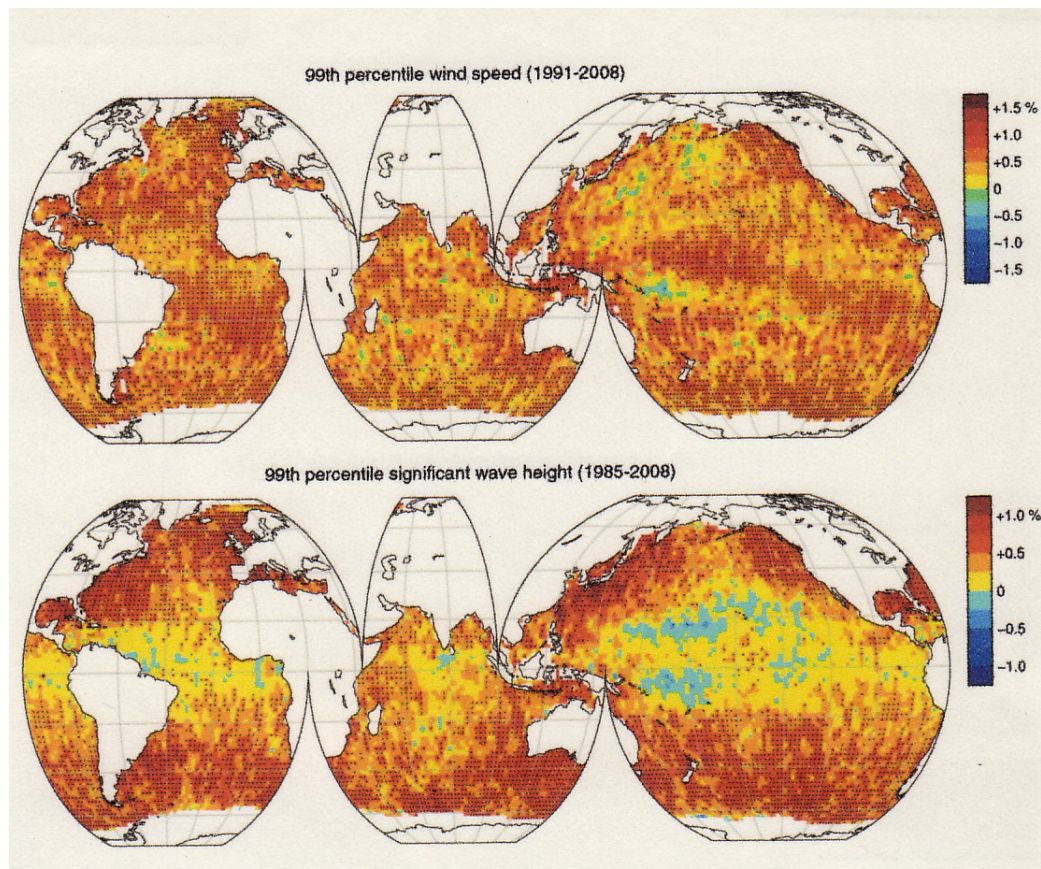
Figure 2-10: Trends of increasing wind speeds and significant wave heights measured by satellites, their 99th-percentile trends (percent per year). [*From* Young et al. (2011)]

Of interest to the present study of Hawke's Bay are the assessments by Young et al. (2011) of the increases in wave heights measured by satellites in the Southern Hemisphere, and specifically around the shores of New Zealand. According to the satellite data, Figure 2-10, the trends of increasing wave heights are even more dominant in the Southern Hemisphere, including along the shores of New Zealand where the increase has been 1% per year (about 5 centimetres per year for Hawke Bay). As will be seen later in this report (Chapter 5), although buoy measurements of waves in Hawke Bay are available for only little more than a decade, they provide supporting evidence for the increasing wave heights found by satellites, yielding essentially the same rate of increase.

2.5 SUMMARY

Multidecadal trends and annual variations in Earth's climate have been positively demonstrated to be major factors in producing enhanced coastal hazards from erosion and flooding. It has been concluded by researchers that the long term trends of increasing sea levels and the intensities of storms and the waves they generate are the result of global warming, although it is recognized that other factors may also have had a role, especially at specific coastal sites. Variations in the erosion processes from year to year can be extreme, resulting in episodes of major coastal impacts, the cause of which might not always be obvious, although the El Niño/La Niña range of climate events has been shown to be important to the impacts along the shores of the Pacific Ocean.

The focus of this chapter has been on the global-scale climate controls that affect the coastal processes important to erosion and flooding — the rate of rise in the global mean sea level and the degree to which it could accelerate in the future, and documentations of increasing storm intensities and the heights of their generated waves. It is the combination of these processes that is important to the erosion and flooding of coastal properties, the summation of the increasing sea levels, the elevated tides due to higher surges caused by more intense storms, and the increased levels to which the higher waves swash up beaches and impact properties. While the global scale of Earth's changing climate has been considered in this chapter, later chapters focus on these enhanced ocean processes and their combined effects on the erosion and flooding hazards along the coast of Hawke's Bay, those occurring at present and projected into the future.

2.6 REFERENCES

Allan, J. C., and P.D. Komar (2006) Climate controls on US West Coast erosion processes: *Journal of Coastal Research*, v. 22, no. 3, p. 511-529.

Bacon, S., and D.J.T. Carter (1991) Wave climate changes in the North Atlantic and North Sea: *International Journal of Climatology*, v. 11, p. 545-558.

Carter, D.J.T., and L. Draper (1988) Has the northeast Atlantic become rougher?: *Nature*, v. 332, p. 494.

Cazenave, A., and R.S. Nerem (2004) Present-day sea level change: Observations and causes: *Review of Geophysics*, v. 42, RG3001.

Cazenave, A., and W. Llovel (2010) Contemporary sea level rise: *Annual Reviews of Marine Sciences*, v. 2, p. 145-173.

CLS/CNES/LEGOS (2013) Google Images from the Centre National d'Etudes Spatiales, France; www.aviso.oceanobs.com/msl

Chen, J.L., B.D. Tapley, and C.R. Wilson (2006) Alaskan mountain glacial melting observed by satellite gravimetry: *Earth and Planetary Science Letters*, v. 248, p. 368-378.

Church, J.A., N.J. White, R. Coleman, K. Lambeck, and J.X. Mitrovica (2004) Estimates of the regional distributions of sea-level rise over the 1950 to 2000 period: *Journal of Climate*, v. 17, n. 13, p. 2609-2625.

Church, J.A., N.J. White and J.M. Arblaster (2005) Significant decadal-scale impact of volcanic eruptions on sea level and ocean heat content: *Nature*, v. 438, p. 74-77.

Church, J.A., and N.J. White (2006) A 20th century acceleration in global sea-level rise: Geophysical Research Letters, v. 33, L01602, doi: 10.1029/2005GL024826, 4pp.

Douglas, B.C. (2001) Sea level change in the era off the recording tide gauge: In *Sea Level Rise: History and Consequences*, edited by Douglas, B.C., M.S. Kearney and S.P. Leatherman, Chapter 3, p. 37-62, Academic Press.

Emanual, K. (2005a) *Divine Wind*: Oxford University Press, 285 pp.

Emanuel, K.A. (2005b) Increasing destructiveness of tropical cyclones over the past 30 years: *Nature*, v. 436, p. 686-688.

Gornitz, V., and A. Solow (1991) Observations of long-term tide-gauge records for indications of accelerated sea-level rise: In *Greenhouse-Gas-Induced Climate Change: A Critical Appraisal of Simulations and Observations*, M.E. Schlesinger (editor), pp. 347-367, Elsevier, Amsterdam.

Gornitz, V., Lebedeff, S., and Hansen, J. (1982) Global sea level trend in the past century: *Science*, v. 215, p. 1611-1614.

Graham, N.E., and H.F. Diaz (2001) Evidence for intensification of North Pacific winter cyclones since 1948: *Bulletin of the American Meteorological Society*, v. 82, p. 1869-1893.

Hansen, J.E., M. Sato, R. Ruedy, K. Lo, D.W. Lea, and M. Medina-Elizade (2006) Global temperature change: *Proc. National Academy of Sciences*, v. 103, p. 14288-14293.

Holgate, S. (2007) On the decadal rates of sea level change during the twentieth century: *Geophysical Research Letters*, v. 34, p. 1-4.

Howat, I.M., I.R. Joughin, and T.A. Scambos (2007) Rapid changes in ice discharge from Greenland outlet glaciers: *Science*, v. 315, p. 1559-1561

IPCC (2007) *Climate Change 2007: The Physical Science Basis; Contribution of Working Group I to the Fourth Assessment Report of the Intergovernmental Panel on Climate Change, IPCC*, Paris, France, 18 pp.

Ishii, M., M Kimoto, and M. Kachi (2003) Historical ocean subsurface temperature analysis with error estimates: *Monthly Weather Review*, v. 131, p. 51-73.

Komar, P.D., and J.C. Allan (2008) Increasing wave heights along the U.S. Central Atlantic shore due to the intensification of hurricanes: *The Journal of Coastal Research*, v. 24, n. 2, p. 479-488.

Komar, P.D., J.C. Allan and P. Ruggiero (2010) Wave and nearshore-process climates: Trends and variations due to Earth's changing climate: *Handbook of Coastal and Ocean Engineering*, edited by Y.C. Kim, World Scientific Publishing Co.

Komar, P.D., J.C. Allan and P. Ruggiero (2011) Sea level variations along the U.S. Pacific Northwest coast: tectonic and climate controls: *Journal of Coastal Research*, v. 27, p. 808-823.

Komar, P.D., J.C. Allan and P. Ruggiero (2013) U.S. Pacific Northwest coastal hazards: tectonic and climate controls: *Coastal Hazards*, edited by C.W. Finkl, Springer, p. 587-674.

Levitus, S., J.I. Antonov, T.P. Boyer, and C. Stephens (2000) Warming of the world ocean: *Science*, v. 287, p. 2225-2229.

Mann, M.E., R.S. Bradley and M.K. Hughes (1998) Global-scale temperature patterns and climate forcing over the past six centuries: *Nature*, v. 392, p. 779-787.

Mann, M.E., R.S. Bradley and M.K. Hughes (1999) Northern Hemisphere temperatures during the past millennium: Inferences, uncertainties, and limitations: *Geophysical Research Letters*, v. 26, no. 6, pp. 759-762.

Mann, M.E., and P.D. Jones (2003) Global surface temperatures over the past two millennia: *Geophysical Research Letters*, v. 30, p. 1820-1823.

Pugh, D. (2004) *Changing Sea Levels: Effects of Tides, Weather and Climate*: Cambridge University Press, 255 pp.

Rahmstorf, S. (2007) A semi-empirical approach to projecting future sea level rise: *Scie3nce*, v. 315, p. 368.

Rahmstorf, S. (2010) A new view on sea level rise: *Nature*, v. 4, p. 44-45.

Ruggiero, P., P.D. Komar and J.C. Allan (2010) Increasing wave heights and extreme-value projections: the wave climate of the U.S. Pacific Northwest: *Coastal Engineering*, v. 57, p.539-552.

Salinger, J., T. Chinn, A. Willsman and B. Fitzharris (2008) Glacier response to climate change: *Water & Atmosphere*, v. 16, n. 3, p.16-17.

Slobbe, D.C., P. Ditmar, and R.C. Linderbergh (2009) Estimating the rates of mass change, ice volume change and snow volume change in Greenland fro ICESat and GRACE data: *Geophys. J. Int.*, v. 176, p. 95-106.

Thomas, R., et al. (2004) Accelerated sea-level rise from West Antarctica: *Science*, v. 306, p. 255-258.

Thompson, L.G., H.H. Brecher, E. Mosley-Thompson, D.R. Hardy and B.G. Mark (2009) Glacier loss on Kilimanjaro continues unabated: *Proceedings of the National Academy of Sciences*, doi:10.1073/pnas.0906029106.

WASSA (1998) Changing waves and storms in the northeast Atlantic?: *Bulletin of the American Meteorological Society*, v. 79, n. 5, p. 741-760.

Young, I. R., S. Zieger and A.V. Babanin (2011) Global trends in wind speed and wave height: *Science*, v. 332, p. 451- 455.

Zhang, R., Guohui Li, Jiwen Fan, Dong L. Wu, and M.J. Molina (2007) Intensification of Pacific storm track linked to Asian pollution: *Proc. National Academy of Science*, v. 104, n. 13, p. 5295-5299.

3 Hawke's Bay Tectonics, Earthquakes and Land Elevation Changes

3.1 INTRODUCTION

New Zealand straddles two of Earth's major tectonic plates, the Pacific and Australian plates that collide and then slide past or beneath one another. In the process they generate destructive earthquakes, at times tsunami, and alter land elevations. The Hawke's Bay region is dominated by the collision of these plates, with the Pacific plate giving way and sliding beneath the Australian plate that includes all of the North Island, its land and offshore continental shelf. The forces of collision have deformed the rocks along this coast, folding them and at times producing movement on faults that generate earthquakes. In particular, the destructive Hawke's Bay earthquake in 1931 owed its origin to the collision of these tectonic plates, an event that also illustrates the significant land elevation changes that can abruptly occur due to this region's tectonic activity. The objective of this chapter is to review these tectonic-related factors important to the multiple hazards faced along the shores of Hawke's Bay, including past and projected occurrences of earthquakes and their generated tsunami. In the context of the erosion and flooding hazards of interest to the analyses undertaken in this study, of significance are the tectonic-related changes in land elevations along this shore, a factor that affects the multi-decadal directions and rates of change in sea levels relative to the land.

This chapter begins with an examination of the plate tectonics setting of Hawke's Bay, the subduction of the Pacific plate along the North Island's east coast, the concern being the potential for a major subduction earthquake and tsunami sometime in the future. There has been considerable research completed by seismologists and geologists during the past decade, investigating this subduction zone and its potential hazards, so an updated review beyond that presented in earlier reports is needed (Komar, 2005, 2010). The plate subduction processes are accompanied by changes in land elevations along this coast, gradual when the plates are locked together and accumulating strain, causing the coast to either slowly rise or subside, but with an abrupt reversal when a subduction earthquake occurs, the change in elevation potentially amounting to on the order of a metre or more. At the same time, as demonstrated by the 1931 Hawke's Bay earthquake, movement on faults within the body of the Australian plate can also be destructive, producing land-level changes of 1 to 2 metres, with that earthquake event 70 years ago still being a significant factor in determining the present day along-coast variations in erosion and flooding experienced on this shore.

3.2 PLATE TECTONICS AND THE HIKURANGI SUBDUCTION ZONE

The forces within the Earth that generate earthquakes and raise mountains are for the most part the result of the tectonic movement and collisions of its crustal plates. The Earth's crust

can be divided into eight major tectonic plates, plus a number of smaller plates, each moving and colliding with one another, sliding horizontally along major faults or with one plate giving way and being pushed beneath another, "subducted" into the Earth's mantle where at depth it is eventually melted and gives rise to the formation of volcanoes. A generalized depiction of the formation, collision, and subduction of a tectonic plate is diagramed in Figure 3-1. New crust is formed at the spreading ridge, consisting of elevated portions of the sea floor that form continuous ridges and rises around the Earth, zones where molten rock arrives from the interior to fill a fracture zone along the ridge, the crust being pulled apart by slowly flowing convection cells within Earth's semi-molten interior (the mantle or aesthenosphere). The newly formed crust (or lithosphere, which includes the solid upper portion of the mantle as well as the crust) moves in opposite directions away from the spreading ridge, giving rise to two areas of crustal plates. This newly formed lithosphere constitutes the tectonic plates that cover the Earth's surface, and in addition to containing the crust of the ocean they also include the land masses, which being less dense than the ocean rocks are in effect "rafted" along within the moving plates.
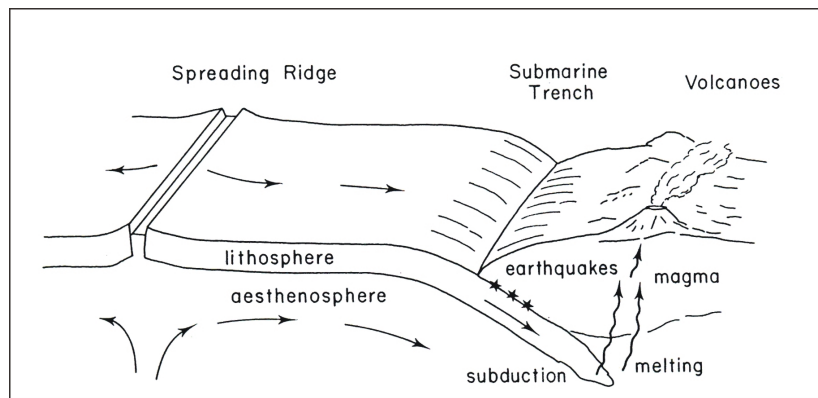
Figure 3-1: The formation of ocean crust at a spreading ridge and its subduction in a submarine trench where the oceanic plate collides with another plate containing a continental land mass. The stars denote earthquakes formed by the plates scraping together during subduction.

Also depicted in Figure 3-1 is the subduction of the oceanic plate when in collides with another plate consisting of a less-dense land mass. The down buckling of the subducted ocean crust forms a submarine trench as it begins its descent beneath the continental plate, the slab of ocean crust scraping against the underside of the continental mass to create a zone of earthquake activity, generating the most intense quakes experienced on Earth (magnitudes 9.2 for the recent 2004 Sumatra and 2011 Japan earthquakes, with the maximum recorded magnitude having been 9.5 in 1960 off the coast of Chile). Heating as it descends into the Earth's mantle, the subducting plate eventually reaches sufficient depths and temperatures that its rocks are melted, forming lava that emerges at the surface as a chain of volcanoes roughly parallel to the subduction zone (Figure 3-1).

Individual tectonic plates are accordingly outlined by zones of earthquakes. Relatively low magnitude, near-surface quakes occur along the lengths of the spreading ridges, where the crust splits apart and magma is injected, adding new crust to the plates. The side edges of the plates, where they slide past one another along transverse faults such as New Zealand's

Alpine Fault, are defined by earthquakes having magnitudes on the order of 7 and 8. But most significant are the destructive earthquakes within Earth's subduction zones, achieving magnitudes greater than 9, associated with the descending plate scraping against the underside of the over-riding plate. As illustrated in Figure 3-1 by the stars representing the epicenters of the subduction earthquakes, near the trench they occur at relatively shallow depths beneath the Earth's surface, but have progressively greater depths with distance inland from the trench.

This basic pattern of plate collisions and subduction is found around the margin of the Pacific Ocean, which has come to be known as the "Ring of Fire" due to its combined earthquakes and volcanic activity. Most of its sea floor consists of the Pacific plate, with its southern portion created at the East Pacific Rise to the west of South America, slowing moving to the west toward New Zealand where it collides with the Australian plate that is moving in the opposite direction toward the northeast. This zone of collision crosses New Zealand as shown in Figure 3-2, where there are three different tectonic responses to the collision: an east-to-west subduction zone along the east coast of the North Island; a west-to-east subduction along the Fjordland coast of the South Island; and with the stretch between these subduction zones grinding sideways past one another along the Alpine Fault.
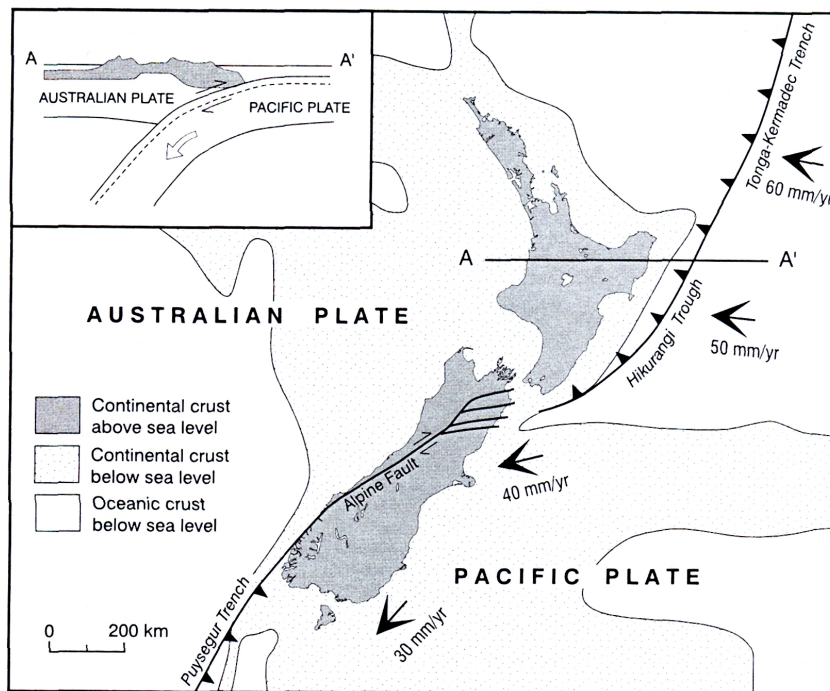
Figure 3-2: The tectonics of New Zealand determined by the collision of the Australian and Pacific plates, with plate subduction occurring at the Hikurangi Trough and Puysegur Trench, the two plates sliding horizontally past one another along the Alpine Fault, a transform fault. [*From* Atkin (1999)]

As diagramed in Figure 3-2, to the east of the North Island the relative rate of movement of the Pacific plate toward the Australian plate is on average about 50 mm per year, where the denser and thinner Pacific plate is being subducted forming the Hikurangi Trough centered about 160 km east of Napier. The tectonics of plate subduction along the Hikurangi Margin

exhibits the principal features typically found in subduction zones as depicted in Figure 3-1, but in several important respects differs in its details. As the Pacific plate is being subducted and descends beneath the North Island, it initially does so at a lower angle than is typical of subduction zones. One result is that a deep trench is not formed, but instead there is a shallower depression whose depths have been further decreased by the accumulation of marine sediments. Due to its shallow depths the depression is generally referred to as a "trough" rather than being a deep "trench".
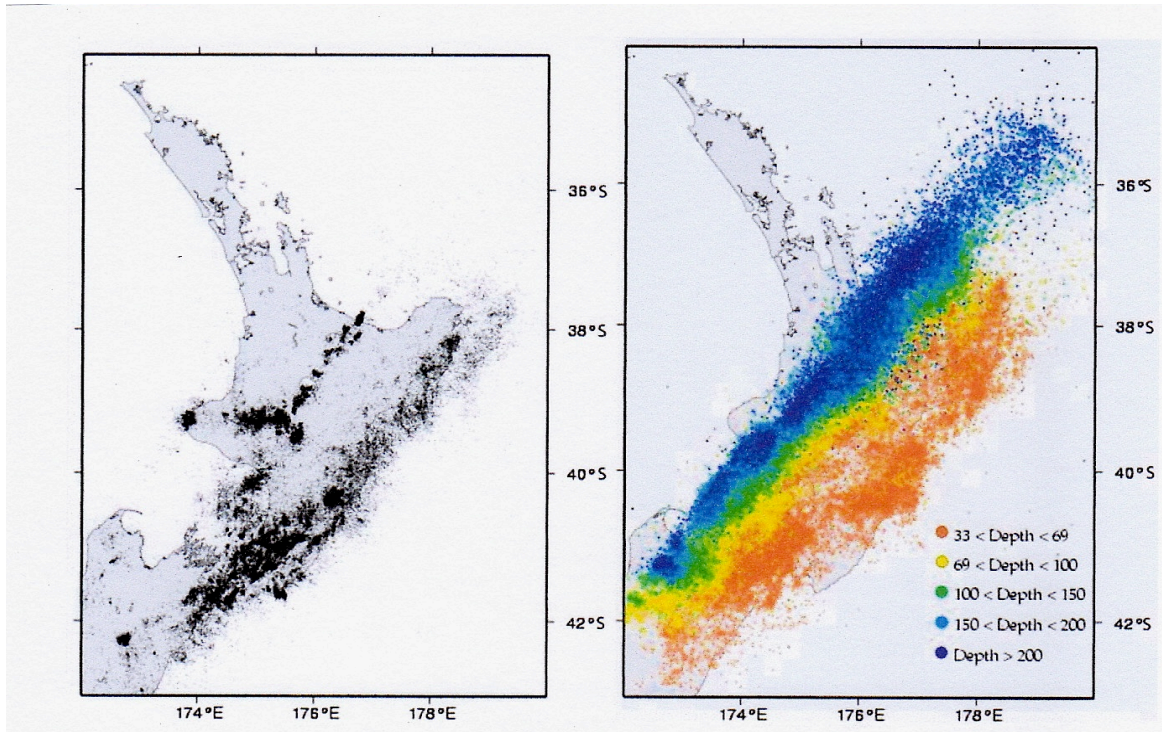
Figure 3-3: Earthquake epicenters that occurred between January 1990 and December 2007. The magnitudes of the events ranged from 0.29 to 6.99. (*Left*) Earthquakes shallower than 33 km, those within the rocks of the Australian plate. (*Right*) Earthquakes greater than 33-km depths defining the interface of subduction between the Pacific and Australian plates, increasing in depths toward the west. [*From* Wallace et al. (2009)]

It is important to distinguish between earthquakes that are directly generated by plate subduction, those that occur on the interface between the plates as they scrape together (Figure 3-3, *Right*), versus those that occur as a result of the deformation and faulting within the continental rocks of the North Island, within the body of the Australian plate (Figure 3-3, *Left*). It is evident in this diagram from Wallace et al. (2009) that the earthquake events at these different levels within the Earth have contrasting distributions of occurrences. Those in the upper crust within the Australian plate form one group of earthquakes in a line that crosses the central North Island, associated with the faulting and volcanic activity of the Taupo region, the second group extending along the full length of the east coast, caused by the compression and faulting of the near-surface rocks, the 1931 Hawke's Bay earthquake having been an important example. In contrast, seismic analyses of earthquake epicenters at depths greater than 33 km closely define the path of the descending subducted Pacific plate beneath the North Island (Figure 3-3, *Right*), progressively increasing in depths toward the

northwest, with the deepest epicenters reaching greater than 200 km beneath the west coast of the North Island (Wallace et al., 2009).

Complicating the plate subduction along the Hikurangi margin is that the rate and direction of plate collision is not uniform along the its length, but instead has a maximum rate of about 60 mm per year north of Gisborne, about 50 mm per year offshore from Hawke's Bay, and reduced still further to 20-30 mm per year where the Pacific plate is being subducted to the east of the Cook Strait (Wallace, et al., 2009, 2010). Furthermore, these rates of convergence between the two plates are not directly straight on, but instead take place obliquely at varying angles from north to south along this margin. The result is a slow rotation of the zone of convergence, but more important there is not only a compressional collision between the Pacific and Australian plates along the Hikurangi Trough, there is also a horizontal sliding between them, with the Pacific plate slipping to the south relative to the Australian plate. This horizontal movement along the Hikurangi Margin continues on the Alpine Fault crossing the South Island, although their respective movements are linked by a series of faults located between Blenheim and Kaikoura, depicted schematically in Figure 3-2.

Whereas major, destructive earthquakes have occurred on the other subduction zones around the Pacific's Ring of Fire, having had magnitudes greater than 9, the Hikurangi Margin has not experienced a significant earthquake on its subduction interface since historic records began about 170 years ago. This absence of a major subduction earthquake can be attributed to two possible causes: (a) the 170-years historic record is too short to encompass their infrequent occurrences, this tectonic margin presently being within an aseismic period that potentially can last for several centuries, during which the subduction zone is "locked" and seismic energy is accumulating and would be expected to be released sometime in the future as an major earthquake; or (b) some of the energy of plate subduction is being aseismically released, not accumulating to the extent that earthquakes greater than magnitude 7 or 8 occur.

It is important to resolve such questions regarding the potential seismic hazards within the Hikurangi Margin, along the entire east coast of the North Island, including the possibility of there being a destructive subduction earthquake sometime in the future, accompanied by a tsunami generated immediately offshore. Answering such questions has been a primary motivation for recent research undertaken by seismologists and geologists, directed toward analyses of plate subduction along this Margin, including the factors important to earthquake occurrences. The products of that research have included a substantial number of journal publications, with those by Wallace et al. (2009, 2010) providing reviews summarizing the main discoveries concerning the tectonics of this subduction zone. The results are already important in having provided an improved understanding of the earthquake and tsunami hazards along this coast. Their investigations are also relevant to our interests in this study concerned with the Hawke's Bay erosion and flooding hazards, in the context of understanding the tectonic controls on land elevation changes and thus the trends in relative sea levels, the combination of the global rise in sea level and local changes in land elevations.

The important characteristics of the Hikurangi Margin are presented in Figure 3-4, summarized by Wallace et al. (2010), highlighting the differences between the Southern, Central and Northern Segments of this subduction zone, Hawke's Bay being within the Central region as

shown in the perspective view of this margin at the top of the figure. The important trends from north to south along the length of this margin include:

- The highest rate of plate convergence is in the north off the coast of Gisborne, decreasing offshore from Hawke's Bay, and with the lowest rate occurring along the Southern Segment;
- While there are numerous seamounts on the surface of the Pacific plate offshore from the Northern and Central Segments, there are fewer offshore from the Southern Segment;
- There is a greater thickness of ocean sediments offshore atop the Pacific plate toward the south, the result being that there is a dominance of accretion along the coast of the Southern Segment as the sediments are scraped off during plate subduction.
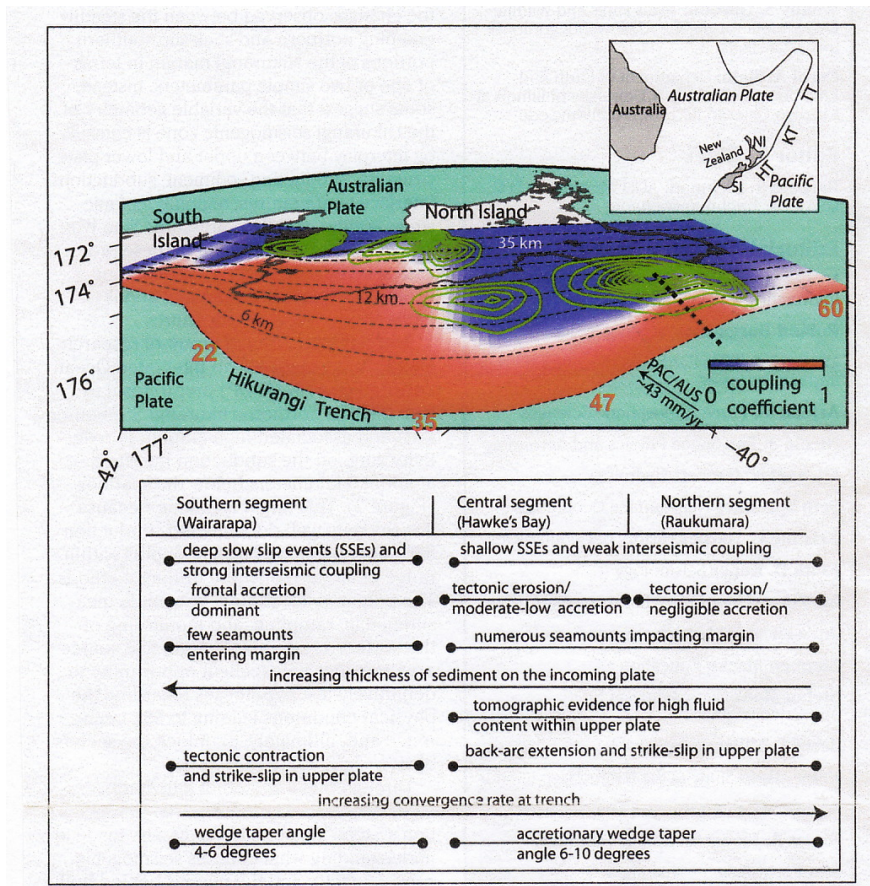
Figure 3-4: Perspective view of the Hikurangi Margin, the blue to red shading denoting increasing values of the Coupling Coefficient, the red regions being those expected to experience "stick-slip" conditions with stronger subduction earthquakes. The green contours show areas where "slow slip events" (SSEs) have occurred since 2002, representing an aseismic release of the subduction energy. The table summarizes the along-coast variations in the characteristics of the segments. [*From* Wallace et al. (2010)]

These along-coast variations in the rates of plate convergence, the numbers of seamounts, and thicknesses of sediments on the subducting Pacific plate are expected to be factors that govern the magnitudes of subduction earthquakes and their frequencies of occurrence.

However, according to Wallace et al. (2009, 2010) there is not a simple correlation individually with these factors, although acting together it is believed that they do affect the behavior of plate subduction, indicated by differences in the tectonics found along the Hikurangi Margin by the recent research investigations, evident in the perspective view of the margin presented in Figure 3-4. As reviewed below, of additional importance to earthquake occurrences and magnitudes along this Margin is evidence that has been found for the presence of high fluid contents within the rocks of the plates, and occurrences of slow movement of the plates at the subduction interface without the generation of an earthquake (aseismic movements), factors that are also listed in Figure 3-4, and to a significant degree account for the differences seen in the perspective view of the margin between the Southern Segment versus the combined Central and Northern Segments.

3.3 EARTHQUAKES — ORIGINS AND MAGNITUDES

The collision and subduction of tectonic plates has its potentially most destructive consequences on margins where the two plates are locked together for long periods of time, in part caused by the friction within the interface between the descending and overriding plates. It is during this locked phase of decades to centuries that significant levels of tectonic energy can be stored. When the resulting force of accumulated energy exceeds the resisting friction at the plate interface, the years of stored energy is suddenly released as a major subduction earthquake. As noted above, the resulting magnitudes of the most extreme events along the Pacific's Ring of Fire have been in the range 9.0 to 9.5. Potentially destructive tectonic margins that follow this cycle are referred to as "stick-slip" subduction zones.

In recent years it has been discovered that within a number of plate subduction zones there are episodes of "slow slip events" (SSEs), which take weeks to years during which there is a prolonged movement between the two plates but without an accompanying earthquake. The plate motion is instead detected by Global Positioning System (GPS) units that record both the resulting horizontal and vertical movements of the Earth's surface. In most cases these SSEs occur along the deeper edges of the zone of plate subduction, while the upper portion closer to the trench can remain locked, storing energy that could later generate a major earthquake.

Both types of responses to plate subduction have been found along the Hikurangi Margin, evident in the perspective view included in Figure 3-4, with a transition occurring about half way along the margin, the Southern Segment primarily being "stick-slip" over almost its entire area of subducting plate, contrasting with the significance of SSE occurrences over the Central and Northern Segments. The red versus blue areas in that diagram represent the range of evaluated Coupling Coefficients, a measure that ranges from 0 to 1 with increasing degrees of locking between the Australian and Pacific plates at the subduction interface, their values having been evaluated by Wallace et al. (2009) from the horizontal movements of the plates measured by GPS units throughout this region. Important is the large area of Coupling Coefficient magnitudes on the order of 1 throughout the Southern Segment, indicating that this region is mostly storing energy and therefore has the greatest potential for future occurrences of major subduction earthquakes and tsunami. In contrast, most of the Central and Northern Segments have low Coupling Coefficients, indicating that some subduction

energy is being released, reducing that being accumulated over time, although the threat of a subduction earthquake remains.

The significance of these patterns of Coupling Coefficient magnitudes have been supported by direct detections of SSEs that are responsible for the release of a portion of the subduction energy, events detected by the GPS units (Wallace et al., 2004; Wallace and Beavan, 2010). During the years from 2002 to 2010 more than eight distinct SSEs were observed along the Hikurangi Margin, in four different locations identified by the green contoured areas in Figure 3-4. In all cases their locations were near the down-dip termination of the zone of locked plates, occurring within the upper portions of the blue zones of low Coupling Coefficients evident in the diagram. According to Wallace and Beavan (2010), SSEs in the Hawke's Bay and Gisborne regions occur fairly often (every 1 to 2 years) but last for only short periods of time (a few weeks), in contrast to the southern region where they rarely occur, perhaps every 5 to 10 years but with each event lasting longer, continuing for 1 to 1.5 years. The largest SSE to date was estimated to have involved up to 35 centimetres of slip on the subduction interface during a 1.5-year time period (2004-2005), representing the release of energy without the generation of an earthquake.

These results from the recent investigations of the Hikurangi Margin tectonics demonstrate the potential for a future major subduction earthquake. Important questions are when it might occur, and what magnitude could it have? The "stick-slip" condition of the Southern Segment presumably represents the greatest potential hazard, but while the Central and Northern Segments including Hawke's Bay appear to pose a somewhat less threat due to the partial energy release by SSEs, the hazards remain significant. At the same time there is also the potential hazard of shallow earthquakes within the body of the Australian plate, their destructive capability being evident from the 1931 Hawke's Bay event. The epicenters of these two classes of earthquakes have been analyzed by Wallace et al. (2009) and are included here in Figure 3-3, having been based on occurrences between January 1990 and December 2007. Considering this represents only 19 years of earthquake events, the considerable number of epicenters and their spatial extent across the North Island demonstrates the significant degree of tectonic activity within this region. Although the magnitudes represented in Figure 3-3 were all less than 7, mostly small energy events, this activity points to the prospects of there potentially being higher magnitude earthquakes in the future.

Within the entire 170-year historic record for New Zealand, dating back to the beginning of European settlement in the 1840s, there have been only relatively moderate earthquakes interpreted as having occurred on the subduction interface. The strongest in the post-1917 seismic records occurred during March and May 1947, having had magnitudes of about 6.9 to 7.1, with each located 50 to 60 km offshore east of the coast between Gisborne and Tolaga Bay (Wallace et al. 2009). Those events are interpreted as having been subduction earthquakes, with their epicenters in locations of seamounts that are being subducted, where seismic energy could accumulate even though SSE occurrences in the surrounding area have acted to release some of the subduction energy.

The concern is that while subduction earthquakes of more extreme magnitudes, in the range 8 to 9, have not occurred anywhere within the Hikurangi Margin during the past 170 years, analyses indicate that high levels of seismic energy could accumulate, particularly within the

"stick-slip" Southern Segment (Wallace et al., 2009). The short historic period associated with this subduction margin could be the primary explanation for not having experienced more extreme earthquake magnitudes. Such a limitation of the historic record is illustrated by the U.S. Pacific Northwest's subduction zone (the Cascadia Margin), where during its similar length of time since European settlement there also has not been a major subduction earthquake. However, geologic evidence along that tectonic margin in the form of coastal marshes that had abruptly subsided and were then covered by tsunami sand, provide positive evidence that a major earthquake occurred some 300 years ago (Atwater, 1987). Its exact date of occurrence was later established by records of the generated tsunami waves that crossed the Pacific and reached the shores of Japan, demonstrating that it took place at 9pm on 26 January 1700, and from the size of the tsunami waves and their destruction along the coast of Japan its magnitude was estimated to have been at least 9 (Sataki et al., 1996). In view of the similarly limited historic record for New Zealand, the potential exists for a future extreme subduction earthquake along the Hikurangi Margin, one that could be expected to reach a magnitude of 8, possibly even 9, just as have occurred along other "stick-slip" Pacific subduction zones.

As undertaken by Wallace et al. (2009), assessments can be made of the potential earthquake magnitudes from the rates of plate collision and subduction, the areas of the coupled plates, the values of the Coupling Coefficients, and factors such as occurrences of SSEs, the factors summarized in Figure 3-4 for the Hikurangi Margin. According to their analysis of the Southern Segment, with it having a potential alongcoast rupture length of about 230 km and being 150 to 185 km wide depending on the rupture limit at depth down the subducting plate, the calculated magnitudes were estimated to be 8.5 to 8.7, with 8 to 12 metres of slip at the plate interface during an earthquake. Based on the rate of plate subduction, the average recurrence interval would be on the order of 300 to 625 years, confirming that the 170-year record is indeed too short to have had a reasonable probability for experiencing a major subduction event. Predictions of potential magnitudes along the Central and Northern Segments are more difficult due to the aseismic SSE release of energy, but an approximate magnitude 8 is possible. If the entire length of the Hikurangi Margin ruptured during a single event, the assessment is again an 8.6 magnitude earthquake with 8 metres of slip that could generate a tsunami (Wallace et al., 2009).

In addition to the subduction earthquakes that occur on the interface of the descending Pacific plate, there have been numerous quakes on faults within the brittle crust above the subduction zone, within the body of the Australian plate closer to the Earth's surface. The epicenters of earthquake occurrences from January 1990 and December 2007, at depths shallower that 33 km, were shown in Figure 3-3 (*Left*) compiled by Wallace et al. (2009); again the magnitudes were less than 7 in this 19-year compilation. There is a significant degree of grouping of the localized epicenters of these shallower earthquakes, one pattern crossing the central North Island associated with the Taupo Volcanic Region, its faulting and volcanism being the result of tension within that portion of the crust overlying the western zone of plate subduction. Most important to the Hawke's Bay earthquake hazards are the epicenters in Figure 3-3 (*Left*) that occurred along the east coast of the North Island, paralleling the Hikurangi Trough and clearly related to the collision and subduction of the Pacific plate, even though these shallow earthquakes were within the Australian plate. This zone landward from the Trough is a region of intense deformation due to the compression that is developed between the colliding plates, producing rock folding and faulting. While

some of this deformation can be seen in rocks exposed at the ground surface, seismic surveys undertaken by geophysicists document the underground extensions of the faults. Examples are shown in Figure 3-5 from Wallace et al. (2009), from top to bottom representing the Southern, Central (Hawke's Bay), and Northern Sections of the margin. Shown as black-dotted curves are the northeast trending reverse faults, "reverse" in the sense that with depth down into the ground they slope (dip) toward the northwest, and when an earthquake occurs the crust above the fault plane moves eastward and upward relative to that below. This pattern is commonly found in zones of plate collision, and having this curvature and separation they are often described by geologists as being "splay faults", or more technically as "imbricate thrust faults", being associated with plate subduction in that as the faults extend downward they merge with the actual zone of plate subduction that is creating them through compression.
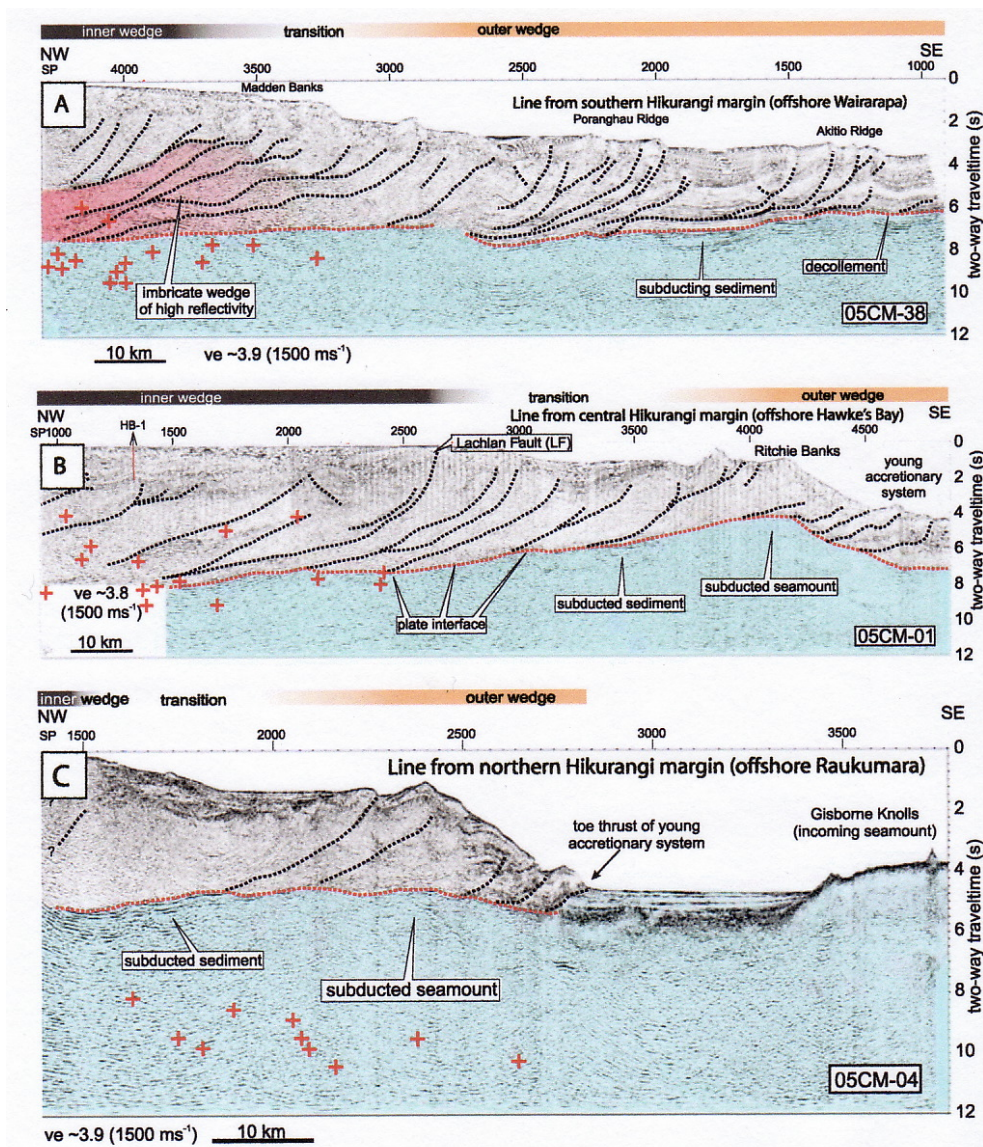
Figure 3-5: Seismic survey lines from the (A) Southern, (B) Central, and (C) Northern Sections, crossing the Hikurangi Margin. Splay faults within the upper Australian plate are shown as black-dotted curves, merging at depth with the subduction interface shown as red dots. [*From* Wallace et al. (2009)]

3 - 10

A generalized version of the tectonic-related features found along the east coast of the North Island is shown in Figure 3-6, from Cole and Lewis (1981) and Berryman (1988). This zone of intense compressional faulting within the Australian plate is referred to as the Accretionary Borderland, landward of which is the Frontal Ridge of mountains, and still further west the Back-Arc Basin of normal faulting produced by tension within the crust, giving rise to the Taupo volcanoes and hot springs. The rocks within the Accretionary Borderland range from conglomerates to sandstones to mudstones, and even limestone, having originated as sediments that were deposited during the past 10 million years in the ocean atop the Pacific plate, but were then accreted to the Australian plate when they were scraped off the Pacific plate as it was being subducted. It should be noted in both Figures 3-5 and 3-6 that this Borderland of intense faulting includes both the land and offshore continental shelf, extending out to the Hikurangi Trough. At least fourteen reverse faults have been found that cross the width of Hawke Bay, posing hazards from both earthquakes and the generation of tsunami.
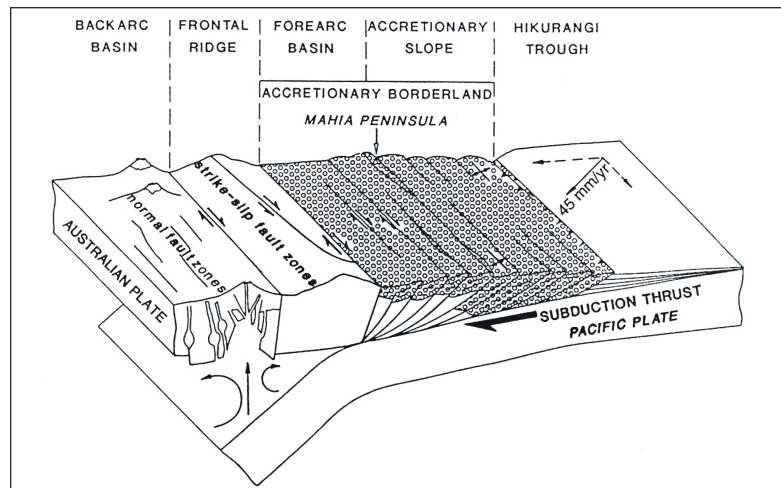
Figure 3-6: The series of reverse faults that dominate the zone of rock compression within the Australian plate due to the subduction of the Pacific plate along the Hikurangi Margin. These faults are found mainly within rocks of the Accretionary Borderland, consisting in part of marine sediments that have been scraped off the Pacific plate as it was being subducted. [*From* Berryman (1988)]

The Hikurangi Margin is again somewhat unusual compared with other subduction zones in that in addition to the reverse movement on the faults within the Accretionary Borderland at times of earthquakes, there is also a horizontal component to the movement, a "strike-slip" motion, so the ground is simultaneously displaced both vertically and horizontally. Typically in the Hawke's Bay area the horizontal movement is some 5 to 6 times greater than the vertical displacement at the time of an earthquake (Berryman, 1988).

Geologists have documented the presence of reverse faults and the accompanying rock deformation throughout this region, and have associated them with historic and pre-historic occurrences of strong earthquakes. Being located within the Accretionary Borderland of the Hikurangi subduction zone and therefore experiencing intense tectonic deformation, Hawke's Bay is one of the most earthquake prone areas of New Zealand. It has a history of at least

nineteen earthquakes felt since settlement by Europeans in 1840 (Aitken, 1999). Of those, five had magnitudes of 7.0 or greater, with the Hawke's Bay earthquake during the morning of 3 February 1931 having been the strongest with a magnitude 7.8. That initial main shock was followed by a number of weaker aftershocks, the strongest having occurred ten days later with a magnitude of 7.3.

The magnitude of an earthquake is a measure of the released energy at its source, its epicenter, but the energy of the ground motions is reduced as it spreads out with distance from the quake's origin. The energy as measured at a particular location distant from the source is called the "intensity", which is assessed using the Modified Mercalli Intensity Scale as a measure of the degree of shaking and the resulting damage experienced at that site on the Earth's surface. The Mercalli scale is recorded with Roman numerals to distinguish it from the magnitude of the energy at the quake's source. On the Mercalli scale the initial 1931 Hawke's Bay earthquake earned a ranking of X, which denotes "general panic, wooden buildings seriously damaged, landslides widespread, and rivers slop over banks" (Aitken, 1999, p. 33). The strongest aftershock ten days later was VII on the Mercalli scale: "General alarm, difficult to stand up, damage to weak masonry buildings, small slides and rock falls". The resulting damage throughout the Hawke's Bay region has been recounted in the book *Quake* by Matthew Wright, containing a number of historic photographs showing the extent of the destruction; 256 lives were lost.

Teams of scientists were immediately dispatched to Hawke's Bay, their objective being to undertake a reconnaissance of the damage to infrastructure and changes in the landscape; their reports appeared as a series of papers published in a 1933 issue of the *New Zealand Journal of Science and Technology*. The epicenter of the earthquake was determined to have been 32 km northwest of Napier, with the focus having been at a depth of 15 to 20 km beneath the surface, that is within what is now recognized to be the Australian plate above the subduction interface. Henderson (1933) provided detailed descriptions of the surface faulting, and the areas of uplift versus subsidence, derived from ground surveys. Marshall (1933) examined the coastline between Cape Kidnappers and Wairoa, and estimated the amount of land-elevation change from tide-gauge data and pre-earthquake high-tide levels. Readily apparent was the abrupt rise of the land that had elevated the Ahuriri Lagoon, with most of its water having rapidly drained into the sea, its floor now being dry land including the region's commercial airport. The increase in land elevations at the time of the earthquake raised the beaches to the north of Napier, up to Tangoio and beyond, whereas to the south at Haumoana, Te Awanga and Clifton, the land subsided so the ocean's water flooded over the beaches, permitting its waves to directly attack coastal properties. This change in land elevations along the Hawke's Bay shore relative to the level of the sea has had a profound effect on the evolution of this coast in the decades subsequent to the 1931 earthquake, and likely is still a factor in accounting for part of the erosion being experienced from Haumoana to Clifton, the area of greatest property losses in the Hawke's Bay region (Komar, 2005, 2010).

The Wellington to Hawke's Bay stretch of the Accretionary Borderland is the region having the most active deformation with strong near-surface earthquakes due to the colliding plates, the activity being greatest there because the deformation of the crust has to make up for the strong coupling at the subduction zone, it having been locked for a long period of time. The strongest historic earthquake in that region was the magnitude 8.1-8.2 Wairarapa event in 1855 that resulted in major damage to Wellington (Grapes, 2000).

In summary, the seismic activity along the east coast of the North Island, caused by its location within the Hikurangi subduction zone, poses a threat of potentially extreme future hazards from major earthquakes, and also from their accompanying tsunami if the fault movement occurs in the offshore on the continental shelf. While historic earthquakes on the subduction interface have at maximum been on the order of magnitude 7 (e.g., the quakes in 1947 off the coast of Gisborne), based on the recent seismology research the protections are that in future subduction earthquakes could have magnitudes on the order of 8.5 to 8.7, possibly even 9 given the uncertainties of such projections and the fact that those magnitudes have occurred on other subduction zones around the Pacific. As evident from the 1931 Hawke's Bay earthquake, movement on faults within the Australia plate can also produce considerable damage, it having had a 7.8 magnitude. To make matters worse and hazard predictions more difficult, there is the possibility that a subduction earthquake at depth beneath Hawke's Bay could simultaneously trigger movement and earthquakes on faults at shallow depths within the upper Australia plate. Investigations reviewed in the following section have found this to be a distinct possibility, offering an explanation for abrupt land-elevation changes and the presence of layers of sand found within bays and estuaries along this coast, attributed to the generation of high tsunami waves by these seismic events (Cochran et al., 2006; Hayward et al., 2006).

3.4 GEOLOGIC EVIDENCE OF PREHISTORIC EARTHQUAKES AND MAJOR TSUNAMI

The Hawke's Bay coast and the Pacific Northwest of the United States, respectively the Hikurangi and Cascadia subduction zones, share a problem in assessing their earthquake hazards in that both have only short historic records, dating back to the mid-19th century. Although significant subduction earthquakes have not occurred on either of those coasts since European settlement, there is the potential for extreme earthquakes together with destructive tsunami, just as recently occurred on the coasts of Sumatra and Japan. In view of this uncertainty as to their potential magnitudes and frequencies of occurrence along the Hikurangi and Cascadia Margins, important has been the search for geologic evidence of pre-historic subduction earthquakes and tsunami that swept far inland, having taken place centuries or even thousands of years in the past.

It was direct evidence derived from investigations by geologists that first established the pre-historic occurrence of a major subduction earthquake and tsunami along the Cascadia Margin, an event that occurred three centuries ago. That initial evidence came from the discovery of buried marshes along the shores of bays and estuaries, ancient marshes that had abruptly subsided by some 1 to 2 metres at the instant of the earthquake, followed a few minutes later by having been covered with a layer of sand carried inland from the ocean beach by the earthquake-generated tsunami waves (Atwater, 1987). Further evidence came from dead trees along the shores of bays, which had been killed by subsidence of the ground, with analyses of their annual growth rings having substantiated the approximate age and even the season when that subduction event had occurred. The catastrophic nature of that event was readily evident, with carbon-14 dating having established that it took place approximately in the year 1700, give or take a few years due to uncertainties of that dating technique. The

exact date and hour of that event was established later by records of the generated tsunami waves that had reached the shores of Japan, demonstrating that the quake had taken place at about 9pm on 26 January 1700 (Sataki et al., 1996; Atwater et al., 2005). From the size of the tsunami waves and the extent of their destruction along the coast of Japan, the intensity of the earthquake was estimated to have been at least magnitude 9.

Since the initial discovery during the 1980s of geologic evidence for that subduction earthquake in 1700 on the Cascadia Margin, continued research by geologists has found additional evidence for that event, as well as for other subduction earthquakes and tsunami that had occurred during the past several thousand years (Darienzo et al., 1994; Hemphill-Haley, 1995; Witter et al., 2003; Goldfinger et al., 2012). Marshes buried by tsunami sands have been found in bays and estuaries along the entire length of the Pacific Northwest coast, from northern California to Vancouver Island, Canada, documenting the numbers and approximate dates of past earthquakes, and with the inland extent of the tsunami deposits providing positive evidence for the extreme hazards represented by those tectonic events.

An unexpected source of evidence for past subduction earthquakes on the Cascadia Margin has come from turbidite sands found in sediment cores collected offshore by oceanographic investigations. Those records provide the most detailed documentations of occurrences of multiple earthquakes throughout the Holocene, with reasonably precise dates for their occurrences, the alongcoast extents of individual events, and implications as to their magnitudes based on the volumes of the turbidite deposits (Goldfinger et al., 2003, 2012). Each individual turbidite is interpreted as having been the product of a major earthquake that generated massive landslides on the continental slope and within submarine canyons, there having been a number of slides along the length of the margin recorded by the spatial extent of the turbidite layers. Analyses based on a large number of sediment cores identified 19 turbidites within the Holocene that are interpreted to having been generated by subduction earthquakes. There are fewer turbidites and associated seismic events in the northern portion of the Cascadia Margin than found in the cores to the south, but those found in the north extend along the full length of the Cascadia Margin, the interpretation being that those particular earthquake events were the most extreme in having affected the entire margin. Additional but less extensive earthquakes occurred in the south, yielding a total of 41 events for that region. The smaller number of northern subduction events therefore yield a longer recurrence interval between earthquakes, on average 500 to 530 years, the recurrence intervals also being indicated by the thicknesses of hemipelagic sediment deposits between the turbidite layers (Goldfinger et al., 2003). For the southern portion of the margin, the sequence of 41 events yields an average recurrence interval of 240 years. The probability for an event occurring again within the next 50 years on the northern margin, and extending the full length of the subduction zone, is 7 to 12 percent; for the southern margin having more frequent events, the probability is 37 to 42 percent for another subduction earthquake in the next 50 years.

Similar investigations have been undertaken along the Hikurangi Margin, searching for geologic evidence of past subduction earthquakes and tsunami. However, the search on this margin and interpretations of the results are inherently more difficult than those along the Cascadia Margin, in that the east coast of the North Island experiences earthquakes both within the body of the Australian plate as well as at the plate subduction interface, and it is likely that in many instances both have occurred during the same tectonic event. A further complication is

the spatial variability in the coastal responses to the earthquakes, with some stretches of coast abruptly subsiding while others are elevated. The result is that evidence for past major earthquakes along the Hikurangi Margin has come from both sediments deposited within bays and lagoons that subsided during the event, similar to the Cascadia Margin, but also from series of uplifted erosional marine terraces cut into the rocky shores (e.g., the Mahia Peninsula).

An early study by Hull (1986) investigated the stratigraphy of sediments deposited in the Ahuriri Lagoon, in what had been its western margin prior to uplift during the 1931 Hawke's Bay earthquake.   The stratigraphic layering of the sediments indicated that there had been a net subsidence of that area (and most of the Lagoon basin) spanning at least the past 4,000 years. Hull concluded, however, that most of that subsidence had occurred between 3,500 years BP and 1,750 years BP, a period of peat accumulation within that area of the Lagoon at an average rate of 4.6 metres per thousand years. A hiatus in peat accumulation occurred between about 1,750 years BP and 500 years BP, interpreted by Hull as having been the result of tectonic uplift, or at least stability in the level of the sea relative to the land. The inundation of that area by the Ahuriri Lagoon in about 500 years BP was likely the result of renewed tectonic subsidence, with the water continuing to cover that area until it was uplifted by the Hawke's Bay earthquake in 1931.

This dominance of land subsidence centered over the Ahuriri Lagoon appears to have extended south to Hastings. Unlike most of the Hawke's Bay region that tectonically rose during the 1931 earthquake, Hastings and its neighboring stretch of ocean shore continued its longer-term trend of subsidence. According to Gibb (1980), water wells in the Hastings area have penetrated estuarine sediments at depths of 10 to 16 metres below the present sea level, deposits that are on the order of 6,500 years old. An investigation by Froggatt and Howorth (1980) analyzed the history of movement on the Wairarapa Fault where it crosses Lake Poukawa southwest of Hastings, movement on that fault having been documented by its effects on the stratigraphy of sediments deposited in the Lake, demonstrating that there had been episodic occurrences of subsidence spanning more than 6,000 years. A cross-section based on a series of bore holes drilled through the sediments revealed that the ash and carbonate layers are displaced vertically where they cross the fault, with the degrees of offset ranging from 0.56 to 1.51 metres, systematically increasing with the age of the layer — the older and deeper the layer, the greater the number of earthquakes and fault movements it has experienced, and hence the greater the cumulative offset. A series of step-function analyses were undertaken, and best-fit agreement with the measured offsets of both sediment and ash layers led them to conclude that eight steps (earthquakes) had occurred during the past 6,500 years, representing on average an earthquake every 800 to 900 years for this site, which taken together account for its total subsidence.

The recent detailed investigations by Hayward et al. (2006) and Cochran et al. (2006) have focused on the regions of net subsidence along the Hawke's Bay coast, respectively the extent of the Ahuriri Lagoon prior to 1931, and the coast of northern Hawke's Bay, the Te Paeroa Lagoon north to the Mahia Peninsula. Both studies documented the stratigraphy of the accumulated sediments in those subsiding areas, with their ages based on carbon-14 dating and the presence of layers of volcanic ash of know dates. Particularly important to their investigations have been paleoecological analyses of the microfossils within the deposits, assemblages of foraminifera and diatoms that have known relationships to water levels on

those shores, permitting determinations of past relative sea levels and how occurrences of earthquakes altered them.

The study by Hayward et al. (2006) was based on the collection of 11 cores (3- to 7.5-metre lengths) of Holocene sediments from the area that had been covered by the Ahuriri Lagoon prior to its uplift and drainage during the 1931 earthquake. The cores spanned the north-to-south extent of the former Lagoon, from what had been its north shore, to core sites central within the bay, and with the greatest concentration being on what had been near the southwest shore. Collectively the stratigraphy of the sediments provided a 7,200-year record of 8.5 metres of subsidence, followed by the 1.5-metre uplift in 1931. The modern-day dependence of foraminifera on water depths served to establish the paleotidal elevations from the assemblages of those microfossils found within sediments sampled along the lengths of the cores, yielding assessments of past relative sea levels. As noted above, age determinations were based on carbon-14 dating and the ages of volcanic ash layers found in the cored sediments. Of primary interest to Hayward et al. (2006) was the identification of probable records of earthquake events, identified in the analyses of the sediments as displacements of the water depths and sea levels, with 6 possible subsidence occurrences having been related to subduction-interface earthquakes: circa 7,000 years BP (-0.6 m subsidence); 5,800 years BP (>-0.5 m); 4,200 years BP (-1.5 m); 3,000 years BP (-1.4 to -1.8 m subsidence); 1,600 years BP (-1.7 m); 600 years BP (-1 m); and the 1.5-metre uplift during the 1931 Hawke's Bay Earthquake. Within this series of subsidence events that are likely related to subduction earthquakes, the return times ranged from 1,000 to 1,400 years.

Associated with these subsidence events and abrupt increases in relative sea levels, found by Hayward et al. (2006) within the Ahuriri Lagoon, were changes in the sediment characteristics ranging from the development of an eroded surface that had been burrowed by estuarine organisms, to an abrupt switch from mud to sand or peat. These changes in the sediments, however, did not positively demonstrate the arrival of tsunami, generated by earthquakes in the offshore. However, just to the north of the Lagoon near the ocean shore of Tangoio are Holocene-age estuarine sedimentary deposits associated with the present-day Pakuratahi Stream. The sediment stratigraphy within cores has been analyzed by Cochran (personal communication, November 2012), having found that the subsidence events occurred in 7,000 years BP, 4,200 years BP and 3,000 years BP, correlating closely with those found in the Ahuriri Lagoon identified by Hayward et al. (2006) [also the summary correlation diagram presented by Wallace et al. (2009, Fig. 6)]. Of significance, Cochran did identify definite tsunami sand layers in the Pakuratahi cores for the 7,000- and 4,200-year events, demonstrating that tsunami had been generated even though not positively identified within the Ahuriri Lagoon.

A similar investigation by Cochran et al. (2006) focused on the Hawke's Bay coast still further to the north, the stretch dominated by subsidence from Wairoa up to the Mahia Peninsula, their research also having had the objective of identifying evidence for past subduction earthquakes and tsunami along the Hikurangi Margin. Five cores were collected from the Te Paeroa Lagoon, in a line perpendicular to the coast in order to document possible inland variations in the sediment stratigraphy representing the inland extent of the flow of extreme tsunami. Another two cores were obtained at Opoho some 10 km to the north along the coast, and two from Opoutama, a low-lying area just to the south and inland from the uplifted Mahia Peninsula. The core stratigraphy from Te Paeroa and Opoho both documented net

subsidence amounting respectively to 4 and 6 metres during the past 7,200 years. In contrast, Opoutama experienced little vertical movement, interpreted to be the result of that site's close proximity to the line of transition between the zone of subsidence to its south versus uplift of the Mahia Peninsula to its northeast.
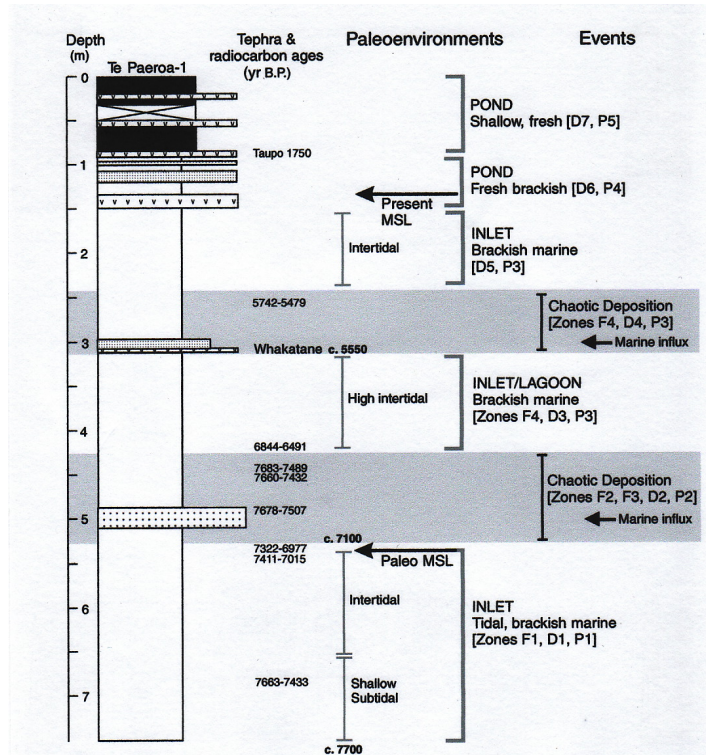
Figure 3-7: The sediment stratigraphy and interpreted paleoenvironments identified in a core from the Te Paeroa Lagoon, containing two layers of coarse sediments (labeled "marine influx") interpreted to having been deposited by tsunami, each overlain by "Chaotic Deposition", sediments that had accumulated due to subsidence at the times of the earthquakes. [*From* Cochran et al. (2006)]

Analyses of the sediment stratigraphies in both Te Paeroa and Opoho showed subsidence events dated circa 7,100 and 5,550 years BP, identified by coarse-grained sediment layers interpreted as having been deposited by tsunami, directly overlain by "chaotically mixed" sediment that appeared to have rapidly filled the accommodation space resulting from the deepened water produced by the earthquake-induced subsidence (Cochran et al., 2006). The sediment stratigraphy and interpreted paleoenvironments identified in the Te Paeroa Lagoon core are shown in Figure 3-7, including two zones of tsunami sand (labeled "marine influx" in the diagram), each having been covered by "Chaotic Deposition". The tsunami deposited layers were based on key diagnostic criteria for having that origin, including being coarser grained than the surrounding sediments, having an extensive distribution across the coastal plain, thinning and fining in the landward direction, and containing marine shells and microfossils. In contrast, the overlying Chaotic sediments have a local origin, derived from erosion by water currents within that coastally enclosed body of water, evident from the sediments containing microfossils and diatoms of brackish to freshwater origins.

While there has been a predominance of land subsidence centered over the Ahuriri Lagoon and the shore south of the Mahia Peninsula, other areas of the Hawke's Bay coast have been dominated by tectonic uplift spanning thousands to millions of years. The rocky stretch of shore north of Tangoio up to Wairoa contains rocks of Plio-Pleistocene marine sediments, some now found at elevations up to 500 metres above sea level, providing clear evidence for a net tectonic uplift spanning at least the past 2 million years (Hull, 1990). Plio-Pleistocene sediments are also found offshore at depth beneath Hawke Bay, indicating net subsidence in the offshore during that same span of time. The interpretation by geologists of such variations in subsidence versus uplift is that compression of the Accretionary Borderland by plate subduction has broadly folded the rocks of the Australian plate into anticlines and synclines, respectively representing net upward and downward movements of the crust. As such, the region extending from the Ahuriri Lagoon to Hastings is central to a developing syncline, while the area to the north where the Plio-Pleistocene sediments have been uplifted represents an anticline, with another found to the south in the Cape Kidnappers area.

Further evidence for this broad folding of the crust, as well as the effects of episodic faulting, has been derived from the study of elevated ancient beaches and wave-cut terraces found on the flanks of Cape Kidnappers and especially on the slopes of the Mahia Peninsula, respectively at the south and north ends of Hawke Bay. An investigation by Hull (1987) of the uplifted terraces on Cape Kidnappers indicated rapid uplift of up to 5 metres since about 2,300 years BP, the Cape being on the eastern flank of the north-south trending Kidnappers Anticline. This uplift of Cape Kidnappers and its anticline therefore likely corresponds to the subsidence of the Ahuriri Lagoon as part of the adjacent syncline, the subsidence recorded by the peat accumulation between 3,500 years BP and 1,750 years BP found by Hull (1986) on the western shore of the Lagoon.

An impressive series of "stair-step" marine terraces covered by ancient beach deposits is found on the flanks of the Mahia Peninsula, recording a long history of significant uplift. The most detailed studies of its terraces are those carried out by Berryman and his co-investigators (Berryman et al., 1989; Berryman, 1993a, 1993b). Each terrace platform represents a period of relative tectonic stability during which waves cut into the rocks of the Peninsula at the intertidal level. It is the rise between successive terraces that represents the record of a tectonic event, an episode of abrupt uplift. Individual amounts of uplift between successive terraces range from about 1 to 4 metres, suggesting that there has been a range in earthquake magnitudes. Berryman's extensive program of radiocarbon dating of intertidal shells found in the beach deposits showed that the terraces located in widespread parts of the Peninsula cluster into five distinct ages: 250, 1600, 1900, 3500 and 4500 years BP. The Mahia terraces are therefore younger than the ages of the tsunami deposits found by Cochran et al. (2006) in the area of subsidence to the south, which represented earthquake events in 5,550 and 7,100 years BP. It is possible that the 5,550-year-old tsunami and earthquake correspond to the 4,500-year-old terrace, that earthquake having been responsible for both the uplift of the Peninsula and subsidence to its south recorded by the tsunami deposits. The time intervals between the ages of the terraces measured by Berryman range from 1,000 to 3,000 years, the average having been about 1,700 years, in reasonable agreement with the sediment records found along this coast by Hayward et al. (2006) and Cochran et al. (2006), there being basic agreement even though the sediment records represent the earthquake intervals, while the terraces are the aseismic periods between those earthquakes.

Berryman concluded that the stair-step series of terraces on the flanks of the Mahia Peninsula is the product of movement on a major reverse fault within the Accretionary Borderland of the Hikurangi subduction zone, specifically the Lachlan Fault in the offshore on the continental shelf, extending along the length of this coast from Hawke Bay to beyond Gisborne in the north (Berryman et al., 1989; Berryman, 1993a, 1993b). Immediately landward from this fault but still in the offshore is the crest of the Lachlan Anticline, with the Mahia Peninsula positioned on its western flank, such that during each earthquake and episode of movement on this fault the rise of the anticline and Peninsula are recorded in the uplift of the terraces and their beach deposits, each occurrence of uplift leading to wave erosion at the base of the Peninsula and the formation of another terrace. Berryman (1993a) estimated that if the entire length of the Lachlan Fault (about 150 kilometres) was to rupture in a single event, the magnitude of the resulting earthquake would be on the order of 7.5 to 8.0, concluding that the past earthquakes recorded in the terraces of the Mahia Peninsula must have been within that range of magnitudes, comparable to the 1931 Hawke's Bay earthquake.

Cochran et al. (2006) similarly considered the possibility that the subsidence and presence of tsunami layers in Te Paeroa and Opoho to the south of the Peninsula occurred in response to earthquakes on the Lachlan Fault, but with those sites being positioned within the syncline adjacent to the Lachlan Anticline. As well as considering this possibility that the Lachlan Fault alone was responsible, they recognized the possibilities that the subsidence and tsunami deposits could have owed their origins to movement and earthquakes on the subduction interface, or that earthquakes occurred essentially at the same time on both the interface and along the Lachlan Fault within the Borderland (this being common on other subducting continental margins). Considering this range of possibilities, Cochran et al. (2006) undertook a series of geophysical analyses representing each; while the model results involving movement on the Lachlan Fault alone best accounted for the combined uplift of the Mahia Peninsula and subsidence to its south, events that included movement on the subduction interface also yielded results that are in close agreement. Their models again led to a conclusion that the earthquakes would have had magnitudes on the order of 7.9 to 8.1.

Similar to the Cascadia Margin of the U.S. Pacific Northwest, turbidites have also been found within the sediments deposited in the Hikurangi Trough, interpreted as providing a record of past major earthquakes along this subduction zone. This has been demonstrated in the recent investigation by Pouderoux et al. (2012), based on a number of sediment cores collected along the northern half of the east coast, from the Trough offshore from Poverty Bay to northeast of the Raukumara Peninsula. Turbidites associated with earthquakes during the past 7,000 years were identified by their containing species of foraminifera that were reworked from sediments that initially had been deposited on the upper continental slope, later to form landslides during earthquakes, generating turbidity currents and their sand deposits found in the Hikurangi Trough. According to Pouderoux et al. (2012), the core stratigraphies provide a more complete record than those found in sediments along the coast, demonstrating the occurrence of a larger number of events with shorter return periods of 270 to 430 years. The longer circa 400-year return periods were found in the Trough sediments in the northern portion of the study region, with the shorter 270-year interval being the average offshore from Poverty Bay, suggesting more frequent earthquakes to the south.

In summary, the geologic investigations of plate subduction along both the Cascadia and Hikurangi Margins have yielded evidence for past major earthquakes and accompanying tsunami. It is evident that past earthquakes along the coast of Hawke's Bay must have had magnitudes of at least 8, possibly greater, with the generation of tsunami whose heights and impacts far exceeded those that have been experienced historically along the coasts of New Zealand, generated by distant earthquake events (e.g., on the Chilean subduction zone in 1960). Uncertainties remain as to the frequencies of occurrences of major earthquakes, the length of time between those destructive events, and to what degree they are generated by movement on the subduction interface between the colliding plates, on faults within the over-riding Australian plate, or the combination of both occurring at essentially the same time. The continuing programs of research by seismologists and geologists can be expected to more fully document past occurrences of subduction earthquakes, supporting improved assessments of potential future hazards to the Hawke's Bay coast.

3.5 TECTONICS AND CHANGING LAND ELEVATIONS

While earthquakes and their accompanying tsunami represent the potentially most extreme hazards faced along the coast of Hawke's Bay, in the context of this investigation of its erosion and flooding hazards, important are the tectonic controls that produce changes in land elevations relative to the level of the sea. As reviewed above, there are extremes in the tectonic land-elevation responses, with significant stretches of this coast having risen in elevations, experiencing a net tectonic uplift over centuries to thousands of years, while other stretches of the coast have been subsiding, forming submergent shores. The latter are of primary concern in this study, since they are most subject to rising sea levels, the consequence being more pervasive erosion and flooding of shorefront properties.

The focus here is on the tectonic factors that affect the Hawke's Bay land elevations, progressively in the long term or episodically during earthquakes, providing a review of the investigations that have been undertaken to document the patterns of subsidence versus uplift along this coast. A difficulty faced in documenting the elevation changes or trends in relative sea levels are the limited availabilities of direct measurements upon which such assessments can be made. Important is the availability of measurements of land elevations obtained from Global Positioning System (GPS) units, and the existence of long-term tide gauge records from which trends in relative sea levels can be determined. In the case of Hawke's Bay, unfortunately there are only a few GPS units in close proximity to its shore, and only one tide gauge, that operated by the Port of Napier, the records of both covering little more than a decade of measurements. These limitations in the availability of important data sets represent a significant problem for Hawke's Bay, in view of there being substantial differences in directions and rates of land-elevation trends along this coast, with parallel variations in relative sea levels and their erosion hazards to coastal properties. There are additional problems in terms of understanding the tectonic factors that cause the changes in land elevations and control the trends in relative sea levels, the complication being that there are both progressive long-term processes related to plate subduction, as well as episodic changes at times of earthquake events, the 1931 Hawke's Bay earthquake being the primary example of the latter.

A regular cycle in the long-term changes in land elevations has been found on other coastal margins that are experiencing plate subduction, associated with their "stick-slip" tectonic behavior. This cycle has been documented on the subduction coast of the U.S. Pacific Northwest (the Cascadia Margin), based on geologic evidence, having found that at times of subduction earthquakes in the past the coast abruptly subsided by up to 1 to 2 metres, but during the aseismic centuries between earthquakes it has experienced tectonic uplift. The progressive aseismic uplift spanning the past century has been documented from periodic resurveys of benchmarks used by surveyors, and more recently by GPS units, further confirmed by data from tide-gauge records showing the existence of along-coast variations in measured relative sea-level trends, reflecting the variations of tectonic uplift of the land (Burgette et al., 2009; Komar et al., 2011). The origin of this cycle of changing directions in land elevations associated with plate subduction is illustrated schematically in Figure 3-8, contrasting the long aseismic period versus the occurrence of an episodic subduction earthquake. During the quiet periods between earthquakes, the accumulation of stress between the locked plates produces a slow uplift of the inland continental crust, while the crust closer to the subduction zone is pulled downward by the descending ocean plate, resulting in subsidence. When an earthquake occurs on the Cascadia Margin the crustal movements are suddenly reversed; inland, the crust abruptly drops down by a metre or more, while that close to the subduction zone is raised. This cycle of ups and downs of the coast, spanning centuries to thousands of years, has had profound effects on the history of erosion along this coast, reflected in its present-day morphology.
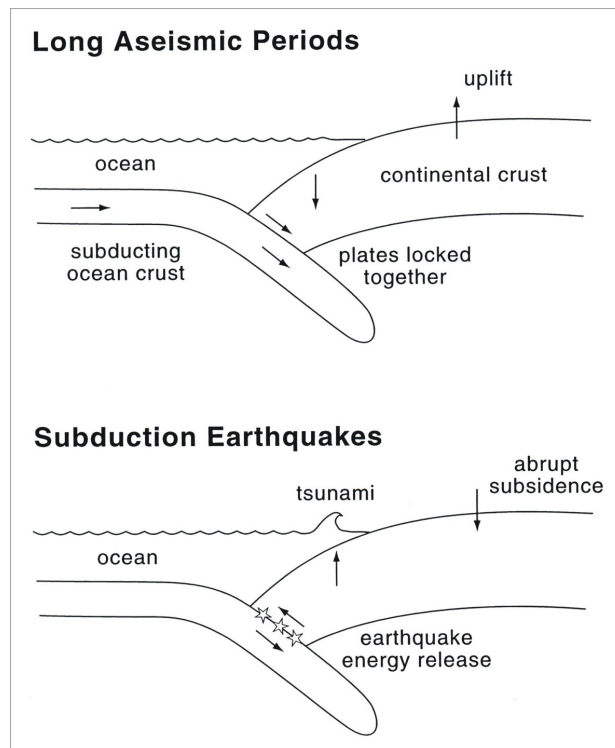
Figure 3-8: The contrasting land-elevation changes that occur during the aseismic period between earthquakes, when the plates are locked in a subduction zone, versus those that abruptly occur when an earthquake takes place, releasing the accumulated strain of the previously locked plates.

It is expected that the Hikurangi Margin could experience this same general pattern of land elevation changes found in other subduction zones, those depicted in Figure 3-8, but this margin is also subject to periodic earthquakes within the overlying Australian plate that more locally alter land elevations. If so, during an aseismic period when the plates are locked, as exists now, the directions of elevation trends would tend to be reasonably consistent along the coast, except when locally interrupted by an earthquake on a fault within the Australian Plate, as occurred in 1931 during the Hawke's Bay event. With the occurrence of the next subduction earthquake, the elevation changes that had been caused by the previously locked plates would abruptly be reversed, as illustrated in Figure 3-8. A complication, however, is the possibility (likelihood) that the subduction earthquake on the interface between the plates would at the same time trigger fault movement and the folding of rocks within the Australian plate, the resulting land elevation change being their combined movements, leading to different net responses of subsidence versus uplift along this coast, evident in this Margin's tectonics.

Important for potentially distinguishing such tectonic effects on the land elevations, of those caused by the long-term subduction cycle versus being produced by faulting and folding within the Australian plate, are measurements by GPS units located throughout the Hawke's Bay region. It can be expected that the ground movements measured by those units in recent years, both horizontal and vertical, are related almost entirely to the plate subduction processes, there not having been a significant earthquake on a fault within the Australian plate during the 2000-2012 decade of GPS data collection. The most important study that has relied on the GPS data to analyze land elevation changes along this coast is the report by Beavan and Litchfield (2009). However, their analyses of the GPS data need to be viewed as providing only a preliminary assessment of the land level changes, considering that only a few active units are in existence along this shore and their record lengths are very short, the most important units having been operational for only 3 to 4 years when their analyses were completed.

Figure 3-9 is the location map from the Beavan and Litchfield (2009) report, the red triangles showing the locations of the GPS units analyzed in their study, there being a total of six in close proximity to the Hawke's Bay shore, each denoted by a 4-character code. From north to south those GPS sites are:

    MAHI   The top of the Mahia Peninsula, a site that has experienced a net uplift
            during the past several thousand years;
    KOKO   The low-lying shore near Opoho, an area that over the long-term has
            experienced a net subsidence;
    LEYL   The north end of the Bay View Littoral Cell, in proximity to Tangoio;
    CKID   Located atop the Cape Kidnappers headland, at the south end of the
            Haumoana Littoral Cell;
    PAWA   The rocky portion of the south-central Hawke's Bay coast, in proximity to
            Pourere;
    PORA   The southern-most stretch of the Hawke's Bay coast, south of Blackhead
            Point.

The location of the Port of Napier's tide gauge (NAPT) is identified by the blue triangle in Figure 3-9, and an additional GPS site to be installed is designated by the green triangle (WAHU), which would fill the shoreline gap between KOKO and LEYL. These six GPS sites include both stretches of coast that have experienced a long-term net uplift, versus others that have been dominated by subsidence. Although the results from all of these GPS units are of interest, only the LEYL and CKID units plus the Port of Napier tide gauge (NAPT) potentially provide measurements that are directly within the stretch of shore of interest in our analyses of the erosion hazards, the Bay View and Haumoana Littoral Cells.
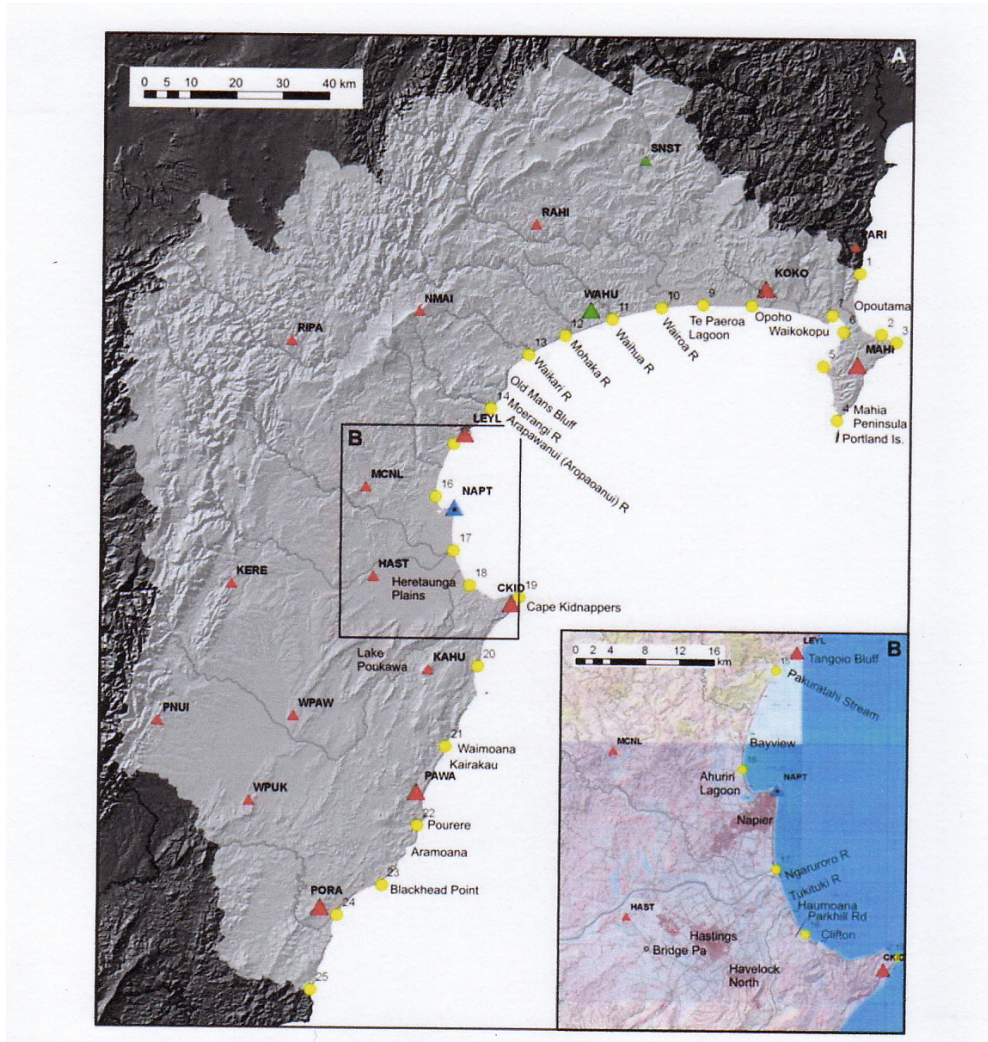
Figure 3-9: Map of Hawke's Bay showing the locations of the active GPS units (red triangles), and the tide gauge at the Port of Napier (blue triangle). [*From* Beavan and Litchfield (2009)]

Figure 3-10 shows the GPS records analyzed by Beavan and Litchfield (2009) for the six sites along the Hawke's Bay shore, with the longer records included at the top of the diagram being from Whangarei (WHNG), Auckland (AUCK), and Wellington (WGTN). The GPS units in Auckland and Wellington provide the longest records, dating back to the year 2000, but even for those units there was only 9 years of measurements available to be analyzed. Auckland and

Whangarei to its north on the west coast of the North Island are a considerable distance from the Hikurangi subduction zone, beyond the effects of significant tectonic activity, and it is seen in Figure 3-10 that both show relatively stable elevations, slow rates of uplift. In contrast, Wellington and all six GPS sites along the Hawke's Bay coast show trends of lowered land elevations, subsidence during this locked phase of plate subduction, although considering the shortness of these records (particularly MAHI and LEYL) the magnitudes of their rates of change are not statistically significant (Beavan and Litchfield, 2009). On the other hand, with these GPS units along the coast being in close proximity to the Hikurangi Trench, where plate subduction is initiated, as diagramed in Figure 3-8 one would expect there to be net subsidence just as indicated by all six coastal units, even including sites such as the Mahia Peninsula (MAHI) and those in the south (PAWA and PORA) that otherwise have experienced long-term net uplift.
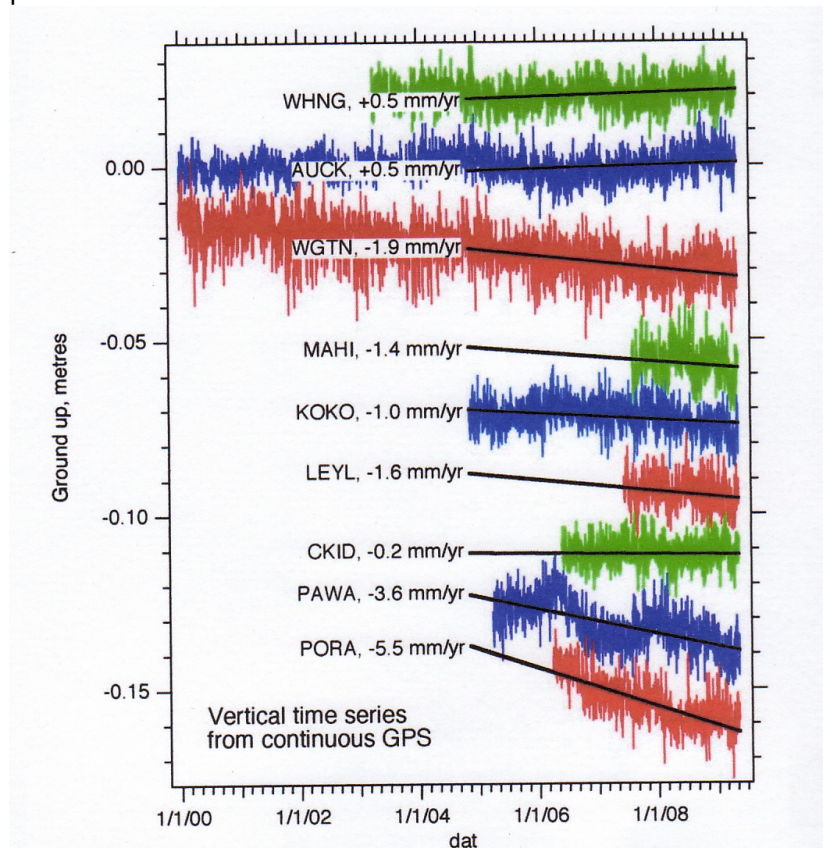
Figure 3-10: Time series of the vertical component of GPS measurements, with decade-long records for Whangari, Auckland and Wellington, but with records from the 6 units along the Hawke's Bay coast ranging from only 3 to 5 years. [*From* Beavan and Litchfield (2009)]

Based on these limited GPS measurements, Beavan and Litchfield (2009) concluded that in considering the entire coast of Hawke's Bay, it cannot be established with confidence whether the vertical land motion along much of that shore is presently upward or downward, and cannot support such conclusions with meaningful magnitudes until significantly longer GPS records become available. Specific to the shore between Tangoio Bluffs southward to Cape Kidnappers, the littoral cells of interest in our hazard analyses, their concluding assessment is that it has been subsiding at a rate between about 0 and 1 mm/year, but with uncertainties having that same order of magnitude.

As will be seen in later chapters, the tide-gauge record from the Port of Napier is only about two decades long, and also contains a major gap of missing data (Chapter 4). Although its analysis directed toward an assessment of the net trend in relative sea level will accordingly be uncertain, it yields an approximate rate of increase of about 1.9 mm/year (Chapter 9), which is in reasonable agreement with the global average rate of rising sea level, and with satellite measurements of changing sea levels along this coast, the implication again being that the present-day change in land elevations is small.

The occurrence of a subduction earthquake in the future could be expected to produce an abrupt uplift along the Hawke's Bay shore, assuming that it follows the reversal of the aseismic trend of subsidence now being measured, similar to found along other Pacific margin subduction zones as depicted schematically in Figure 3-8. One might expect that this abrupt rise in the land along the shore would be on the order of a metre, possibly more, similar to experienced along other subduction zones (e.g., the Cascadia Margin). It is uncertain, however, what the net change in land elevations would be, if one considers the full cycle of movements on this "stick-slip" margin, subsidence followed by uplift during the next subduction earthquake. Furthermore, while the alongcoast variations in the net displacement of the land elevations attributable to this subduction cycle is important in contributing to the observed differences between the long-term uplifted shores versus those that have subsided, undoubtedly more important have been earthquakes within the body of the Australian plate, either triggered at the same time as a subduction earthquake, or being an isolated occurrence as was the case during the 1931 Hawke's Bay event.

The consequences of land-elevation changes that can result from movement on faults within the Australian plate are dramatically illustrated by the Hawke's Bay earthquake in 1931. Immediately evident was the uplift of the Ahuriri Lagoon, a major portion of which rapidly drained into the sea, permanently converting that area to land. In his reconnaissance investigations, Marshall (1933) created a map that showed the aerial extent of the uplifted floor of the Lagoon, estimating that the total area of new dry land was 3,170 acres, about 13 square kilometres. Henderson (1933) derived assessments of the land elevation changes by compiling earlier land surveys and comparing them with post-quake re-surveys. This included the levees along the banks of the Tukituki, Ngaruroro and Tutaekuri Rivers, but of particular interest to changes along the Bay's shore were resurveys of the railway line from Wairoa in the north to Opapa, 45 kilometres south of Napier, a total along-coast distance of about 160 kilometres. A more recent analysis of this survey data throughout the region was completed by Hull (1990), with the results shown in Figure 3-11, documenting a zone of uplift defined by a northeast trending elongate dome having a maximum length of about 90 kilometres and a width of at least 17 kilometres. The maximum uplift of 2.7 metres occurred near Oldmans Bluff on the coast just north of the mouth of the Aropaoanui River, about 5 kilometres north of Tangoio. The tide gauge in the Port of Napier recorded an uplift of 1.8 metres, representative of the rise along the shore of the Bay View Littoral Cell, but further to the south within the Haumoana Cell the amount of uplift was progressively less, becoming 0 at about Awatoto, and with a zone of subsidence found still further to the south, centered on Hastings where the land elevation had dropped by about 1.0 metre. The line of zero change in land elevations, the so-called "hinge line" in this tectonic event, extended in the southwest direction from Awatoto on the coast, through Bridge Pa west of Hastings (Figure 3-11).
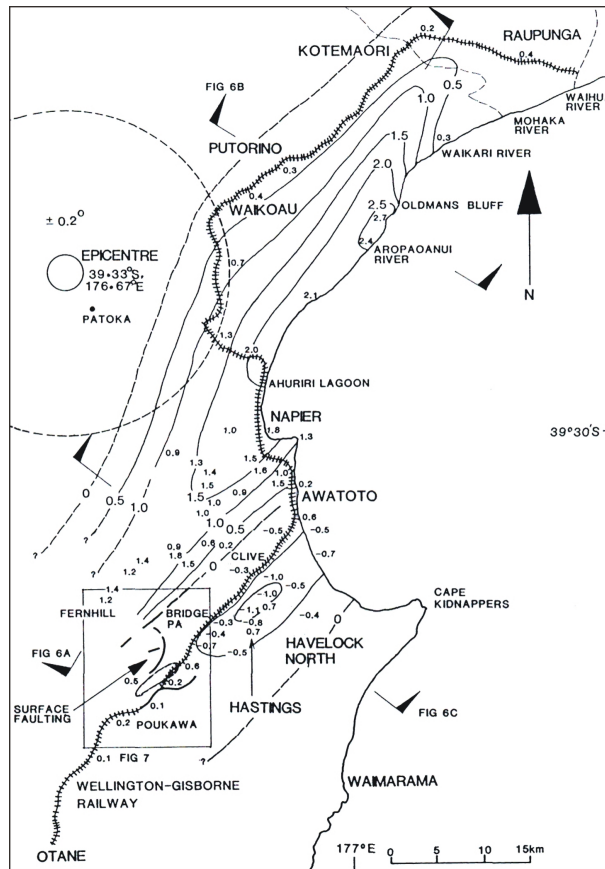
Figure 3-11: Land elevation changes produced by the 1931 Hawke's Bay earthquake. Negative values centered on Hastings and extending to the coast denote land subsidence. [*From* Hull (1990)]

The northeast trending dome of tectonic uplift formed during the 1931 earthquake, evident in Figure 3-11, for the most part produced the greatest increases in elevations in close proximity to the coast itself, or immediately inland, thereby reducing the gradients of the river channels as they flow eastward from the mountains toward the Bay. Most important have been the decreased channel slopes of the Ngaruroro and Tutaekuri Rivers, which reach the shore of the Haumonana Littoral Cell, the reductions in the gradients having cut off the transport and delivery of gravel to that Cell's beaches, representing a significant loss of sediment sources important in maintaining its beach. Only the Tukituki River further to the south has continued to supply gravel to the Haumoana shore, its channel being positioned within the zone of land subsidence. Within the Bay View Littoral Cell, the gradient of the Esk River was also reduced by the development of the elevated dome, so it similarly is no longer a source of gravel to that shore, on supplying some sand.

Marshall's (1933) reconnaissance efforts immediately following the earthquake were directed primarily toward a detailed documentation of the elevation changes along the Hawke's Bay shores, complimenting his recently completed studies of its mixed sand-and-gravel beaches (published in 1927 and 1930). His assessments were directed toward determinations of the elevation changes relative to mean sea level based on the altered high-tide strand lines, including the position of the line of detritus deposited by the wash of waves on the beaches,

and displacements of intertidal marine life. Of interest was the degree of uplift of the Port's breakwater and the entrance to the Ahuriri Lagoon:

> The rise in level at the breakwater tide-gauge was 6 feet, and this appears to have been uniform throughout its extent. Calcareous seaweeds were growing generally on the surface of the piles of the wharf that extended northwards from the shoreward part of the breakwater. After the elevation these became bleached by the sun and indicated clearly the previous sea level. Between the breakwater and the entrance to Port Ahuriri the effect of the 6-foot uprise was most evident. The shore here had a wide apron of limestone boulders which had been shed from Scinde Promontory. Beneath the low-tide level these had become coated with calcareous algae, which died when exposed after the elevation. The remains of these soon bleached.

Marshall (1933) extended his observations of the extent of beach uplift to the north of Napier, finding that from Ahuriri to Petane (Bay View) the uplift continued to be about 6 feet (1.8 metres) but then gradually increased to approximately 6.5 feet (2.0 metres) at Tangoio, reaching a maximum of 9 feet (2.7 metres) at Moeangiangi, but then about 3 kilometres further north near Old Man's Bluff the amount of uplift rapidly decreased.

In an investigation of the elevation changes caused by the 1931 earthquake and the resulting processes of erosion, Single (1985) surveyed cross-shore profiles of the beach and backshore ridge at twelve sites north and south of Napier. His results are graphed in Figure 3-12, comparing his surveyed elevations of the beach ridge with the change in elevations documented by the resurvey of the railway line by the Public Works Department, where the railway was positioned immediately landward from the beach. Single's surveyed beach-elevation changes and the increased elevations of the railway line following the earthquake are largely in agreement, showing gradual increases in uplift toward the north, with subsidence on the order of 1 metre at the south end of this shore. The main difference between his beach surveys and those along the railway line occurs at Whirinaki immediately north of the mouth of the Esk River, having been affected by the shifting mouth of the river.
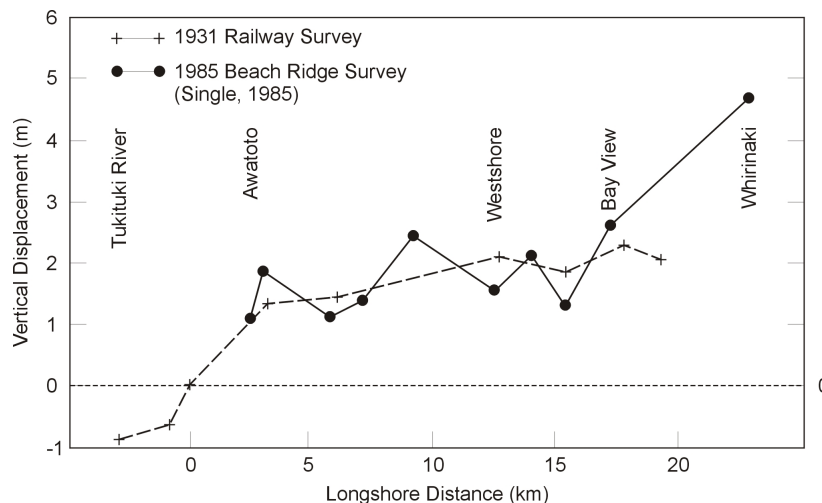
Figure 3-12: Land elevation changes along the shore of Hawke's Bay produced by the 1931 earthquake. The dashed line is from the 1931 resurvey of the railway line, while the solid curve is based on surveys by Single (1985) of profiles across the elevated beaches.   [*After* Single (1985)]

The changes in land elevations at the time of the Hawke's Bay earthquake significantly altered the morphology of this coast, a change that has had lasting importance in governing the susceptibilities of shorefront properties to erosion and flooding. The uplift and drainage of the Ahuriri Lagoon resulted in the Westshore area being changed from a narrow, low-lying spit that had experienced frequent wave overtopping events during storms, into an elevated gravel barrier ridge that now fronts a large expanse of land, including the region's commercial airport. There was also an immediate change in the fronting beach along Weestshore, with its width having increased in proportion to its slope and the degree of uplift. According to Campbell (1975, p. 161), uplift by the earthquake altered this beach from a "dangerous shingle bank to a placid sand expanse", and as a result it became increasingly popular for recreational swimming and surfing, continuing up to the present. According to Smith (1986), this fronting sand beach was formed by the onshore transport of the sand by the waves in the weeks to months after the uplift of this area, but during the subsequent decades the sand was progressively lost, being essentially gone by the late 1950s or 1960s.

With the added 1- to 2-metre increase in elevations of the barrier gravel ridge along the entire length of the Bay View Littoral Cell, and the widening of its beaches, the shore-front properties no longer experienced wave overwash and flooding during storms, and their susceptibilities to wave erosion have been significantly reduced. This similarly has been the case along the northern half of the Haumoana Cell, south to approximately Awatoto, even though its uplift was not as great (Figure 3-12). According to Marshall (1933, p. 33): "Two weeks after the earthquake it was found that the shingle beach on the south side of the breakwater (Pacific Beach in Napier) had been built out by as much as 1 chain." [1 chain = 20 metres], the extent of expansion expected to have been produced by the 2-metre uplift of the beach at that location, with its slope being on the order of 1-in-10. Local residents immediately noticed that the water had receded, leaving a considerable width of additional beach exposed above the high-tide levels. Prior to uplift and beach widening, storm waves were at times able to wash across the Marine Parade and flow into downtown Napier. The uplift by the earthquake therefore provided significantly increased protection from storms. However, the raised beach was later leveled, and together with the addition of debris from the ruined buildings in the city, provided the foundation for recreational development along the downtown area, including the addition of the Marine Parade parkland. A new seawall was constructed to protect this area from erosion and flooding.

While the coastal response to uplift produced by the 1931 earthquake, therefore, generally resulted in the increased elevations of the barrier gravel ridge and expansion of the beaches, providing additional protection to shore-front properties, the subsidence experienced south of Awatoto had the opposite effect, producing an immediate landward retreat of the shoreline by tens of metres, followed by a prolonged period of continued erosion. Investigations of this stretch of shore have concluded that the chronic erosion at Haumoana, Te Awanga and Clifton is still in part a response to the shoreline retreat induced by the coastal subsidence at the time of the Hawke's Bay earthquake, and can be expected to continue for an indefinite period into the future, especially with an accelerated rate of rising sea levels due to global warming (Smith, 1977; Daykin, 2010; Komar, 2005, 2010).

3.6 SUMMARY AND DISCUSSION

The tectonic setting of the Hikurangi Margin is of major importance to the range of potential hazards faced along the coast of Hawke's Bay, it being where two of Earth's tectonic plates collide with the oceanic Pacific plate sliding and being subducted beneath the Australian plate. The objectives of this chapter have included a consideration of the most extreme hazards created by future potential occurrences of subduction earthquakes and accompanying tsunami, much as have occurred along other subduction zones around the Pacific Ocean's "Ring of Fire". The Hikurangi Margin stood out as an anomaly in that while significant earthquakes such as the 1931 Hawke's Bay event had occurred on land within the Australian plate, there has been no historic earthquakes positively identified as having occurred on the subduction interface, certainly none having a significant magnitude. This raised questions concerning an occurrence sometime in the future — when might it occur, and what magnitude could it have? For the most part, recent research undertaken by seismologists and geologists has answered those questions. Their findings and conclusions include the following:

- The Hikurangi Margin is a "stick-slip" subduction zone, there being long periods (centuries to more than a thousand years) during which the plates are locked together, accumulating energy from the colliding plates;
- When the accumulated forces reach a level that exceeds the resisting friction at the interface between the two plates, a subduction earthquake occurs together with the likely generation of destructive tsunami waves;
- Large numbers of low magnitude events in recent decades on the subduction interface define the geometry of the subducting plate as it progressively deepens toward the west beneath the North Island, its shallowest depth being at the Hikurangi Trough where it begins its descent;
- The collision of the plates along this tectonic margin has resulted in the compression of the rocks within the overriding Australian plate, folding them into series of anticlines and synclines, also creating a large number of reverse faults that slope toward the west, merging at depth with the subduction interface;
- Movement on these faults within the Australian plate can produce moderately high-magnitude earthquake events, the 1931 Hawke's Bay earthquake being an example of the resulting impacts;
- A strong subduction earthquake on the plate interface is likely to trigger movement and earthquakes on reverse faults within the Australian plate, enhancing the destructive impacts and land-elevation changes;
- Investigations by geologists of sediments within lagoons and other bodies of water along this coast have found evidence for multiple prehistoric subduction earthquakes, some dating back thousands of years, documenting the sudden subsidence of those areas (e.g., the Ahuriri Lagoon region) at the times of major earthquakes, while other stretches of the coast (e.g., the Mahia Peninsula) have experienced net uplift, raising their elevations;
- There have been positive identifications of sand layers deposited by tsunami at coastal sites that have experienced subsidence (Te Paeroa Lagoon and Opoho), interpreted as having been generated by offshore earthquakes that occurred either on the subduction interface or within the Australian plate, possibly both;
- Estimates based on the geometry and other characteristics of the Hikurangi subduction zone yield estimates on the order of 300 to 600 years for the

recurrence periods of subduction earthquakes, with magnitudes potentially reaching 8.5, whereas sediments in coastal water bodies attributed to subsidence and tsunami generated by earthquakes suggest recurrence intervals of major events on the order of 1,000 to 1,500 years.

These conclusions reached in investigations undertaken by seismologists and geologists point to the potential extreme hazards faced by those living along the shores of Hawke's Bay, from earthquakes that could be substantially stronger and destructive than experienced in 1931, and with those occurring in the offshore also generating tsunami waves that far exceed the heights of those that have reached this shore from distant sources (e.g., the 1960 Chilean earthquake), having the potential for producing far greater impacts.

This tectonic setting of Hawke's Bay is also important to its short-term impacts from erosion and flooding, "short" representing frequent occurrences during this century at times of severe storms. The role of tectonics involves its controls on changes in land elevations along this coast, at present and in the recent past, with some stretches of shore subsiding while others have experienced a net uplift relative to the level of the sea. The local directions and rates of land-elevation changes, and the corresponding variations along this shore of the trends in relative sea levels, have in the long-term determined the morphologies of the contrasting coasts, the subsiding shores of the Haumoana and Bay View Littoral Cells versus the tectonically rising coast north of Tangoio with its high sea cliffs, and of the Mahia Peninsula with its "stair-step" series of uplifted marine terraces. The present-day hazards from erosion and flooding are governed in large part by recent tectonic events, foremost having been the 1931 Hawke's Bay earthquake that elevated a significant stretch of this shore, thereby increasing its stability, while the shore from Awatoto southward within the Haumoana Cell subsided, that occurrence 70 years ago likely still being a factor in its continued problems with erosion. Future hazards depend on the rates of rising sea levels that are predicted to accelerate due to global warming, and possible increases in storm intensities and the energies of their generated waves.

The local rate of increasing sea levels along the Hawke's Bay coast depends on the global rise in sea levels and its climate controls, plus the local changes in land elevations along its shores. There is uncertainty regarding the present-day directions and rates of land elevation changes, the main source of measurements being derived from GPS units along this coast, but with their records limited to less than a decade, and with the most important units closest to the shore being only 4 to 5 years in length, insufficient for determinations of statistically significant magnitudes of elevation changes. However, the directions are such that all six units in closest proximity of the shore indicate that subsidence is occurring, even at those sites that have experienced a long-term net uplift (the Mahia Peninsula). This ongoing subsidence is consistent with those found along other subduction zones such as the Cascadia Margin of the U.S. Pacific Northwest, in that with the Hawke's Bay shore being positioned close to the zone of plate subduction, the Hikurangi Trough, the locked plates drag down the overlying plate causing its subsidence. It follows that as experienced on other subduction zones, when a subduction earthquake does occur again along this margin, sometime in the future, it can be expected that with the release of tension within the subduction interface, this outer portion of the Accretionary Borderland will abruptly rise, possibly by on the order of 1 to 2 metres. On the other hand, if the subduction earthquake also triggers movement and earthquakes on faults within the overriding Australian plate, their combined effects could

result in an abrupt net rise of the land along some stretches of shore, while there are enhanced degrees of subsidence along other shores.

3.7 REFERENCES

Aitken, Jefley J. (1999) *Rocked and Ruptured: Geological Faults in New Zealand*: Reed Books, Auckland, 88 pp.

Atwater, B.F. (1987) Evidence for great Holocene earthquakes along the outer coast of Washington State: *Science*, v. 236, p. 942-944.

Atwater, B.F., and others (2005) *The Orphan Tsunami of 1700: Japanese Clues to a Parent Earthquake in North America*: U.S. Geological Survey in association with the University of Washington Press.

Beavan, R.J., and N.J. Litchfield (2009) *Sea Level Rise Projections Adjusted for Vertical Tectonic Land Movement Along the Hawke's Bay Coastline*: GNS Science Consultancy Report 2009/128, 42 pp.

Berryman, K. R. (1988) Tectonic geomorphology at a plate boundary: A transect across Hawke Bay, New Zealand: *Zeitschrift für Geomorphologie N.F.,* Suppl.-Bd. 69, p. 69-86.

Berryman, K. R. (1993a) Age, height, and deformation of Holocene marine terraces at Mahia Peninsula, Hikurangi subduction margin, New Zealand: *Tectonics*, v. 12, p. 1347-1364.

Berryman, K. R. (1993b) Distribution, age, and deformation of Late Pleistocene marine terraces at Mahia Peninsula, Hikurangi subduction margin, New Zealand: *Tectonics*, v. 12, p. 1365-1379.

Berryman, K. R., Y. Ota, and A. G. Hull (1989) Holocene paleoseismicity in the fold and thrust belt of the Hikurangi subduction zone, eastern North Island, New Zealand: *Tectonophysics*, v. 163, p. 185-195.

Burgette, R.J., R.J. Weldon, and D.A. Schmidt (2009) Intersiesmic uplift rates for western Oregon and along-strike variation in locking on the Cascadia subduction zone: *Journal of Geophysical Research*, v. 114, B01408.

Campbell, M. D. N. (1975) *Story of Napier 1874-1974*: Napier City Council.

Cochran, U., and others (2006) Paleoecological insights into subduction zone earthquake occurrences, eastern North Island, New Zealand: *Geological Society of America Bulletin*, v. 118, no. 9/10, p. 1051-1074.

Cole, J. W., and K. B. Lewis (1981) Evolution of the Taupo-Hikurangi subduction system: *Tectonophysics*, v. 72, p. 1-21.

Darienzo, M.E., C.D. Peterson, and C. Clough (1994) Stratigraphic evidence for great subduction-zone earthquakes at four estuaries in northern Oregon: *Journal of Coastal Research*, v. 10, no. 4, p. 850-876.

Daykin, N. (2010) *Haumoana Littoral Cell: Coastal Storm Analysis*: Asset Management Group Technical Report, Hawke's Bay Regional Council, 113 pp.

Froggatt, P. C., and R. Howorth (1980) Uniformity of vertical faulting for the last 7000 years at Lake Poukawa, Hawke's Bay, New Zealand: *New Zealand Journal of Geology and Geophysics*, v. 23, p. 493-497.

Gibb, J. G. (1980) *Late Quaternary Shoreline Movements in New Zealand*: Unpublished Ph.D. thesis, Victoria University, Wellington, 217 pp.

Goldfinger, C., C.H. Nelson, and J.E. Johnson (2003) Holocene earthquake records from the Cascadia subduction zone and northern Sand Andreas fault based on precise dating of offshore turbidites: Annual Review of Earth and Planetary Sciences, v. 31, p. 555-577.

Goldfinger, C., and others (2012) Turbidite Event History — Methods and Implications for Holocene Paleoseismicity of the Cascadia Subduction Zone: U.S. Geological Survey Professional Paper 1661-F, 170pp.

Grapes, Rodney (2000) *Magnitude Eight Plus: New Zealand's Biggest Earthquake*: Victoria University Press, 208 pp.

Hayward, B. W., and others (2006) Micropaleontological evidence of large earthquakes in the past 7200 years in southern Hawke's Bay, New Zealand: *Quaternary Science Reviews*, v. 25, p. 1186-1207.

Hemphill-Haley, E. (1995) Diatom evidence for earthquake induced subsidence and tsunami 300 years ago in southern coastal Washington: *Geological Society of America Bulletin*, v. 107, p. 367-378.

Henderson, J. (1933) The geological aspects of the Hawke's Bay earthquakes: *New Zealand Journal of Science and Technology*, v. 15, p. 38-75.

Hull, A. G. (1986) Pre-AD 1931 Tectonic subsidence at Ahuriri Lagoon, Napier, Hawkes Bay, New Zealand: *New Zealand Journal of Geology and Geophysics*: c. 29, p. 75-82.

Hull, A. G. (1987) A late Holocene marine terrace on the Kidnappers coast, North Island, New Zealand: some implications for shore platform development processes and uplift mechanisms: *Quaternary Research*, v. 28, p. 183-195.

Hull, A. G. (1990) Tectonics of the 1931 Hawkes Bay earthquake: *New Zealand Journal of Geology and Geophysics*, v. 33, p. 309-320.

Komar, P. D. (2005) *Hawke's Bay, New Zealand: Environmental Change, Shoreline Erosion, and Management Issues*: Report for the Hawke's Bay Regional Council.

Komar, P. D. (2010) Shoreline evolution and management of Hawke's Bay, New Zealand: Tectonics, coastal processes and human impacts: *Journal of Coastal Research*, v. 26, n. 1, p. 143-156.

Komar, P.D., J.C. Allan and P. Ruggiero (2011) Sea level variations along the U.S. Pacific Northwest Coast: Tectonic and climate controls: *Journal of Coastal Research*, v. 27, n. 5, p. 808-823.

Marshall, P. (1933) Effects of the earthquake on the coastline near Napier: *New Zealand Journal of Science and Technology*, v. 15, p. 79-92.

Pouderoux, H., J.-N. Proust, G. Lamarche, A. Orpin and H. Heil (2012) Postglacial (after 18 ka) deep-sea sedimentation along the Hikurangi subduction margin (New Zealand): Characteristics, timing and origin of turbidites: *Marine Geology*, v. 295-298, p. 51-76.

Satake, K., K. Shimazaki, Y. Tsuji, and K. Ueda (1996) Time and size of a giant earthquake in Cascadia inferred from Japanese tsunami records of January 1700: *Nature*, v. 379, p. 246-249.

Single, M. B. (1985) *Post-Earthquake Beach Response, Napier, New Zealand*: Master of Arts Degree, University of Canterbury, 150 pp.

Smith, R. K. (1977) *Coastline Changes and Beach Sediments in Southern Hawke Bay*: Unpublished report, Ministry of Works and Development, Napier.

Wallace, L. M, J. Beavan, R. MCaffrey, and D. Darby (2004) Subduction zone coupling and tectonic block rotation in the North Island, New Zealand: *Journal of Geophysical Research*, v. 109, B12406.

Wallace, L. M., and others (2009) Characterizing the seismogenic zone of a major plate boundary subduction thrust: Hikurangi Margin, New Zealand: *Geochemistry, Geophysics, Geosystems*, v. 10, n. 10, 32pp.

Wallace, L. M., and others (2010) Subduction systems revealed: Studies of the Hikurangi Margin: *EOS, Transactions, American Geophysical Union*, v. 91, no. 45 (9 November 2010), p. 417-418.

Wallace, L. M., and J. Beavan (2010) Diverse slow slip behavior at the Hikurangi subduction margin, New Zealand: *Journal of Geophysical Research*, v. 115, B124012, 20pp.

Witter, R.C., H.M. Kelsey, and E. Hemphill-Haley (2003) Great Cascadia earthquakes and tsunamis of the past 6,700 years, Coquille River estuary, southern coastal Oregon: *Geological Society of America Bulletin*, v. 115, p. 1289-1306.

4 Measured Tides and Extreme Water Levels

4.1 INTRODUCTION

The changing levels of the tides can be a significant factor in causing beach and property erosion, controlling the mean water elevations atop which waves break and swash up the sloping beach. Whether or not a storm results in property damage can depend in large part on the timing of the tide and occurrences of the highest storm waves, the impacts being greatest if the waves reach the shore coincident with an extreme spring tide. Also important is the degree to which the levels of the measured tides are above their predicted elevations, for example raised by a storm surge. These are the main process components in models that have been developed to evaluate erosion and flooding hazards, wherein the measured tides and swash runup levels of the waves at the shore are added to determine the total water elevations, which can then be compared with the elevation of the junction between the beach face and backshore property (the base of a sea cliff or the toe of foredunes). This model has seen frequent application in our analyses of erosion hazards along the shores of the U.S. Pacific Northwest, the states of Oregon and Washington (Ruggiero et al., 2001; Komar et al., 2013). This model will similarly be employed in our analyses of the erosion hazards along the shores of Hawke's Bay, after analyses have been completed of the tides, the deep-water waves, and nearshore processes of wave breaking and swash runup on the Hawke's Bay beaches.

The objective of this chapter is to examine the tides that have been measured by the Port of Napier's gauge, to document the frequency distribution of its elevations. In assessments of the erosion and flooding hazards, of primary interest are the extreme magnitudes of the highest water levels reached by the measured tides. However, a documentation of these extremes derived from the Port's gauge is limited by the shortness of its record, hourly measurements being available only since 1989, and with a gap of missing data from 1995 to November 1998. Considering this limitation in the available measurements, our goal in this chapter is primarily to determine the general distribution of the measured water elevations, providing some indication of their potential extremes. Assessments of the long-term extremes will be based in part on a review of past investigations by others of storm surges along the shores of New Zealand, in order to provide a better understanding of their origins and magnitudes during the most severe storm events.

4.2 TIDES ALONG THE COASTS OF NEW ZEALAND

The tide is a periodic hour-to-hour rise and fall in the level of the sea during the span of a day, generated by the gravitational attraction of the Moon and Sun on the ocean's water, it being the relative motions of the Earth, Moon and Sun in their orbits that account for most of the

tidal variations. The actual motions of the generated tides are then governed by the rotation of the Earth on it axis (the Coriolis "force"), with their complexity further enhanced by the irregular depths of the oceans and outlines of the shores such as the presence of capes and embayments. Being generated by these planetary forces, the predictions are referred to as the "astronomical tides", capable of being calculated well into the future but with the variations differing from site to site along the coast. In spite of the complexities in their generation and the multiple factors that determine their motions, model-predicted tides are on average reasonably close to the tides measured by gauges, so reasonably accurate predictions of the astronomical tides can be made. This is true for the coasts of New Zealand (Walters et al., 2001), although as discussed below its tides have unusual characteristics that differ from those observed on most other coasts.

Tides are the most significant factor affecting variations in mean water levels along the New Zealand coast; overall, they account for 96% of the variations (Goring, 1997). Other oceanic and atmospheric processes give rise to the remaining 4% of the variations found in the measured tides, their hour-to-hour departures from the predicted astronomical tides. These departures include seasonal variations in monthly-mean water levels caused by changes in water temperatures and ocean currents, but the most significant departures generally are storm surges created by the winds and lowered atmospheric pressures of cyclonic storm systems, which on the New Zealand coast can raise the measured tides above predicted levels by on the order of a metre, potentially having an important role in producing episodes of erosion and flooding.

New Zealand's tides are semidiurnal, there being two high tides per day having nearly the same heights, separated by low tides that similarly have nearly identical levels. However, the tides vary considerably from place to place along the coast, in both their amplitudes and in their general patterns of varying water levels. There is a monthly variation in the tidal ranges, but this pattern of change differs markedly between the west and east coasts of New Zealand. On the west coast (the Tasman Sea) there is a monthly variation of spring tides when the range in greatest, and neap tides when the range is lowest, the spring tides occurring when the forces of the Moon and Sun are aligned to reinforce one another (that is, at times of the full and new Moon); the neap tides occur when the forces of the Moon and Sun oppose one another. This is the pattern and cause of spring versus neap monthly variations in tides generally found throughout the world's oceans. However, the monthly variations in the tides on the east coast of New Zealand differ in their relationship to the gravitational forces of the Moon and Sun. While the tides are generally semidiurnal with two highs and two lows each day, one high tide reaches a slightly higher elevation than the other (there being a small diurnal inequality). A more significant difference in the tides on New Zealand's east coast is that while there is a spring versus neap cycle, it does not correspond to the astronomical alignments of the Moon and Sun; the highest tides do not occur during full and new Moon when their forces combine. The monthly variation on the east coast is instead produced by the varying distance of the Moon from the Earth, this distance determining the force of attraction by the Moon on the Earth's ocean water, being greatest when the Moon is closest to the Earth at perigee in its monthly orbit, resulting in the highest tidal range of the month (Goring, 1997). The lowest tidal range occurs at apogee, when the Moon is farthest from the Earth. Every seven months the full or new Moon coincides with the Moon's perigee, and this produces somewhat larger than normal perigean spring tides, the highest predicted astronomical tides of the year.

Table 4-1 lists the water-level statistics for the Hawke Bay predicted astronomical tides, published in the *New Zealand Nautical Almanac*, based on harmonic analyses of the measured tides to determine their primary tidal constituents. The water levels listed are related to two elevation datums: the Chart Datum (CD) that generally is used in reporting tidal elevations and water depths, while the LINZ datum is relative to mean sea level (MSL) and is employed in land surveys. The Chart Datum is defined as corresponding to the predicted Lowest Astronomical Tide (LAT) for that tide gauge, this choice having the result that all of the predicted tides would be expected to have positive values. However, according to the Land Information Agency of the New Zealand government, the CD datum for the Napier tide gauge is more precisely 0.06-metre (www.linz.govt.nz), so that extreme low predicted tides could in rare instances have small negative values.   It is seen in Table 4-1 that the two datums for the long-term predicted mean sea level (MSL) differ by 0.95 metre, which is also the value we have obtained in our analyses for the mean sea level based on measurements derived from the Port of Napier's tide gauge.

Table 4-1: The predicted astronomical tides for Hawke Bay.
(*New Zealand Nautical Almanac*)

Tidal Level	LINZ (metres)	Chart Datum CD (metres)
HAT	1.05	2.00
MHWS	0.96	1.91
MHWN	0.61	1.56
MSL	0	0.95
MLWN	-0.56	0.39
MLWS	-0.93	0.02
Chart Datum	-0.95	0

It is seen in Table 4-1 that the mean high water level at the time of spring tides (MHWS) for Hawke Bay, 1.91-metre CD, is on average 0.35 metre higher than the 1.56-metre level during neap tides (MHWN). The range of the tides based on the difference between the mean high spring tides (MHWS) and spring lows (MLWS) is about 1.9 metres. The highest predicted astronomical tide (HAT) of the year is 2.00-metres CD, this essentially being the full tidal range of predicted water levels for Hawke Bay. Having this range, the tides are classified as "microtides" by Davies (1964), only just reaching the "mesoscale" range at their maximum. Therefore, the ranges of tides are modest in comparison with those that occur on most coasts.

4.3 MAGNITUDES OF MEASURED TIDES IN HAWKE BAY

Tide data have been collected by the Port of Napier's Geddis Wharf gauge since 1989, their measured elevations being graphed in Figure 4-1, showing that there is a significant 3-year gap from 1995 to 1999. Furthermore, the pre-1995 data were recorded to only 1-centimetre resolution. As a result, while tide predictions have been available for Hawke Bay and its harbor for more than a century, quality measurements are available for only little more than a decade. Of interest, it is evident in Figure 4-1 that beginning in about 2008 there have

been occurrences of unusually high tides, including the highest water level measured since 1989. This grouping of high water levels in recent years is likely due to occurrences of more extreme storms and their surges, the trend for the rise in sea level based on the Port's tide-gauge record having been only 1.9 mm/year (Chapter 8), amounting to only 2 cm during the decade of measurements, therefore not accounting for these recent elevated water levels.
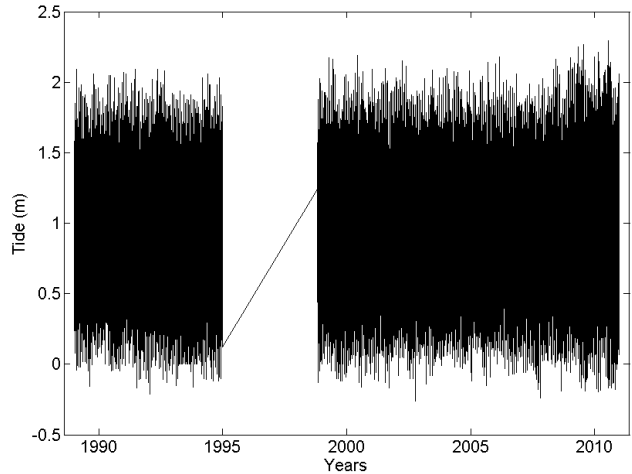
Figure 4-1: The tides measured by the Port of Napier's gauge since 1989, referenced to the Chart Datum (CD) that corresponds approximately to the Lowest Astronomical Tide (LAT). The predicted mean sea level is 0.95 metre CD (Table 4-1).

Of interest are the monthly variations and the general distribution of measured water elevations throughout a year, respectively graphed in Figures 4-2 and 4-3 based on data from the year 2010, representative of the recent increase in measured levels. Most apparent in Figure 4-2 are the monthly cycles with superimposed variations between the highest and lowest ranges of tides. Occasional spurious hourly measurements are evident in this graph, there being both abnormally high and low water levels, concluded in most cases to being erroneous data.
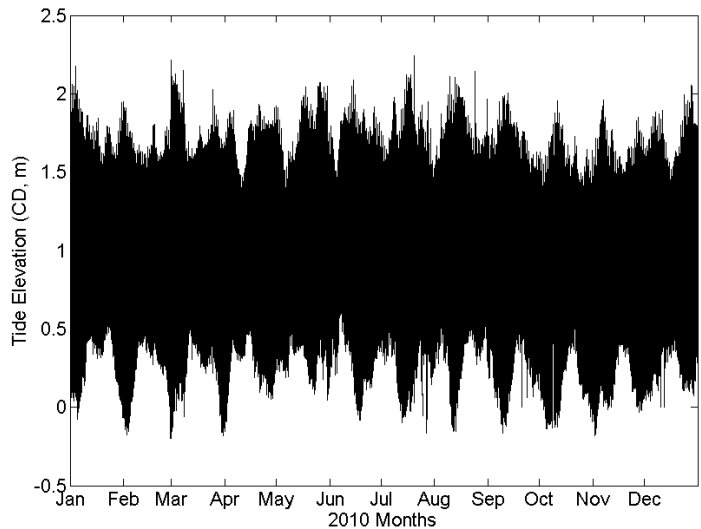
Figure 4-2: The hourly measured tides during 2010, showing the monthly cycles.

4 - 4

Histograms for the frequency distribution of the hourly-measured tides during 2010 are presented in Figure 4-3, graphed using both linear and log scales for the numbers of observations. The linear plot, shown in gray, is the conventional form of graphing distributions, whereas the log plot in red is more informative in our applications to hazard assessments in that it emphasizes the few occurrences of the extreme highest measured tides (Komar and Allan, 2007). Based on the distribution using the log scale, it is seen that the most extreme measured tides (5 occurrences) are on the order of 2.25-metres CD, 0.25 metre above the predicted Highest Astronomical Tide (HAT), but with the surge magnitudes that likely caused those extremes undoubtedly having been substantially greater since they did not actually occur during the maximum HAT predicted level. The mean value of all measured tidal elevations during 2010 is 0.95-metre CD, which as noted above corresponds to that obtained when analyzing the predicted astronomical tides over a number of decades; this value, therefore, represents the Mean Sea Level (MSL) at least for the year 2010, and probably close to the MSL over a number of years since the trend of change is relatively small (Chapter 8). The modes of most frequent occurrences in Figure 4-3 are at approximately 0.5- and 1.5-metres CD, which respectively depend on the ranges of the daily low and high tides, although these modes differ somewhat from the predicted mean low tides and mean high tides according to Table 4-1. An overall asymmetry is evident in the distribution graphed in Figure 4-3, with the maximum elevation (2.25-metres CD) being 1.30 metres above the MSL, whereas the lowest measured tide is 1.10 metres below MSL. It is likely that this skewness toward higher measured tides has for the most part been produced by storm surges that enhanced the high water levels, amounting to 10s of centimetres above the predicted tides and accounting for the most extreme measured high water levels.
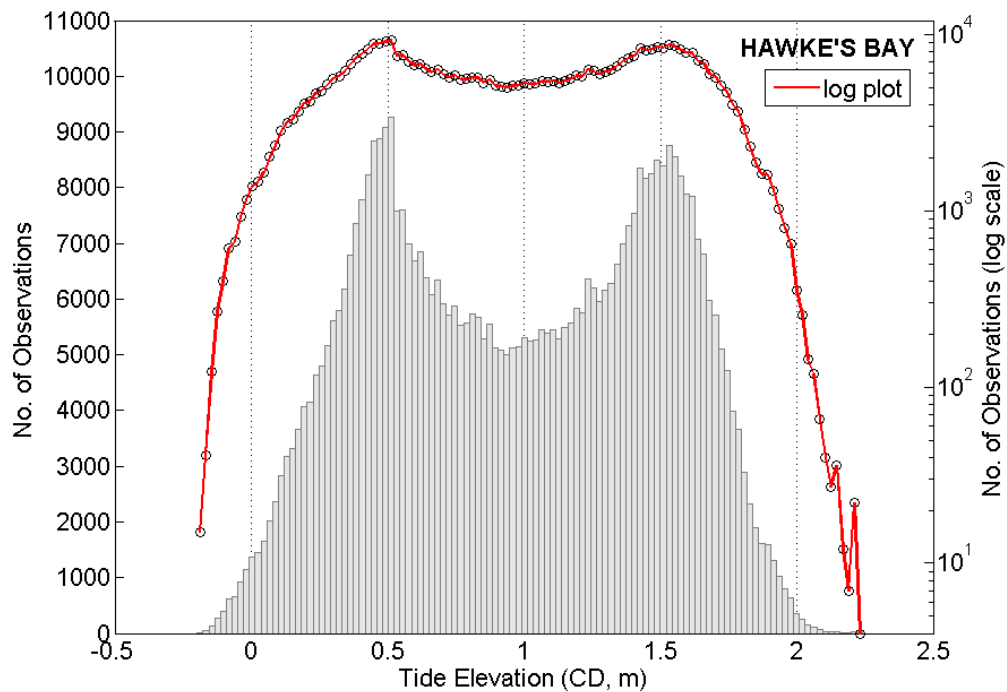
Figure 4-3: Frequency distributions of the hourly measured tidal elevations during the year 2010, the numbers of observations graphed on linear and log-scale axes.

4.4 SEASONAL VARIATIONS IN MEAN WATER LEVELS

While the above analyses determined that the mean value of all measured tidal elevations during 2010 was 0.95-metre CD, this also being the mean sea level according to the predicted astronomical tides, there potentially could be seasonal variations in the monthly-mean water levels that are important to coastal erosion and flooding, particularly if the monthly means are elevated during the storm season of most extreme waves, contributing to the total water levels. These seasonal variations in the monthly mean water levels recorded by tide gauges have been demonstrated to be caused by a number of processes: water temperatures, with the warmer water of the summer commonly producing a thermal expansion and elevated water levels; the Coriolis effect due to the rotation of the Earth, producing a deflection of ocean currents that act to turn their flow to the right in the Northern Hemisphere, to the left in the Southern Hemisphere; the monthly occurrences of storms and their surges, generally elevating the tides but at times lowering the water levels; and annual variations such as the El Niño/La Niña range of climate events, which can affect multiple processes including the water temperatures and ocean currents.
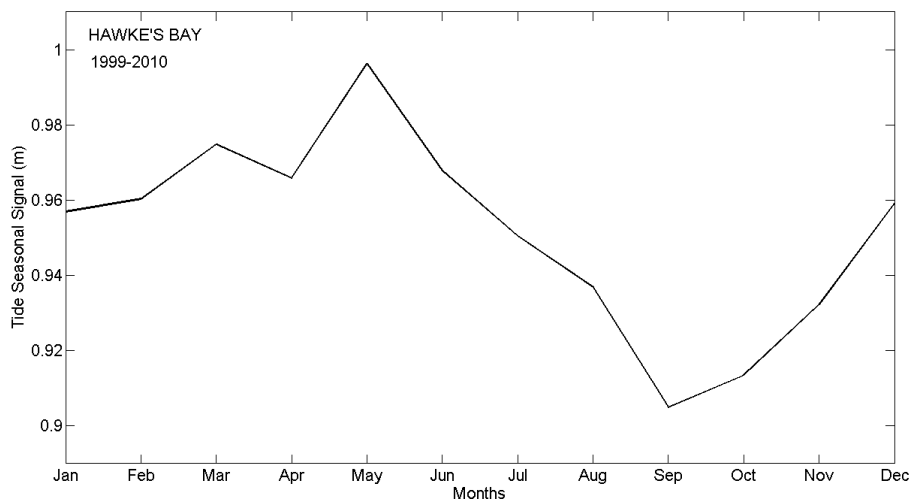
Figure 4-4: The seasonal cycle of monthly-mean water levels, calculated from the 1999-2010 Port of Napier's hourly tide-gauge measurements.

An analysis of the monthly-mean water levels based on the 1999-2010 "quality" measurements from the Port of Napier's tide gauge is presented in Figure 4-4, showing that the highest water levels occur during the winter months of roughly March to June, with a marked decline into the summer, reaching a low in September. A similar analysis but limited to the year 2010, yielded almost identical results. This monthly variation for Hawke Bay contrasts with the more commonly found seasonal cycle where the highest monthly-mean water levels occur during the summer to early fall, a result of the warmer water and its thermal expansion. That typical seasonal variation has been reported by Bell et al. (2000) for other New Zealand tide gauges, with the variation amounting to about 0.2 metre, the highest water levels occurring during the summer. It is seen here in Figure 4-4 for Hawke Bay that the difference between the winter and summer amounts to only about 0.1 metre, representing a factor in having contributed to the total water levels and episodes of coastal erosion. Although we have not undertaken analyses to account for the factors that produce this

inverse seasonal variation for Hawke Bay, it is likely that the elevated water levels of this magnitude are produced by storms and their surges that dominate the winter, while the effects of seasonal variations in water temperatures are negligible.

4.5 STORM SURGES ON THE COASTS OF NEW ZEALAND

The tidal statistics listed in Table 4-1 for Hawke Bay (Napier) are the predicted astronomical tides, whereas our analyses undertaken here have been the tides measured by the Port's gauge, with the 2010 record having been used to determine the general distribution of water-level elevations (Figure 4-3). Of concern in our examination of coastal erosion and flooding hazards are occurrences when the measured tides are substantially higher than predicted, which generally happens during the generation of a surge at the time of a major storm event, when its intense winds and low atmospheric pressures combined to pile water up along the coast. Typically a storm surge achieves significant levels for only a day or two at the height of the storm, but can persist for several days depending on the duration of the low pressures and winds, and the rate at which the storm passes through the area. The objective here is to broaden our consideration of storm surge occurrences along the coasts of New Zealand, in order to provide a better documentation of their extremes than permitted by the short-term tide-gauge record from Hawke Bay.

According to the analyses by de Lange (1996), on average 50% of the storm surge elevations experienced along the New Zealand coast are produced by the lowered atmospheric pressures of the storm's center, the other 50% being caused by the strong winds of the storm. The atmospheric pressure component is generally termed the "inverse barometer effect", wherein the sea surface elevation increases by 0.01 metre (1 centimetre) for each 1-millibar decrease in the atmospheric pressure. This correlation is based on a static response of the sea level to the reduced atmospheric pressure at the center of the storm's cyclonic rotation. However, the dynamic effects of a moving storm system can alter this correlation, shown by Goring (1995) in his analyses of storm surges recorded by tide gauges around the coasts of New Zealand; included in his analyses were tides measured by the Port of Napier's gauge from September 1986 through December 1988. In general, Goring found that the storm surge response depends on the exposure of the site to the predominant westerly winds, such that along the west coast the surge response was higher than the inverse barometer static correlation, whereas along the more sheltered east coast the response was generally smaller. However, during some events on the east coast, Goring found that the response could in fact be greater. To further complicate matters, cases were found where the storm surge was measured well in advance of the arrival of the storm, and in a few cases the storm surge displayed a secondary peak following the passage of the low-pressure system. Such unusual responses have been interpreted as resulting from the generation of coastal-trapped waves, in effect a long-period bulge in the level of the sea that is held against the coast by refraction over the sloping continental shelf, with its movement affected by the Earth's rotation (the Coriolis force). Such surges have been observed along both the east and west coasts of New Zealand, moving southward along the west coast and northward along the east coast (Heath, 1979; Stanton, 1995). If this alongcoast movement corresponds to the path of the storm that generated the surge, the trapped shelf wave could amplify the rise in the water levels directly associated with the low atmospheric pressure and winds within the storm, thereby

enhancing the total surge elevations, but the trapped wave can also travel along the coast independently from the storm.

Analyses by de Lange (1996) of measured storm surges found that the maximum expected elevations for the New Zealand coast are in the range 0.8 to 1.0 metre, having achieved those levels with return periods of 100 years or longer. Therefore, a value of 0.9 metre has commonly been added to the MHWS tidal elevation to provide an estimate of potential storm surge elevations having a 1% probability of occurrence each year (i.e., the 100-year event). This would be significant on the coast of Hawke's Bay where the predicted high tides are relatively modest, about 1 metre above mean sea level (Table 4-1), significant to the extent that the measured high tide elevated by a storm surge could be doubled to be on the order of 2 metres above mean sea level. In terms of the distribution of measured tides graphed in Figure 4-2 using the Chart Datum (CD), an extreme surge could reach an elevation of 3 metres CD, some 0.75-metre higher than the highest measured tides during 2010. The effect on a typical mixed sand-and-gravel Hawke's Bay beach is that the mean-water shoreline could advance landward by some 15 to 20 metres, which at high tide brings the water much closer to shore-front properties such that the swash runup of the waves also generated by the storm could forcefully impact and erode those properties.

Detailed analyses by de Lange and Gibb (2000) of occurrences of storm surges measured between 1960 and 1998 by tide gauges in Tauranga Harbour on the Bay of Plenty demonstrated the occurrence of decadal variations in response to cycles in Earth's climate. In particular, they found that there was a marked shift in the magnitudes and frequencies of storm surges in about 1976; the period 1960-1976 showed a greater occurrence of surges compared with 1976-1998. They suggested that this change was a response to a shift of the Inter-decadal Pacific Oscillation (IPO), which reversed its phase in about 1976. A phase shift in the IPO includes a coherent change in sea-surface temperatures spanning the entire Pacific Ocean, affecting the paths of tropical cyclones in the southwest Pacific, and also representing a shift in the dominance of El Niños versus La Niñas between the separate phases; the 1960-1976 phase was dominated by La Niñas, whereas El Niños prevailed during 1976-1998. As a result, there is an association between storm surges that are both more frequent and achieve higher elevations, and the IPO La Niña phase when there are more frequent storms. In discussing these results, de Lange and Gibb (2000) pointed out that the assessments of coastal hazards due to occurrences of storm surges have largely been based on measurements obtained from tide gauges during the post-1976 phase of the IPO when the magnitudes and frequencies of surges were reduced, so the results can be expected to under-predict the hazards during the opposite IPO phase. This distinction is significant in that climatologists have concluded that the IPO shifted its phase in about 1998, having returned to a condition comparable to that in 1960-1976 with more frequent La Niñas. This may account for the higher water levels of the measured tides in Hawke's Bay since 1999 than seen in the earlier data, evident in Figure 4-1, and in particular the marked increase since 2009.

The magnitudes of storm surges in Hawke Bay and the climate effects on their frequencies and magnitudes have received little attention by coastal scientists and engineers due to the availability of only a short record of tide measurements, 1989 to the present. The one significant study is the report by Worley (2002), which analyzed measurements during the 4-year period from 1 November 1998 to 31 October 2002. The objective was to establish the criteria to be used in the design of the Port's facilities, with their analyses having included

assessments of extreme waves and tides. The mean water level was calculated for each year from the measured tides, and was found to vary from 0.87 to 0.95-metre CD, which is reasonably consistent with the mean sea level of 0.95-metre CD for this site's predicted astronomical tides (Table 4-1) and found in our analysis of the 2010 record (Figure 4-3. A tidal constituent analysis was undertaken by Worley (2002), of the same type employed to derive the predicted tides, but were limited to one year, 27 May 2001 to 3 June 2002, at that time the longest set of continuous measurements without missing data. Of particular interest in their analysis were the "tidal residuals", the portion of the water-level variation that is not accounted for by the astronomical tides, having resulted mainly from occurrences of storm surges. Eighteen storm surges were identified in that 1-year record when measured tidal elevations reached at least 0.75-metre higher than the predicted tides. The results of an extreme-value analysis of the residuals showed that they are on the order of 0.9 metre, which is consistent with the results obtained by de Lange (1996) based on his analyses of storm surges along the entire coast of New Zealand. As noted above, this value is commonly added to the predicted MHWS tide elevation (Table 4-1) to provide an estimate of potential storm surge elevations having a 1% probability of occurrence each year; for Hawke's Bay this would yield a water level of 2.86-metres CD or 1.91-metre LINZ, that is, nearly 2 metres above the mean sea level.

As an alternative assessment of extreme measured tides for Hawke Bay, one that provides a less conservative estimate of total water levels, Worley (2002) undertook a joint probability analysis that combined the astronomical tides and tidal residuals. Based on 18,000 Monte Carlo simulations, effectively representing 1,000 years of simulated tides, the result was that the 100-year extreme is 2.70-metres CD (1.75-metres LINZ). Beyond that, Worley (2002) also added 0.2 to 0.4 metre as the potential rise in sea level during the next 50 years, to project future water levels in the range 2.9 to 3.1-metres CD (2.0 to 2.9-metres LINZ), used in their applications for the design of the Port of Napier facilities. These results are also applicable to analyses of potential extreme water levels on the Hawke's Bay shores, important in assessments of coastal erosion and flooding hazards.

4.6 REFERENCES

Bell, R. G., D. G. Goring and W. P. de Lange (2000) Sea-level change and storm surges in the context of climate change: *IPENZ Transactions*, v. 27, no. 1/Gen, p. 1-10.

Davies, J. L. (1964) A morphogenic approach to world shorelines: *Zeitschrift für Geomorphologie*, v. 8, p. 127-142.

de Lange, W. P. (1996) Storm surges on the New Zealand coast: *Tephra*, v. 15, no. 1, p. 24-31.

de Lange, W. P., and J. G. Gibb (2000) Seasonal, interannual, and decadal variability of storm surges at Tauranga, New Zealand: *New Zealand Journal of Marine and Freshwater Research*, v. 34, p. 419-434.

Goring, D. G. (1995) Short-term variations in sea level (2-15 days) in the New Zealand region: *New Zealand Journal of Marine and Freshwater Research*, v. 29, p. 69-82.

Goring, D. G. (1997) Tides around New Zealand: a pictorial essay: *Water & Atmosphere, NIWA*, v. 5, n. 1, p. 13-16.

Heath, R. A. (1979) Significance of storm surges on the New Zealand coast: *New Zealand Journal of Geology and Geophysics*, v. 22, p. 259-266.

Komar, P.D., and J.C. Allan (2007) A note on the depiction and analysis of wave-height histograms: *Shore & Beach*, v. 75, n. 3, p. 1-5.

Komar, P.D., J.C. Allan and P. Ruggiero (2013) U.S. Pacific Northwest coastal hazards: tectonic and climate controls: *Coastal Hazards*, edited by C.W. Finkl, Springer, p. 587-674.

Ruggiero, P., P.D. Komar, W.G. McDougal, J.J. Marra, and R.A. Beach (2001) Wave runup, extreme water levels and the erosion of properties backing beaches: *Journal of Coastal Research*, v. 17, no. 2, p. 407-419.

Stanton, B. R. (1995) Sea level variability along the west coast of New Zealand: *Journal of Physical Oceanography*, v.25, p. 1265-1272.

Walters, R. A., D. G. Goring and R. G. Bell (2001) Ocean tides around New Zealand: *New Zealand Journal of Marine and Freshwater Research*, v. 35, p. 567-579.

Worley (2002) *Port of Napier: Design Criteria Report for Outer Breakwater Extension*: 20 December 2002 report to the Port of Napier, Worley Infrastructure Pty Ltd, Perth, Australia.

5 The Hawke Bay Wave Climate

5.1 INTRODUCTION

The heights, periods and energies of storm-generated waves are the dominant environmental factors important on most coasts, with their extremes accounting for episodes of beach erosion and impacts to backshore properties. Important is the development of what is termed the "wave climate", a documentation of the waves that have been experienced during past decades, including projections of the potentially most extreme storm-wave events that could occur in the future, posing a threat to the coast and its infrastructure (Komar et al., 2010).

The establishment of wave climates has been of fundamental significance to coastal engineers and scientists, the former requiring them in the design of ocean and coastal structures so they can withstand the forces of the most severe storm waves. The requirements by coastal scientists are similar, for example in the establishment of coastal-hazard zones to maintain homes and other developments safe from severe storm events. This places demands on the assessment of a wave climate, ideally one based on wave data that spans several decades of measurements by buoys, or is derived from storm hindcast analyses. Important is that reasonably confident projections can be made of the most extreme waves expected during a century or longer (e.g., the 100-year event, the storm that has a 1% probability of occurring each year). This projection becomes one of the most significant parameters used in coastal engineering applications and in hazard assessments.

The goal of this chapter is to develop a deep-water wave climate for Hawke's Bay, required in considerations of its coastal hazards, those existing at present and the potentially enhanced extremes that could occur with future increased storm intensities and wave heights. Important will be an application of the resulting wave climate in analyses of wave breaker heights and swash runup levels on the Hawke's Bay beaches (Chapter 6), which depend on both the deep-water wave heights and periods (and also on the slope of the beach). In Chapter 7 the vertical component of the calculated runup will be added to the measured tides to determine the total water elevations, their extremes then being compared with the elevations of the beaches and backshore properties to assess the potential hazards from erosion and flooding.

5.2 STORMS AND WIND-GENERATED WAVES

Waves along the coasts of New Zealand are generated primarily by the dominant westerly winds and superimposed extratropical storm systems that occur in the Southern Hemisphere between 30°S and 70°S. New Zealand itself extends from 34°S to 47°S, with Hawke's Bay centered at about 39°S, within this zone of westerly winds but with the strongest storms occurring over the Southern Ocean between New Zealand and Antarctica. During the winter the belt of westerly winds and storms shifts to the north, extending across New Zealand with the storms crossing the land from west to east.

The clockwise pattern of winds surrounding the lows in atmospheric pressures of these cyclonic storms produce onshore winds to their south sides as they cross the east coast, locally generating the highest waves. Located on the east coast on the North Island, Hawke's Bay is on the lee shore relative to the storm tracks, and as expected the wave heights are on average smaller than occur along the west coast. However, due to the alignment of the country in a northeast-southwest direction, waves generated in the Southern Ocean by the strongest storms can progress northward and travel up the east coast, reaching Hawke's Bay from the south to southeast.

Tropical cyclones originating during the summer in the equatorial region to the north of New Zealand can generate waves that have the potential for reaching Hawke's Bay from the northeast. However, according to the analyses presented in this chapter, waves with significant energies generated by tropical cyclones appear to be rare on the Hawke's Bay coast, generally representing a minor contributor to its wave climate.

Of interest in this chapter are the waves generated by the westerly winds and storms, reaching the shores of Hawke's Bay. Data for the heights and periods of the waves, serving as the basis for the development of a wave climate, are available from investigations that have relied on wave hindcast methodologies, assessments of the wave parameters derived from the storm-wind velocities, fetch distances (areas), and storm durations. In August 2000 the Port of Napier installed a wave buoy in 16-metres water depth offshore and to the north of its breakwater. The hourly measurements of the wave heights and periods collected during the past 13 years serve as the primary basis in this study for the development of a wave climate for Hawke Bay. Here we first review the past studies that have analyzed the waves applying hindcast techniques, and the reports that have summarized the direct measurements of wave heights and periods collected by the Port's buoy. Following those reviews of past studies, we expand the analyses of the buoy data with the objective of developing a deep-water wave climate that in Chapter 6 can be applied to compute the beach processes of wave breaking and swash runup levels, required in the hazard assessments.

5.3 WAVE DATA SOURCES

5.3.1 Hindcast data

Prior to the deployment of the Port of Napier's buoy in August 2000, the only direct assessment of the wave conditions in Hawke Bay was the limited collection of visual observations spanning brief periods of time. This was generally true for the entire coast of New Zealand, and for that reason Gorman et al. (2003a, 2003b) undertook analyses of the wave climates based on hindcast methodologies, for storms that occurred during the 20-year period 1979-1998. Their analyses still provide the most detailed assessments of the wave climates around the coast of New Zealand, including that for Hawke Bay.

Their hindcasts were derived using the wave generation model WAM (WAve Model), based on data for the daily winds across the ocean's expanse. In their analyses they included the latitudes from 10°S near the Equator southward to the coast of Antarctica, and 100°E to 220°E in longitude, New Zealand being positioned approximately at the center of that area. The hindcasts were undertaken at 3-hour intervals for 1979 through 1998. In the first of their pair of companion papers, Gorman et al. (2003a) presented the hindcast results and

compared them with wave-buoy data at eight representative sites around the New Zealand coast (Gisborne being closest to Hawke's Bay). When the comparison was with a buoy that is well offshore and fully exposed to the waves, good agreement was found, whereas when the comparison was with an inshore buoy (e.g., Gisborne) there was as expected poorer agreement due to the effects of wave refraction and sheltering by the land. In their second paper, Gorman et al. (2003b) compared the WAM hindcast data of deep-water wave heights and periods with those measured by altimeters from satellites. It was found that the long-term mean significant wave heights from the hindcasts were generally 0.3- to 0.5-metre lower than wave heights from the satellite altimeter; the distributions of the hindcast significant wave heights matched the satellite data reasonably well, but tended to underestimate the occurrences of the more extreme-wave events. It is uncertain whether this disagreement represents a systematic error in the satellite measurements or in the hindcast results.

The wave hindcasts by Gorman et al. (2003a, 2003b) show the expected patterns of wave conditions along the coasts of New Zealand. The largest mean significant wave heights were found in the Southern Ocean where the westerlies are strongest and have long fetches around Antarctica. North of that band the waves propagate to the north along both the west and east coasts, with diminishing mean wave heights, especially along the east coast due to the blocking effect of the land mass. Figure 5-1 from their study contains graphs of the significant wave heights versus the simultaneously evaluated spectral-peak wave periods, while Figure 5-2 presents the distributions of significant wave heights derived from their 20-year hindcasts at the six selected deep-water sites. The site to the east of the North Island (latitude 34.875°S, longitude 168.750°N) and closest to Hawke Bay shows the mode of greatest significant wave height occurrences being about 2 metres, while the maximum significant wave height during the 20-years hindcast was 10.7 metres. Figure 5-1 shows that the highest storm wave heights corresponded with wave periods centered at about 12 to 13 seconds.
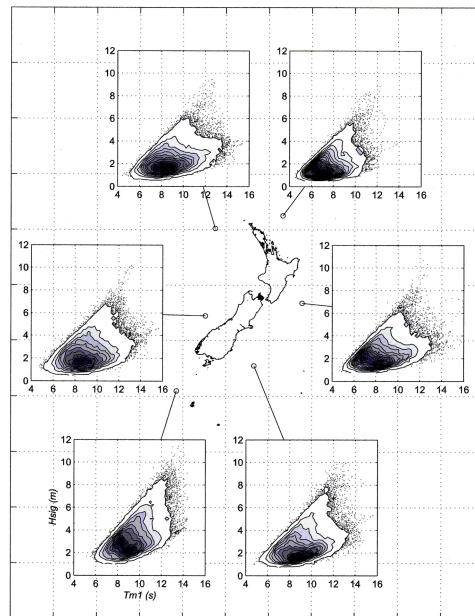
Figure 5-1: "Scatter diagrams" of significant wave heights versus periods around the coast of New Zealand, based on the 20-year WAM hindcasts. [*From* Gorman et al. (2003b)]
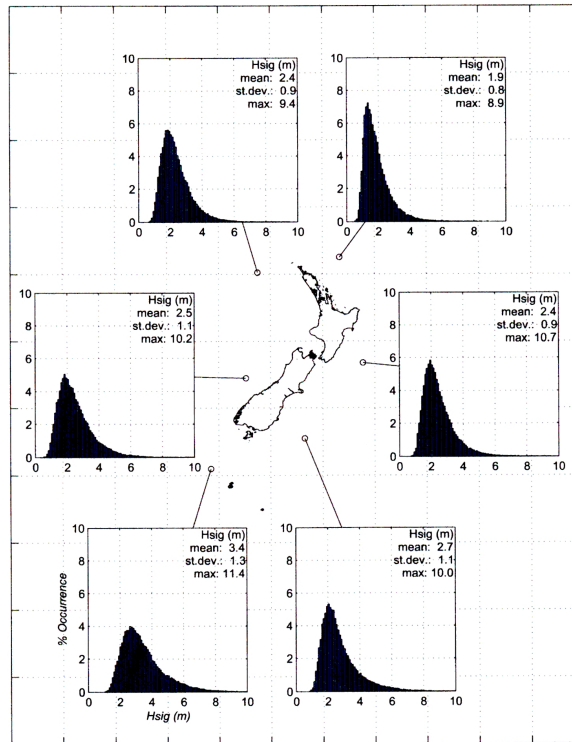
Figure 5-1: Distributions of significant wave heights at the six sites around the coast of New Zealand, derived from hindcasts. [*From* Gorman et al. (2003b)]

Tonkin and Taylor (2003) employed the WAM hindcast data of Gorman et al. (2003a) to evaluate the significant wave heights and periods at the 200-metres water depth directly seaward from Hawke Bay, presented as histograms in Figure 5-3, to serve as the local deep-water wave climate in their analyses of waves in shallow water along this coast. The mean significant wave height is 1.76 metres, the maximum significant wave height being 8.56 metres, the mean period of the waves found to be 10.4 seconds.

The hindcast data demonstrated the existence of a seasonality to the wave conditions, with the analyzed site east of the North Island having experienced the highest waves during the winter months of May through August, when the monthly averages of the significant wave heights were on the order of 2.75 metres, reduced to about 2.0 metres during the summer (Gorman et al., 2003b). Some dependence was found in the waves on the range of climate events from El Niños to La Niñas, expected in that the winds varying between those climate events with an El Niño generating more southwesterly winds while a La Niña produces northeasterly winds. As a result, correlations were found between the wave heights around the New Zealand coast with those climate events, El Niños tending to enhance the wave heights along much of the coast since that event reinforces the effects of the prevailing westerlies, while to the north in the Bay of Plenty the winds and waves increased during La Niñas. According to the analysis results of Gorman et al. (2003b), Hawke Bay is positioned within the zone of transition so its wave climate might be expected to experience only a small influence by the El Niño/La Niña range of climate events, but this has not been investigated in detail.

5 - 4
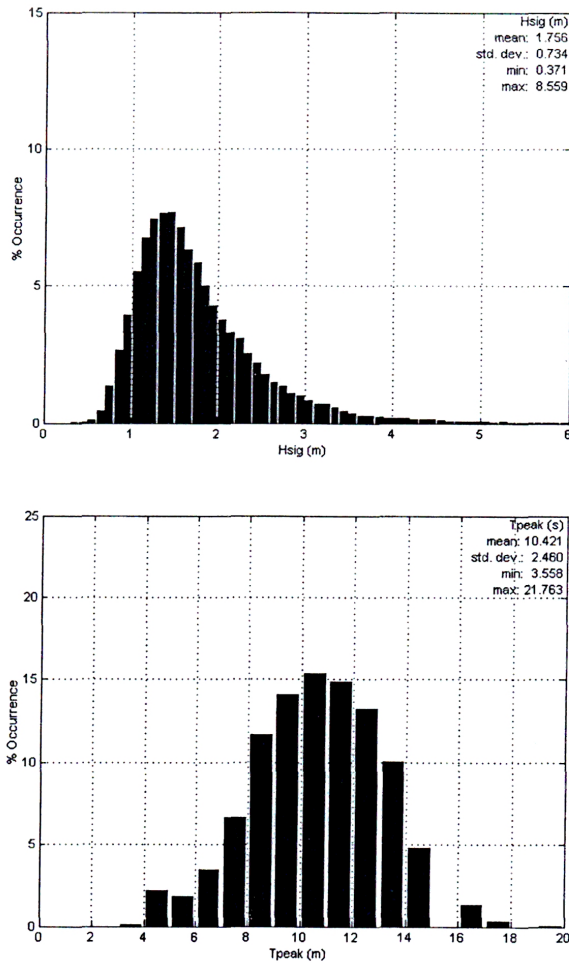
Figure 5-2: The WAM hindcast deep-water wave climate directly offshore from Hawke Bay. [*From* Tonkin & Taylor (2003)]

The deep-water wave hindcasts by Gorman et al. (2003a, 2003b) for the period 1979 through 1998 continue to be important in defining the wave climate for Hawke Bay. Their climatology has recently been complemented by similar hindcast analyses undertaken by MetOceans (2008, 2011), covering the 12-year period from 1997 through 2010. While the analyses included the deep-water wave conditions, the primary objective of their 2008 report was directed toward documenting the shallow-water waves in the Westshore area of Napier, and how they might be altered by the construction of a seawall/breakwater proposed to provide improved property protection. The 2011 report extended the analyses, having the objective of providing shallow-water wave climates for 15 sites along the Hawke's Bay shore, corresponding approximately to the 5- and 10-metre water depth contours. In both reports the MetOceans analyses modeled the energy losses in the wave spectra due to bottom friction and wave-wave interactions. While not explicitly having reported the ranges of deep-water significant wave heights and periods, as did the Gorman et al. (2003a, 2003b) investigations, the MetOceans analyses are important in having confirmed their hindcast results in comparisons with the Port's buoy measurements in 16-metres water depth, and with satellite-derived wave data.

The wave hindcast results from Gorman et al. (2003a, 2003b) and MetOceans (2008, 2011) will be compared later in this chapter with our analyses based on the Port's buoy measurements, the goal being to develop a unified deep-water wave climate where there is basic agreement between the Port's wave data and the hindcast analyses as to the ranges and extremes in magnitudes of the significant wave heights and periods. Furthermore, the analyses by Tonkin and Taylor (2003) and MetOceans (2011) have documented the extent of refraction as the waves cross the continental shelf from deep water and approach the shores of Hawke's Bay, with the significant wave heights changing as they shoal and refract, results that are of importance in our analyses of its coastal hazards, presented in later chapters.

5.3.2 The Port of Napier's offshore buoys and wave measurements

The Port of Napier installed a Triaxys directional wave-rider buoy in August 2000, in 16-metres CD water depth offshore and to the north of the Port's breakwater (39°27'27"S and 176°56'3"E). At that depth the dominant waves are in intermediate to shallow water, depending on their period, not representing the desired deep-water conditions. The buoy records 20 minutes of water surface elevations, and then calculates a number of wave parameters including the significant wave height (H_s), the 10% exceedence wave height, the maximum wave height (H_{max}), the wave period at the peak of the energy-density spectrum (T_p), and the average and range of wave directions. During the first three years of operation the buoy collected measurements once each hour, but in 2004 it began to collect data twice per hour.

The buoy data have been analyzed and presented in a series of reports by Worley, an engineering consulting firm, prepared for the Port of Napier with the analysis results reviewed here having been for the data collected from August 2000 to September 2004 [Worley (2004), reviewed in Komar (2005)]. Monthly mean significant wave heights and periods are listed in Table 5-1 for that 4-year period. The results show that the highest wave conditions occurred during July and August, with their averages being on the order of 1.2 metres, the lowest occurring in the summer months of November through January when they averaged about 0.7 metres. This general pattern is found each year, but with the maximum wave heights of the most severe storms variously occurring in June through September. Included in Table 5-1 are the numbers of storm events each month, defined as occurrences when $H_s > 2$ metres, together with the mean values of the maximum significant wave heights of the storms measured since August 2000. These columns reinforce the general pattern of July and August being the months having the greatest numbers of storms, but in terms of the maximum wave heights it is seen that high wave conditions can occur during essentially any month. Each of the Worley reports tabulates the individual storms, which demonstrates that individually they generally have maximum significant wave heights between 2 and 4 metres, with a 4.68-metres significant wave height on 2-4 April 2002 having been the largest measured during those 4 years. Table 5-2 compares the annual storm conditions that occurred during the 4 years of buoy measurements, demonstrating that there can be substantial differences from year to year. Based on these measured storm wave heights, Worley (2004) undertook an extreme-value analysis in which the 25-, 50- and 100-year projected significant wave heights were respectively 5.4, 5.8 and 6.2 metres. Since those assessments were based on only 4 years of data, they can only be suggestive of the extremes in the Hawke Bay wave climate as measured at the 16-metres water depth of the buoys.

Table 5-1: Monthly-mean significant wave heights and periods, the numbers of storm events each month defined as occurrences when $H_s > 2$ metres, and mean values of the maximum significant wave heights for the period of wave measurements by the Port's buoy, August 2000 through September 2004. [*From* Worley (2004)]

Month	Ave. Significant Wave Height (m)	Wave Period (s)	Number of Storms	Ave. Maximum Wave Heights (m)
January	0.73	11.4	3	2.25
February	0.74	10.0	2	2.35
March	0.87	11.4	6	2.47
April	0.85	11.6	3	3.15
May	0.86	11.6	5	2.25
June	0.83	11.9	4	2.80
July	1.12	11.7	9	2.73
August	1.22	11.9	11	2.90
September	0.8	11.9	5	2.71
October	0.78	10.7	1	2.35
November	0.68	10.2	0	0
December	0.64	10.9	1	2.13
Mean	0.86	11.4	50	2.65

Table 5-2: The numbers of storm events each year and numbers of hours during which $H_s > 2$ metres, and the average maximum significant wave heights each year [*From* Worley (2004)].

Year	Number of Storm Events	Mean Number of hours $H_s > 2$ m	Maximum H_{max} (m)
Aug 2000-July 2001	12	14	2.55
Aug 2001-July 2002	9	30	3.18
Aug 2002-July 2003	13	23	2.57
Aug 2003-July 2004	11	11	2.39

The mean peak-energy wave period for the 4-years of wave measurements was 11.4 seconds (Table 5-1), while averages for the stormiest months, July and August, yielded values of 11.7 and 11.9 seconds. A scatter diagram of wave periods versus significant wave heights prepared by Worley (2004) demonstrated that while $H_s > 3.5$ metres can correspond to a wide range of periods above 8 seconds, the primary occurrences of waves when $H_s > 4$ metres had periods of 14 to 16 seconds. Specifically, the highest wave event in April 2000 with $H_s = 4.68$ metres had a period of 15 seconds. In that the wave power depends on both the height and period (as do runup elevations of the wave swash on the beaches), this combination of high wave heights and long periods for the most severe Hawke Bay storms is important to coastal erosion and flooding occurrences.

The Port's Triaxys wave-rider buoy also measures the direction of the peak wave energy, the direction of the dominant waves on the coast. A joint-frequency analysis by Worley (2004) of the directions versus the range of measured significant wave heights showed a strong prevalence of the largest waves arriving from the directions 90 to 120°, that is east-southeast, representing 71.9% of the measured waves. Only a small portion of the waves arrived from northeasterly directions, a total of 12.6% from 0 to 90°, with 7.7% arriving from

75 to 90°. As expected, this pattern is also seen in the joint-frequency diagram of wave periods and directions, the longest period waves having arrived from the 90° to 120° quadrant.

5.4 ANALYSES OF THE BUOY-MEASURED WAVE CLIMATE

5.4.1 Goal and Scope of the Analyses

As reviewed above, previous documentations of the deep-water wave climate for Hawke Bay were based on hindcast analyses derived from the storm parameters (Gorman et al., 2003a, 2003b; MetOceans, 2008, 2011). Our decision instead in this study has been to base the hazard analyses on data from the Port's buoy, representing the only extensive set of directly measured waves in Hawke Bay. Furthermore, it is of broad interest to integrate the buoy data into the Bay's wave climate, merging it with the hindcast results. This choice is also something of a personal preference in that in our past studies of hazards along the coast of the U.S. Pacific Northwest, we have relied exclusively on buoy data. Finally, this choice for Hawke Bay has been governed by the ready availability of that data for use in our analyses, having been provided by the Hawke's Bay Regional Council. It is recognized, however, that this reliance on the buoy data results in complications in that the buoy is located in a water depth of only 16 metres, such that the storm waves of particular interest are technically in "intermediate" water, not representing "deep-water" wave parameters desired in a wave climate. The wave heights measured by the Port's buoy have been significantly altered while crossing the continental shelf from deep water, generally having been reduced in their heights and energies, while their periods remained essentially the same.

Beyond the desire to have any coastal wave climate be based on deep-water wave conditions, the equation we employ to calculate the swash runup levels along the shores of Hawke's Bay is that derived by Stockton et al. (2006), which depends on the deep-water significant wave heights and periods, as well as on the local beach slope. Those calculations will be undertaken in Chapter 6, with the resulting runup levels later added to the measured tides to determine the hourly total water levels and their extremes relative to the elevations of the beach profiles and backshore properties (Chapters 7 and 9).

The analyses presented here directed toward the development of a deep-water wave climate, based on the measurements by the Port's buoy, involve several stages in the methodology. First, analyses will be undertaken of the directly measured significant wave heights (SWHs) and periods by the buoy, in effect yielding a wave climate at that 16-metre water depth, this being of some interest due to its proximity to the Port and the community of Westshore. That initial analysis of the buoy data will be followed by calculations of the reverse shoaling transformations of the waves, to derive their equivalent deep-water SWHs. It is recognized, however, that this shoaling transformation based on wave theory does not account for the effects of wave refraction[1] and bottom friction, which would have reduced the buoy-measured wave heights and energies; therefore, this inverse calculation based on only the shoaling transformations would systematically underestimate the magnitudes of the deep-water SWHs.

---

[1] The refraction of ocean waves is analogous to the refraction of light through a glass lens, changing the direction of the ocean waves as they advance in shallow water, due to the rate of movement of their crests being dependent on the water depth such that the portion of the crest in deeper water advances more rapidly than that in shallow water, resulting in the rotation of the crest so it becomes more nearly parallel to the shore (Komar, 1998, p. 189-196).

To on average correct for this systematic difference, the final step in the analyses will be directed toward deriving a correction factor, which when applied yields a reasonable merging of the Port's buoy data with the hindcast-based deep-water SWHs, a unified wave climate that will be suitable for our hazard assessments, and possibly in other applications.

5.4.2 Climate of buoy-measured waves

Our analyses of the Hawke Bay wave climate are based on the 11 years of measurements derived from the Port of Napier buoy, 2000 through 2010. From the beginning of the buoy's operation until September 2003, measurements were recorded once per hour; since that date, recording has been twice per hour. A second, redundant buoy was installed in close proximity to the first, at the same water depth; its measurements have been used whenever the first buoy was not operational, yielding a nearly complete set of wave data for those 11 years.

The buoys are located to the northeast of the Port's breakwater, sufficiently distant that measurements of the waves would have experienced minimal effects such as reflection from the breakwater. Both buoys are in a water depth of 16.4 metres relative to mean sea level, inferring that most measurements represent intermediate to shallow-water conditions, not the desired deep-water significant wave heights and periods. These limits are defined as

Deep water	$h/L_\infty > 1/4$	
Intermediate water	$1/4 > h/L_\infty > 1/20$	(5-1)
Shallow water	$h/L_\infty < 1/20$	

where h is the water depth relative to the wavelength in deep water, calculated with the equation $L_\infty = (g/2\pi)T^2$, being dependent only on the wave period T. In contrast to this deep-water dependence on the wave period, in shallow water the wavelength depends only on the water depth, while in intermediate water the dependence is on both the period and depth, requiring that the more complex general equations be used in analyses (Komar, 1998). The simpler deep-water and shallow-water approximations are generally limited to the condition where the maximum error in their application is less than 5% compared with having utilized the complex general equations.

Previous analyses based on the Port's buoy data utilized its measurements directly, since the Port of Napier is interested in the wave conditions in the immediate proximity to their harbour. For completeness, our initial analyses again directly utilized the measured significant wave heights and periods, in effect yielding a wave climate at the buoy's 16-metres water depth. The original measurements are graphed in Figure 5-4 as a scatter diagram of the SWHs versus their periods. The blue Xs are the mean SWHs for each band of reported periods. The vertical dashed lines at 6.5 and 14.5 seconds delineate the separate regions of deep, intermediate and shallow-water wave conditions, according to the limits defined by the above equations. It is seen in this scatter diagram that the measured wave periods range from approximately 2 to 25 seconds. A large number of the measurements have periods less than 6.5 seconds, and therefore are still in deep water at the buoy depth; they will have experienced minimal shoaling transformations and refraction prior to having been measured by the buoy. The highest measured significant wave heights during storms for the most part have periods within the range 9 to 16 seconds, being predominantly in intermediate water depths such that the heights measured by the buoy will be slightly lower than in deep water due to shoaling

transformations, and further reduced by refraction and bottom friction as they cross the continental shelf. The largest waves are seen to have reached SWHs on the order of 4 to 4.5 metres.

This graph is fairly typical of wave-scatter diagrams, the waves having periods less than about 5 to 6 seconds for the most part having been locally generated by winds, and therefore have smaller heights due to not having had a large fetch or sufficient time to have grown larger, and because short-period waves are stable without breaking only if their heights are small. All of the waves with periods greater than 20 seconds are seen in Figure 5-4 to have heights smaller than about 1 metre, representing low-steepness swell, presumably generated by distant storms, likely being the forerunners of the 10 to 12-second waves with greater heights that arrived hours to days later.
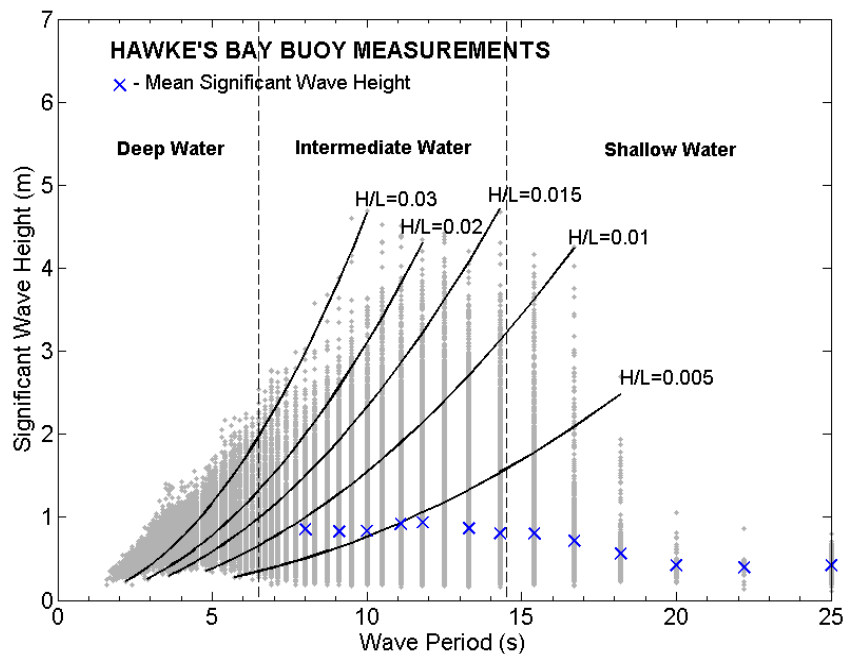
Figure 5-4: The scatter diagram of significant wave heights versus periods measured in 16-metres water depth by the Port of Napier's buoy from 2000 through 2010.

The overall pattern in Figure 5-4 of the otherwise scattered data and the mean X values is therefore what one would expect for the arrival of waves generated by distant storms, the first to reach Hawke Bay being the long-period, low-height forerunners, followed by progressively lower periods but having appreciably higher SWHs, the highest waves being those having periods on the order of 10 seconds. As indicated, the lowest period waves, those less than about 5 seconds, are for the most part probably generated in close proximity to Hawke's Bay, not being the product of distant storms.

Figures 5-5 and 5-6 are respectively histograms of the measured SWHs and periods directly measured by the buoy from 2000 through 2010. The SWHs are graphed as a pair of histograms, one version being the numbers of observations plotted with a conventional linear scale, the second (in red) graphing the same data but using a log scale for the numbers of observations to emphasize the more extreme but rare SWHs, 10^0 representing 1 occurrence during the 11 years of measurements (Komar and Allan, 2007). Within that span of time the

largest individual SWHs generated by major storms and measured by the buoy are seen to have ranged from 4 to about 5 metres. The mode of maximum occurrence is at about 0.6 metre, which according to the scatter diagram in Figure 5-4 could correspond to the full range of wave periods, but predominantly consists of locally generated waves having periods on the order of 5 seconds or less.
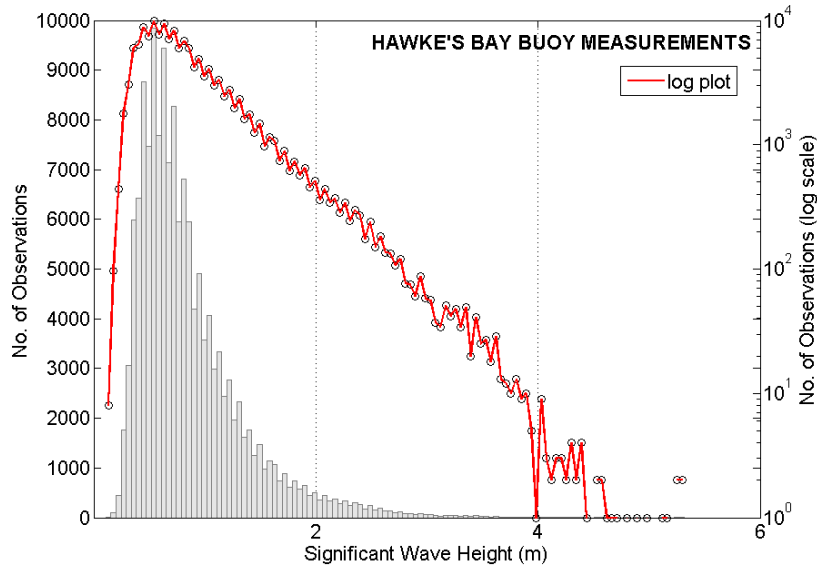
Figure 5-5: Histogram of significant wave heights (SWHs) measured by the Port's buoy from 2000 through 2010.

The histogram of measured wave periods, Figure 5-6, has the conventional form using linear scales, now including axes for both the numbers of observations during the 11 years of data collection and the percentages of occurrence. The results are largely as expected, with the dominant periods ranging from about 9 through 15 seconds. This again confirms that most of the measured waves by the buoy are "intermediate", within the 6.5- and 14.5-second boundaries. While this histogram is for the periods measured by the buoy in its 16-metres water depth, the histogram would be essentially the same in deep water since the periods for the most part are unaltered during shoaling.
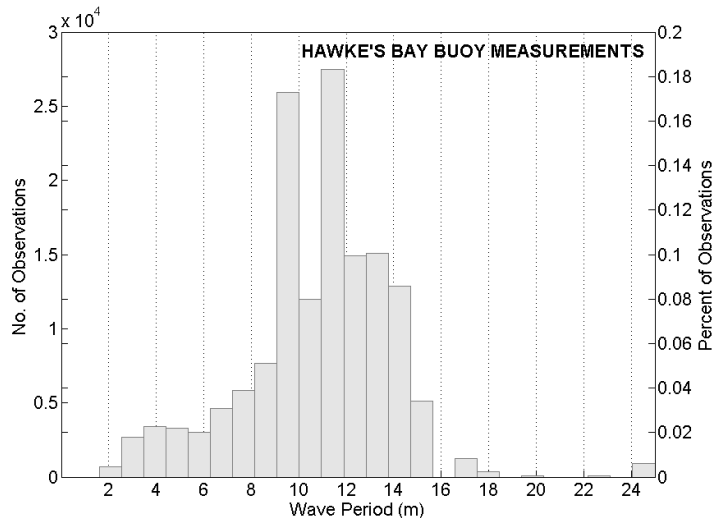
Figure 5-6: Histogram of buoy-measured wave periods.

Figure 5-7 is a graph of the SWHs versus their directions of arrival when measured by the Port's buoy. The range of directions is 0 degrees for waves arriving from due north, 90 degrees from the east, and 180 degrees from the south. As expected, the waves primarily arrive from the east to southeast, generated by extratropical storms in the circum-Antarctica Southern Ocean or crossing the South Island. With the directions having been measured in 16-metres water depth, most would already have experienced some refraction as they crossed the continental shelf; while still offshore in deep water, prior to having undergone refraction, the waves would have arrived from an even more southeasterly quadrant, the higher the wave period the greater the change in direction compared with that in deep water. In spite of this complexity governing the measured wave directions, it is evident that the main source of arriving waves is from storms to the southeast of Hawke Bay.
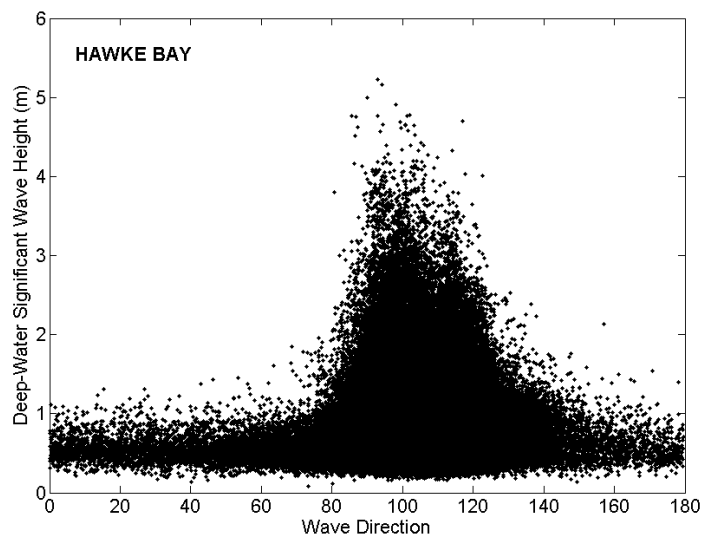
Figure 5-7: Significant wave heights versus wave directions measured by the Port's buoy, with the 90-degree direction being to the east, the plot showing that the highest waves arrive from the east to southeast.

It is also evident in Figure 5-7 that there is an absence of more extreme waves arriving from the north-northeast, which might have been attributed to their generation by tropical cyclones whose tracks take them southward from Equatorial regions, moving toward the southeast where they would pass Hawke's Bay to its northeast. Examinations of the tracks of tropical cyclones that occurred during those 11 years of buoy measurements indicated that generally they were well offshore, and by that stage had decreased in intensity from being a fully developed cyclone to a weaker tropical storm. There were no high wave events measured from 2000 to 2010 by the buoy that could positively be identified as having been generated by a tropical cyclone, but such an occurrence is certainly possible in the future.

5.4.3 Equivalent deep-water significant wave heights

As already discussed, in developing a wave climate for a coastal region the general practice is to formulate it for the deep-water conditions, the primary reason being that a wave climate based on mid- to inner-shelf depths represents waves that are intermediate to shallow water, having been altered by shoaling transformations, refraction, and by some loss of energy due

to bottom friction. The resulting wave climate would therefore be different from site to site, depending on the local water depth and extent of refraction. This represents an obvious limitation of the wave climate developed above for the 16-metre depth of the Port's buoy, it really only being of interest to the operation of the Port of Napier and the community of Westshore. Of broader interest in applications is to develop an equivalent deep-water wave climate that is otherwise based on the Port's buoy data, the only extensive set of directly measured waves in Hawke Bay. This has been accomplished in our analyses by first employing the equations derived from wave theory to calculate what represents the "equivalent" SWHs in deep water, corresponding to the heights and periods measured hourly by the buoy. However, with the buoy-measured SWHs also having been reduced by refraction and bottom friction, as well as altered by shoaling, the transformation to more meaningful deep-water equivalents requires the inclusion of assessments that account for those factors. Analyses will therefore be directed toward deriving a "correction factor" wherein there is basic agreement between the buoy data and the hindcast deep-water wave climates, those obtained by Gorman et al. (2003a, 2003b) and by Tonkin and Taylor (2003) specifically for Hawke Bay. Once an integrated deep-water wave climate has been determined, it can then serve as the basis for calculations of wave breaking and swash runup levels on the Hawke's Bay beaches (Chapter 6), followed by comparisons of the total water elevations (tides plus the wave runup) with the beach profiles and elevations of backshore properties (Chapter 7).
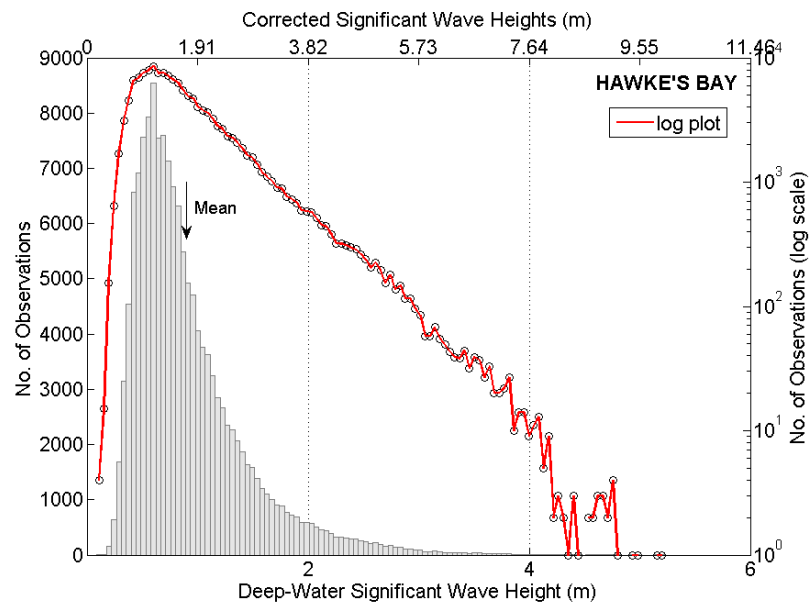
Figure 5-8: Histogram of the deep-water SWHs calculated from the Port's buoy measurements.   The bottom axis accounts for the shoaling transformations but not refraction and bottom friction reductions of the wave heights, while the top axis for the "Corrected" magnitudes results in basic agreement with the histogram of Figure 5-3 for the hindcast deep-water significant wave heights.

In our analysis the transfer of the Port's wave-buoy measurements to deep-water equivalents first yielded the SWHs graphed in Figure 5-8, again presented as a pair of histograms respectively using linear and log scales for the numbers of observations. The methodology of this transfer initially involved simple calculations of the shoaling transformations, the result represented by the lower SWH axis in the graph. At this stage there actually isn't much difference between this histogram and that in Figure 5-5 based on the original buoy

measurements, this similarity having been expected in that as noted above the lower period waves are still in deep water at the 16-metre depth of the buoy, and according to linear wave theory the waves in intermediate water depths would have equivalent deep-water SWHs that are only slightly higher than the buoy-measured values. The long-period waves that were already in shallow water at the buoy's depth, those having periods greater than 14.5 seconds and evident in the scatter diagram of Figure 5-4, would yield somewhat smaller deep-water equivalent SWHs according to the shoaling transformation. However, most of the shallow water increase in the wave heights would be expected to occur as they approach still closer to shore than the buoy's 16-metres depth, so the similarity between the histograms of Figures 5-5 and 5-8 is again not surprising. Although this level of correction accounting for the shoaling transformations turns out to have been relatively minor, any further difference between the histogram of SWHs based on the Port's buoy measurements versus the hindcast predictions can be attributed mainly to wave refraction, with some loss of wave energy due to bottom friction as the waves crossed the continental shelf.

There is a substantial difference compared with the ranges of deep-water SWHs derived from the hindcast analyses, the histogram in Figure 5-3 from Tonkin and Taylor (2003) for Hawke Bay. A direct comparison between the statistics of the distributions is given in Table 5-3, including the mean SWHs, the modes of most frequent occurrences, and the respective minimum and maximum SWHs. It is evident that the magnitudes in this series of statistics are substantially higher for the hindcast analyses than inferred from the buoy data, an expected result in that there generally is substantial refraction of the waves in Hawke Bay, especially for the dominant and largest waves arriving from the southeast. In particular, the initial assessment in Figure 5-8 for the maximum SWH based on the buoy measurements is only on the order of 5 meters, considerably less than the 8.6-metre maximum SWH based on the hindcast analyses by Gorman et al. (2003a, 2003b), and reported by Tonkin and Taylor (2003) for Hawke Bay.

Table 5-3: Comparisons between the statistics of the wave hindcast deep-water significant wave heights (Figure 5-3), and those calculated from measurements by the Port of Napier's buoy (Figure 5-9). The final column is the "corrected" buoy assessments, based on the 1.91 factor.

	Hindcast (m)	Buoy (m)	Corrected (m)
Mean	1.76	0.92	1.76
Mode	1.4	0.62	1.2
Minimum	0.37	0.09	0.17
Maximum	8.6	5.2	9.9

The procedure we have followed has been to "correct" the values derived from the buoy measurements by simply applying a multiplication factor, the ratio of the means determined respectively for the hindcast analyses (1.76 metre) and the buoy measures (0.92 metre), the resulting ratio and correction factor being 1.91 to make them equivalent. This 1.91 factor was then applied as an empirical "correction factor" for the entire histogram of deep-water SWHs derived from the Port's buoy, a uniform shift of all values that is directly accomplished by the upper axis in Figure 5-8, the Corrected Significant Wave Heights. With this empirical correction, it is evident in the third column of Table 5-3 that there is now reasonable agreement between the magnitudes of the deep-water SWHs derived from the Port's buoy, and those based on the wave hindcast analyses. The maximum SWHs are now respectively 8.6 metres for the hindcast analyses, and 9.9 metres for the deep-water equivalent maximum

SWH based on the Port's buoy data, reasonably good agreement in view of the contrasting approaches (hindcasts versus buoy measurements) for their assessments, and with the expected uncertainties in both values.

Furthermore, this 1.91 correction factor employed to empirically account for wave refraction is in approximate agreement with Snell's Law. Based on the wave directions measured by the buoy, graphed in Figure 5-7, and their reasonably expected directions in deep water arriving predominantly from storms located to the southeast, simple calculations using Snell's Law yield factors on the order of 1.2 to 1.4. The difference from our 1.9 empirical correction implies that bottom friction and wave-wave interactions and instabilities leading to breaking have also been important, as suggested by the SWAN model analyses completed by Tonkin and Taylor (2003) and MetOceans (2008, 2011).

The analysis results for the buoy-equivalent deep-water SWHs versus their corresponding periods are graphed as a scatter diagram in Figure 5-9, with the left axis being the deep-water SWHs having accounted for the shoaling transformations, while the right axis is that corrected with the 1.91 factor to account for wave refraction. The overall pattern of the data here for the deep-water equivalent SWHs and periods is similar to that in Figure 5-4 for the 16-metre water depth wave climate, with the Xs again being the mean SWHs for each band of reported periods. As discussed earlier, the pattern of data scatter seen here in Figure 5-9 can be explained by the hourly changes in SWH and period combinations arriving from distant storms, with the long period but low wave heights being the forerunner swell, the first to reach Hawke Bay, while the waves in the range of periods from about 7 to 17 seconds are the later arrival of the largest swell waves generated by those distant storms. In contrast, the lower waves with periods less than 5 to 6 seconds are for the most part locally generated in close proximity to Hawke Bay.
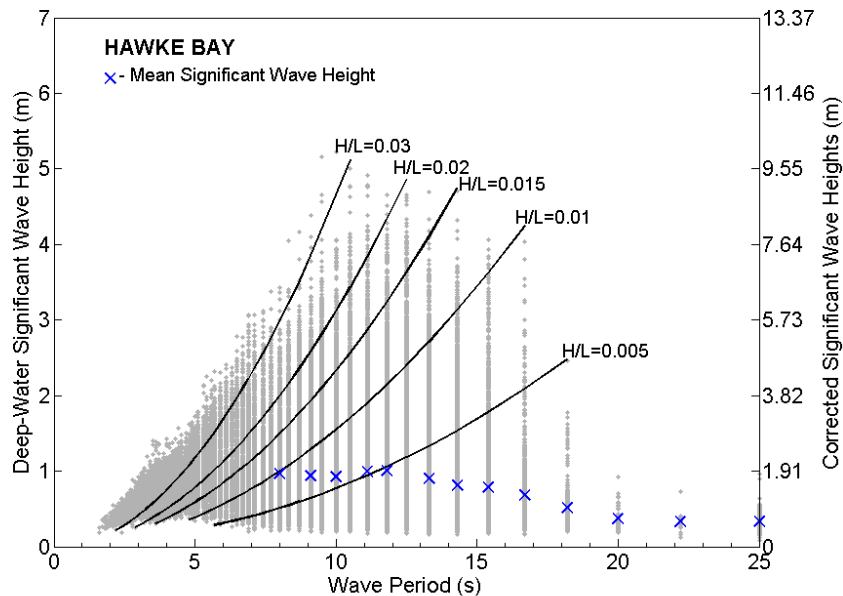
Figure 5-9: Scatter diagram of the "equivalent" deep-water SWHs versus periods, derived from measurements by the Port's buoy. The left axis accounts for wave shoaling, while the right axis applies a 1.91 correction factor so that the magnitudes agree with the hindcast analyses.

We recognize the potential shortcomings undertaken here in our analyses of the Hawke's Bay deep-water wave climate. First is the limited availability of hourly measurements derived from the Port's buoy, having analyzed only one decade of measurement (2000 through 2010). While this was sufficient to generally define the Bay's wave climate as graphed in Figures 5-8 and 5-9, absent is a sufficient documentation of the infrequent extreme wave events, generated by the most severe storms, supporting projections of the 50- to 100-year SWH extremes. However, our methodology to integrate the analysis results based on the buoy data with the distributions of deep-water SWHs derived from wave hindcasts (Gorman et al., 2003a, 2003b; Tonkin and Taylor (2003) yielded a reasonable level of agreement in their overall distributions of SWHs (Table 5-3), including the extremes, providing us with a unified wave climate that covers 30 years of wave data, hindcasts plus buoy measurements. We recognize that our methodology of converging the wave data through the use of a single empirical "correction factor", 1.91, is oversimplified in having accounted for the effects of wave refraction experienced in Hawke Bay. Although this factor may approximately represent an average refraction coefficient and the degree of wave energy loss due to bottom friction, each hourly combination of the measured SWH, period and direction of arrival measured by the buoy at its 16-metre water depth would require a different correction factor. To have accomplished such an analysis would in effect require that we repeat the SWAN model refraction analyses previously undertaken by Tonkin and Taylor (2003) and MetOceans (2008, 2011), but in the opposite direction starting with the hourly buoy measurements and reverse shoaling them to deep water from the 16-metre buoy depth, yielding an individual correction for each set of hourly wave measurements. While such an improved merging of the Port's ongoing buoy measurements with the hindcasts would constitute the preferred approach to developing a deep-water wave climate for Hawke Bay, it was beyond the scope of this study directed toward hazard assessments, our conclusion having been that it would not sufficiently improve our projections of those hazards, considering the remaining uncertainties involved in making those projections.

The histogram of SWHs in Figure 5-8 and the scatter diagram of Figure 5-9, based on the hourly measurements of waves by the Port's buoy, will see applications in subsequent chapters, first to calculate the corresponding climates of wave breaker heights and swash runup levels on the Bay's beaches (Chapter 6), in turn yielding assessments of the total water levels at the shore when the runup is combined with the corresponding tide measurements (Chapter 7). The resulting total water levels are important in being compared with the elevations of the beaches and backshore properties along this coast (Chapters 7 and 9), at present and in the future as the rise in global sea level also becomes an important factor in the magnitudes of those impending hazards.

5.4.4 Seasonal variations and the decadal trend in deep-water wave heights

Remaining to be examined are the seasonal variations in wave heights measured by the Port's buoy, and whether there has been any trend of net change during the 11 years of data collection. The monthly variations in mean SWHs are graphed in Figure 5-10, including plots for each of the individual years, the bold line being the average seasonal cycle for the entire record while its standard deviation is shown in blue. For the 11-year averages it is seen that there is the expected seasonal variation, with the highest waves on average having occurred in July (mid-winter). However, from the graphs for the individual years it is apparent that

there has been a considerable variation from year to year, there being the possibility for occurrences of significant storm events virtually every month. The conclusion is that although there is on average a seasonal variation, its development is less prominent than found on most coasts, such that erosion and flooding events can occur throughout the year.
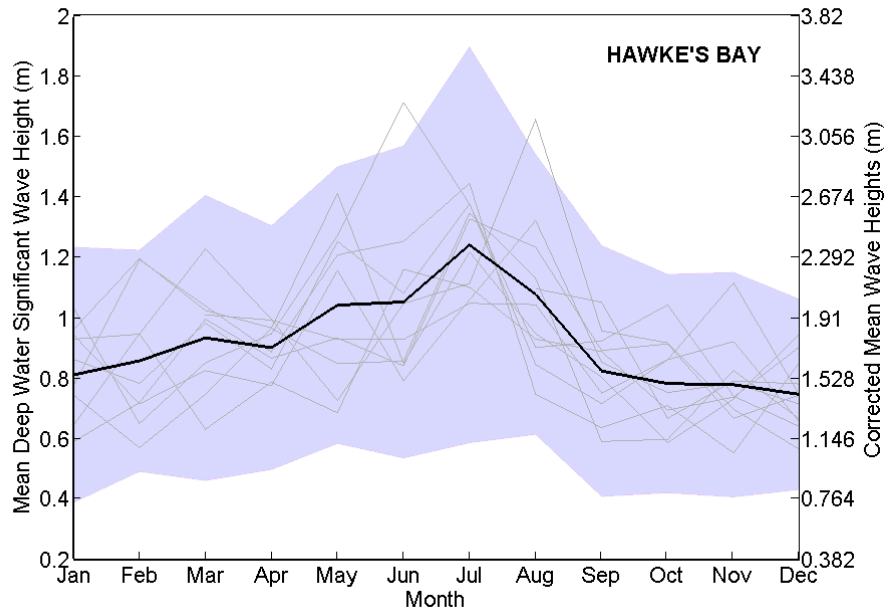
Figure 5-10: The seasonality of monthly-mean deep-water SWHs derived from the buoy data, the dark curve being the 11-year averages while the light-colored curves are for individual years.

The analysis graphed in Figure 5-11 is of the decadal-long trend in the annual average deep-water SWHs, the linear regression suggesting that there has been an increase at a rate of roughly 0.008 m/year. Although this rate might seem small, it amounts to about a 10-centimetre increase in 11 years, a 6% increase above the 1.66-metre mean deep-water SWH measured during the first year (2000) of buoy operation. The existence of such an increase is consistent with the trend found by Young et al. (2011), based on satellite measurements for 1985 through 2008, reviewed in Chapter 2. Their graph is for the trend of change in the 99th-percentile SWH across the world's oceans, with the shores of New Zealand showing a net increase on the order of 1% per year. Assuming that the 9-metre maximum SWH measured by the Port's buoy (Table 5-3) corresponds approximately to this 99th percentile, its rate of increase might be expected to be on the order of 0.09 m/year according to the satellite data; if that same rate is applied to the average SWH, 1.76 metres, the rate of increase would be approximately 0.02 m/year, closer in magnitude to that based on the Port's buoy data[2]. With both the buoy measurements and satellite data being based on only limited records, it clearly is not possible to conclude with confidence that there has been a climate-controlled increase in wave heights around the coasts of New Zealand in recent decades, including on the shores of Hawke's Bay. However, as reviewed in Chapter 2, there is firm evidence locally from buoys

---

[2] This result for Hawke Bay, showing more extreme wave heights increasing at a greater rate than the average, is consistent with analyses of the trends of increasing wave heights along the coast of the U.S. Pacific Northwest (Allan and Komar, 2006; Ruggiero et al., 2010), and as discussed by Wigley (1988) for climate-controlled environmental data in general (global temperatures, river discharges, etc.) that have skewed distributions.

and from the satellite data across the world's oceans that global warming has resulted in stronger storm intensities, both extratropical and tropical systems, resulting in trends of increasing wave heights. The evidence therefore is that in addition to rising sea levels, the increase in storm intensities and wave heights will be important to the future hazards on the Hawke's Bay shores, but a much longer record derived from the Port's buoy is required to establish its existence and the magnitude of the rate of increase.
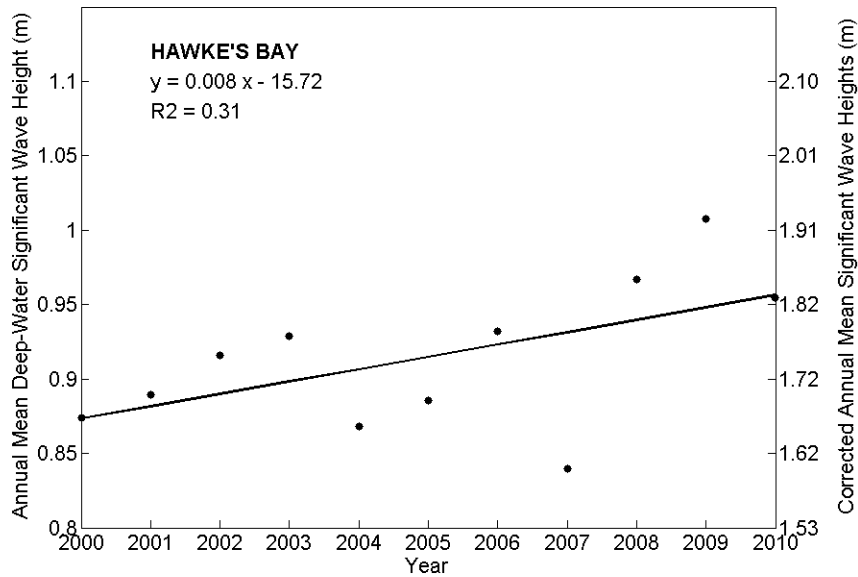
Figure 5-11: The regression trend of increasing annual average deep-water SWHs derived from the Port of Napier's buoy measurements.

5.5 SUMMARY

The objective of this chapter has been to develop a deep-water wave climate for the coast of Hawke's Bay, to be applied in the following chapter to calculate wave breaker heights and wave-swash runup levels on its beaches, components in the nearshore processes climates required in evaluations of erosion and flooding hazards. The decision was to rely principally on measurements obtained by the Port of Napier's buoy, which is located in proximity to its harbour at a water depth of 16 metres. Aspects of a wave climate were first determined for that water depth, based directly on the measured significant wave heights and periods, of potential use in the engineering design and management operations of the harbour. However, our main goal was to derive the deep-water equivalent significant wave heights generally desired in a wave climate, and specifically needed in our hazard assessments. This was accomplished by first applying the equations derived from wave theory, which account for wave shoaling changes in the significant wave heights between deep water and the buoy's 16-metres water depth. Those results were then compared with the range of magnitudes of the deep-water significant wave heights obtained by investigations using hindcast analysis methodologies based on the storm parameters. That convergence in the results between the buoy data and the hindcast wave assessments was accomplished simply by shifting the histogram for the significant wave heights based on the buoy (Figure 5-9) to higher magnitudes determined by the hindcasts, a correction factor of 1.91 producing a match of the mean values in their respective distributions. Important is that this shift also produced

reasonable agreement between their entire distributions, including the modes of most frequent height occurrences, and with the extreme magnitudes measured by the Port's buoy corresponding to the extreme derived in the hindcasts by Gorman et al. (2003a). A significant product of our analyses, therefore, has been a unified deep-water wave climate based on the hourly measurements derived from the Port of Napier's buoy, beginning in the year 2000, with the earlier 20-year hindcasts by Gorman et al. (2003a, 2003b) adapted for use by Tonkin and Taylor (2003) in Hawke Bay. Important in this study, the resulting wave climate is suitable for applications in the following chapters to evaluate the nearshore processes that have fundamental roles in affecting this coast's erosion and flooding hazards.

Of interest and concern to the future erosion and flooding hazards along the shores of Hawke's Bay is the evidence for increasing wave heights in recent decades, measured by the Port of Napier's buoy since the year 2000 and by satellites since 1985, and also found on other ocean shores, implying that Earth's changing climate is enhancing the intensities of the storms that have generated the waves. Although the results for Hawke's Bay are uncertain in having been based on only short records, the prospect for continued increases in storm intensities and generated extreme wave heights obviously needs to be included in assessments of this coasts potential future hazards.

5.6 REFERENCES

Allan, J. C., and P.D. Komar (2006) Climate controls on US West Coast erosion processes: *Journal of Coastal Research*, v. 22, no. 3, p. 511-529.

Gorman, R. M., K. R. Bryan and A. K. Laing (2003a) A wave hindcast for the New Zealand region: Nearshore validation and coastal wave climate: *New Zealand Journal of Marine and Freshwater Research*, v. 37, p. 567-588.

Gorman, R. M., K. R. Bryan and A. K. Laing (2003b) A wave hindcast for the New Zealand region — Deep water wave climate: *New Zealand Journal of Marine and Freshwater Research*, v. 37, p. 589-611.

Komar, P.D. (1998) *Beach Processes and Sedimentation*: 2nd edition, Prentice Hall, 544pp.

Komar, P. D. (2005) *Hawke's Bay, New Zealand: Environmental Change, Shoreline Erosion, and Management Issues*: Report for the Hawke's Bay Regional Council.

Komar, P.D., and J.C. Allan (2007) A note on the depiction and analysis of wave-height histograms: *Shore & Beach*, v. 75, n. 3, p. 1-5.

Komar, P.D., J.C. Allan and P. Ruggiero (2010) Wave and nearshore-process climates: Trends and variations due to Earth's changing climate: *Handbook of Coastal and Ocean Engineering*, edited by Y.C. Kim, World Scientific Publishing Co.

MetOceans (2008) *Westshore Reef Surf Conditions*: MetOcean Solutions Ltd., New Plymouth, New Zealand, 65 pp.

MetOceans (2011) *Hawkes Bay Wave Climate*: MetOcean Solutions Ltd., New Plymouth, New Zealand, 42pp.

Ruggiero, P., P.D. Komar, and J.C. Allan (2010) Increasing wave heights and extreme-value projections: the wave climate of the U.S. Pacific Northwest: *Coastal Engineering*, v. 57, p. 539-552.

Stockdon, H.F., R.A. Holman, P.A. Howd, and A.H. Sallenger (2006) Empirical parameterization of setup, swash, and runup: *Coastal Engineering*, v. 53, p. 573-588.

Tonkin and Taylor (2003) *Hawke's Bay Nearshore Wave Climate*: report to the Hawke's Bay Regional Council, 13 pp + Appendices.

Wigley, T.M.L. (1988) The effect of changing climate on the frequency of absolute extreme events: *Climate Monitoring*, v. 17, p. 44-55.

Worley (2004) *Wave Data Report, August 2003 - September 2004*: 2 November 2004 report to the Port of Napier, Worley Infrastructure Pty Ltd, Perth, Australia.

Young, I. R., S. Zieger and A.V. Babanin (2011) Global trends in wind speed and wave height: *Science*, v. 332, p. 451- 455.

6 Wave Breaker Heights and Swash Runup Levels on Hawke's Bay Beaches

6.1 INTRODUCTION

In the preceding chapter a deep-water wave climate was developed for Hawke Bay, based primarily on the Port of Napier's buoy data but with the magnitudes calibrated to correspond with the results derived from the wave-hindcast analyses. With this integrated climate representing the deep-water waves prior to their shoaling and refraction as they cross the continental shelf, its significant wave heights (SWHs) and periods are essentially the same for the entire coast of interest in this study, the Bay View and Haumoana Littoral Cells. However, of most immediate relevance to occurrences of coastal erosion and flooding along those shores, as well as to its future hazards, are the processes that occur directly on the beaches, including the ranges of wave breaker heights and the levels to which the waves swash up the sloping beaches. These factors are depicted schematically in Figure 6-1, representing the components of what is termed the "nearshore processes climate", analogous to and dependent on the deep-water wave climate (Komar and Allan, 2002).
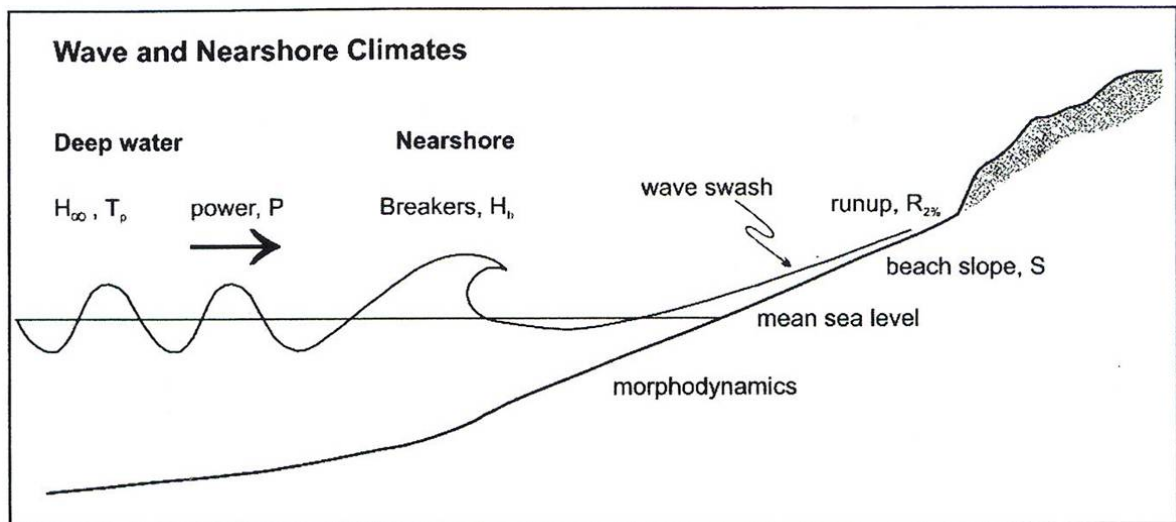
Figure 6-1: The nearshore processes climate that includes the ranges of breaking wave heights and swash runup levels on the sloping beach. [*From* Komar and Allan (2002)]

The processes occurring on the beaches depend on the hour-to-hour combinations of wave heights and periods generated by storms in deep water, and in the case of the wave runup there is also a dependence on the slope of the beach. The extremes in breaker heights and runup at the shore therefore correspond to occurrences of extremes in the deep-water storm

waves. Furthermore, on coasts where the deep-water wave heights and periods have been increasing over the decades, the nearshore processes climate can be expected to respond in tandem, with the resulting multidecadal increases in the energy of the breaking waves and runup elevations of the swash at the shore, being important to the resulting impacts from erosion and flooding.

The development of nearshore processes climates has been important in our work along the shores of the U.S. Pacific Northwest, in assessments of the impacts of episodic major storms, and in the longer term produced by their enhanced magnitudes due to Earth's evolving climate. The goal in this chapter is to similarly undertake analyses of wave breaker heights and swash runup levels along the shores of Hawke's Bay.

6.2 MODEL ANALYSES OF COASTAL WAVE HEIGHTS

An important step in establishing the link between the deep-water wave climate and the nearshore processes is through model analyses of the shoaling and refraction of the waves as they cross the continental shelf. The significance of wave refraction in Hawke Bay was first demonstrated by Gibb (1962) in his construction of refraction diagrams for waves approaching this coast from various directions. In particular, the dominant waves from the south to southeast quadrants experience significant changes in directions as they travel toward the coast, with their crests progressively rotating counter-clockwise by on the order of 90° as they pass from deep water to the shores of the Bay View and Haumoana Littoral Cells. The most important consequence to investigations of the coastal hazards is that this degree of refraction will significantly decrease the heights of the waves and swash runup levels on the beaches. Recent analyses of the wave refraction for Hawke Bay have been undertaken in the reports by Tonkin and Taylor (2003) and MetOceans (2008, 2011), applying models that evaluated in detail the wave shoaling and refraction, also accounting for energy losses caused by bottom friction. Their investigations in effect yielded climates of SWHs and periods in the immediate offshore from the beaches, at water depths of 5 and 10 metres.

The analyses by Tonkin and Taylor (2003) were based on the wave hindcasts obtained in the study by Gorman et al. (2003a, 2003b), representing the deep-water wave climate in 200-metres water depth off the Hawke's Bay coast. They employed the SWAN (Simulating WAves Nearshore) model to transform this deep-water data to 19 nearshore sites along the 10-metre CD water depth contour within Hawke Bay (9 metres below Mean Sea Level). The results are listed in Table 6-1 for the mean SWHs, maximum SWHs, mean periods, and mean directions. Sites 2 through 5 are located to the south of Cape Kidnappers, while sites 16 through 20 are to the far north, in proximity to the Mahia Peninsula. Of specific interest to the present study are sites 6 through 10 within the Haumoana Littoral cell, the stretch of beach between Cape Kidnappers and the barrier represented by Bluff Hill and the Port's breakwater within the city of Napier, and sites 11 to 15 in the Bay View Cell from Westshore immediately north of Bluff Hill to Tangoio, beyond which is the rocky stretch of coast still further to the north. Tonkin and Taylor (2003) tested the results derived from their model analyses against the Port's buoy accumulated measurements; although the time frames differed, there was good agreement supporting the validity of their model results.

Table 6-1: Mean and maximum significant wave heights (metres), mean periods, and directions of arrival (degrees clockwise from the north) in 10-metres water depth at sites along the coast of Hawke's Bay. [*From* Tonkin and Taylor (2003)]

Site	Significant Wave Heights (m) Mean	Maximum	Wave Periods	Wave Arrival Directions
Deep-Water Offshore				
1	1.76	8.56	10.4	
South of Cape Kidnappers				
2	1.53	7.81	10.6	
3	1.47	7.88	10.5	
4	1.50	8.00	10.4	
5	1.43	8.13	10.8	
Haumoana Littoral Cell (Cape Kidnappers to Napier)				
6	0.60	3.32	10.7	86.8
7	0.52	3.36	10.2	83.7
8	0.52	3.49	9.9	94.8
9	0.59	3.82	10.2	101.3
10	0.62	4.09	10.5	105.7
Bay View Littoral Cell (Ahuriri to Tangoio)				
11	0.46	3.35	10.7	99.4
12	0.58	3.93	10.7	108.8
13	0.64	4.15	10.7	113.4
14	0.69	4.44	10.8	116.2
15	0.70	4.26	10.9	120.0
Rocky Coast (Waipatiki Beach)				
16	0.74	4.25	10.5	131.2
Wairoa Littoral Cell (Waikari to 10km west of the Mahia Peninsula)				
17	0.87	4.66	10.7	148.7
18	0.97	4.77	11.0	163.1
19	1.16	4.88	11.4	182.9
20	0.97	5.31	11.6	191.9

Site 1 in Table 6-1 lists the mean and maximum deep-water SWHs, respectively 1.76 and 8.56 metres, values obtained in the hindcasts by Gorman et al. (2003a, 2003b), discussed in Chapter 5 and graphed in the histogram of Figure 5-3. It is seen here in Table 6-1 that the wave-height magnitudes for Sites 2 through 5 remain comparable to those in deep water, that stretch of coast being rocky within which are individual pocket beaches composed of sand, whose orientations are such that there is only a small degree of refraction as the waves cross the shelf. In contrast, as evident in Table 6-1 the wave heights for the 10 sites within the Haumoana and Bay View Littoral Cells have decreased substantially from those in deep water, the mean SWHs ranging from about 0.5 to 0.7 metre, the corresponding maximum extremes ranging from 3.3 to 4.4 metres at the 10-metre water depth.   The lowest means and maximums occur at the south ends of the cell's shorelines, to the north of Cape Kidnappers, caused by the sheltering of that extensive headland from the dominant waves arriving from the southeast, and similarly to the north of Bluff Hill, which together with the Port's breakwater combine to protect the Westshore community within Napier. For the waves to reach those sheltered shores, a considerable degree of refraction is required, this primarily accounting for the lowered wave heights.

The recent analyses by MetOceans (2008, 2011) are similar to those undertaken by Tonkin and Taylor (2003), having refracted the deep-water waves to the inner-shelf depths of Hawke Bay. As summarized in Chapter 5, the MetOceans study developed its own wave hindcasts to represent the deep-water wave climate, covering the 12-year period from 1998 to 2009. They also employed the SWAN model to analyze the transformations of the waves as they cross the continental shelf, undergoing refraction and losses of energy due to bottom friction. The MetOceans reports similarly tabulated the mean and maximum SWHs at the 10-metre water depth contour, but also at the 5 metres depth, bringing the assessments still closer to the Bay's shorelines, demonstrating that there are further decreases in wave heights as the waves cross the inner shelf. As expected, the decrease is greatest at the south ends of the littoral cells, again attributed to the sheltering effects of Cape Kidnappers and Bluff Hill, with the transitions from the 10- to 5-metre depths occurring within their shadow zones, resulting in greater degrees of refraction.

Although the analysis procedures followed by Tonkin and Taylor (2003) and MetOceans (2008, 2010) are much the same, there are differences in their respective results in the evaluated SWHs at the 10-metre depth contour where they can be compared, indicative of there being a level of uncertainty in these SWAN model analyses. Furthermore, a substantial degree of additional refraction of the waves would occur between that 5-metre depth and the nearshore where the waves have increased in their heights to the point where they become unstable and break, and then swash up the sloping beach. In our analyses of the wave breaker heights and swash runup levels undertaken here and in subsequent chapters, we do not actually apply the magnitudes of the SWHs at the 10- and 5-metre depths derived in those studies, instead utilizing them only as indicators of the extent of refraction that has occurred from deep water to those depths, and how it varies along the lengths of these shores, there expected to be parallel variations in the magnitudes of the wave breaker heights and runup levels.

In summary, it is noteworthy that at all of the Hawke's Bay coastal sites within the Bay View and Haumoana Littoral Cells analyzed by Tonkin and Taylor (2003) and MetOceans (2008, 2011), the wave heights have been reduced from their deep-water values due to the combination of shoaling transformations, wave refraction and bottom friction. The resulting degrees of reduction have produced alongcoast variations in the shallow-water wave climates within the littoral cells, with the reduction having been greatest in the stretches of shore immediately north of Cape Kidnappers and at Westshore north of Bluff Hill, due to the partial sheltering by those promontories of the dominant storm waves arriving from the southeast. The consequence is that there will be parallel longshore variations in the calculated wave breaker heights and swash runup levels on the beaches, although the runup could also be affected by differences in beach slopes.

6.3   WAVE BREAKER HEIGHTS

A major component in any nearshore processes climate is an assessment of the ranges and extremes in wave breaker heights on the beach, of obvious importance to coastal erosion hazards (Komar and Allan, 2002). Therefore of interest here are analyses of the breaking wave heights experienced on the Hawke's Bay beaches. The initial analysis will be directed toward the transformation of the deep-water wave climate derived in Chapter 5, to its equivalent nearshore climate of breaker heights, this being accomplished by employing a simple formula.

However, that initial assessment does not account for the energy reductions due to wave refraction and bottom friction, requiring that corrections be applied based on guidance from the analyses by Tonkin and Taylor (2003) and MetOceans (2008, 2011) of the SWHs at the 10- and 5-metre water depths offshore, directly seaward from the site where are to be made of the wave breaker heights in the nearshore.

Several studies have developed semi-empirical formulae that directly correlate the heights of measured breaking waves on beaches to their corresponding deep-water wave heights and periods [see review in Komar (1998, p. 214-217)]. The measurements to establish these formulae have come from both controlled laboratory wave tank experiments and field studies at a number of beach sites representing a variety of morphologies and wave-energy levels. The most successful correlation for the breaker height, H_b, is the formula

$$H_b = 0.39g^{1/5}(TH_\infty^2)^{2/5} \tag{6-1}$$

where T is the wave period and H_∞ is the deep-water wave height. Note that, perhaps unexpected, according to this formula and those developed by others there is not a dependence on the slope of the beach, this having been the conclusion based on data collected over a large range of beach slopes. Equation 6-1 does not account for wave refraction that would alter the energy of the waves and thus the breaker heights, this being particularly significant in Hawke Bay as already discussed. Furthermore, uncertain is the degree to which this formula accounts for energy losses due to bottom friction, although it is presumed to empirically on average include some effect, especially in the field measurements that were used to derive this formula.

Equation (6-1) is applied here to Hawke Bay to calculate values of the wave breaker heights on a typical mixed sand-and-gravel beach, the heights they would have reached had they not been reduced by wave refraction, which will differ alongshore from site to site. The calculations are based on the deep-water SWHs and periods determined in Chapter 5, the heights graphed in Figure 5-8 after corrections had been made such that the buoy measurements correspond in magnitudes with those of the wave hindcast data. The input data to the calculations here are therefore the hourly pairs of deep-water SWHs and periods (H_∞ and T), yielding a corresponding value for the wave-breaker height, H_b (its SWH).

The resulting histogram of calculated wave-breaker SWHs is shown in Figure 6-2, representing the 11 years of wave measurements by the Port's buoy (2000 through 2010). As expected, the distribution of breaker heights is closely similar in form to that of the deep-water wave heights (Fig. 5-8), but is systematically shifted to higher values as expected from the shoaling transformations, and also because at this stage we have not accounted for the reduction caused by refraction. In the calculations thus far, the mode of most frequent occurrences is at about 1.9 metres, the mean is about 2.3 metres, and the maximum calculated breaker heights are on the order of 10 metres. These calculated magnitudes are in reasonable agreement with those found by Tonkin and Taylor (2003) and MetOceans (2011) in their SWAN analyses for the waves south of Cape Kidnappers, on the sandy pocket beaches where refraction is less significant. However, it is evident that these results derived from our initial calculations using equation (6-1) are well off the mark for the shores of the Haumoana and Bay View Littoral Cells where refraction is significant, our calculated values being substantially higher than the breaking waves observed along those shores.

In Chapter 5 we empirically corrected the magnitudes of the SWHs measured by the Port's buoy in 16-metres water depth, so they would correspond to the wave hindcast assessments, combined to yield a deep-water wave climate. Here a similar analysis is undertaken, but in the opposite direction to transform the deep-water wave heights to the 10- and 5-metre depths determined by Tonkin and Taylor (2003) and MetOceans (2008, 2011) in their SWAN analyses, and ultimately providing a correction factor for our calculated breaker heights graphed in Figure 6-2. In Chapter 5 the correction factor was 1.91 to transform the buoy data to their "equivalent" deep-water SWHs, so the inverse correction would be 1/1.91 = 0.52, but a further correction is required to account for the additional transformations of the waves to the 10- and 5-metre water depths, and then to wave breaking in shallow water on the beaches. Here the transformations become complex in that simple shoaling will act to increase the heights of the waves, whereas refraction and bottom friction act to reduce the wave heights, important being the net balance between these opposing trends.
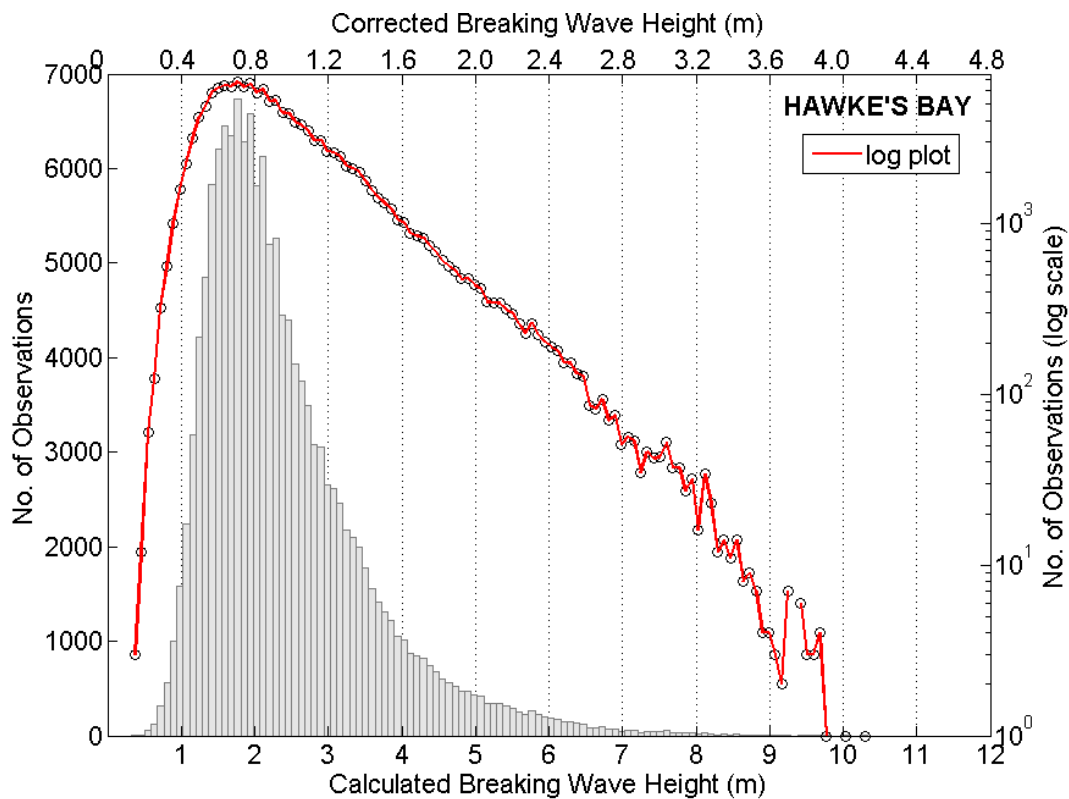
Figure 6-2: Wave-breaker significant wave heights initially calculated with equation (6-1) from the deep-water wave climate, yielding the values given by the lower axis, the upper axis having been corrected using a 0.4 factor to account for the reduction by wave refraction.

As reviewed in Chapter 5, the transition from intermediate to shallow water in the shoaling analysis is given by the ratio $h/L_\infty = 1/20$ of the water depth h to the deep-water wave length $L_\infty = (g/2\pi)T^2$, the transition therefore being dependent on the wave period. This relationship indicates that at the 10-metre water depth all waves having periods greater than 11 seconds are in shallow water, and at the 5-metre depth waves having periods greater than 8 seconds are in shallow water. The significance is that effectively all of the dominant waves reaching this

6 - 6

shore are already in shallow water at those depths, and therefore would be expected to increase in their heights as they approach the beaches, tending to increase up to the point where they achieve their maximum heights, become unstable and break on the beaches. Considering only shoaling, the SWHs could increase by about 50% from their heights in 10-metres depth. However, this potential increase from shoaling is offset by the reduction of the wave energy and wave heights caused by additional wave refraction. In that the extent of refraction varies along the shores of the Bay View and Haumoana Littoral Cells, the resulting balance between shoaling and refraction will change from site to site, as will the net correction factors. To provide and example result, in Figure 6-2 a 0.4 correction factor has been applied to the initially calculated wave breaker heights obtained with equation (6-1), yielding the "corrected" axis in the graph representing in general the central portion of shore within the Bay View Littoral Cell. With that correction, the mean breaker height is reduced to about 1.0 metre, and the maximum SWH to on the order of 4 metres. These results imply some increase in wave heights from the 5-metre depth assessments by MetOceans (2011), where the mean and maximum were respectively 0.8 and 3.8 metres for this relatively exposed shore; there has been a net increase as the waves continue to approach the nearshore, expected from the common observation that the waves rapidly increase as they approach the beaches, increasing their heights until they break. The results in Figure 6-2 are offered only as an example analysis of the wave breaker heights, the results differing on other sites along the shores, with the magnitudes of the breaker heights being less that estimated for this relatively exposed shore that has experienced a smaller degree of wave refraction.

It is recognized that this empirical approach in the analyses of the wave-breaker heights is only approximate, but the goal has been to develop a methodology that yields a reasonable depiction of the ranges of wave breaker heights within the nearshore processes climate, representing the general levels of wave energies important to the erosion hazards at that site. The results, however, are not actually employed in a quantitative sense to evaluate hazard zones or set-back distances for the safer construction homes, more important in that application being the wave swash runup levels.

6.4   WAVE SWASH RUNUP LEVELS ON HAWKE'S BAY BEACHES

In considerations of coastal hazard assessments, the most important component in the nearshore processes climate is the wave swash runup levels at the shore, particularly their extremes during storms. Analyses here are directed toward calculations of the runup for Hawke's Bay. In Chapter 7 the addition of the runup levels and the simultaneously measured tides will determine the total water elevations and their extremes, which can then be compared with the elevations of the beach and backshore properties to assess their potential impacts. Here calculations of the runup levels are derived from the hourly values of the deep-water SWHs and periods derived based on the Port's buoy measurements (Chapter 5), yielding a histogram for the range of its magnitudes and extremes. The analysis of the runup is much the same as that undertaken above for the wave breaker heights, again initially being based on a formula that directly calculates the runup from the deep-water wave climate, but with that magnitude similarly being corrected to account for the local effects of wave refraction that will reduce the runup magnitudes along the shores of the littoral cells.

Formulae are available from the published literature that can be applied to calculate the wave swash runup levels, their vertical components, for each hourly combination of deep-water SWHs and periods. Unlike the wave breaker heights, the swash runup also depends on the beach slope; however, as will be seen in Chapter 7 where analyses are undertaken for several survey sites, the beach profiles of these mixed sand-and-gravel beaches are consistently close to a slope of about 0.1 (1-in-10), a value that is used here in developing an example of the analysis procedures and its results.

The formula employed in this application originated in analyses of field measurements by Holman and Sallenger (1985) and Holman (1986), collected at the Field Research Facility of the U.S. Army Corps of Engineers in Duck, North Carolina. Their measurements were analyzed to determine both the components due to wave setup[1] and the swash of individual waves above that mean water elevation. While their analyses considered these separate components and derived individual formulae for each, they also obtained an equation for the combined setup and swash, the total water level associated with the waves, this being of prime interest in our applications to assess the erosion and flooding of shore-front properties in Hawke's Bay.

As part of our investigations of erosion hazards along the coast of the U.S. Pacific Northwest, we collected additional measurements of swash runup levels and related their magnitudes to the deep-water SWHs and periods (Ruggiero et al., 2001). With that data, together with field measurements from previous studies, we derived the formula

$$R_{2\%} = 0.27(SH_\infty L_\infty)^{1/2} = 0.108(gSH_\infty T^2)^{1/2} \qquad (6\text{-}2)$$

where S is the beach slope and $L_\infty = (g/2\pi)T^2$ is again the deep-water wave length, its substitution yielding the second form of the relationship of equation (6-2). The measured runup level, $R_{2\%}$, represents the 2% exceedance value within the distribution of individual measured swash maxima, an extreme in the distribution but occurring sufficiently often during an hour that it represents a meaningful factor to the impacts of backshore properties. Again, this is the vertical component, and includes both the wave setup and runup of individual waves.

A still later development of a runup formula is that by Stockdon et al. (2006), who analyzed time series of water-level measurements derived from ten field investigations, representing diverse beach morphologies including dissipative, intermediate and reflective categories in the morphodynamics classification of Wright and Short (1983). Their semi-empirical analyses separately considered the mean wave setup at the shore and the additive wave swash, with separate analyses of the latter to consider both the incident and infragravity energies within the motions and maximum levels of the swash runup. The general expression they obtained for all data sets from various beaches and including these multiple causative processes is

$$R_{2\%} = 1.1\left\{0.35S(H_\infty L_\infty)^{1/2} + \tfrac{1}{2}[H_\infty L_\infty(0.563S^2 + 0.004)]^{1/2}\right\} \qquad (6\text{-}3)$$

---

[1] The wave setup is produced by the momentum of the waves as they approach the shore, locally increasing the mean water levels above the measured tides, contributing to the total water elevation associated with the waves.

one that is seen to have a similar dependence on the waves and beach slope shown in Figure 6-2. This formula has been applied in our calculations of wave swash runup levels on the Hawke's Bay mixed sand-and-gravel beaches, having a mean slope $S = 0.1$. The calculations are based on hourly pairs of deep-water wave heights and periods, initially derived from the Port's buoy measurements (Chapter 5).

An example of a distribution of wave swash runup levels is graphed in the histogram of Figure 6-3, consisting of 11 years of calculated runup magnitudes. As in the case for the wave breaker heights (Figure 6-2), there are two axes representing the $R_{2\%}$ runup magnitudes, the bottom axis being that for the initial evaluations derived from equation 6-3, while the axis at the top of the diagram introduces a correction factor to account for the effects of wave refraction, and also possibly in this case the decrease in the runup level and cross-shore distance due to percolation of the water into these coarse-grained Hawke's Bay beaches. Again, these are vertical-component magnitudes for the runup, not elevations relative to a datum such as the mean sea level, that being accomplished later in Chapter 7 where we calculate and analyze the total water elevations, the summation of the runup and the measured tides, it being the tides that determine the water-level elevations relative to mean sea level and land-elevation datums.
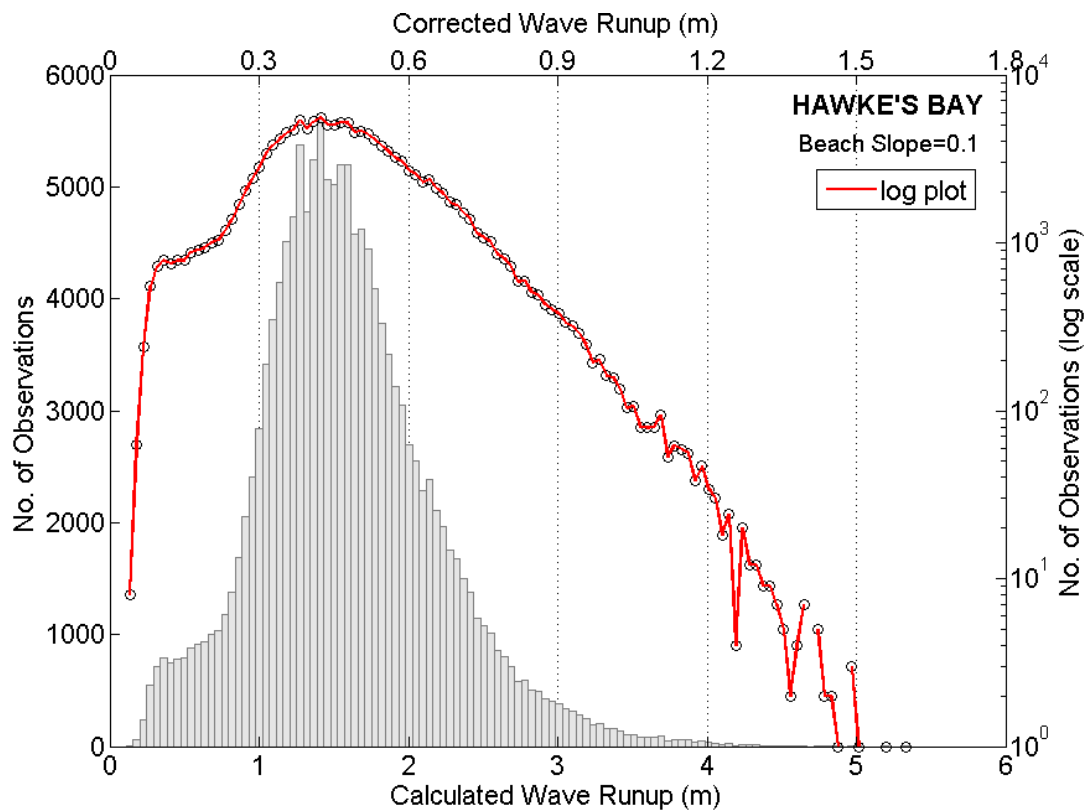
Figure 6-3: Linear and log graphs of the wave swash runup levels (vertical component), calculated with equation (6-3) from the deep-water wave climate and for a $S = 0.1$ beach slope. The upper axis for the "Corrected" values includes a 0.3 multiplication factor to account for the reduction caused by wave refraction water percolation into the beach face.

The runup histograms in Figure 6-3 show a mode of most frequent occurrence at about 1.5 metres for the initially calculated magnitudes, the most extreme being on the order of 5 metres. With a beach slope of 0.1, the horizontal components of the runup corresponding to these vertical levels would respectively be 15 and 50 metres. As will be seen in Chapter 7, the vertical and horizontal distances of the entire beach profiles are respectively on the order of 15 and 50 metres, indicating that as in the case of the initial calculations of wave-breaker heights, the runup magnitudes calculated from equation (6-3) are similarly too large, again due to not having accounted for the effects of refraction and energy losses due to bottom friction. Here we have employed a correction factor of 0.3 to account for this reduction, yielding the axis for the Corrected Wave Runup magnitudes. The maximum vertical component of the wave runup is now about 1.6 metres, representing a 16-metre horizontal swash distance, more reasonable for the Hawke's Bay mixed sand-and-gravel beaches. This example using a 0.3 correction factor was arbitrarily selected, on the bases that it yielded seemingly reasonable results. Its value is not as clearly established by the extent of wave refraction in that equations (6-2) and (6-3) for the calculation of the runup depend primarily on the wave period that is not altered by refraction, there being a reduced dependence on the SWH that could be substantially reduced by refraction. More meaningful site-specific assessments of this correction factor will be undertaken in Chapter 7, where the model results for the total water elevations are in effect calibrated through comparisons with the junction elevations between the site's beach and backshore properties, this geomorphic feature providing the primary evidence for the extreme magnitudes of total water elevations experienced during storms and high tides.

6.5 DECADAL TRENDS OF BREAKER HEIGHTS AND RUNUP LEVELS

It was seen in Chapter 5 (Figure 5-11) that there is evidence for a decadal net trend of increasing annual-average SWHs measured by the Port's wave buoy, consistent with increases found by Young et al. (2011) in analyses of satellite measurements along the coasts of New Zealand. In that the wave breaker heights and swash runup levels depend on the deep-water SWHs, increases in those nearshore processes would be expected.

An analysis of the annual-average wave breaker heights is presented in Figure 6-4, corresponding to the magnitudes in the histogram in Figure 6-2 with the 0.4 correction factor having been included. As expected there is a significant degree of data scatter, but linear regression suggests that on average there has been an increase at a rate of 0.0135 m/year, amounting to a 15-centimetre increase during the 11-year record, somewhat higher than the 0.008 m/year rate for the annual averages of the deep-water SWHs. Although this rate of increase in the breaker heights might seem small, it amounts to a 6% increase above the 2.35-metre mean breaker heights in the year 2000. However, as noted in Chapter 5 concerning the decadal increase in the deep-water wave heights, having been based on a limited record of data it is not possible to conclude with confidence that a climate-controlled increase in breaking wave heights has occurred on the Hawke's Bay beaches, and would be expected to continue in the future.
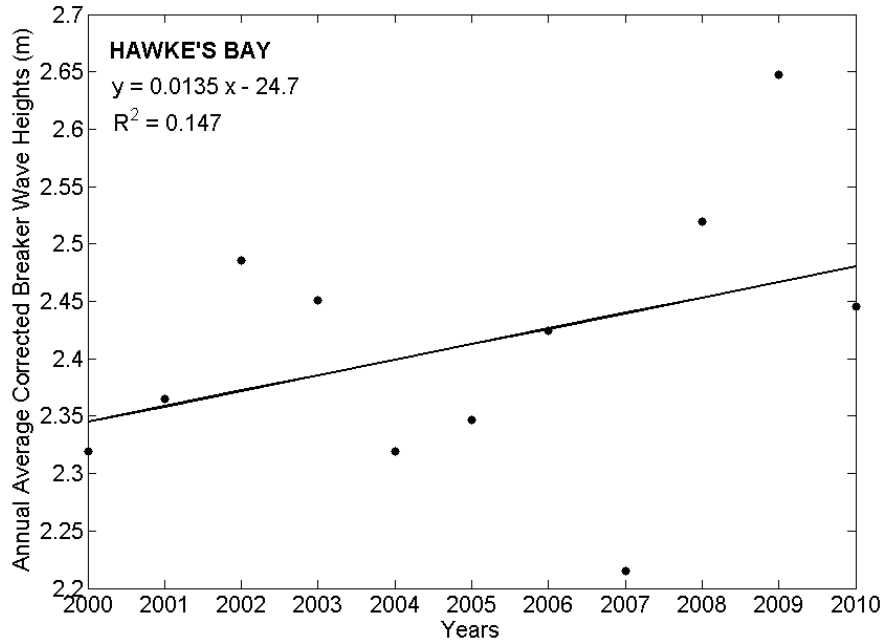
Figure 6-4: Trend of increasing annual-average wave breaker heights calculated from the deep-water wave climate, the result being comparable to that in Chapter 5 for the annual averages of the deep-water SWHs.

Comparable analyses of the annual-average swash runup levels are graphed in Figure 6-5, but the results are seen to be extremely scattered, with no discernable decadal trend. This contrast from there being decadal trends in the deep-water and breaking wave heights might initially seem puzzling in that one would expect there to also be a trend of increasing swash runup levels on the beaches. This lack of a trend for the swash runup is understandable, however, when one compares the formulae we have used in our calculations. For the deep-water wave climate, the trend for the annual averages was based directly on the hourly data for the SWHs, H_∞ (Figure 5-11). In the case of the wave breaker heights, according to equation (6-1) the relationship is $H_b \propto H_\infty^{4/5} T^{2/5}$, there being a strong dependence on the deep-water wave heights but only a weak dependence on the wave period. In contrast, from equations (6-2) and (6-3) for the swash runup levels, the dependence is altered to $R_{2\%} \propto H_\infty^{1/2} T^1$, a much weaker dependence on the deep-water SWHs, the wave period instead having become the primary controlling factor. Although one would expect increases in both the deep-water wave heights and periods as storms become stronger due to climate controls, the increase in the wave heights would be substantially greater than the shift in periods to higher values; this has been shown in our analyses of wave climate trends in the U.S. Pacific Northwest, with both the wave heights and periods having increased over the decades, but with the change in periods having been much smaller (Allan and Komar, 2006). This difference for wave breaker heights versus swash runup, respectively equations (6-1) and (6-3), is undoubtedly the cause of the contrasting results found here, with the annual average deep-water SWHs and breaker heights showing trends of increasing magnitudes, whereas the runup levels do not show the expected corresponding increase.

6 - 11
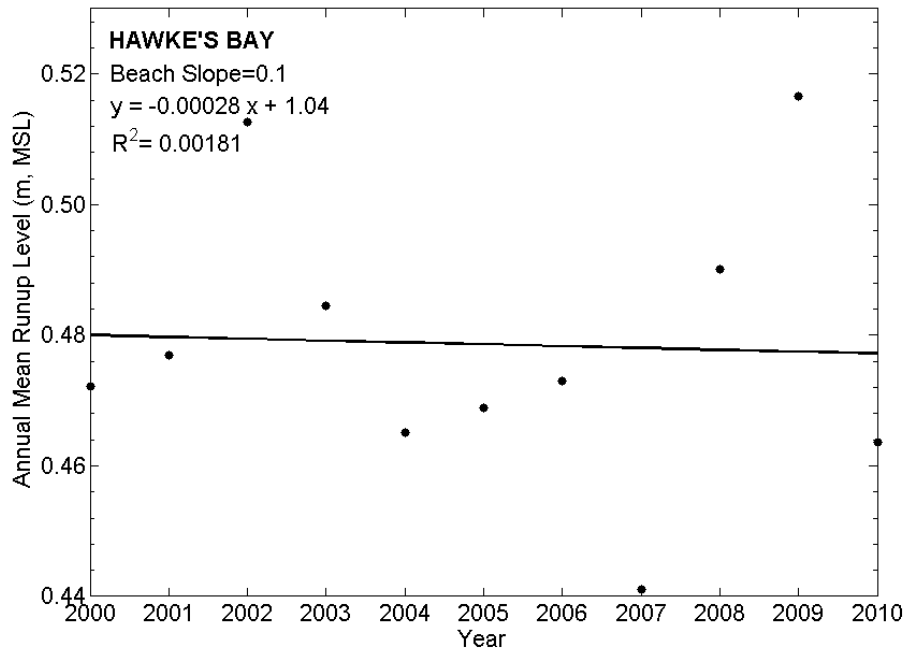
Figure 6-5: Annual-average wave runup levels, calculated from the deep-water wave climate using equation (6-3).

This difference can be traced to the contrasting approaches taken in deriving their respective equations used in our calculation. The relationship between the breaker heights and those in deep water is logically based on the energy flux or power of the waves, the basis for analyzing wave-shoaling transformations. The runup on the sloping beach is instead analyzed as a function of the dimensionless Iribarren Number, $S/(H_\infty/L_\infty)^{1/2}$, the ratio of the beach slope to the deep-water wave steepness (Holman, 1986; Stockdon et al., 2006), which emphasizes the importance of wave periods rather than wave heights.

Considering these seemingly disparate results, the trends of increasing deep-water wave heights and breaking wave heights on the Hawke's Bay beaches are consistent with the increase found by Young et al. (2011) in analyses of satellite measurements, globally and along the shores of New Zealand. It is logical to expect that the swash runup levels on the beaches would similarly increase, in spite of the outcome of the analyses here. While the $R_{2\%} \propto H_\infty^{1/2}T^1$ process dependence in the runup formulae might statistically predict the magnitudes of the runup through its combination of wave heights and periods, it appears that the weak dependence in the formulae on the deep-water wave heights is incapable of demonstrating the expected decadal increase in runup levels. This difficulty is of course exacerbated by our presently having only an 11-year record of wave measurements to analyze, it actually being of some surprise that we have been able to find evidence that the deep-water wave heights and wave breaking heights appear to have increased during that short period of time.

6.6 SUMMARY

The goal in this chapter has been to establish a methodology for analyses of the nearshore processes climates along the central coast of Hawke's Bay, the heights of wave breaking and swash runup levels on the steeply sloping mixed sand-and-gravel beaches found in the Bay View and Haumoana Littoral Cells. Important to assessments of the erosion and flooding hazards along those shores, the analyses of those processes involved the transformation of the deep-water wave climate developed in Chapter 5, to the resultant processes of potential significance to impacts on ocean-front properties and infrastructure. The analyses developed in this chapter have been general rather than site specific, providing only example assessments in the methodologies. Expanded analyses of the distributions of swash runup levels will be undertaken in the following chapter, which are then combined with the measured tides to determine the hourly total water elevations, the results being site specific through comparisons with surveyed profile elevations of the beaches and backshore properties. That comparison in effect empirically calibrates the process analyses and model assessments developed thus far, such that there is agreement with the geomorphology of the Hawke's Bay beaches, the junction elevations between the beach face and the wave-cut backshore bluff that provide direct evidence for past extreme water levels that have occurred during major storms, with the elevations of the barrier gravel ridges where overwash events have taken place offering further evidence for the magnitudes of the extreme total water levels.

6.7 REFERENCES

Allan, J. C., and P.D. Komar (2006) Climate controls on US West Coast erosion processes: *Journal of Coastal Research*, v. 22, no. 3, p. 511-529.

Gibb, J.G. (1962) Wave refraction patterns in Hawkes Bay: *New Zealand Journal of Marine and Freshwater Research*, v. 6, p. 435-444.

Gorman, R. M., K. R. Bryan and A. K. Laing (2003a) A wave hindcast for the New Zealand region: Nearshore validation and coastal wave climate: *New Zealand Journal of Marine and Freshwater Research*, v. 37, p. 567-588.

Gorman, R. M., K. R. Bryan and A. K. Laing (2003b) A wave hindcast for the New Zealand region — Deep water wave climate: *New Zealand Journal of Marine and Freshwater Research*, v. 37, p. 589-611.

Holman, R.A. (1986) Extreme value statistics for wave run-up on a natural beach: *Ocean Engineering*, v. 9, p. 527-544.

Holman, R.A., and A.H. Sallenger Jr. (1985) Setup and swash on a natural beach: *Journal of Geophysical Research*, v. 90, n. C1, p. 945-953.

Komar, P.D. (1998) *Beach Processes and Sedimentation*: 2nd edition, Prentice Hall, 544pp.

Komar, P.D., and J.C. Allan (2002) Nearshore-process climates related to their potential for causing beach and property erosion: *Shore & Beach*, v. 70, n. 3, p. 31-40.

MetOceans (2008) *Westshore Reef Surf Conditions*: MetOcean Solutions Ltd., New Plymouth, New Zealand, 65 pp.

MetOceans (2011) *Hawkes Bay Wave Climate*: MetOcean Solutions Ltd., New Plymouth, New Zealand, 42pp.

Ruggiero, P., P.D. Komar, W.G. McDougal, J.J. Marra, and R.A. Beach (2001) Wave runup, extreme water levels and the erosion of properties backing beaches: *Journal of Coastal Research*, v. 17, no. 2, p. 407-419.

Stockdon, H.F., R.A. Holman, P.A. Howd, and A.H. Sallenger (2006) Empirical parameterization of setup, swash, and runup: *Coastal Engineering*, v. 53, p. 573-588.

Tonkin and Taylor (2003) *Hawke's Bay Nearshore Wave Climate*: report to the Hawke's Bay Regional Council, 13 pp + Appendices.

Wright, L. D., and A. D. Short (1983) Morphodynamics of beaches and surf zones in Australia: *In Handbook of Coastal Processes and Erosion*, ed. P.D. Komar, pp. 35-64, CRC Press, Boca Raton, Florida.

Young, I. R., S. Zieger and A.V. Babanin (2011) Global trends in wind speed and wave height: *Science*, v. 332, p. 451- 455.

7 Water Levels, Beach Morphologies and Erosion Hazards

7.1 INTRODUCTION

The objective of this study has been to analyze the ocean processes that are responsible for occurrences of erosion and flooding along the coast of Hawke's Bay, undertaken at representative sites within the Bay View and Haumoana Littoral Cells. This includes projections of those hazards into the future with rising sea levels and potentially increasing storm intensities. In preparation for those assessments, in earlier chapters we analyzed the ranges and extremes in the measured tides (Chapter 4), the deep-water wave heights and periods (Chapter 5), and evaluated the nearshore processes of wave breaker heights and swash runup levels on the mixed sand-and-gravel beaches in these littoral cells (Chapter 6). The goal of the present chapter is to combine these processes, specifically the measured tides plus the swash runup levels, to determine the hour-to-hour variations in total water levels, and then compare their extremes with the elevations of the beaches and backshore properties to assess the present-day erosion and flooding hazards.

In this comparison between the ocean processes and the geomorphic evidence in the surveyed beach profiles for past significant erosion events, it is our working hypothesis that the junction elevations between the beach face and the wave-cut backshore bluff, and also the elevations of barrier gravel ridges where overwash events have taken place, each provide the most direct estimates of past extreme total water levels. The deep-water wave climate for Hawke's Bay contains significant uncertainties, especially in its assessments of extreme significant wave heights (SWHs) during major storms, and even in applications of the most up-to-date models to evaluate the wave refraction and energy losses while crossing the continental shelf, uncertainties remain in the resulting evaluations of the corresponding SWHs in shallow water (5- to 10-metres depths) offshore from the beaches. And we recognize that our calculations in Chapter 6 of the wave swash runup levels also include uncertainties, in part due to the unknown extent of water percolation beneath the swash as it flows across the coarse-grained mixed-sand-and-gravel beaches of the Bay View and Haumoana Littoral Cells.

In this chapter we consider the present-day ranges in magnitudes of the ocean processes, the tides and ocean waves measured by the Port of Napier's tide gauge and buoy, used to calculate the hour-to-hour variations in the total water levels, which are then compared with the surveyed beach profiles in order to assess the processes that were responsible for the geomorphic evidence of past erosion events, with implications as to their extreme occurrences. Deferred for consideration are projections through the 21st century (Chapters 8 and 9), the global rise in sea levels and possible climate-controlled increases in wave heights, with analyses of the potential future impacts to the shores of Hawke's Bay through the 21st century.

7.2 SURVEYED BEACH PROFILES

Important to the management of the Hawke's Bay beaches, specifically in assessments of their multidecadal trends of erosion versus accretion, has been a monitoring program with its emphasis placed on the collection and analysis of periodic surveys of beach profiles at a large number of stations along the shores of the Bay View and Haumoana Littoral Cells. The history, procedures, and products of this monitoring program have been summarized by Gibb (1995a, 1995b), while studies such as that by Tonkin and Taylor (2003) have relied on the survey data in applications, at the same time having provided reviews of the status of the accumulated profiles. The report by Edmondson et al. (2011) provides the most recent analyses of the profile surveys, their results being important in this study.

The efforts directed toward monitoring the beaches, including the surveys of profiles, were initiated in reaction to past impacts from erosion. According to Gibb (1995a), the earliest profiles date back to 1914 in East Clive, surveyed in response to the erosion that threatened the Hastings sewer outfall. In 1916 New Zealand Railways established 15 profile sites at Westshore to monitor the threat to their railway line, having surveyed them at regular intervals until 1961. Over the years additional profiles have been added, again mainly in response to episodes of erosion and flooding. The beach-profile monitoring program now underway was established in 1974 by the Hawke's Bay Regional Council (HBRC), having included many of those earlier profile sites but adding others so that the entire lengths of the Bay View and Haumoana Littoral Cells are now included (as are other beaches within Hawke's Bay). The existing coverage of sites in those littoral cells is shown in Figure 7-1, there being 12 evenly-spaced sites covering the shore of the Haumoana Littoral Cell, and 11 in the Bay View Cell. The beaches of those sites have been surveyed monthly, annually, or on a bi-annual basis, as well as occasionally following major storm events.

The updated analyses by Edmondson et al. (2011) included profiles from the 1970s to December 2010, the actual numbers of profiles depending on the site. In order to assess the extent of the erosion or accretion over the decades, Edmondson et al. (2011) analyzed the horizontal movement of the shoreline at the 1.5-metre elevation above mean sea level, and the volumes of beach sediment per metre of shoreline length above that elevation. Such assessments of the trends in shoreline positions and beach sediment volumes have been important in establishing meaningful hazard zones, so the construction of homes or other developments are safer from the potential dangers inherent to living in close proximity to the ocean. Past studies specifically directed toward hazard-zone assessments include those by Gibb (1996, 2002), Oldman et al. (2003), and Tonkin and Taylor (2003). Other uses of the monitoring profiles have included the development of sediment budgets, or were directed toward specific management issues such as assessments of the impacts produced by the commercial beach sediment mining at Awatoto, and to determine the effectiveness of the beach nourishment program at Westshore.

To meet the objectives of this study, six representative sites have been selected for analyses, three from each of these littoral cells. In order from south to north the sites are:

> HB03:   Representing the Hawke's Bay shore that has experienced the greatest impacts from erosion, affecting the communities of South Haumoana to Te Awanga, the erosion attributed to there being a significantly negative balance in its sediment

budget, and possibly in part a result of the subsidence of that shore during the 1931 Hawke's Bay earthquake (Chapter 3);

HB06: Located in the community of East Clive, approximately midway along the shore of the Haumoana Littoral Cell, an undeveloped barrier gravel ridge having low elevations, susceptible to overwash occurrences during storms;

HB10: The southern edge of the city of Napier, in the vicinity of the aquarium, with its parking lot having experienced minor flooding during storms;

HB14: Westshore, at the south end of the Bay View Littoral Cell, sheltered by Bluff Hill and the Port's breakwater from the dominant waves that arrive from the southeast, this profile site being north of the stretch of shore where sand and gravel is placed in the nourishment program;

HB17: Located in the community of Bay View, approximately midway along the length of this littoral cell, a site that has experienced some erosion of the barrier ridge following its uplift during the 1931 earthquake, but is comparatively stable now;

HB20: The community of Whirinaki, representing the northern one-third of the Bay View Cell's shoreline, characterized by a higher bluff cut into the uplifted gravel ridge, with evidence for there having been recent occurrences of erosion by high tides and storm waves.
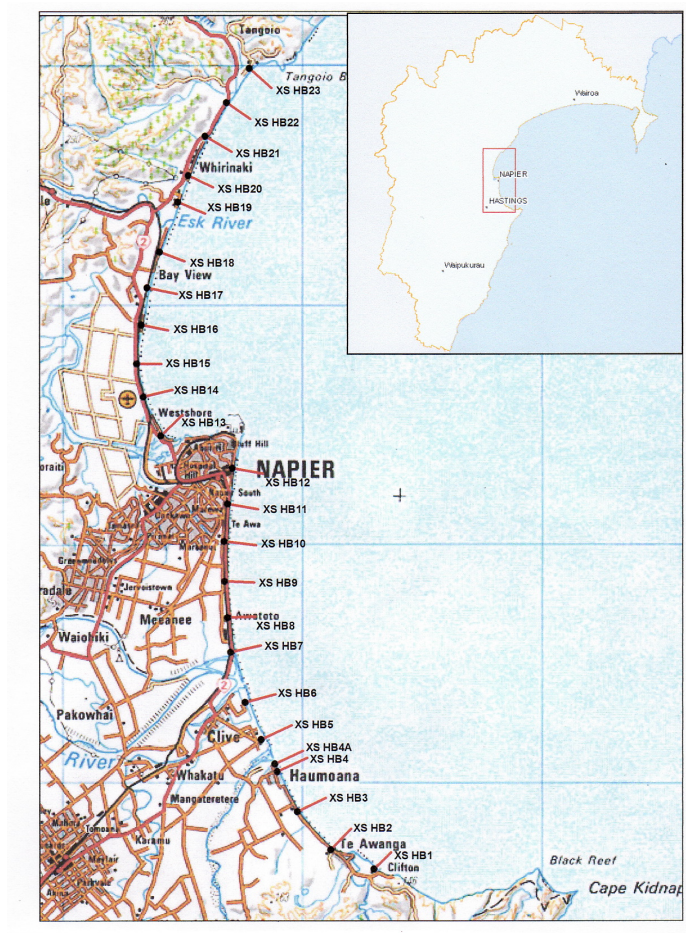
Figure 7-1: Locations of the beach profile sites surveyed as part of the Hawke's Bay Regional Council's monitoring program. [*From* Edmondson et al. (2011)]
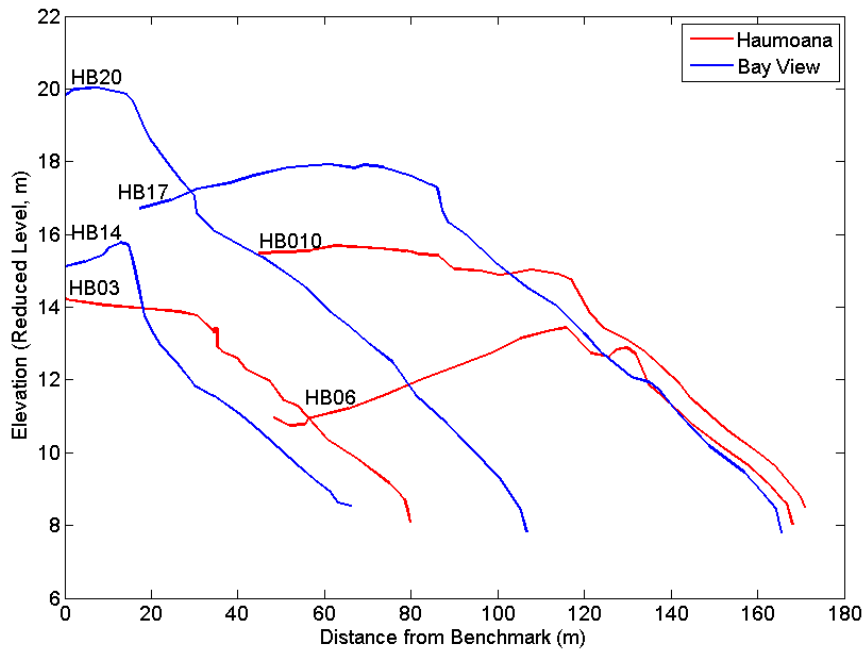
Figure 7-2: Representative beach profiles (2010) from the Haumoana and Bay View Littoral Cells, the focus of hazard assessments based on analyses the total water levels of measured tides plus the wave swash runup.

Recently surveyed (2010) profiles of these six sites are graphed in Figure 7-2, showing their overall morphologies and permitting general comparisons between the elevations of the beaches and backshore gravel ridges. Both the surveyed elevations and cross-shore distances are relative to established benchmarks, the elevation datum being denoted as the "Reduced Level" (RL), with the mean sea level being approximately at the 10-metre RL elevation. The horizontal distances and positions of the profiles relatively to one another in the graph depend on the locations of their respective benchmarks, and therefore have no significance with respect to their trends of erosion versus accretion, or to their potential erosion hazards. Of primary interest are comparisons between the elevations of these profiles, being highest at the north within the Bay View Cell (HB20), followed by the next profile to the south (HB17), with the two in Napier (HB14 and HB10) having approximately the same elevations even though they are in separate littoral cells, respectively being north and south of the Bluff Hill headland. The profiles of the two sites to the south within the Haumoana Littoral Cell (HB06 and HB03) are still lower, having subsided during the 1931 earthquake. There are also systematic alongcoast variations in the junction elevations between the active beach and eroded backshore escarpment cut into the gravel ridge, providing direct evidence for the elevations of the wave runup and tides experienced as those sites during past storms. This evidence for past water elevations that resulted in erosion of the barrier gravel ridge, derived from the morphologies of the surveyed profiles, will be compared with the extreme combinations of tides plus the wave runup, being the focus of analyses presented later in this chapter.

Table 7-1 summarizes the characteristics of these six profile sites, including their multidecadal net rates of shoreline erosion or accretion analyzed by Edmondson et al. (2011), the values of their surveyed beach/bluff junction elevations derived from the profiles in Figure 7-2, and the elevations of the backshore that in most cases represent the seaward portions of the shore-front properties or undeveloped open space. As expected from the tectonic-induced land elevation changes during the 1931 earthquake, the elevations of the backshore landward from the active beaches are highest at the north end of the Bay View Littoral Cell (Profiles HB20 and HB17) where the greatest uplift occurred, somewhat lower at the south end of that Cell (HB14), and with the backshore elevations of the profiles at the south end of the Haumoana Cell (HB03 and HB06) being significantly lower; the total difference is on the order of 3 to 5 metres between the highest in the north to the lowest in the south. Although this systematic alongcoast variation for the most part can be accounted for by the tectonic induced land-level changes during the 1931 earthquake, the ocean processes had also been factors, the levels of storm washover that occurred along essentially the entire length of the coast prior to its tectonic uplift, similarly to what now occurs but is limited to the low-elevation shores of the south Haumoana Cell (e.g., at East Clive, HB06).

Table 7-1: Trends of shoreline change (Edmonson et al., 2011) and elevations of the beach/bluff junctions and maximum of the backshore gravel ridge.

	Shoreline Trend (metre/year)	Beach/Bluff Elev. (metres RL)	Backshore Ridge Elevation (metres RL)
Haumoana Littoral Cell			
HB03 (South Haumoana)	-0.607	13.0	14.2
HB06 (East Clive)	-0.333	12-13	13.5
HB10 (South Napier)	+0.561	13.7	15.7
Bay View Cell			
HB14 (North Westshore)	+0.045	12.5-13.5	15.8
HB17 (Bay View)	+0.062	16.5	18.0
HB20 (Whirinaki)	-0.288	16.5	20.0

There are parallel alongcoast variations in the beach/backshore junction elevations, Table 7-1, but they have nothing to do with the tectonic-induced changes, instead being a record of the extremes in total water elevations that are a consequence of combinations of elevated tides and swash runup levels during major storms that have occurred since 1931. Those decades of erosion processes and their total water levels have been imprinted into the uplifted beach ridges subsequent to the earthquake, notching out escarpments into the barrier ridge that backs the active beach in the Bay View Cell, whereas both erosion and overtopping of the gravel ridge have occurred in the Haumoana Cell. As evident in the profiles graphed in Figure 7-2 and in the values listed in Table 7-1, the highest elevations of the beach/backshore junctions occur along the northern portion of the Bay View Cell (HB17 and HB20), it being fully exposed to the waves, while the junction elevations are significantly lower to the south in that cell (HB14), at Westshore which is sheltered from the waves. The beach/backshore junction elevations are also lower in the Bay View Cell, although as discussed later they are not as well defined since ridge overwash events occur at many sites, partly obscuring the records from erosion at the lower elevations.

Systematic alongcoast variations in elevations have been documented in detail by Gibb (2002) for the stretch of shore within the Bay View Cell, from Westshore sheltered by Bluff Hill, northward 10 kilometres to the mouth of the Esk River. His survey results are graphed in Figure 7-3, where the elevations are relative to Mean Sea Level (MSL). Graphed in blue are the elevations of the crest of the uplifted beach ridge, while shown in red are the elevations at the top of the active beach where it generally meets the toe of the scarp that has been eroded into the ridge subsequent to its uplift, the beach/backshore junction elevation of interest in our analyses. Gibb's survey shows that the barrier crest height increases significantly to the north, from an average elevation of 3.6 metres above MSL at South Westshore to an average of 8.4 metres MSL at Le Quesne Road (and then decreases near the Esk River, having been cut back by the river). Gibb (2002) correctly interpreted this trend in the elevation of the top of the gravel ridge as having resulted from the progressively increased exposure of the shore toward the north to greater wave heights and runup levels, reduced to the south by the sheltering of Bluff Hill and the Port's breakwater. It is known from historic records that prior to its uplift in 1931, South Westshore adjacent to the inlet into the Ahuriri Lagoon experienced frequent overwash events due to its low elevations, having made it nearly impossible to develop that shore until the earthquake elevated those properties (Komar, 2005, 2010).
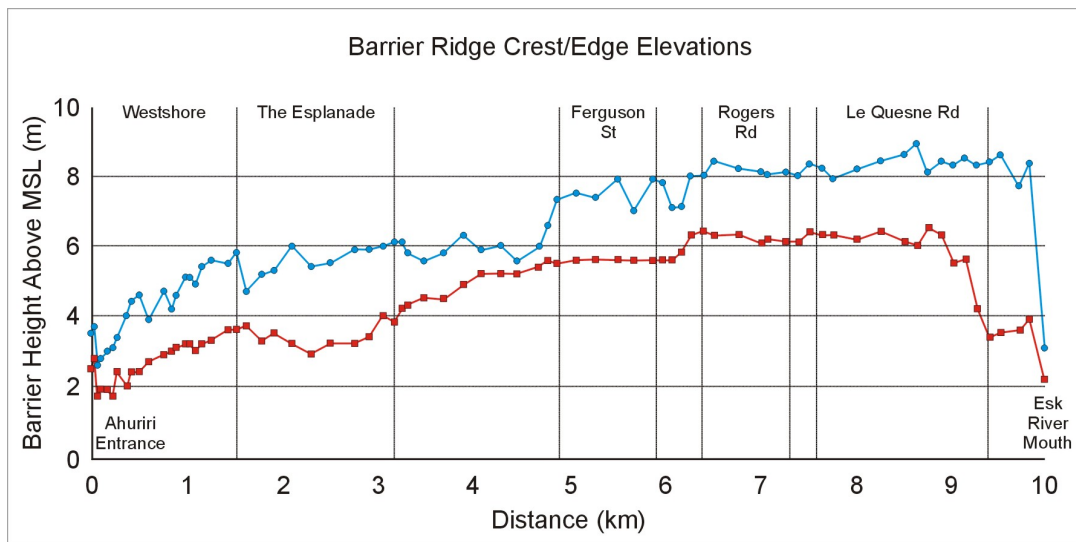
Figure 7-3: The elevations relative to Mean Sea Level of the crest of the raised gravel ridge (blue) and the edge of the eroding toe of the bluff scarp (red) where it meets the active beach, representing the beach/backshore junction elevation. [*From* Gibb (2002)]

Essentially the same alongshore trend is evident in the elevations of the beach/backshore junction, Figure 7-3, which again increases systematically to the north, from an average of 2.3 metres above MSL at South Westshore to 6.3 metres at Le Quesne Road. On average the difference in elevations of the crest top of the barrier ridge and its eroding junction elevations is about 1.8 metres, which Gibb (2002) correctly interpreted as having been produced by the uplift of this ridge at the time of the 1931 earthquake, with the present crest top corresponding approximately to the alongcoast shape of the ridge crest that had formed by overwash events prior to its uplift. There are local anomalies in this comparison, evident in

Figure 7-3; for example, according to Gibb (2002) the pronounced dip in the elevation of the ridge crest between The Esplanade and Ferguson Avenue was produced by earth-moving equipment. It is also evident that the beach/backshore junction elevations have been affected by the beach nourishment program at Westshore, in operation since 1987. Gibb's (2002) interpretation was that the dip in its elevation along The Esplanade is the result of the beach nourishment, such that the lower edge (the top of the beach foreshore) reflects the elevations reached by storm waves only since 1987 when nourishment began, whereas elsewhere along the shore the higher elevations of the junction represent total water levels that had occurred during the 80 years since uplift took place, representing longer-term and more extreme events in the total water levels of tides plus storm-wave runup.

Important to assessments of the erosion hazards for Hawke's Bay is the question of how old the evidence is for past erosion events and the total water levels they infer, derived from the morphologies of the barrier gravel ridges and fronting beaches, with the series of profiles at most dating back to the 1970s, some only to the 1990s. The age of this evidence will depend in part on the history of erosion of the fronting beach; for sites experiencing a net retreating shore, the expectation is that the escarpment has similarly experienced erosion, representing comparatively recent storms, whereas accretion of the fronting beach opens the possibility of preserving much older evidence for past and more extreme erosion events. As listed in Table 7-1, of the six sites selected for analyses, according to the results of Edmonson et al. (2011), three of those beaches have experienced net erosion in recent decades, while three show trends of accretion. However, as noted earlier, these trends represent the horizontal shifts in the shoreline at the 1.5-metre elevation above mean sea level, that is within the active beach, the results not necessarily representing the extent of erosion of the barrier gravel ridge backing that beach site.

To examine the respective changes between the beaches and escarpments cut into the gravel ridges, the earliest surveyed profiles were compared with recent surveys (2010) for each of the six analysis sites. The comparisons for the Bay View Littoral Cell are graphed in Figure 7-4. The profiles for the Whirinaki site (HB20) include some 36 years of surveys, and it is evident in the comparison between the oldest (1974) and a recent profile (2010) that while the beach has experienced significant net erosion during that period (a rate of -0.288 metre/year according to Table 7-1), there has been almost no change in the position of the escarpment, although there now is a somewhat more prominent notch at its base where it meets the beach. However, the elevation of that notch has not changed, contrasting with the seaward elevations of the beaches where more erosion has occurred, lowering its level by 1 to 2 metres. In contrast, profile HB17 from the community of Bay View covers a time span of only 15 years (1995-2010), showing profiles that are essentially congruent, both in the ridge scarp and in the elevations of the fronting beach, agreeing with the near-zero rate of change (+0.064 metre/year) in Table 7-1. This difference between Whirinaki and Bay View in their trends of changing shorelines corresponds with the cell-wide patterns found by Edmonson et al. (2011), based on all of the profile sites within the Bay View Littoral Cell, there having been net erosion in the northern half of that shore, net accretion in the southern half. The absence of a change in the beach profiles in Figure 7-4 for Bay View is can therefore be explained by its location at the node in the oscillation between those eroding and accreting shores, there being a longshore transport of the beach gravels (north to south) but not a change in the sediment volumes and shoreline positions at that node. Somewhat unexpected in this comparison are the minimal changes in the scarps in recent decades that have been eroded into the uplifted barrier gravel

ridge, at least since the 1970s. It is noteworthy that the elevations of the beach/backshore junctions are the same at both sites, being about 16.5 metres, probably having experienced the same extreme storm events and total water levels, with that level possibly having been reached multiple times during the past 36 years documented by these profiles.
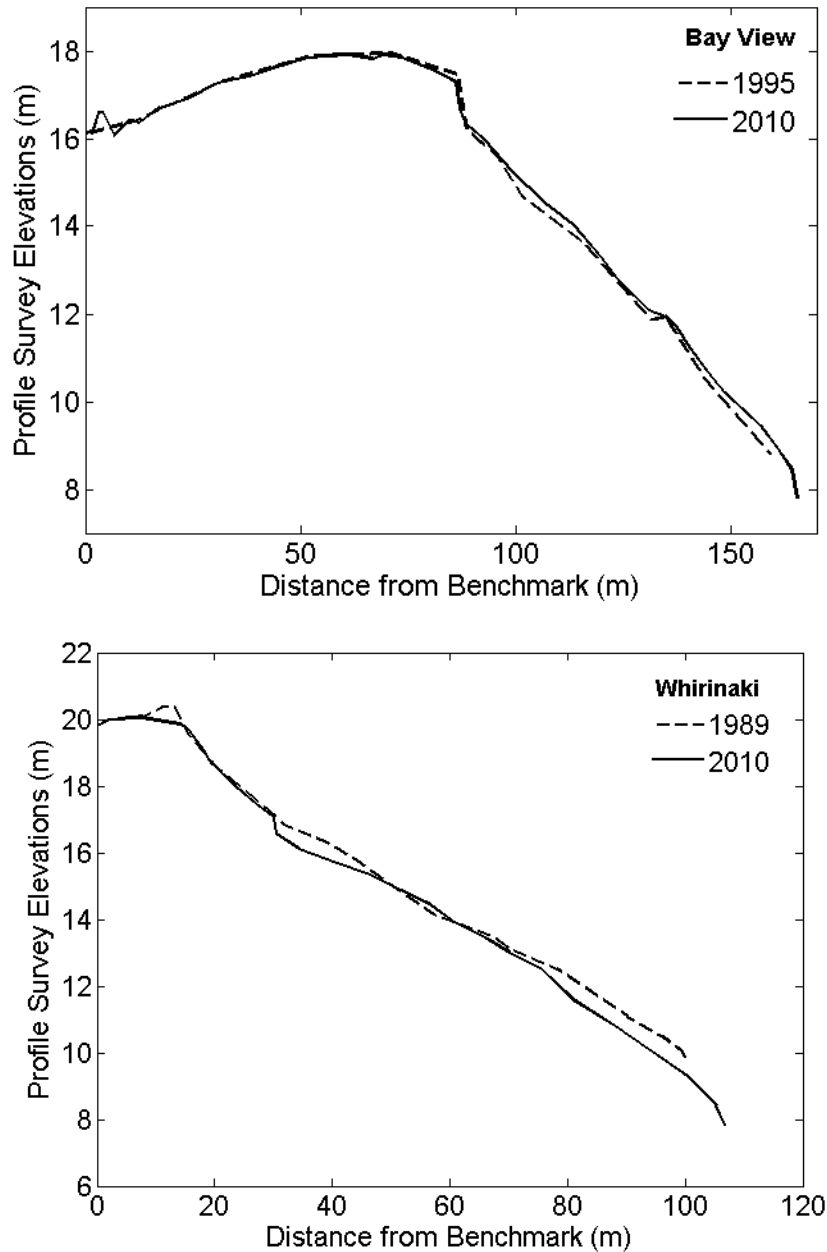
Figure 7-4: Decadal changes in the surveyed profiles at Bay View (HB17) and Whirinaki (HB20) within the Bay View Littoral Cell.

Figure 7-5 shows the similar profile comparison for the surveyed series at East Clive (HB06), the profiles surveyed in 1989 and 2011, with the ocean again being to the right in this graph. There is a surprising amount of change in the gravel barrier ridge at this site, although it could have been expected in that the ridge had experienced storm overtopping events during that period (Daykin, 2010). However, considering that this pair of surveys represents only 22

years, a significant volume of sediment is seen to have accumulated on the landward flank of the gravel ridge, with erosion of the ocean beach, an expected response from overtopping events, eroding gravel from the beach and transporting it over the top of the ridge to its landward side. In spite of the significant volumes of gravel having been carried by waves washing over the ridge, its crest has experienced relatively little change, maintaining an elevation at about 13.5 metres RL. The implication is that the total water levels of major storms have reached this elevation, producing overtopping by the wave swash, but not more extreme overwash that are know to breach barrier ridges, resulting in significant flooding of inland properties.
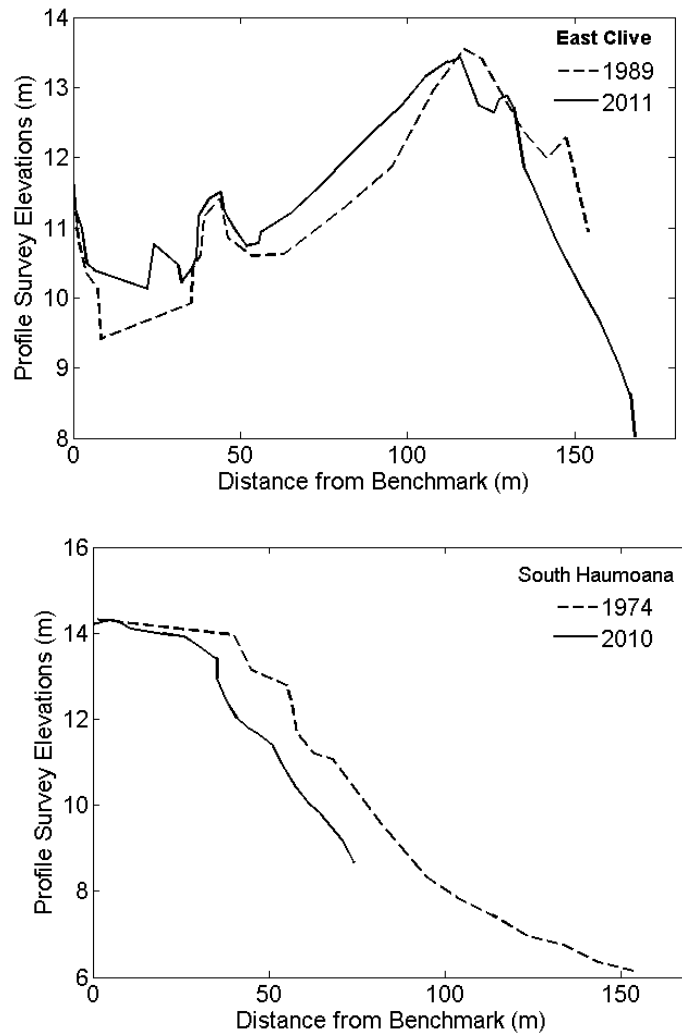
Figure 7-5: Changes in the beach profiles at East Clive (HB06) and South Haumoana (HB03) within the Haumoana Littoral Cell, the ocean being at the right in the diagrams.

Also included in Figure 7-5 are profiles from South Haumoana (HB03), comparing that in 1974 to the recent profile of 2010. As expected, there has been a significant retreat in the profiles, the net rate having been -0.607 metres/year (Table 7-1), attributed to this shore's beach sediment budget bing significantly "in the red", posing a threat of loss of a number of homes

along this shore (Dayton, 2010). A variety of seawalls have been constructed along this shore to protect the homes, with one being evident in Figure 7-5. The elevation of the junction between the beach and seawall is at about 13.0 metre, essentially the same at East Clive and South Napier to its north within the Haumoana Littoral Cell, suggesting that Haumoana experiences minimal sheltering by Cape Kidnappers at the south end of the Cell, also accounting for its problems with erosion.

7.3 ANALYSIS METHODOLOGY

The processes that impact ocean-front properties depend on the deep-water wave heights and periods generated by storms, which determine the levels of the wave swash runup on the sloping beaches, combining with the surge that is also generated by the storm, elevating the measured tides. Important is the summation of these processes, the resulting total water levels (TWLs) and in particular their extremes when a major storm occurs at the same time as the predicted astronomical tides are high. Whether or not erosion or flooding occurs then depends on the beach and property elevations, the toe of a foredune or the base of a sea cliff, it being this morphology compared with the TWLs that determines whether backshore erosion results from the wave impacts, and with the overall elevation of the properties governing whether overwash and flooding occur. These relationships between the ocean processes and coastal morphology have been formalized in the model developed by Ruggiero et al. (2001), shown schematically in Figure 7-6, depicting the summation of the measured tides that can be elevated well above their predicted levels, and with the vertical component of the wave runup superimposed to determine the total elevations reached by the water. According to the model as depicted in this diagram, the total water level TWL can be expressed simply as

$$TWL = E_T + C_r R_{2\%} \qquad\qquad (7\text{-}1)$$

where E_T is the elevation of the measured tide and $R_{2\%}$ is the wave swash runup level calculated from the deep-water wave height and period. As measured by a gauge, the tide includes both the predicted astronomical tides and processes that can elevate the water to still higher elevations. As reviewed earlier, these processes include the normal seasonal cycle of monthly-mean water levels, storm surges that raise water levels lasting hours to days, and possibly climate controls such as the range of El Niño/La Niña events that can result in extremes in the monthly-mean sea levels. The wave runup, $R_{2\%}$, is the 2% exceedence level as calculated with the relationships given in Chapter 6, in this report the equation of Stockton et al. (2006). The coefficient C_r is included in equation (7-1) to account for the effects of wave refraction and the loss of energy due to bottom friction, discussed in Chapter 6 and illustrated in Figure 6-3 for an example distribution of runup levels based on the Hawke's Bay wave measurements, in that example with $C_r = 0.3$. In the long term the projected rise in the relative sea level can also be added to determine the elevated TWLs and hazards expected decades into the future (Chapters 8 and 9).

For a site-specific application of this model, of importance is the corresponding elevation E_J of the beach/backshore junction, and also an elevation of the top of the backshore property E_{DC}, the comparison depicted in Figure 7-6 being a foredune backing the beach. The model as developed by Ruggiero et al. (2001), focusing on the toe erosion, can be extended conceptually

to include considerations of the elevations of the foredunes and their potential overtopping during storms, or in the case of the uplifted gravel ridges along the shores of the Bay View and Haumoana Littoral Cells, to assess the potential hazards from overwash and property flooding.
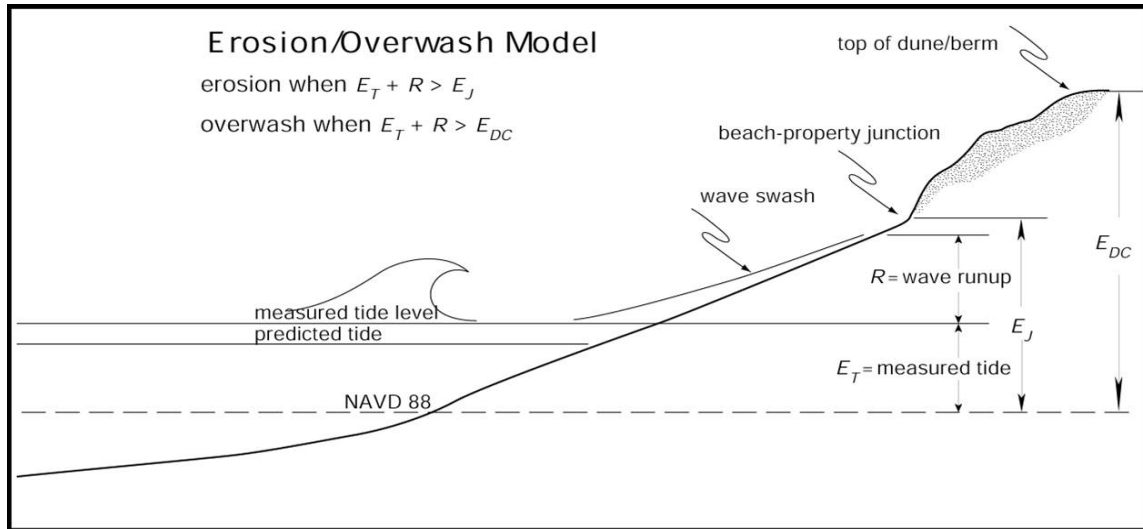
Figure 7-6: Model to assess the total water level resulting from the summation of the predicted tide, processes such as a storm surge that elevates the measured tides above their predicted levels, and the contribution of the vertical component of the wave-swash runup, the TWL (its elevation) being compared with the elevation of the toe of a foredune or sea cliff. [*Modified from* Ruggiero et al. (2001)]

Conceptually this model is relatively simple, but its applications generally require detailed data analyses, with various approaches being possible. In applications to the coast of the U.S. Pacific Northwest, Ruggiero et al. (2001) utilized the available long-term tide gauge records to document the hour-to-hour variations in the measured tides, the records having been sufficiently long that a large number of significant extratropical storm events were represented by their range of surge levels (which can be on the order of 1.5 metres on that coast), and included the 1982-83 major El Niño that raised measured tides by on the order of 0.5 metre above predicted levels throughout the entire winter. Hourly buoy measurements of the waves were also available spanning the decades back to the 1970s, permitting hourly assessments of the runup levels on the beaches. Analyses of the TWLs, the measured tides plus the swash runup, yielded a multidecadal documentation of the numbers of hours during which those combined processes could impact the base of a foredune or sea cliff, depending on its elevation. Based on multiple sites along the coast of the U.S. Pacific Northwest, it was demonstrated that the long-term net rate of sea cliff recession correlated with the annual numbers of wave impact hours, the erosion having also been governed by the compositions of the cliffs and the inherent resistance their rocks to wave impacts. Such data analyses also permitted assessments of the major storm events that had occurred over the decades, the extremes in TWLs that are most important to assessments of the erosion and flooding hazards.

The Ruggiero et al. (2001) model has served as the foundation in erosion hazard analyses along the coast of the U.S. Pacific Northwest, including having been applied to investigate individual

major storms that resulted in past property losses, then extended to make projections of future extreme events that could result in still greater occurrences of property impacts, supporting the determination of hazard zones (set-back lines) through the 21st century in which projections of future sea levels and increasing wave heights have been included (Allan and Komar, 2002; Komar et al., 2002; Komar et al., 2013). Similar analyses have been undertaken in the present study for the coast of Hawke's Bay, presented in this chapter to represent the present-day processes and hazards, while those in Chapters 8 and 9 project the hazards through the 21st century with accelerated rates of rising sea levels and increased storm intensities.

7.4 HAWKE'S BAY WATER ELEVATIONS AND BEACH MORPHOLOGIES

7.4.1 Introduction

Applications of the Ruggiero et al. (2001) model to Hawke's Bay are affected by the limited availability of hourly measurements of simultaneous waves and tides, there being little more than a decade of data, well short of that required to confidently project magnitudes of future extreme events. In view of this limitation, the objective in our initial analyses presented here will be directed toward developing a typical annual range of total water levels (TWLs), the sum of the hourly tides and wave runup. That analysis will be followed by a comparison between the extreme TWL magnitudes and morphologies of the beaches, particularly their beach/backshore junction elevations produced by past erosion events. The analyses will be based on the wave and tide data for the year 2010, for which we have complete records of both waves and tides collected by the Port of Napier, with that year also having been exceptional in its extremes, having experienced the highest measured waves and tides in the decade-long records. Analyses will also be presented to document the details of major storms that occurred during 2010, their hour-to-hour variations in wave heights, tides, and $TWLs$. To compliment those analyses limited to the year 2010, efforts will be directed toward assessments of the longer-term extremes through the development of "scenarios", combinations of high tides plus wave runup and surges generated by extreme storm events, combinations that while being possible, could represent what might be the most extreme hazards from erosion and flooding faced along the Hawke's Bay coast, when a major storm having extremes in its wave heights, runup levels and surge heights coincides with a high spring tide.

7.4.2 Histograms of total water levels

The calculations of total water levels (TWL) with equation (7-1) depend on the summation of the hourly measured tides (E_T) and the vertical component of the wave swash runup ($R_{2\%}$) on the beach face, determined from the measured waves. In this application to Hawke's Bay the tide at any specific hour can be assumed to essentially have the same elevation at all profile sites within the Bay View and Haumoana Littoral Cells, therefore not contributing to alongcoast variations in the TWLs. The surveyed variations in the beach/backshore junction elevations along this coast, evident in the profiles of Figure 7-2 to be analyzed here, and also those in Figure 7-3 from the surveys by Gibb (2002), must therefore be accounted for by differences in the levels of the wave runup ($R_{2\%}$) together with its correction factor C_r that accounts for the extent of refraction, it systematically changing along the length of the shore from exposed to sheltered sites. It is seen in Table 7-1 that the beach slopes in the intertidal zones of the six profiles are all nearly the same, essentially having a slope of 0.1 (1-in-10); this value is used in

the following analyses, such that changes in beach slopes are not a factor in accounting for alongcoast variations in swash runup levels and the eroded beach/backshore junction elevations.

In application to Hawke's Bay, the initially calculated value for $R_{2\%}$ represents the potential maximum runup level for a 0.1 beach slope, and hence the maximum TWL that would occur along that shore for a given combination of the deep-water significant wave height and period, the calculated runup not having been reduced by refraction or other energy losses. However, at shoreline sites where the refraction has been significant, such as at Westshore, the value of C_r will be significantly less than 1.0, in order to account for the reduced effective runup and resulting TWL, a reduction that will be required to provide a match with the lowered beach/backshore junction elevations along sheltered shores. Therefore, important in our Hawke's Bay analyses is the range of C_r magnitudes from 1.0 down to about 0.1, representing progressively decreasing wave runup contributions and therefore reduced TWL elevations. A C_r value of 0 would in effect be a shore where the beach morphology is determined only by the range of tides, the waves being negligible to absent.

In Chapter 6 a histogram of $R_{2\%}$ runup levels was calculated (Figure 6-3), with the initial un-refracted maximum magnitudes having then been reduced by a factor $C_r = 0.3$, serving as an arbitrarily selected example of the effects of wave refraction, yielding the Corrected Runup Level axis in that histogram, representing $C_r R_{2\%}$ in equation (7-1). In the analyses developed here of the TWLs and their relationship to the morphologies of the beach profiles at the monitoring sites, we are interested in the full range of $C_r R_{2\%}$ magnitudes supporting matches between the extreme TWLs and the elevations of the beach/backshore junctions. Also of general interest are the changes in the forms of the TWL histograms as C_r ranges from 0.1 to 1.0, how the distributions systematically change from being dominated by the tidal variations to where the waves become the most important process.

Calculations of TWL histograms have been completed at 0.1 increments from $C_r = 0.1$ to 1.0, based on the 2010 data sets for the waves and tides, with the results illustrated in Figure 7-7 by four of the ten histograms. The upper-left histogram calculated with $C_r = 0.1$ represents a condition of relatively small waves and runup, their contribution to the elevations reached by the water on the beach being small compared with the tides. As expected, the form of the distribution of TWLs in this case is dominated by the tides, with two prominent modes of maximum occurrences within the intertidal zone across the beach face. As discussed in Chapter 4, the distribution is somewhat asymmetric and shifted to higher values compared with that of the predicted tides, due to occurrences of storm surges that elevate the measured tides. Here in Figure 7-7, the shift to higher TWLs by surges has been further increased by inclusion of the wave swash runup. The following two histograms are for $C_r = 0.4$ and 0.7, the tides not having changed but there having been increased magnitudes of the swash runup produced by higher waves having reached the shore. In these transitional examples it is seen that the pair of modes of maximum occurrences contributed by the tides progressively disappear, the distributions instead having a central plateau of TWL magnitudes in the range 10 to 12 metres RL, increasingly dominated by the waves. The final histogram (lower right) with $C_r = 1.0$ represents the exposed coast condition where there essentially has been no wave energy reduction by refraction, representing the potential maximum wave input for Hawke's Bay according to its deep-water wave climate. For this end-member condition, the TWL distribution has become essentially unimodal, centered at about 11.5 metres RL for the 2010 measured waves and tides.
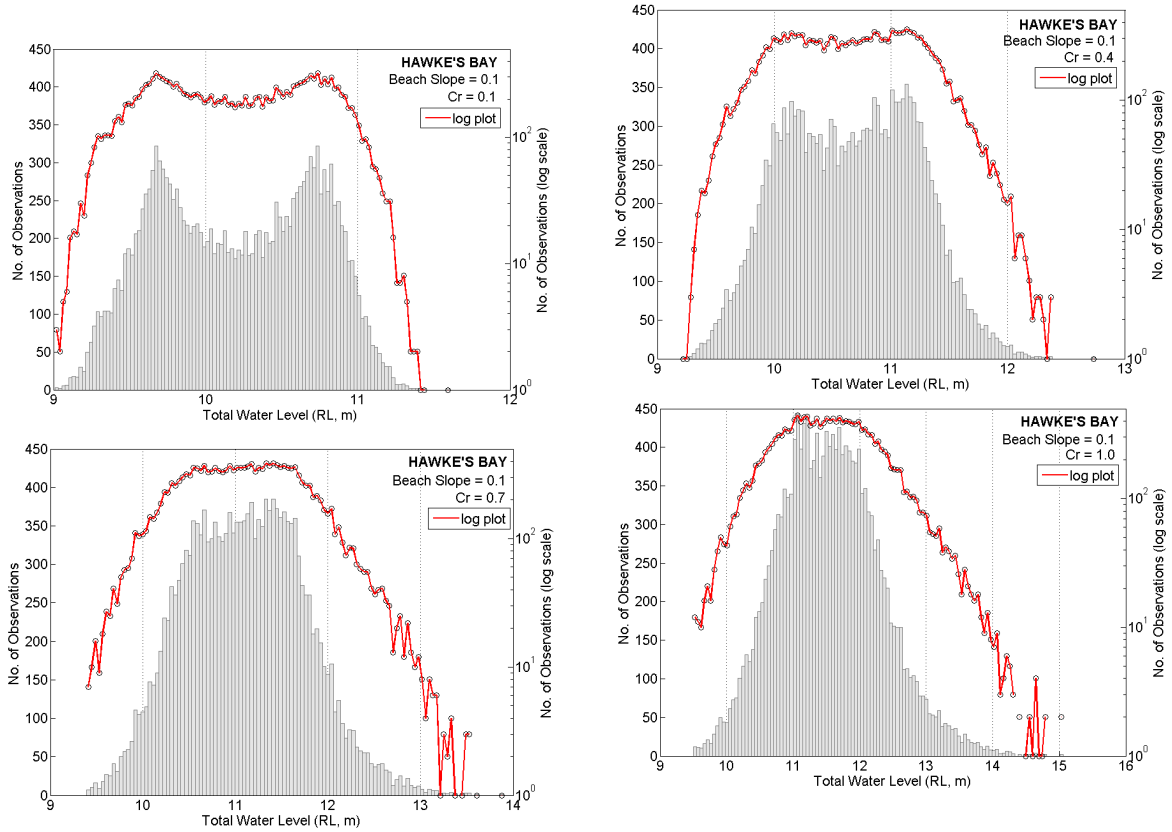
Figure 7-7: Representative examples of TWL distributions based on the 2010 Hawke's Bay measured waves and tides, for a series of C_r values representing increased swash runup levels determined by the extent of wave refraction.
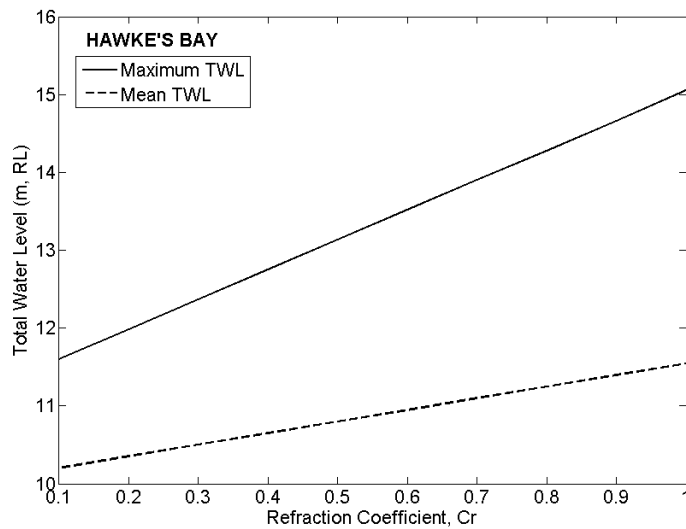
Figure 7-8: Means and maximums in the series of TWL histograms for C_r values ranging from 0.1 to 1.0, derived from Figure 7-7.

As expected, the ranges of TWL magnitudes in this series of histograms systematically shift to higher values as the coefficient C_r increases from 0.1 to 1.0, there progressively being higher swash runup levels superimposed on the measured tides that otherwise have remained the same. This increase is most evident in the maximum TWL values, which are graphed in Figure 7-8 together with the mean values of the distributions. The TWL maximums are seen to increase at a greater rate than the means, a consequence of the asymmetries of the runup and TWL histograms. The maximum TWL magnitudes range from about 11.5 to 15 metres RL, an encouraging result in that as graphed in Figure 7-2 the beach/backshore junctions of the profiles at the six representative monitoring sites within the Bay View and Haumoana Littoral Cells have comparable elevations.

### 7.4.3 Water elevations and beach morphology comparisons

Here we undertake comparisons between the analyses completed above for the TWLs, and the elevations of the beach/backshore junctions of the surveyed profiles, and also with ridge-crest elevations where wave overtopping events have occurred in recent years (HB06 East Clive). These comparisons between the processes and surveyed beach profiles generally involve a choice of the C_r dependent histogram and its extremes that provide the best agreement between the maximum water levels and elevations of the beach profile that provide direct evidence of past major storm events. This comparison in turn requires an interpretation of the storm that could have cut into the beach ridge at that junction elevation, whether it occurred early during the 80 years since this shore was uplifted by the 1931 earthquake, or perhaps records a storm that took place recently.

Along the shore of the Bay View Littoral Cell, the 2-metre uplift would have resulted in the initially rapid erosional retreat of the elevated former beach, forming a scarp on the seaward flank of what was now a ridge, with the eroded gravel reworked to form a new fronting beach. As seen in the beach and ridge profiles from the central to northern stretch of that shore, graphed in Figure 7-4, there has been minimal erosion of the scarp in several decades, even where the beach itself has experienced some erosion. There is a prominent beach/backshore junction at an elevation of 16.5 metres RL in both the Whirinaki (HB20) and Bay View (HB17) profiles, the latter including profiles from 1974 and 2010, indicating that TWLs have achieved that elevation by multiple storms over the years, but apparently have not reached still higher elevations to erode the scarps.

Such interpretations are more complex in the Haumoana Cell, due to its alongcoast differences in uplift versus subsidence at the time of the 1931 earthquake, having varied systematically from north to south along that shore (Chapter 3). Adding to this complexity is this cell's budget of beach sediments, with the locations of the main sources of gravel and sand being located at the south end of its shore, derived from the Tukituki River and erosion of Cape Kidnappers, supporting a net northward longshore sediment transport driven by waves that dominantly arrive from the southeast (Komar, 2005, 2010). While transported to the north, there is a progressive loss of gravel due to its abrasion, and in past decades due to its commercial extraction from the beach at Awatoto. It is evident in the records from the beach surveys collected by the monitoring program that substantial net erosion has prevailed along the southern half of this stretch of shore, with some accretion along its northern half (Edmondson et al., 2011). It will be evident in the analyses developed here, comparing the

TWLs with the beach profile elevations, that both the land-level changes at the time of the earthquake and the local processes governed by the site's wave heights and runup levels have determined the resulting erosion and occurrences of overtopping along the Haumoana Cell's barrier ridge, there being significant differences with the Bay View Cell.

Comparisons can now be undertaken between the morphologies of the beach profiles graphed in Figure 7-2 and the histograms of TWLs illustrated by those in Figure 7-7, for the six sites along the shores of these littoral cells. This involves matching their beach/backshore junction elevations or ridge-crest levels to the magnitudes of TWLs in the series of histograms generated for the range of C_r coefficients, using the curves in Figure 7-8. In this comparison C_r in effect becomes an empirical "matching factor" such that the model-evaluated water levels correspond to the evidence for past occurrences of erosion of the scarp, or of overwash events. Although this selection for a match may appear to be rather arbitrary, it is undertaken with a recognition that the results should be consistent with assessments of the extent of refraction experienced by the waves prior to having reached that profile site on the shore, that is with the expected reductions in nearshore wave heights and runup levels. It also needs to be recognized, however, that as discussed earlier the C_r coefficients have absorbed significant uncertainties in the refraction analyses and degrees of wave-height reductions, and also those that occur in our calculations of $R_{2\%}$ runup levels, in the applicability of the Stockton et al. (2006) to these mixed sand-and-gravel beaches.
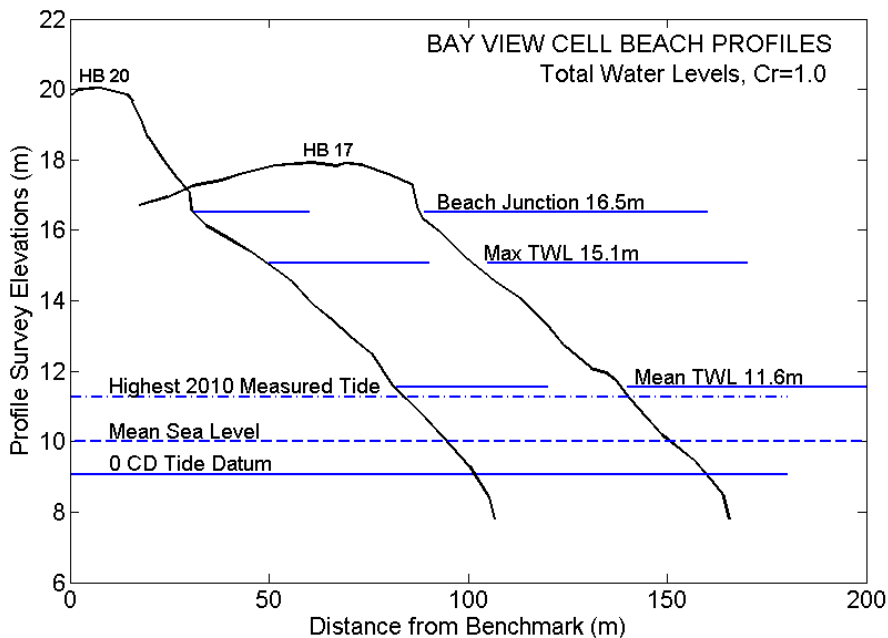
Figure 7-9: Model analysis of TWLs compared with morphologies of beach profiles surveyed at Whirinaki (HB20) and Bay View (HB17) within the Bay View Littoral Cell.

The analysis results for the Bay View Cell are graphed in Figure 7-9 for profiles HB17 and HB20. As discussed in Komar (2005, 2010), with minimal sediment inputs into this littoral cell its shoreline in the long term (centuries) has rotated clockwise so that it faces toward the prevailing waves that arrive from the southeast. The consequence is that the extent of wave refraction is reduced, the potential being that the most extreme calculated TWL magnitudes

could occur along this cell's central to northern shore that is fully exposed to the waves. This interpretation is supported by the 16.5-metre beach junction elevations being the same for both profiles. However, a problem has arisen in that modeling of the water levels yielded a maximum TWL = 15.1 metres in the histogram calculated with C_r = 1.0, the value when there has been little or no reduction due to wave refraction. The difference between the results for the calculated TWL elevation and the beach/backshore junction is about 1.4 metres, the model analyzed water levels being too low, evident in the graphical comparison in Figure 7-9.

The cause of this difference is open to interpretation, including a degree of speculation. The occurrence of some refraction of the waves from deep water to the shore, as well as bottom friction, would of course result in a still lower model analyzed TWL than the 15.1-metres extreme, yielding an even greater difference with the junction elevation. The 1.4-metre difference may be a problem with the formula we have applied to calculate the swash runup levels, that developed by Stockton et al. (2006); due to its empirical basis, it might not be successful when applied to the steeply sloped Hawke's Bay mixed sand-and-gravel beaches. However, the most probable explanation for this difference between the evaluated TWLs and beach/backshore junction elevation is that the histograms for the water levels were based on tide and wave data for only one year, 2010, even though that year had produced the highest elevated tides and wave heights within the decade of availability simultaneous measurements. Based on the profile surveys for HB17 and HB20 having shown essentially no evidence for the erosional retreat of their ridge-front scarps since the 1970s, and with the beach/backshore junction having remained at the 16.5-metre elevation, the inference is that the storm that generated this TWL elevation occurred prior to the decade of wave and tide measurements applied in our derivations of the TWL histograms, that this earlier storm had both higher wave runup levels and possibly a greater surge level than have occurred in our limited data sets; or perhaps the predicted astronomical tide was simply higher at the time of that earlier storm, with the waves and surge not necessarily having been that much greater than found in our data, this perhaps being more likely in view of the evidence that storm intensities and their generated waves appear to be increasing with time.

The problem experienced here for HB17 and HB20 in matching an extreme TWL with the beach/backshore junction elevations did not occur for the other surveyed profiles, the evidence for erosion events being at lower elevations, having experienced reduction in the waves and runup due to refraction. Although reasonable matches could be found for C_r coefficients well below 1.0, being within the range graphed in Figures 7-7 and 7-8, the cause of the problem with the exposed sites within the Bay View Cell likely remains, with the coefficient C_r providing a match having become an empirical "matching" factor, although it is still strongly affected by the degree of the site's exposure to the waves and the extent of wave refraction.

The Westshore development at the south end of the Bay View Littoral Cell has experienced occasional episodes of erosion, with the impacts to its undeveloped Reserve in the 1980s having received considerable attention from homeowners in that community, leading to the implementation of the program of annual beach nourishment. Its erosion has commonly been attributed to the construction of the Port's breakwater in the late 19th century, but in a review of the problem it was concluded that the breakwater together with Bluff Hill instead acts to protect this shore from storm waves (Komar, 2005, 2010). The relatively rare and minor erosion occurrences have instead been attributed to alongcoast oscillations of the sand volumes within this pocket-beach littoral cell, under the varying directions of arriving waves, possibly

associated with climate cycles such as the El Niño/La Niña range important to the coastal processes.

Westshore is represented in the present study by profile HB14 in Figure 7-2. It has lower backshore elevations than the exposed profiles to the north, which have been analyzed in Figure 7-9. Its beach/backshore scarp junction is ill defined, there being a steepened slope shoreward from about the 12-metres RL elevation, with 14 metres RL approximately being the base of the wave-eroded scarp. As discussed earlier in connection with the detailed surveys of this stretch of shore by Gibbs (2002), Figure 7-3, Westshore beach has been significantly modified by the nourishment undertaken annually since 1985, likely accounting for the gradual but steepened slope of the surveyed HB14 profile. Edmondson et al. (2011) reported a net rate of accretion of -0.045 m/year for its profile series since 1977. The elevation of the Reserve backing the bluff has also been artificially increased to prevent overtopping and flooding; it is seen in the HB14 profile, Figure 7-2, that the crest of the ridge immediately landward from the scarp has an elevation of about 16 metres RL, dropping down to about 15 metres further landward within the Reserve.

According to the results from the series of TWL histograms and the graph of their mean and maximum elevations in Figure 7-8, a coefficient C_r = 0.4 yields a maximum water level of about TWL = 13 metres RL, providing a reasonable assessment for the base of the wave-cut scarp in the Westshore HB14 profile, which would have occurred during storms prior to the beach nourishment operation, the storms whose erosion of the Reserve alarmed homeowners. This degree of reduction in the C_r value is reasonably consistent with the extent of wave refraction along this stretch of shore sheltered by Bluff Hill and the Port's breakwater, and the reduced wave heights for this shore derived in the refraction analyses by Tonkin and Taylor (2003) and MetOceans (2008, 2011), reviewed in Chapter 6.

Figure 7-10 presents a similar analysis of the HB06 and HB10 beach profiles in the Haumoana Littoral Cell, respectively from East Clive approximately midway along the cell's shoreline, and at the south end of Napier, in proximity to the Aquarium (Figure 7-1). While the beach slopes are essentially the same as those in the Bay View Cell ($S \approx 0.1$), the widths of the active beaches are somewhat less, and the elevations of the backshore are 1 to 2 metres lower than those of profiles HB17 and HB20 analyzed in Figure 7-9. It is evident that the barrier beach ridge at East Clive (HB06) would be expected to be susceptible to wave overtopping during storms, and there are reports that the Aquarium in proximity to the Napier profile HB10 has occasionally experienced water washing into its parking lot during storms, even though it is set well back from the ocean's shore. As surveyed, profile HB06 shows the presences of a small accretionary mound or ridge running along the length of its shore, probably formed by recent moderate to low wave conditions; during a storm that ridge would quickly be cut away, leaving an evenly sloped beach over which the wave runup might overtop the crest of this barrier ridge. There is a subtle beach/backshore junction in the HB10 profile that might represent an episode of beach erosion up to its 13.7-metre RL elevation, but of greater interest are the potential TWLs that could result in overwash of the ridge crest at East Clive, or still higher flows over the 15.5-metre RL elevation of the South Napier backshore.

The TWL analyses presented in Figure 7-10 focuses on the water level that would result in overtopping of the crest of the East Clive profile, the C_r = 0.6 histogram with a maximum TWL = 13.7 metres achieving this. Of interest, it is evident that this water level would also

reasonably account for the beach junction elevation on HB10 in Napier. This result is consistent with the wave swash runup from the dominant storm waves arriving from the southeast, being less than determined in Figure 7-9 for the HB17 and HB20 profiles at similar exposed positions within the Bay View Cell, the shoreline of the Haumoana Cell trending obliquely to their dominant arrival direction, a condition that accounts for the net northward longshore sediment transport along this shore, but significant here being that this orientation also results in a greater degree of wave refraction and a decrease in the C_r "matching" coefficient. The rare and mild overtopping of profile HB10 in South Napier, with a backshore elevation of about 15 metres, could be explained by storm waves arriving directed from the east to northeast, having experienced minimal refraction, the C_r = 1 model results in Figures 7-7 and 7-8 yielding that elevation for the maximum $TWLs$.
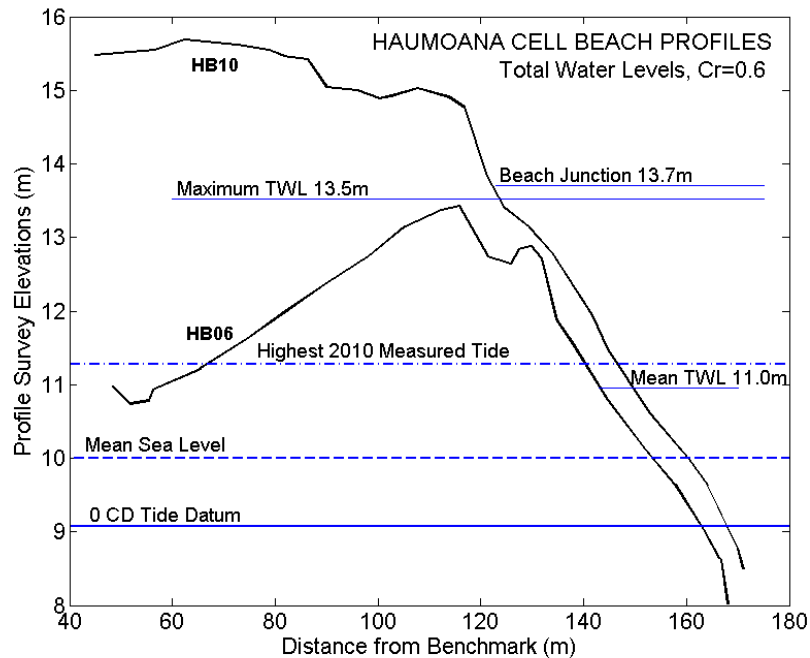
Figure 7-10: Comparisons between the $TWLs$ and beach junction elevations and ridge crests for beach profiles within the Haumoana Littoral Cell, East Clive (HB06) and South Napier (HB10).

The southern portion of the Haumoana Cell's shoreline has experienced the greatest erosion and flooding impacts within Hawke's Bay, including from north to south the communities of East Clive, Haumoana, Te Awanga and Clifton. The report by Daykin (2010) documents the occurrences and extent of the impacts during major storms from 1996 to 2010, including overwash events in the area of profile HB06 on the East Clive shore, with massive erosion damage to shorefront homes in Haumoana and Te Awanga. Profile HB03 for South Haumoana, with surveys graphed in Figures 7-2 and 7-5, is representative of this erosion-impacted shore; seen in the profile is one of the many seawalls that have been constructed in an attempt to protect the homes. Figure 7-2 including all six profiles illustrates the significance of the contrasting elevations along this coast, with HB03 in South Haumoana being about 4 metres lower than HB17 in the Bay View Cell, 2 metres lower than HB10 in South Napier, and slightly higher than HB06 in East Clive where ridge overtopping occurs during storms. These elevation variations can be attributed primarily to the land level changes at the time of the 1931

earthquake, still being a factor 80 years later in the locations of erosion and flooding impacts. However, it is also clear that the erosion concentrated along the southern shore of the Haumoana Cell, seen in Figure 7-5 showing the retreat of the beach at South Haumoana, to a significant degree results from the negative net balance in its sediment budget [see reviews in Komar (2005, 2010), and in Chapter 9 of this report]. According to analyses of the profile trends by Edmondson et al. (2011), the erosion at South Haumoana (HB03) has averaged about -0.607 metre/year, the shoreline retreat at East Clive (profile HB06) having been about -1.6 metre/year.

7.5 SCENARIOS OF EXTREME STORM EVENTS

An obvious limitation in the above analyses is that our assessments of the extreme TWL magnitudes have been based on wave and tide measurements collected only during a single year, 2010, even though that year was particularly significant in storm occurrences during the decade of wave and tide measurements. While the range of TWL histograms included in Figure 7-7 on average provided reasonable documentations of this important component in the nearshore processes climate, the extremes TWL magnitudes in those histograms in all probability fall short of the 50- to 100-year projected extremes, or those that might have occurred during the 80 years since the Hawke's Bay earthquake that altered elevations of most of this shore. Missing would be the severe but rare storms that generated both extreme waves and a surge that elevated the measured tides, which by chance also corresponded in time with a reasonably high predicted astronomical tide. With the total records of waves and tides for Hawke's Bay being little more than a decade, even if we had calculated the TWLs for that entire record, projections of the potential extremes would most likely still have been too low.

In our investigations to develop hazard analyses along the coasts of the U.S. Pacific Northwest, we had some 40 years of simultaneously measured tides and waves that were applied in calculating the hourly TWLs, those longer records having captured a number of major storms and represented years for both strong El Niños and La Niñas. Such extended records were capable of supporting meaningful calculations of the 50- and 100-year extreme significant SWHs and TWLs, affected by various climate controls (Ruggiero et al., 2001, 2010). However, even for the U.S. Pacific Northwest it has been informative to develop "scenarios" of the potentially most extreme combinations of predicted tides, their enhancement by the normal seasonal variations in monthly-mean water levels, the elevated water levels measured throughout the year of a strong El Niño, and the processes during severe storms, the surge plus the swash runup of the extreme waves (Komar et al., 2002). With a scenario representing combinations of these processes and their respective extremes, it is not possible to precisely assess their probabilities of joint occurrences, but the chosen combinations could be such that they reasonably represent an extreme though rare event, one that is possible and could occur, posing the present-day greatest threat from erosion and flooding to coastal developments and infrastructure, prior to any future rise in sea levels and increased storm intensities.

The objective here is to develop such a scenario for the coast of Hawke's Bay, in this case the procedure being particularly important due to the limited availability of wave and tide measurements. Fortunately, although there is only a decade of data, the analyses we have completed thus far of the waves and tides provide guidance as to their overall distributions of

magnitudes, making possible fairly reasonable estimates of their individual extremes, and considerations of their potential joint occurrences.

As reviewed in Chapter 4, predictions of the astronomical tides for Hawke Bay have been available for more than a century, the analysis having yielded a 1.91-metre CD elevation for the Mean High Water Spring (MHWS) statistic, and a 2.00-metre CD elevation for the Highest Astronomical Tide (HAT); the maximum tidal range is therefore about 2.0 metres. However, our analyses of the tides measured by the Port's gauge during 2010 demonstrated that the distribution of its magnitudes is skewed to higher values, the maximum measured elevation that year having been about 2.25 metres CD (Figure 4-3). This enhancement of the elevations of the measured tides versus their predicted levels can result from a number of environmental processes, ranging from the normal seasonal cycle of monthly-mean water levels to surges generated by storms. The seasonal cycles in monthly-mean water levels along New Zealand's shores are relatively small, the range from summer to winter being on the order of 0.2 metre, in the case of Hawke Bay according to the Port's tide-gauge record the highest monthly average occurring during the winter. More important are the magnitudes of storm surges, which in analyses by de Lange (1996) of the highest occurrences along the New Zealand coast were found to range from 0.8 to 1.0 metre, levels that have return periods on the order of 100 years. The only detailed study of storm surges measured by the Port's tide gauge in Hawke Bay was that by Worley (2002), having analyzed the "tidal residuals", the portion of the water-level variations that is not accounted for by the astronomical tides, the residuals having resulted mainly from surge events. Eighteen significant surge occurrences were identified in the 1-year record analyzed (May 2001 to June 2002), when the measured elevations reached at least 0.75 metre higher than the predicted tides. An extreme-value analysis of the residuals yielded a magnitude on the order of 0.9 metre, consistent with the results of de Lange (1996). In hazard assessments along the New Zealand coast that account for extreme water levels, it has been common to add this 0.9-metre surge to the predicted MHWS tide elevation to provide an estimate of potential water-level elevations having a 1% probability of occurrence each year (the 100-year event). For Hawke Bay this would yield 2.86 metres CD (12.0 metres RL), nearly 2 metres above the Mean Sea Level.

The results from these analyses of the measured versus the predicted astronomical tides for Hawke Bay demonstrate the significance of storm surges to potential occurrences of erosion and flooding along its shores. Considering that the highest possible predicted tide (HAT) would achieve a tidal elevation of 2.0 metres CD (11.1 metres RL), the addition of another 1 metre by a storm surge represents a substantial increase on this coast that otherwise experiences a relatively small range of tidal variations. On a typical mixed sand-and-gravel beach having a slope of 0.1 (1-in-10), a 1-metre enhanced level due to a surge would shift the mean shoreline landward by 10 metres. In terms of the 12.0-metre RL extreme water levels projected based on surge measurements by de Lange (1996) and Worley (2002), the water could reach significant elevations even in the absence of waves, with the beaches along the southern portion of the Haumoana Littoral Cell (profiles HB03 and HB06) and at Westshore (HB14) nearly being inundated by the elevated tides. On the other hand, the higher elevation beaches and backshores toward the north ends of the littoral cells (HB10, HB17 and HB20) would have only half of their profiles covered by water during those extreme tides. Although it is evident that this degree of tide-level enhancements by storm surges represents an important component in the potential erosion and flooding of shorefront properties, an equally important role must be the extreme waves generated by severe storms, their swash runup levels on the beaches.

From the analyses in Chapter 5 of the deep-water wave climates, it was demonstrated in the histogram of SWHs (Figure 5-8) that the mean value measured over a 11-year period (2000-2010) was 1.76 metres, the maximum measured SWH having been about 10 metres; from this, a projected extreme might be expected to be on the order of 11 to 12 metres. Based on the wave heights and periods measured by the Port's buoy during that decade, calculations were completed in Chapter 6 for the vertical components of the wave runup on a beach having a 0.1 slope, a representative of the monitoring profiles, with the results again presented as a histogram (Figure 6-3). For a beach located along the shore where wave energy reduction is expected to be relatively small (e.g., the north shores of the littoral cells), the mean runup level was on the order of 1.7 metres, the maximum occurrences during those 11 years having been about 5.4 metres; projected extremes could therefore be on the order of 6.0 to 6.5 metres. In the case of shores where reductions due to wave refraction are significant (e.g., Westshore), the mean runup level might only be on the order of 0.5 metre, the maximum measured being 1.6 metres (Figure 6-3), with the projected extremes roughly 1.8 to 2.0 metres. These results in terms of the wave runup levels demonstrate that on a sheltered beach such as found at Westshore, the runup is comparable to the storm surge in governing the total water levels, TWL, but on shores more exposed to the waves the runup is substantially greater than the surge enhancement of the measured tides. In that the measured tides enhanced by a storm surge will be effectively the same along the shores of the Hawke's Bay littoral cells, it is the alongcoast variation in the extreme magnitudes of the wave swash runup levels that produce different "scenarios" for shores that are exposed versus those that are protected from the waves arriving from deep water.

It is evident that the most severe erosion and flooding event for the Hawke's Bay coast is one that occurs during what would be the most extreme storm event, represented by extremes in the measured tides enhanced by a storm surge, and extremes in the measured deep-water wave heights that in turn produce the greatest swash runup levels. It is therefore reasonable to assume that the 100-year projections of these processes are likely produced by the same major storm event, and if they are combined to determine the extreme TWL the result is again approximately the 100-year event. Even if it does exceed that statistical extreme, this combination still has a reasonable expectation for its occurrence. Presented in Table 7-2 are the resulting assessments of the extreme total water levels (TWL) derived by adding the respective extremes for the measured tides and calculated wave-swash runup levels, yielding a pair of scenarios representing "Exposed" versus "Sheltered" shores along the Bay View and Haumoana Littoral Cells, respectively beaches that are impacted directly by the waves with minimal refraction, versus a beach such as Westshore where there is signification sheltering and the waves have undergone considerable refraction prior to having reached that shore. An elevation of 12.0 metres RL is used in both scenarios for the extreme tide, based on the investigations by both de Lange (1996) and Worley (2002), who used different analysis procedures to arrive at this value. The difference in this pair of scenarios is in the extreme values of the swash runup levels, reflecting the range of different degrees of protection by headlands and in the case of Westshore by the Port's breakwater, and also the extent of wave refraction required by the waves as they pass from deep-water to those shoreline sites. This difference is significant, the magnitudes of the swash runup extremes being 6 versus 2 metres respectively for the Exposed and Sheltered shorelines.

Table 7-2: Scenarios of extremes in the measured tides and wave swash runup levels, yielding extremes in the elevations of the total water levels (TWL) on Exposed versus Protected shorelines in Hawke's Bay.

    Exposed Shores
        Extreme measured tides   12.0 metres RL
        Extreme swash runup level   6.0 metres
            Total Water Elevation   18.0 metres RL

    Sheltered Shores
        Extreme measured tides   12.0 metres RL
        Extreme swash runup level   2.0 metres
            Total Water Elevation   14.0 metres RL

For the Exposed Shore, the addition of this 6-metre runup to the assessed measured tide, 12 metres RL, yields a TWL extreme of 18 metres RL. This appears to be a reasonable order-of-magnitude assessment in that the extreme TWL of the histogram in Figure 7-7 for $C_r = 1$, based on only one year of measurements, would likely be about 16 metres RL. This fully exposed beach environment, having experienced minimal refraction, is most closely represented by profiles HB17 and HB20 on the north-central shore of the Bay View Littoral Cell (Figure 7-9). Of interest, the 16.5-metre RL beach/backshore junction elevations found on both profiles correspond to the 16.0-metre projected extreme indicated by the TWL histogram, expected to be a more modest projection considering it is based on only 1 year of measured tides and waves. The more extreme projection of 18 metres RL provided by the scenario developed in Table 7-2 could be expected to overtop the ridge crest on profile HB17 in the community of Bay View, but the 20-metre elevation of the HB20 backshore is clearly too high for any conceivable overwash, although this 18-metre water level projected by this scenario would reach the scarp of the bluff backing the beach and could be expected to result in some erosion, the amount depending on the duration of the storm.

Profile HB10 at the north end of the Haumoana Littoral Cell is also fully exposed to the arriving waves, although those from the dominant southeast would have experienced more refraction than the waves reaching HB17 and HB20 in the Bay View Cell, due to the contrasting shoreline orientations. The development of a scenario for the HB10 site yields an extreme on the order of 16 metres RL, whereas the TWL histograms of Figure 7-7 project an extreme of 14 to 15 metres RL. With a crest elevation of 15.5 metres in this profile, Figure 7-10, these projected water levels would be expected to result in occasional occurrences of overwash events, as have been observed at this shore position to the immediate south of Napier, having occasionally flooded the Aquarium's parking lot.

The "Sheltered Shore" scenario given in Table 7-2 can be viewed as representing only an approximate assessment to be compared with Westshore at the south end of the Bay View Cell, sheltered by Bluff Hill and the Port's breakwater, and also for the southern-most shore of the Haumoana Cell sheltered by Cape Kidnappers. This scenario includes a 2.0-metre level for the extreme runup, accounting for the reduced heights of the waves, yielding a TWL extreme of 14.0 metres RL for those shores partially protected from the storm waves arriving from the southeast. As seen in Figure 7-2, the HB14 profile from Westshore has a backshore elevation of 15 to 16 metres RL, so that significant overwash events are doubtful, but the 14-metre water levels would reach well up onto the face of the scarp along the Reserve, with the expectation of

there being significant erosion during a 100-year storm at a time of high tides. The HB03 profile at South Haumoana has a backshore elevation of about 14 metres RL, 13 metres at the toe of its vertical seawall (Figures 7-2 and 7-5), suggesting that overwash into the backshore properties are possible. However, based on the frequency of property inundation occurrences during storms that have been documented by Daykin (2010), the 14-metre RL scenario for the TWL on a Sheltered Shore as given in Table 7-2 may actually represent a fairly frequent event for that southern stretch of shore within the Haumoana Cell, and that the 100-year extreme is more likely to be on the order of 15 metres RL.

## 7.6 STORMS AND HOURLY VARIATIONS IN TOTAL WATER LEVELS

Applications of the Ruggiero et al. (2001) model to calculate the TWLs at the shore and to compare them with the beach morphology can also be directed toward the hour-to-hour variations in waves and tides during a specific storm event, yielding more detailed analyses of its resulting erosion and flooding. Such analyses have been undertaken for the coast of the U.S. Pacific Northwest (Allan and Komar, 2002), for storms during the El Niño winter of 1997-98 when tides were elevated by 10s of centimetres and several significant storms occurred, and also for the following winter of 1998-98 when unusually severe storms producing the most extreme waves in recent decades. Similar analyses are undertaken here in application to Hawke's Bay, illustrated by three of the strongest storms that occurred during 2010, the results complementing our earlier analyses where the hourly total water levels (TWL) were presented as histograms, their extremes having been compared with the beach morphologies.

In an investigation of the erosion and flooding impacts in recent decades along the shore of the Haumoana Littoral Cell, Daykin (2010) included analyses of the hourly variations in wave heights and tides during major storms, measured by the Port of Napier's buoy and tide gauge. An example of his analyses is given here in Figure 7-11, a storm that occurred during March 2010, including the hourly averages, hourly maximums, and the significant wave heights, wave periods, and the cycles of the measured tidal elevations. This example in particular illustrates how the waves first progressively increased in heights and periods, having been generated by a distant storm, reaching a maximum on 08 March 2010, and then gradually decreased in both the wave heights and periods. The greatest impacts during this storm would be expected to have occurred at the time of the combination of the highest waves and high-tide water levels. Our corresponding analysis results applying the Ruggiero et al. (2001) methodology to this storm are graphed in Figure 7-12, extending the analysis to calculations of the wave-swash runup levels ($R_{2\%}$) and total water elevations (TWL). Of interest is that the maximum values of the runup lag by nearly half a day behind the magnitudes of the deep-water significant wave heights, caused by the strong dependence of the runup on the periods of the waves, as well as their heights. Figure 7-12 also illustrates how the TWL responds on an hourly basis to the summation of the wave runup and the cycle of the tides, with the maximum TWL having reached nearly 15 metres RL. This analysis did not include a reduction in the runup elevation produced by wave refraction, that is in equation 7-1 to evaluate the TWLs the correction coefficient was set at $C_r = 1$. Therefore, the comparison in Figure 7-9 with the Whirinaki and Bay View beach profiles involved this March 2010 storm, having yielded the maximum TWL of that year. If this analysis in Figure 7-15 of the hourly variations in the TWLs applied equally to the Haumoana Littoral Cell with its beach/backshore junction elevations being in the range 12 to 13.5 metres, it is evident that erosion of the foredunes would have been continuous for 3 to 4 days, and the

gravel ridge crest at East Clive with an elevation of 13.5 metres (Figure 7-10) would have experienced wave overtopping during three successive tides, having been most extreme on 8 March 2010 when the calculated TWL exceeded its elevation by more than 1 metre.
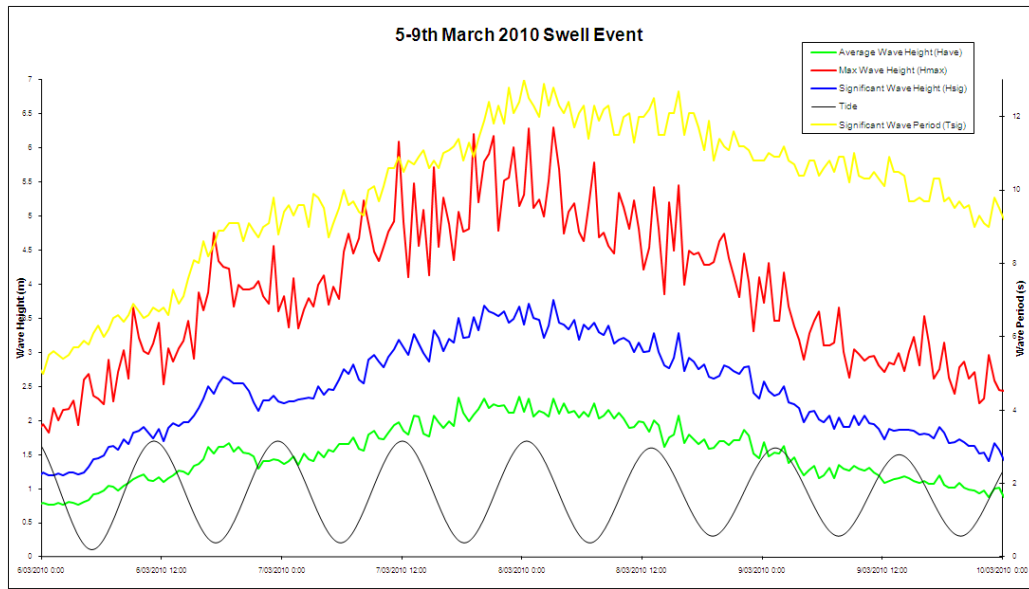
Figure 7-11: Analyses by Daykin (2010) of the hourly buoy-measured significant wave heights and periods during a major storm in March 2010, together with cycles in the levels of the tides.
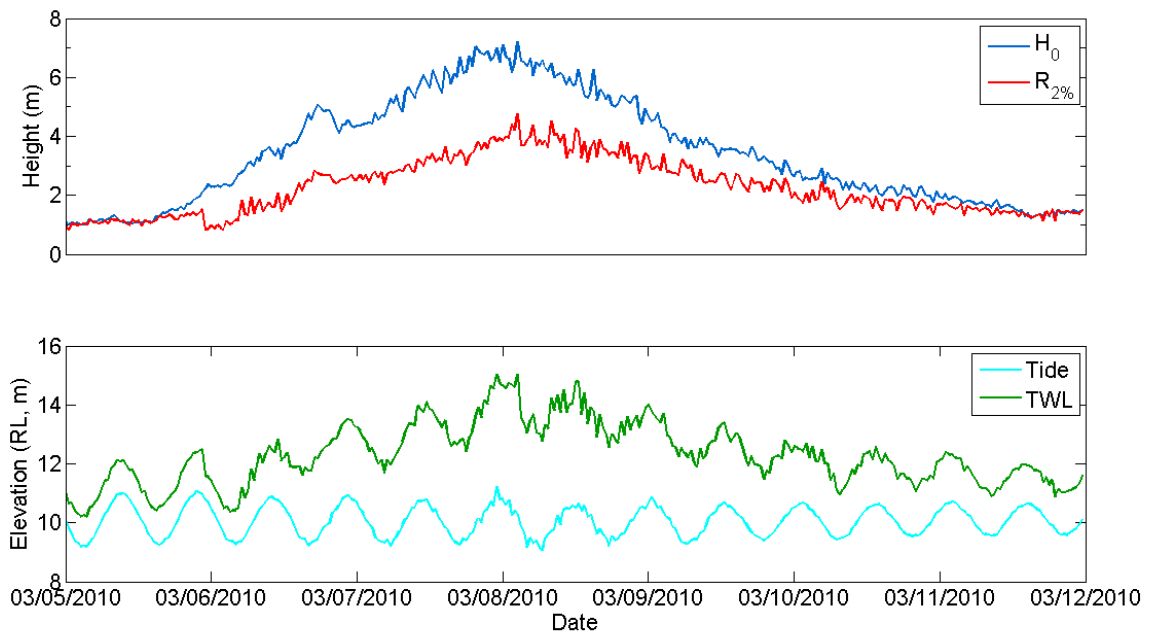
Figure 7-12: Analysis of the March 2010 storm, including the deep-water significant wave heights derived from the buoy data, the calculated swash runup at the shore ($R_{2\%}$), the measured tides, and the resulting hour-to-hour variations in the total water levels (TWL).

7-25

Two additional analyses are presented in Figures 7-13 and 7-14, respectively for storms in May and August-September 2010, again including the hourly variations in $R_{2\%}$ and TWLs. The August storm is of interest in that it had a significantly different pattern of variations with abrupt increases in the significant wave heights and runup levels, resulting in a TWL increase within a few hours to a maximum 14-metre RL elevation, the subsequent decrease having spanned several days. This pattern presumably reflects the passage of a storm moving from west to east as it crossed New Zealand, probably close by to the south of Hawke's Bay; the sharp increase in generated wave heights would have recorded the first arrival of the storm over the ocean, having crossed the eastern shore of the North Island.
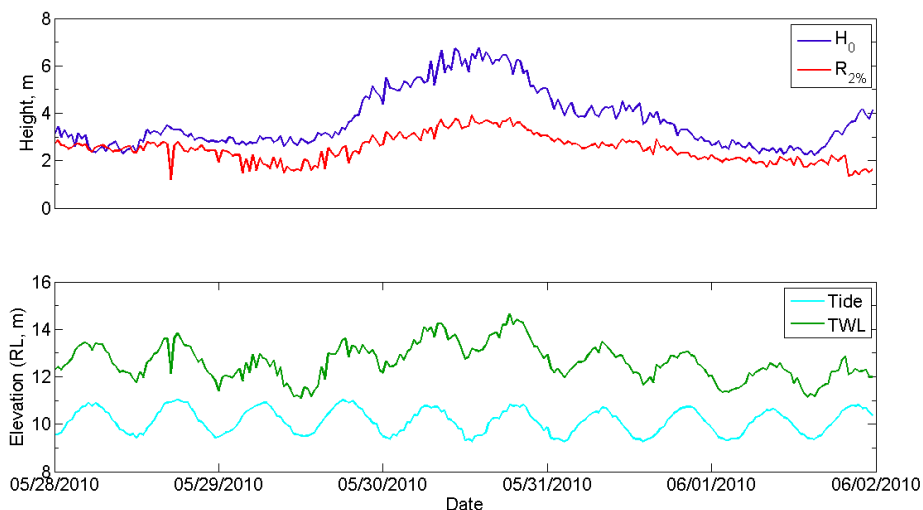
Figure 7-13: Hourly variations in measured waves and tides during the May 2010 storm, and the calculated runup and total water levels.
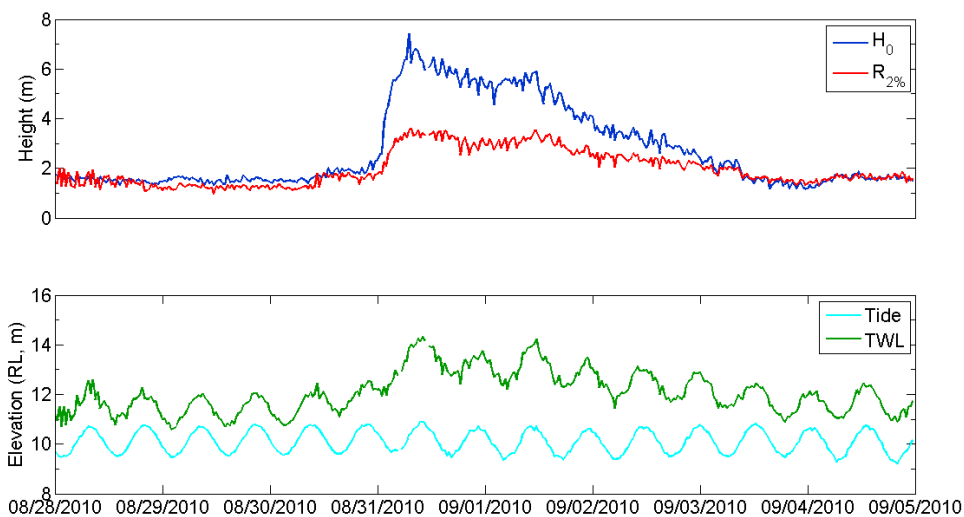
Figure 7-14: Measured waves and tides, calculated runup levels, and total water elevations during the August-September 2010 storm.

The intent in this section has been to illustrate the potential application of the Ruggiero et al. (2001) model in analyses of individual storm events that have impacted the Hawke's Bay coast. With the inclusion of detailed analyses of the storms themselves (winds and atmospheric pressures), and their generated deep-water waves, measurements of the concurrent tides enhanced by a storm surge, and the inclusion of analyses of the details of the nearshore processes climate (wave breaker heights and swash runup levels), the results of such analyses lead to assessments of the hour-to-hour variations in total water levels at the shore, providing a understanding of the resulting property erosion and flooding impacts that have been documented in the report by Daykin (2010) for the Haumoana Littoral Cell.

7.7 SUMMARY AND DISCUSSION

The objective in this chapter has been to combine the analyses completed in previous chapters of the Hawke's Bay tides, waves and nearshore processes, into assessments of the elevations of the total water levels (TWL) at the shore. This can be viewed as essentially the summation of the predicted astronomical tide and the processes related to storm occurrences, the surge that is primarily responsible for the elevation of the measured tides above its predicted elevations, and the levels of the swash runup on the sloping beach, being dependent on the wave heights and periods, and the degree of refraction as the waves cross the continental shelf and reach the shore. In that the analyses themselves are based on the hourly measured tides derived from the Port's gauge, all of the factors and processes that determine the mean water levels are automatically included, although it has been shown that the more extreme enhanced levels of the Hawke's Bay tides are the result of storm surges, which can elevate the water by about 1 metre. Considering that the total range of tides is relatively small, about 2 metres, it is apparent that occurrences of storm surges can represent a significant control on the water levels, being an important factor in the resulting erosion and flooding impacts.

On the shores of Hawke's Bay that are sheltered from the waves (e.g., Westshore), the mean water level of the astronomical tide plus a storm surge can inundate the entire beach profile, reaching the elevation of the toe of the bluff at the back of the beach. But even though the waves are reduced in energy and have relatively low runup levels, they are still important as an agent of erosion, impacting and cutting away the scarp at the landward extent of the beach. The importance of the waves and the magnitudes of their swash runup levels as agents of erosion are more evident on the exposed shorelines, the analyses in this chapter having shown that if considered alone the measured tides would reach only about half way up the beach face, the wave runup during storms being required to span the remaining distance as well as providing the impact forces to erode the gravel ridges, or in the extreme to produce overwash that results in property flooding.

The primary accomplishment in this chapter has been to analyze the total water elevations, the sum of the measured tides and calculated wave runup levels, to determine the hourly TWL magnitudes. This included the development of the TWL nearshore climate in the form of histograms based on simultaneous wave and tide data for the year 2010, and also analyses of the hour-to-hour TWL variations during the more severe storm events that occurred. The TWL histograms, specifically their extreme elevations, were compared with the morphologies of

surveyed beach profiles from the Bay View and Haumoana Littoral Cells, of interest being the correspondence with their beach/backshore junction elevations that represent evidence for occurrences of past scarp erosion events. A reasonable correspondence was found, with an approximate match between the alongshore variations in the junction elevations in the profiles, becoming progressively lower along the sheltered shores, accounted for by the reduced TWLs due to the lowered waves and swash runup. The analyses also reasonably accounted for occurrences of overwash events in the Haumoana Cell where the crests of the beach ridges are sufficiently low that the TWLs during storms and high tides can reach higher elevations.

The primary shortcoming in the TWL analyses developed in this chapter is the limited data availability of measured tides and waves, less than two decades. Although the general distributions in the histograms of TWL magnitudes are reasonably well defined, this limited data is insufficient to account for the magnitudes of the extreme events, particularly the 50- to 100-year projections. Accomplishing that would require at least another decade or two of tide and wave measurements, only then yielding what is generally considered to be an acceptable degree of confidence in such projections. In an attempt to provide assessments of the potential extreme events in terms of the erosion processes, "scenarios" were developed based on the possible extreme magnitudes of the individual processes and their joint occurrences (tides, storm surges, deep-water wave heights, and swash runup levels), providing indications of the potentially most severe hazards to Hawke's Bay from erosion of the seaward edges of the uplifted barrier beach ridges, or flooding due to overwash occurrences.

All of the conditions considered in this chapter represent the present-day hazards, not having included the potential increase in global sea levels expected during the 21st century, nor the possibility that a climate-induced increase in storm intensities and wave heights, apparently already being experienced, will continue though this century. Their inclusions in the hazard assessments are undertaken in the following chapters.

7.8 REFERENCES

Allan, J. C., and P.D. Komar (2002) Extreme storms on the Pacific Northwest coast during the 1997-98 El Niño and 1998-99 La Niña: *Journal of Coastal Research*, v. 18, no. 1, p. 175-193.

Daykin, N. (2010) *Haumoana Littoral Cell: Coastal Storm Analysis*: Asset Management Group Technical Report AM05/18, Hawke's Bay Regional Council.

de Lange, W. P. (1996) Storm surges on the New Zealand coast: *Tephra*, v. 15, no. 1, p. 24-31.

Edmondson, E., N. Daykin, and Sara Bailey (2011) *Hawke's Bay Coastal Profile Monitoring 2011*: Asset Management Group Technical Report AM11/01, Hawke's Bay Regional Council, 219 pp.

Gibb, J. G. (1995a) *Review of the Physical Coastal Monitoring Programme of Hawke's Bay Regional Council, Volume I*: Report prepared for Hawke's Bay Regional Council, 61 pp.

Gibb, J. G. (1995b) *Review of the Physical Coastal Monitoring Programme of Hawke's Bay Regional Council, Volume II, Beach and Offshore Profile Data and Survey Costs*: Report prepared for Hawke's Bay Regional Council.

Gibb, J. G. (1996) *Coastal Hazard Zone Assessment for the Napier City Coastline between the Ahuriri Entrance and Esk River Mouth*: Report prepared for Napier City Council, C.R. 96/2, 80 pp.

Gibb, J. G. (2002) *Review of the 1996 Coastal Hazard Zone between Ahuriri Entrance and Esk River Mouth*: Report prepared for Napier City Council, 56 pp + Appendices.

Komar, P. D. (2005) *Hawke's Bay, New Zealand: Environmental Change, Shoreline Erosion, and Management Issues*: Report for the Hawke's Bay Regional Council.

Komar, P.D. (2010) Shoreline evolution and management of Hawke's Bay, New Zealand: Tectonics, coastal processes and human impacts: *Journal of Coastal Research*, v. 26, n. 1, p. 143-156.

Komar, P.D., J.J. Marra, and J.C. Allan (2002) Coastal erosion processes and assessments of setback distances: *Proceedings, Solutions to Coastal Disasters Conference*, Amer. Society of Civil Engineers, p. 808-822.

Komar, P.D., J.C. Allan and P. Ruggiero (2013) U.S. Pacific Northwest coastal hazards: tectonic and climate controls: *Coastal Hazards*, edited by C.W. Finkl, Springer, p. 587-674.

MetOceans (2008) *Westshore Reef Surf Conditions*: MetOcean Solutions Ltd., New Plymouth, New Zealand, 65 pp.

MetOceans (2011) *Hawkes Bay Wave Climate*: MetOcean Solutions Ltd., New Plymouth, New Zealand, 42pp.

Oldman, J. W., R. K. Smith and R. Ovenden (2003) *Coastal Erosion Hazard Assessment of the Foreworld Sites between Gill Road and Franklin Road, Bay View, Hawke Bay*: NIWA Report for Foreworld Development Ltd., Napier, 64 pp.

Ruggiero, P., P.D. Komar, W.G. McDougal, J.J. Marra, and R.A. Beach (2001) Wave runup, extreme water levels and the erosion of properties backing beaches: *Journal of Coastal Research*, v. 17, no. 2, p. 407-419.

Stockdon, H.F., R.A. Holman, P.A. Howd, and A.H. Sallenger (2006) Empirical parameterization of setup, swash, and runup: *Coastal Engineering*, v. 53, p. 573-588.

Tonkin and Taylor (2003) *Hawke's Bay Nearshore Wave Climate*: report to the Hawke's Bay Regional Council, 13 pp + Appendices.

Worley (2002) *Port of Napier: Design Criteria Report for Outer Breakwater Extension*: 20 December 2002 report to the Port of Napier, Worley Infrastructure Pty Ltd, Perth, Australia.

8 Rising Sea Levels along the Shores of Hawke's Bay

8.1 INTRODUCTION

The evidence for global warming produced by human emissions of greenhouse gases into the atmosphere was examined in Chapter 2, including a review of investigations that evaluated average rates of the resulting rise in globally-averaged sea levels spanning the 20th century. Those results in turn led to projections of future accelerated rates of rising sea levels, expected from continued global warming. One of the major concerns to society is that the elevated levels of the sea will lead to greatly enhanced impacts from coastal erosion and flooding, potentially achieving catastrophic levels along low-lying stretches of the world's shores. Considerations of such dyer prospects have become important in efforts directed toward the sound management of our coasts, for the protection of shorefront properties from the increased hazards and to preserve resources such as the recreational use of its beaches. Such an assessment for Hawke's Bay is the primary goal of this report, and specifically in this chapter where we analyze the potential accelerated rates of increasing sea levels along its shores, to determine the water elevations that could be reached by the year 2100. The resulting erosion and flooding impacts will be considered in the following chapter.

The preceding series of chapters focused on the related ocean processes important to the erosion and flooding hazards along the Hawke's Bay coast: its measured tides that include their enhanced levels due to storm-induced surges (Chapter 4); the deep-water wave climate and its extremes that occur during the most severe storms (Chapter 5); and the resulting nearshore processes of wave breaker heights and swash runup levels on the Hawke's Bay beaches, being of direct importance to the impacts of its shore-front properties (Chapter 6). Having applied the Ruggiero et al. (2001) model that combines the effects of these processes, the present-day ranges and extremes in total water levels (tides plus wave-swash runup) were evaluated and compared with the morphologies and elevations of the Hawke's Bay beaches and backshore properties (Chapter 7). Those analyses thereby provided assessments of the ocean processes that are important to the present-day hazards from erosion and flooding, supporting the establishment of improved hazard zones required for safer development, that otherwise have been based primarily on multidecadal trends of shoreline changes determined from annual surveys undertaken in the HBRC monitoring program. The goal here and in the following chapter is to project into the future the expected enhanced coastal hazards associated with Earth's evolving climate, the result of accelerated rates of rising sea levels, and potential increases in storm intensities and the heights of their generated waves.

The analyses in Chapter 7 of the present-day erosion and flooding hazards did not include a consideration of the fact that the global mean level of the sea has been increasing throughout the 20th century, with tide gauges along the coasts of New Zealand having shown a

comparable rise. Remaining to be analyzed in this chapter are the changes in sea levels that could occur during the 21st century, the results of which will be incorporated into models in the following chapter to project the future hazards faced along the shores of Hawke's Bay.

8.2 NEW ZEALAND'S CHANGING SEA LEVELS

A primary factor governing the occurrence and extent of coastal erosion and flooding is the direction and rate of change in its relative sea level, the combination of the trend in the eustatic level of the ocean compared with the net uplift or subsidence of the land. Depending on this combination, a stretch of coast could either be submergent if the sea is rising faster than the land, or even more so if the land is subsiding, while emergent coasts occur where the land is rising faster than the sea. Over thousands of years sea levels have undergone large changes in response to the alternating growth and melting of glaciers, its level having been some 125 metres lower 18,000 years ago at the time of the last maximum expansion of the glaciers during the Ice Ages. With their subsequent melting the sea rapidly rose until about 7,000 years ago, by which time it had nearly reached its present level. As reviewed in Chapter 2 (seen in Figure 2-3), the longest tide-gauge records show relatively constant sea levels until late in the 19th century, when they began to rise and have continued to do so through the 20th century. The recent analyses by Church and White (2006) and Holgate (2007) of world-wide tide gauge records yielded almost identical rates, the latter study having obtained a mean rate of 1.74 mm/year for the 20th century, a net increase of 17 centimetres in 100 years. This magnitude of rising sea levels has been found in analyses specifically for New Zealand, although locally the tide-gauge records are expected to be affected by its tectonics and resulting changes in land elevations.

Gibb (1986) investigated sea levels along the New Zealand coast spanning the past 10,000 years, with his results having similarly documented the global rise in sea level that occurred when the Ice Age glaciers began to melt, returning water to the oceans. The results of his study are shown in Figure 8-1, based on 82 radiocarbon dated sea-level indicators found on both the North and South Islands, collected on relatively stable shores; data from Hawke's Bay were not included due to its tectonic instability and land-elevation changes (Chapter 3). The sea-level indicators used by Gibb (1986) included beach-ridge elevations, shell beds deposited in estuaries, brackish carbonaceous mud, and layers of peat deposits. He analyzed this data to separate the eustatic worldwide component of sea-level rise from the local tectonic induced land-level changes. The resulting sea-level graph in Figure 8-1 shows that the eustatic sea level rose from about -34 metres below its present level 10,000 years ago to about -9 meters 7,500 years before the present. About 6,500 years ago the sea level approximately attained its present elevation, and according to Gibb's (1986) data it has remained at that level with only small variations up to the 20th century when the increase associated with global warming began. His analyses also provided assessments of local changes in land elevations due to tectonic uplift or ground subsidence; those values are included in Figure 8-1 for the individual sites, ranging from 0.1 to 0.3 metre per 1,000 years (0.1 to 0.3 mm/year) for the areas of tectonic uplift, and -0.05 to -0.1 metre per 1,000 years (-0.05 to -0.1 mm/year) for the areas of subsidence. In general, these magnitudes for the local land elevation changes are in accord with the relatively stable settings of the sites where Gibb (1986) collected his data.
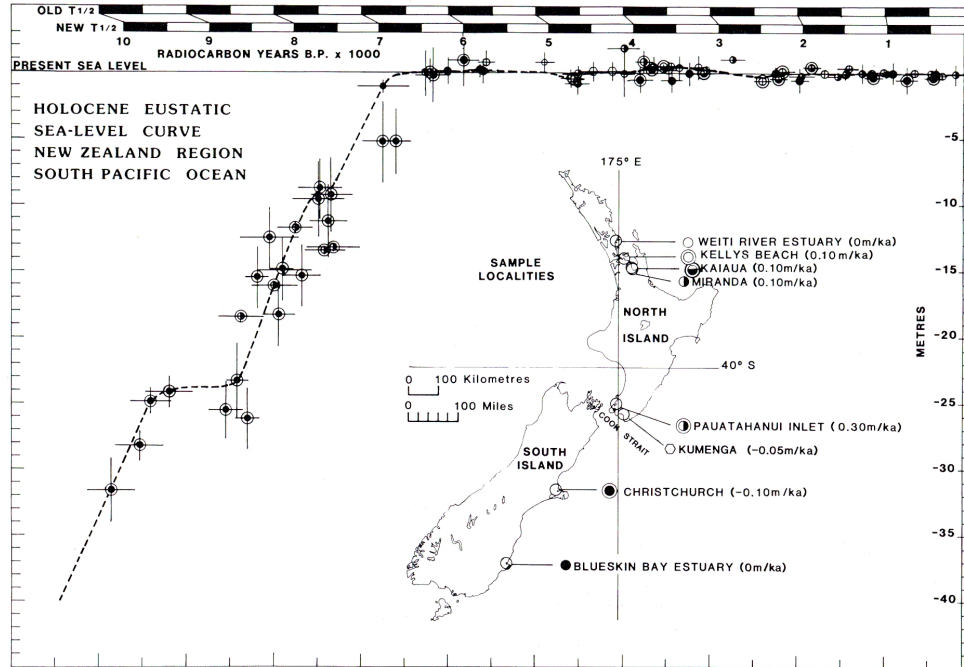
Figure 8-1: The regional Holocene eustatic sea-level curve for New Zealand, the data being from the sites identified on the map. The values in parentheses are the estimated rates of change in land elevations. [*From* Gibb (1986)]

Of interest, Figure 8-2 is a comparison between the Holocene sea-level changes found by Gibb (1986) with those determined by Cochran et al. (2006) for episodic changes in land and sea-level elevations along the Hawke's Bay coast, reviewed in Chapter 3. The upper-most graph includes only Gibb's (1986) data for the eustatic sea level, it being essentially the same as that in Figure 8-1. The study by Cochran et al. (2006) was based on sediments in cores collected in the Te Paeroa Lagoon and at Opoho, with the results respectively shown in the lower diagrams of Figure 8-2, revealing clear evidence for abrupt episodes of subsidence and the arrival of large tsunami waves, attributed to occurrences of major earthquakes within the Hikurangi subduction margin. Both sites demonstrate that there has been a net subsidence during the past 7,200 years, respectively having been about 4 and 6 metres. An equivalent net rate of rise in the relative sea level would have been roughly 0.6 and 0.8 mm/year for those two sites, although these assessments are solely the result of the two major earthquakes and accompanying episodic land subsidence, the interpretation being that the eustatic water level had not changed as indicated by Gibb's (1986) data.

The 20th century rise in sea level along the coasts of New Zealand was first documented by Hannah (1990, 2004) based on data from four tide gauges in operation since 1900, located on relatively stable shores: Auckland, Wellington, Lyttelton (Christchurch), and Dunedin. His results up through 1989 are graphed in Figure 8-3. It is seen for each of the gauges that there have been higher rates of rising sea levels during the post-1930 era than occurred earlier, suggestive of there having been a transition from the relatively constant sea levels during the 19th century (Chapter 2), also representing a transition to the nearly constant Holocene sea levels found by Gibb (1986) on the coast of New Zealand for the preceding 7,000 years, graphed here in Figures 8-1.
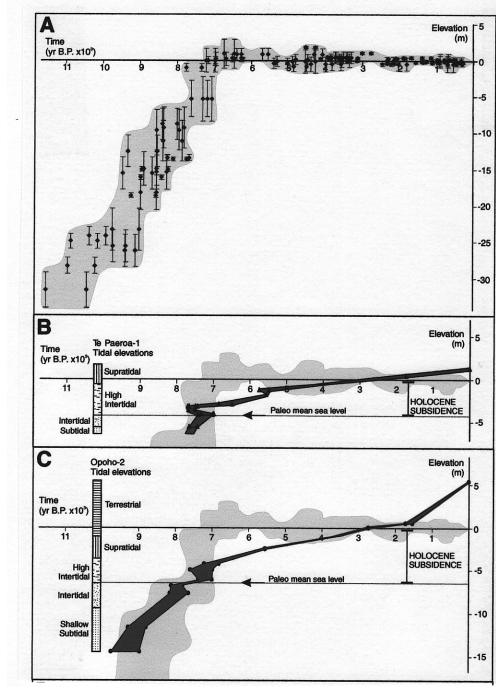
Figure 8-2: (A) Gibb's (1986) Holocene sea-level curve for New Zealand. (B and C) Comparisons with changes in sea levels based on sediments found in cores collected within the Te Paeroa Lagoon and at Opoho on the Hawke's Bay coast, showing episodes of subsidence that resulted in a rise in the relative sea level. [*From* Cochran et al. (2006)]
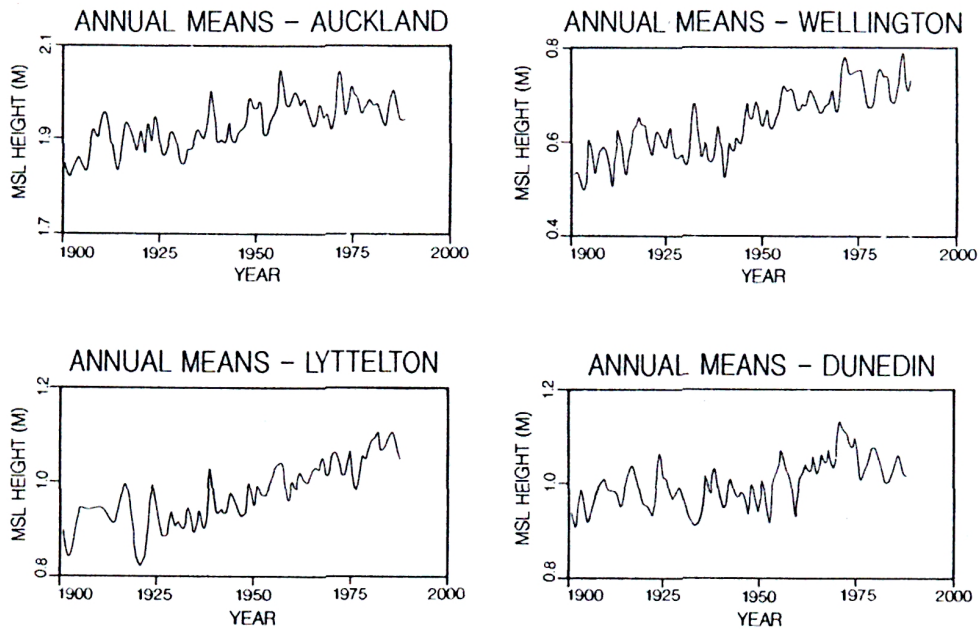
Figure 8-3: Annual mean sea levels derived from long-term New Zealand tide-gauge records on relatively stable coasts. [*From* Hannah (1990)]

1- 4

Recently, Hannah and Bell (2012) updated analyses of the trends for these long-term tide gauge records, and also analyzed measurements from gauges that have records spanning only a few decades, having applied improvised methodologies to analyze short time series. Their assessments for the updated rates of rise in relative sea levels for the four long-term tide gauges are:

Auckland	1.7 ± 0.14 mm/year
Wellington	2.2 ± 0.13 mm/year
Lyttelton	2.0 ± 0.15 mm/year
Dunedin	1.3 ± 0.15 mm/year

Six shorter tide-gauge records were included in their analyses: Whangarei, Moturiki and New Plymouth on the North Island; Nelson, Timaru and Bluff on the South Island. The trends in relative sea levels of those gauges agreed with the long-term records, collectively the six gauges now yielding an average rate of 1.7 ± 0.1 mm/year for the rise in relative sea levels along the coasts of New Zealand. This rate is effectively identical to the 1.74-mm/year global average found by Church and White (2006) and Holgate (2007), based on tide-gauge records throughout the world. However, all of these New Zealand sites are located on relatively stable shores, so this 1.7 mm/year rate might not necessarily be applicable to the tectonically active coast of Hawke's Bay where significant land elevation changes could be occurring, the evidence discussed below being that it is subsiding.

It is evident in Figure 8-3 that there can be significant variations in annually-averaged mean sea levels based on tide-gauge records, the peaks in those variations possibly being important to coastal erosion and flooding hazards since they represent reasonably persistent elevated water levels for that year, being particularly important if the highest levels in the seasonal cycle occur during the winter, in conjunction with major storms. Such variations are typical of tide-gauge records throughout the world, and it has been determined that they commonly are a response to year-to-year changes in the climate. In particular, it has been shown that they can result from the range of climate events between El Niños and La Niñas; for example, along the coast of the U.S. Pacific Northwest, strong El Niños elevate monthly-mean sea levels during the winter by up to 50 centimetres, whereas the levels are depressed during La Niñas, a difference produced by changes in water temperatures and ocean currents (Komar et al., 2011). In order to investigate such effects on New Zealand's sea levels, NIWA has installed ten open-coast sea-level measurement sites constituting their Sea-Level Network (Bell et al., 2000, 2001). Nine of these sites were installed between 1994 and 1998; this includes their Riverdale gauge south of Hawke's Bay, which began operation in August 1997. The tenth site, Moturiki Island near Mt Maunganui in the Bay of Plenty, has the longest record, yielding quality data since June 1973. One key finding has again been a demonstration of the important role of the El Niño/La Niña climate range in producing variations in mean sea levels from year to year, but the conclusion having been that La Niñas are accompanied by a rise in the annual mean sea level, whereas El Niños result in a drop (Bell et al., 2000, Fig. 2), opposite to those found along the U.S. west coast.

Longer-term cycles in Earth's climate are also recognized in the New Zealand tide-gauge records, including a dependence on the Inter-decadal Pacific Oscillation (IPO) that has a periodicity on the order of 25 years. The alternate phases of this oscillation are a "warm"

period when El Niño occurrences dominate, versus a "cool" phase with more La Niñas. The control of the IPO climate index on New Zealand's annual sea levels was also investigated by Bell et al. (2000), with the results shown in Figure 8-4 where the IPO cycles since 1900 are compared with the annual mean sea levels derived from the Port of Auckland's tide gauge. Although there is a great deal of variability from year to year, a pattern emerges wherein decades of rapid sea-level rise have occurred during the cool IPO phases when La Niñas dominated, whereas there was little or no net increase in sea levels spanning the decades during the warm phases with El Niños. For example, prior to about 1975 the IPO had been in its cool phase since 1948, during which there was a rapid rise in sea level. In contrast, during the twenty-five years from 1975 to 1998 the warm phase produced essentially no additional net increase in the sea level. Climatologists have concluded that in about 1998-99 the IPO again reverted to its cold phase, and Bell et al. (2000) accordingly predicted that there would be a return to rising sea levels such as occurred from 1948 to 1975. As seen in Figure 8-4, there was an abrupt step increase in the year 2000, amounting to on the order of 5 centimetres, attributed to the occurrence of a particularly severe La Niña, but since that major occurrence the annual mean sea levels have largely leveled off, as recorded on the tide gauges along New Zealand's coasts (Hannah and Bell, 2012, Fig. 2).
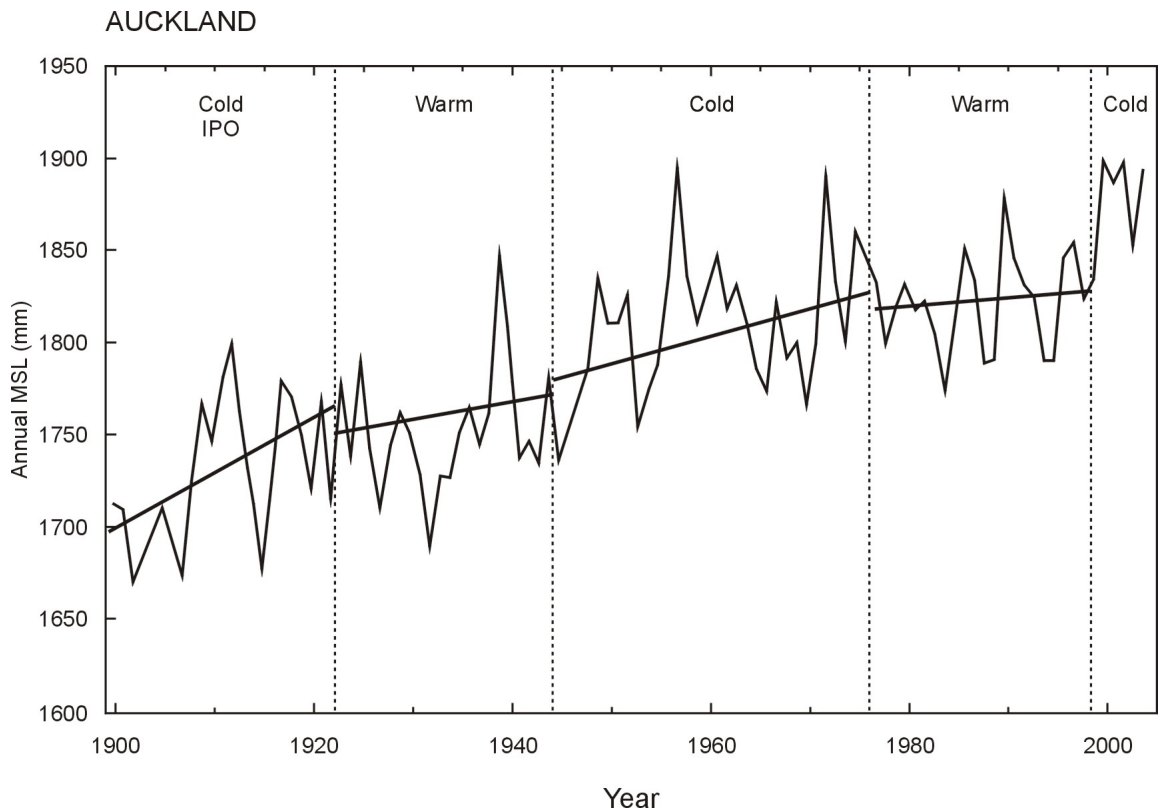
Figure 8-4: Annual mean sea levels derived from analyses of tide-gauge records from the Port of Auckland, contrasting the trends during the warm (W) and cold (C) phases of the IPO climate cycle. [Graph courtesy of Rob Bell, NIWA; also see Bell et al. (2000), and Goring and Bell (2001)]

8.3 THE HAWKE BAY TREND OF RISING SEA LEVELS

The hourly variations in the Hawke Bay tides measured over the years by the Port's gauge were analyzed in Chapter 4 to determine their ranges and extremes in water levels, the primary interest having been the highest elevations reached when the predicted astronomical tides were raised by storm surges. It was seen that tide data have been collected only since 1986, with a 4-year gap from 1995 to 1999, this limited availability of measurements having inhibited the derivation of assessments of the more extreme water levels (e.g., the 100-year extreme elevation).

Also important to this coast's hazard assessments is that the Port's measurements of the tides potentially could also yield a trend for the rate of increase in the relative sea level for this coast since 1986, the summation of the eustatic rise in the ocean level and any change in land elevations at the site of the gauge. However, the problem again is that the results will be uncertain due to its limited record, spanning only 24 years. Of interest will be the magnitude of the rate of rise in the relative sea level determined from the tide-gauge data, compared with independent measurements of the eustatic rise in water levels measured by satellites, and the GPS measurements of the land elevation changes along this shore.

The report by Beavan and Litchfield (2009) investigated the land-elevation changes based on geologic evidence to determine the long-term directions of uplift versus subsidence, but focused primarily on the Global Positioning System (GPS) data that provides direct measurements of the elevation changes. The results of those analyses were reviewed in Chapter 3, but again the GPS data are limited to a mere decade or less for the sites of interest immediately along this shore, suggesting directions of uplift versus subsidence, but yielding uncertain magnitudes for their trends. Beavan and Litchfield (2009) also analyzed the tide-gauge records from the North Island, the long-term measurements by the Auckland and Wellington gauges, and those collected by the Port's gauge in Hawke Bay, having analyzed the trends in mean sea levels but with their primary objective having been to provide additional assessments of the relative rates of changes in land elevations between those sites. A linear regression through the Wellington tide data for the monthly mean water levels, extending back to 1945, yielded a trend of 2.2 ± 0.2 mm/year for the rate of rise in its relative sea level. Regression results for the Napier data were not provided in their report, but it appears from their graph of the data that the trend is close zero.

With their interest having been on the changing land elevations, they subtracted the monthly mean water levels of the Wellington gauge from those in the Hawke Bay record, this removing the eustatic water-level changes that are assumed to be essentially the same at both sites, yielding a trend for their respective changes in land elevations. Subtraction of these records also had the positive effect of reducing the data scatter in the difference, Beavan and Litchfield (2009) having noted that there is a close correspondence in the year-to-year variations for these North Island sea levels, presumably due to having had essentially the same climate and oceanographic controls. Their analyses accordingly provided a smoothed comparison between the land-elevation trends for the Wellington and Port of Napier tide-gauge records. The graph obtained by Beavan and Litchfield (2009) from subtracting the monthly-averaged relative sea levels from these respected tide gauges yielded the linear regression

$$SLR_N - SLR_W = \text{-1.7} \ \pm \ 0.6 \ \text{mm/year}$$

where SLR_N and SLR_W respective represent the rates of change in measured sea levels for Napier and Wellington, this difference also representing the different trends in land elevations. Having determined that $SLR_W = 2.2$ mm/year for Wellington, this -1.7 mm/year rate for the difference in turn yields $SLR_N = 0.5$ mm/year for the corresponding Hawke Bay trend of its relative sea level, a low magnitude as expected from their graph. However, the use of the 2.2 mm/year rate for Wellington in this calculation carried with it a ± 0.2 mm/year uncertainty, which together with the ± 0.6 mm/year uncertainty in the trend for the difference in their rates signifies that this 0.5 mm/year indirect determination for the Hawke Bay rate of change in the relative sea-level rise must be viewed as highly questionable.

These high uncertainties in the analyses of sea-level trends by Beavan and Litchfield (2009) are likely in part due to their having been based on monthly averages. In our analyses of sea-level trends on the coast of the U.S. Pacific Northwest based on its tide-gauge records, we undertook a comparison between three methodologies: linear regressions of the monthly averages; the monthly averages but having subtracted the long-term seasonal cycle to reduce the data variations; and the traditional approach based on a regression of the annual averages (Komar et al., 2011). The analyses based on the monthly averages, the methodology followed by Beavan and Litchfield (2009), retained by far the greatest scatter in the data and the lowest statistical confidence in the derived regression trends for the relative sea levels. Based on that experience it was decided in the present study of Hawke's Bay to adopt the other methodologies in the analyses of the sea-level trend based on the Port's tide-gauge data. The results are graphed respectively in Figures 8-5 and 8-6, yielding essentially the same rates of sea-level rise from the linear regressions; a 1.90 mm/year trend based on the monthly averages where the seasonal cycle has been removed, and 2.07 mm/year for the trend of the annual average sea levels. Nearly the same magnitudes are also obtained when the analyses are based on only the "quality" tide measurements from 1999 to the present, although the uncertainties are increased by having limited the analyses to little more than a decade of measurements.
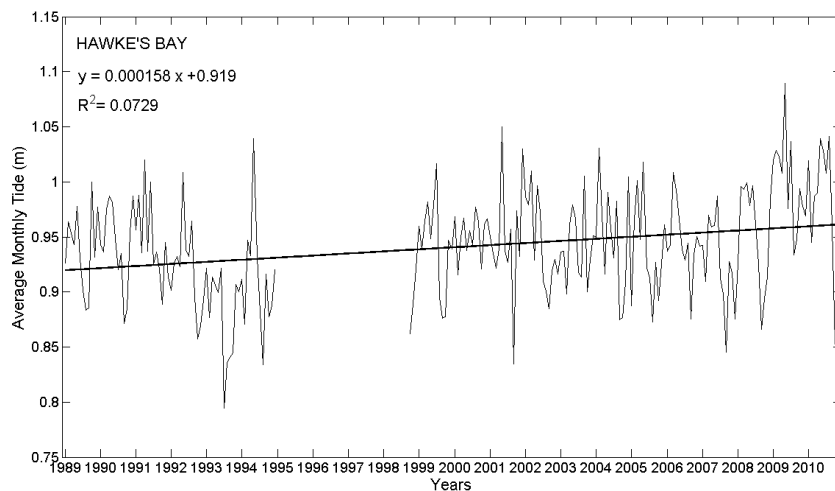
Figure 8-5: The trend in relative mean sea levels for the Port of Napier's tide-gauge based on the monthly averages with the mean seasonal cycle having been subtracted. The regression rate of 0.000158 metre/month is equivalent to 1.90 mm/year.
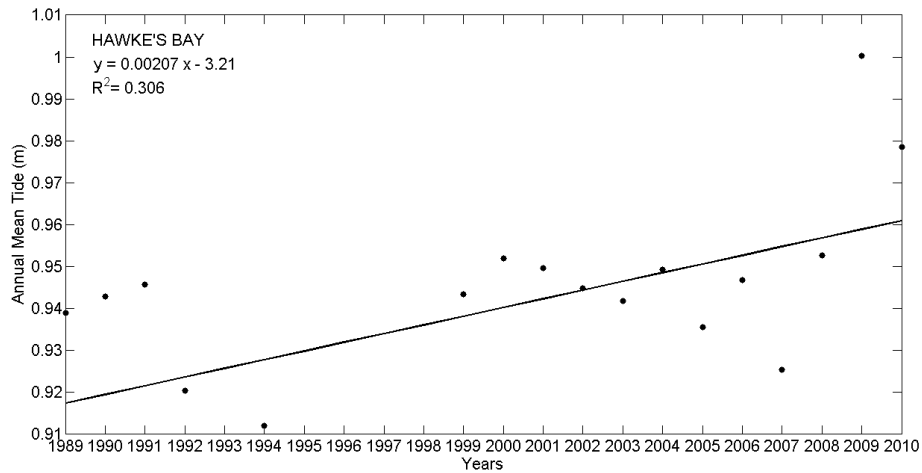
Figure 8-6: Trend in relative mean sea levels for the Port's tide-gauge measurements based on the annual averages, yielding 2.07 mm/year for the rate of rise.

Both graphs continue to show significant scatter in the data, more than generally found in such analyses according to our experience. This scatter is not random, however, as the plot in Figure 8-5 of the monthly averages for the Hawke Bay water levels is almost identical to that in an analysis of the tide-gauge measurements from Wellington, a coherence in the variations that had also been noted by Beavan and Litchfield (2009). The implication is that the scatter in both can be attributed in large part to climate controls that affect water temperatures and salinities along the shores of the North Island, combining to produce variations in the water densities, and possibly due also in part to ocean currents.

The rates found in this pair of analyses, Figure 8-5 and 8-6, about 2.0 mm/year for the rise in the relative sea level in Hawke Bay, are reasonably consistent with those determined by Hannah and Bell (2012) for individual long-term tide gauge records (Wellington and Lyttelton) on the New Zealand coast, being somewhat greater than their 1.7 mm/year average rate based on all the tide-gauge records and also found in assessments of global average rates spanning the 20th century. A somewhat higher rate for Hawke Bay would be expected in view of its tectonic setting, and with Beavan and Litchfield (2009) having concluded from the GPS measurements that this stretch of shore containing the Port's tide gauge has been subsiding, although the magnitude of its rate is uncertain due to the shortness of those records.

An interpretation of these results for Hawke Bay based on its tide-gauge record is, however, unclear with respect to the component of its relative rate of change in sea level produced by the local eustatic rise in water levels along the New Zealand coast. As reviewed in Chapter 2 (Figs. 2-6 and 2-7), satellite data of the changing eustatic sea levels from October 1992 to March 2010 reveal the occurrence of significant variations across the world's oceans, interpreted as having been caused almost entirely by changes in water temperatures and the resulting thermal expansion or contraction respectively producing a rise or fall in the local water levels. Of significance, the rate of increase for the South Pacific as a whole has been about 2.34 mm/year, while off the east coast of New Zealand's North Island the rate appears to have been higher, possibly on the order of 3 to 5 mm/year. With the addition of the GPS component due to the subsidence of this shore, the net rate of increase in the relative sea

level would be still greater, their summation being substantially higher than the 2.0 mm/year rate inferred from our analyses of the tide-gauge records. These uncertainties based on the independent measurements from the Port's tide gauge, the GPS data of land elevations, and satellite measurements of eustatic water levels, clearly result from shortness of these data sets; when longer records become available, it can be expected that these inconsistencies will be resolved, providing a better assessment of the trend of the rising relative sea level along the Hawke's Bay coast, and of its components, the eustatic rise in the ocean's water and the contribution from the subsidence of the land.

8.4 PROJECTED FUTURE SEA LEVELS

As reviewed in Chapter 2, projections into the future have predicted that there will be accelerated rates of rising sea levels associated with continued global warming. Although projections of future sea levels by various investigators have differed in their rates and magnitudes, depending on their analysis methodologies and assumptions as to the extent of future global warming, the predicted levels by the year 2100 generally range from an increase of about 50 centimetres to over 1 metre. The goal in this section is to present a "consensus" scenario for the projected global increase in sea levels based on the recent analyses by climatologists, and then to apply those global projections specifically to Hawke Bay, with the resulting projected relative sea levels taking into account its changing land elevations.

Graphical projections of future sea levels were presented in Chapters 2 (Fig. 2-5), the diagram prepared by Cazenave and Llovell (2010) for the global average sea levels consisting of a curve though the 19th century based on geological observations, and the 20th-century curve derived from tide-gauge records and recent satellite data; those measured trends were then projected through the 21st century, represented by shaded regions that illustrate both the expected increases and their levels of uncertainty. Included in that diagram were the IPCC 2007 climate model projections (Meehl et al., 2007), and the more extreme projected ocean levels derived by Rahmstorf (2007). The overall concave-up curvature of that graphical synthesis developed by Cazenave and Llovell (2010) provides a sense of the acceleration in the rate of sea-level rise over the centuries, considering that there had been minimal increase during the 19th century prior to significant global warming, some acceleration throughout the span of the 20th century, and with future projections predicting significantly higher rates of acceleration leading to much higher ocean levels by the year 2100 than at present.

The IPCC projections were based on detailed numerical climate models and assumptions for the potential future greenhouse gas emissions, the result being a range of uncertainties in the future global mean sea levels, an increase ranging from approximately 20 to 60 centimetres during the 21st century (Meehl et al., 2007). The more extreme projections by Rahmstorf (2007) amount to an increase of 50 to 120 centimetres by the year 2100, based on a semi-empirical correlation between the global sea-level rise and Earth's past changes in mean temperatures, directly representing the degree of global warming. Similar projections have been offered by other investigators, again based on statistical models similar to that developed by Rahmstorf (2007). These have been reviewed by Rahmstorf (2010), the list of their projected increases by the year 2100 being listed in Table 8-1. The consensus from these later analyses is that future increases in global mean sea levels will in all probability be greater than those projected by IPCC, that the increase could be more than 1 metre by the end of the 21st century. Such projections are of considerable importance to assessments of

the resulting erosion and flooding hazards faced along the world's coastlines, but it is clear that large uncertainties remain in the expected magnitudes of the potential sea-level increase by the year 2100. This continues to be an active area of research by climatologists, and in such circumstances it is necessary to be conservative in projecting what might be the worst-case scenario. Later when the science has advanced and there is a greater degree of consensus, adjustments could then be made, either increasing or decreasing the recommended hazard zones for the development of shore-front properties.

Table 8-1: Ranges of projected increases in global average sea levels by the year 2100, derived by recent investigations.

|	Sea-Level Rise (metres)
IPCC (Meehl et al., 2007)	0.2 to 0.6
Rahmstorf (2007)	0.5 to 1.2
Horton et al. (2008)	0.5-1.0
Grinsted et al. (2009)	0.9-1.3
Vermeer and Rahmstorf (2009)	0.75-1.90
Jevrejeva et al. (2010)	0.6-1.6

The approach we have followed in developing hazard zones along the coast of the U.S. Pacific Northwest consisted of applying the above projections of future global mean sea levels, accounting for the local trends of changing land elevations on that coast in order to determine the combined future increases in relative sea levels (Baron, 2011; Harris, 2011; Komar et al., 2011; Komar et al., 2013). Faced with the wide range of projections listed above for the future sea levels, a "consensus" projection was developed that is based on the curves published by Horton et al. (2008), Vermeer and Rahmstorf (2009), Grinsted et al. (2009), and Jevrejeva et al. (2010). For each of their projected curves of rising sea levels, values were extracted at the decadal intervals 2030, 2040, 2050, 2070, 2080, and 2100, graphed as the "data" points in Figure 8-7 (Baron, 2011; Harris, 2011). A quadratic curve has been fitted through the averages of the middle or "best guess" curves published by those authors to create our "Average" projection, with similar curves having been derived to represent the ranges, the "High" and "Low" estimates. For the year 2100 the Average projected sea level increase is 0.95 metre, the range being 0.63 to 1.34 metres, significantly higher than the 0.2- to 0.6-metre IPCC projection but representative of the ranges in the more extreme water levels derived by Rahmstorf (2007) and in analyses by other climatologists listed in Table 8-1.

The "consensus" sea-level projections graphed in Figure 8-7 have been applied in our assessments of future relative sea levels along the U.S. Pacific Northwest coast, with two examples shown in Figure 8-8 representing present-day submergent and emergent shores (Komar et al., 2013). The three "consensus" curves for Average, High and Low projections have been attached extending the trends of the regression lines based on the tide-gauge analyses for those two sites, providing estimates of future sea levels out to the year 2100. Being tangent to the linear regressions based on the tide-gauge data, these projections account for the present-day trends in relative sea levels that depend on the local changes in land elevations. This is evident in the contrasting results for Yaquina Bay (Newport) on the mid-Oregon coast where there is already a trend of increasing relative sea levels, versus that for Crescent City on the coast of northern California where the tectonic uplift of the land is greater than the present-day eustatic rise in sea level, at present resulting in an emergent

shore. However, according to the Average projection for Crescent City, Figure 8-8, in roughly the year 2025 the rise in the eustatic water level could be expected to accelerate to the extent that it exceeds the rate of uplift of the land, that coast then becoming submergent with an expected increase in erosion and flooding hazards. In total we analyzed 16 tide gauges along the coast of the U.S. Pacific Northwest, to determine their multidecadal trends in relative sea levels, defining both the present-day submergent and emergent shores and how they are expected to change in the future (Komar et al., 2011, 2013).
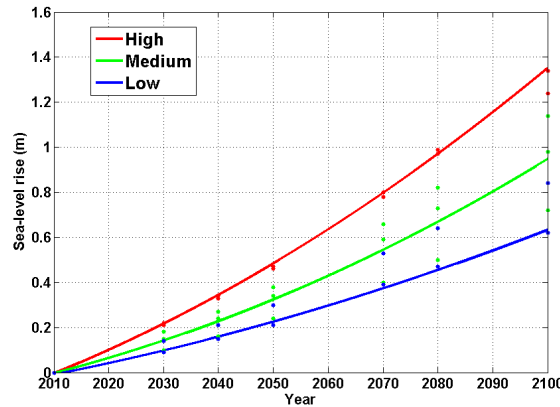
Figure 8-7: Global sea-level projections through 2100 based on recent analyses by climatologists, yielding High, Medium and Low curves for the "consensus" projections.   [*From* Baron (2011) and Harris (2011)]
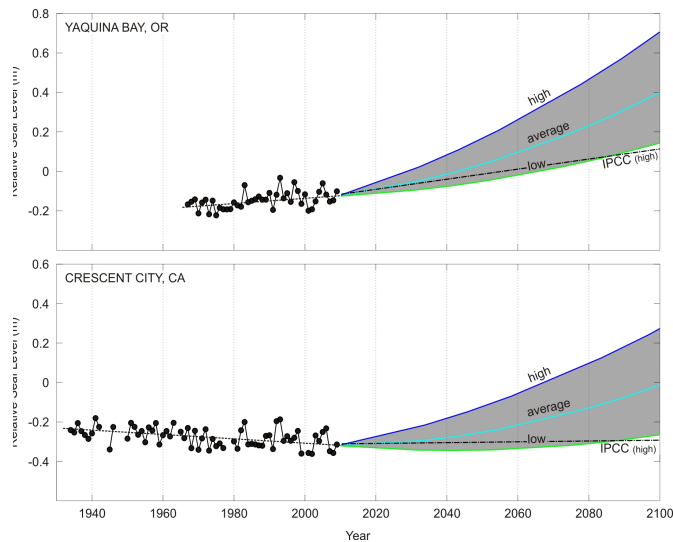
Figure 8-8: Projected relative sea levels beyond those measured by the Yaquina Bay (Newport) tide gauge on the central Oregon coast, and for Crescent City on the northern coast of California where the tectonic uplift of the land presently exceeds the eustatic rise in sea level, but is projected to become a submergent coast in the future. [*From* Komar et al. (2013)]

These analysis procedures applied on the coast of the U.S. Pacific Northwest have been followed in the present study to project future elevations of the Hawke Bay rising sea levels during the 21st century, with the results graphed in Figure 8-9. The curve for the annual average sea levels obtained in Figure 8-6, based on the Port's tide-gauge records, similarly serves as the regression trend beyond which the projections extend, the latter being the three

1- 12

"consensus" curves in Figure 8-7 for the Average, High and Low projections. The results indicate that by the year 2050, the Average assessment is that the relative sea level could be expected to rise by about 30 centimetres above its present elevation, and that by 2100 the rise could amount to on the order of 90 centimetres. These projections represent the most probable increases based on the analyses by climatologists. The more extreme potential future coastal hazards due to rising sea levels are given by the High consensus curve in Figure 8-9; it shows that the increase could amount to 50 centimetres by mid-century, and be as much as 130 centimetres by the end of this century. The Low ranges of projections respectively for 2050 and 2100 are on the order of 20 and 50 centimetres, corresponding approximately to those projected in the IPCC 2007 report. These projected magnitudes are in reasonable agreement with the original ranges listed in Table 8-1 for the assessments by climatologists of potential increases in the global average eustatic sea levels. On the other hand, since the intent in Figure 8-9 is to project the increase in the relative sea levels for Hawke Bay, the expectation was that the magnitudes would be somewhat greater, depending on the rate of land subsidence at the site of the Port's tide gauge; however, as discussed above, its assessment remains uncertain, and apparently is sufficiently low as to not have significantly affected the future projections. These projections here for Hawke Bay are consistent with those used elsewhere in New Zealand, and in Australia, applied in their hazard assessments.
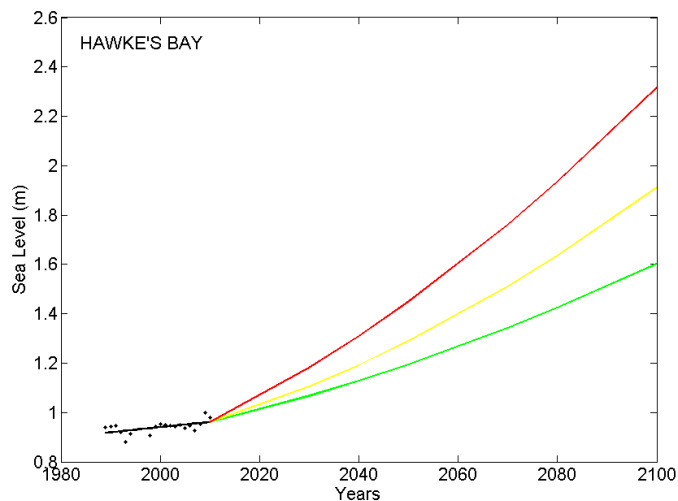
Figure 8-9: Projected future relative sea levels for Hawke Bay due to global warming, based on the Port's tide-gauge measurements that defined the trend from 1989 to 2010, with the projections given by the "consensus" curves in Figure 8-7.

8.5 SUMMARY AND DISCUSSION

The objective of this chapter has been to examine the changing sea levels along the coasts of New Zealand, beginning thousands of years ago as the Ice Age came to an end and sea levels rose at rapid rates when the melting glaciers returned water to the oceans. As reviewed in Chapter 2, globally the initial high rate of rise in the mean level of the sea slowed significantly beginning about 7,000 years ago, but returned to increasing rates during the late 19th century and has continued to do so up to the present, an increase that clearly can be attributed to global warming. The primary goal of this chapter has been to analyze the present-day trend of sea-level rise along the coast of Hawke's Bay, based on the Port of

Napier's tide-gauge records, and to project the future accelerated rates of increase through the 21st century based on the research results by climatologists.

As expected, the changes in sea levels along the coasts of New Zealand have largely corresponded to the variations found globally. This is true for the rapid rise in sea levels following the end of the Ice Age, seen here in Figure 8-1 from the study by Gibb (1986), with that rapid increase transitioning about 7,000 years ago to a long period of nearly constant levels along this coast. Those thousands of years of stable sea levels ended in the late 19th century, as found on other coasts throughout the world, due to the inception of global warming. The longest tide-gauge records available on the New Zealand coast date back to 1900, their analyses by Hannah (1990, 2004) and Hannah and Bell (2011) having determined that the 20th century average rate of rise has been on the order of 1.7 mm/year, essentially the same as found for the global average (1.74 mm/year). However, this average for New Zealand's rate of rise in the relative sea level is based only on tide gauges located on relatively stable coasts, and the results might not necessarily apply to the coast of Hawke's Bay due to its tectonic setting on the Hikurangi Margin, the geological evidence and recent measurements by GPS units along this coast indicating that this shore is slowly subsiding.

Important in this chapter has been our analyses of the Port of Napier's tide-gauge records to determine its trend in relative sea levels, affected by both the eustatic change in the ocean levels and any trends of change in the land elevations. The results are graphed in Figures 8-5 and 8-6, respectively based on analyses of the monthly-mean water levels and the annual averages; the results from their linear regressions are nearly the same, a trend of 1.90 mm/year based on the monthly averages where the seasonal cycle has been removed, and 2.07 mm/year for the trend of the annual averages. However, these results are based on only 25 years of water level measurements derived from the Port's gauge, with both the monthly and annual averages being highly variable due to changes in water temperatures and possibly ocean currents. In that generally it is considered that some 40- to 50-years of tide-gauge records are required to derive statistically meaningful trends of change in relative sea levels, the approximately 2.0 mm/year magnitude for the rate of rise obtained here for Hawke Bay should be viewed as only an approximate estimate, although it is clear that there has been a net rise in its levels over the decades, approximately at the rate of the globally-average rate of increase plus some subsidence of this coast as evident in the GPS records from these shores.

Projections of future rates of sea-level rise along the coast of Hawke's Bay are critical to analyses of its potential erosion and flooding hazards through the 21st century. Such projections remain problematic for any coast, in view of the significant ranges derived by climatologists in their analyses of sea-level responses to global warming, evident in the list given in Table 8-1 where the projections of global averages range from 1.0 to 1.9 metres. The projections we have derived for Hawke Bay, graphed in Figure 8-9, were based on a "consensus" set of curves representing the products of those analyses by climatologists, extending into the future the regression line based on the Port's existing tide-gauge record. The results indicate that by the end of the century (the year 2100), according to the Average ("most probable") assessment the relative sea level could be expected to rise by about 90 centimetres, but the more extreme High assessment is that it could amount to on the order of 130 centimetres. Although these projections for Hawke Bay are affected by numerous uncertainties, the magnitudes themselves seem reasonable in comparison with those applied in

hazard assessments on other coasts where the analyses are based on longer data sets for the tides and trends in sea levels. The results found here will therefore be incorporated in the following chapter into models that project future erosion and flooding hazards faced along the shores of Hawke's Bay, produced by Earth's evolving climate.

8.6 REFERENCES

Baron, H.M. (2011) *Coastal Hazards and Community Exposure in a Changing Climate: The Development of Probabilistic Coastal Change Hazard Zones*: Masters of Science thesis, Oregon State University, 95 pp.

Beavan, R.J., and N.J. Litchfield (2009) *Sea Level Rise Projections Adjusted for Vertical Tectonic Land Movement Along the Hawke's Bay Coastline*: GNS Science Consultancy Report 2009/128, 42 pp.

Bell, R. G., D. G. Goring and W. P. de Lange (2000) Sea-level change and storm surges in the context of climate change: *IPENZ Transactions*, v. 27, no. 1/Gen, p. 1-10.

Bell, R. G., T. M. Hume and D. M. Hicks (2001) *Planning for Climate Change: Effects on Coastal Margins*: New Zealand Climate Change Programme, Ministry for the Environment, Wellington, 100 pp.

Cazenave, A., and W. Llovel (2010) Contemporary sea level rise: *Annual Reviews of Marine Sciences*, v. 2, p. 145-173.

Cochran, U., and others (2006) Paleoecological insights into subduction zone earthquake occurrences, eastern North Island, New Zealand: *Geological Society of America Bulletin*, v. 118, no. 9/10, p. 1051-1074.

Church, J.A., and N.J. White (2006) A 20th century acceleration in global sea-level rise: Geophysical Research Letters, v. 33, L01602, doi: 10.1029/2005GL024826, 4pp.

Gibb, J. G. (1986) A New Zealand regional Holocene eustatic sea-level curve and its application for determination of vertical tectonic movement: *Royal Society of New Zealand Bulletin*, v. 24, p. 377-395.

Goring, D. G., and R. Bell (2001) Sea level on the move?: *Water & Atmosphere, NIWA*, v. 9, n. 4, p. 20-22.

Grinsted, A., J.C. Moore, and S. Jevrejeva (2009) Reconstructing sea level from paleo and projected temperatures 200 to 2100 AD: *Climate Dynamics*, v. 34(4), p. 461-472.

Hannah, J. (1990) Analysis of mean sea level data from New Zealand for the period 1899-1988: *Journal of Geophysical Research*, v. 95 (B8), p. 12,399-12,405.

Hannah, J. (2004) An updated analysis of long-term sea level change in New Zealand: *Geophysical Research Letters*, v. 31, L03307, doi: 10.1029/2003GL019166.

Hannah, J., and R.G. Bell (2012) Regional sea level trends in New Zealand: *Journal of Geophysical Research*, v. 117, C01004, doi:10.1029/2011JC007591, 7 pp.

Harris, E.L. (2011) *Assessing Physical Vulnerability of the Coast in Light of a Changing Climate: An Integrated, Multi-Hazard, Multi-Timescale Approach*: Masters of Science thesis, Oregon State University, 91 pp.

Holgate, S. (2007) On the decadal rates of sea level change during the twentieth century: *Geophysical Research Letters*, v. 34, p. 1-4.

Horton, R., C. Herweijer, C. Rosenzweig, J. Liu, V. Gornitz, and A.C. Ruane (2008) Sea level rise projections for current generation CGCMs based on the semi-empirical method. *Geophysical Research Letters*, v. 35, L02715, 5 pp.

Jevrejeva, S., J.C. Moore, and A. Grinsted (2010) How will sea level respond to changes in natural and anthropogenic forcings by 2100?: *Geophysical Research Letters*, v. 37, L07703, 5 pp.

Komar, P.D., J.C. Allan and P. Ruggiero (2011) Sea level variations along the U.S. Pacific Northwest coast: tectonic and climate controls: *Journal of Coastal Research*, v. 27, p. 808-823.

Komar, P.D., J.C. Allan and P. Ruggiero (2013) U.S. Pacific Northwest coastal hazards: tectonic and climate controls: *Coastal Hazards*, edited by C.W. Finkl, Springer, p. 587-674.

Meehl, G.A., T.F. Stocker, W.D. Collins, P. Friedlingstein, A.T. Gaye, J.M. Gregory, A. Kitoh, R. Knutti, J.M. Murphy, A. Noda, S.C.B. Raper, I.G. Watterson, A.J. Weaver and Z.-C. Zhao (2007) Global Climate Projections. In: Climate Change 2007: The Physical Science Basis. Contribution of Working Group I to the Fourth Assessment Report of the Intergovernmental Panel on Climate Change, [Solomon, S., D. Qin, M. Manning, Z. Chen, M. Marquis, K.B. Averyt, M. Tignor and H.L. Miller (eds)]. Cambridge University Press, Cambridge, United Kingdom and New York, NY, USA.

Rahmstorf, S. (2007) A semi-empirical approach to projecting future sea-level rise: *Science*, v. 315, p. 368-370.

Rahmstorf, S. (2010) A new view on sea level rise: *Nature*, v. 4, p. 44-45.

Ruggiero, P., P.D. Komar, W.G. McDougal, J.J. Marra, and R.A. Beach (2001) Wave runup, extreme water levels and the erosion of properties backing beaches: *Journal of Coastal Research*, v. 17, no. 2, p. 407-419.

Vermeer, M., and S. Rahmstorf (2009) Global sea level linked to global temperature: *Proceedings of the National Academy of Sciences*, v. 106 (51), p. 21527-21532.

9 Increasing Sea Levels and Storm Intensities — Coastal Responses and Future Hazards

9.1 INTRODUCTION

The century-long rise in global-average sea levels was reviewed in Chapter 2, documented from tide-gauge records and more recently using satellite measurements, the 0.17-metre increase during the 20th century having been attributed to global warming. In Chapter 8 the trends in relative sea levels along the shores of New Zealand were examined, including analyses undertaken for Hawke Bay based on the Port of Napier's tide-gauge record. With the expectation of there being continued emissions by humans of greenhouse gases into the atmosphere, projections by climatologists are that rates of sea-level rise will accelerate, with the global mean level increasing by the order of 1 metre by the end of this century, dwarfing the increase during the past century. At the same time there is evidence that the intensities of storms are becoming stronger, leading to increased wave heights across most of the world's oceans, including Hawke's Bay according to both satellite measurements and data from the Port's wave buoy. The climate-induced rising sea levels, combing with the elevated surges and heights of waves generated by extreme storms, are expected to result in enhanced coastal-erosion processes and property impacts, becoming substantially greater than occurred in past decades. The objective of this study has been to investigate these climate-affected ocean processes and the resulting enhanced erosion and flooding along the Hawke's Bay coast, projected through this century to serve as the basis for the establishment of rational hazard zones to protect homes and infrastructure.

This chapter begins with a general review of the responses of coasts to rising sea levels and major storms, the effects on the beach morphologies with our focus being on coarse-grained gravel beaches such as those found along the shores of the Bay View and Haumoana Littoral Cells. An emphasis will be placed on models that have been developed to provide quantitative assessments of the resulting erosion and flooding of shorefront properties. However, the extent of the future erosion will also depend on factors beyond the responses to elevated sea levels and storm intensities, important being the sediment budgets for the Hawke's Bay beaches that account for the gains and losses of gravel and sand from their shores, with the balance in those budgets expected to be significantly modified by the climate-altered processes.

The goal of this chapter is to combine these multiple ocean processes and factors important to the erosion of the Hawke's Bay shorefront properties, to provide quantitative assessments of the future evolution of its protective barrier gravel-beach ridges. An important question is whether the gravel ridges will continue to provide protection to homes and infrastructure along these shores, or whether destructive losses from erosion and flooding can be expected as the 21st century progresses.

9.2 COASTAL RESPONSES TO RISING SEA LEVELS

With the prospects for increased impacts along the world's ocean shores due to global warming, field research programs have been directed toward investigations of the coastal responses to elevated water levels, including the changes in morphologies of beaches and to low-lying backshore areas that are flooded by the surge and waves of major storms. The results of those investigations have supported the development of models that can be applied to predict future changes in the morphology, including assessments of the associated rates of erosional retreat of shorefront properties. The vast majority of those research investigations have been undertaken on sand beaches, with comparatively few on coarse-grained beaches composed of pebbles and cobbles. The products of the research efforts for gravel beaches will be summarized in this section, the focus being on the effects of increasing sea levels and storm intensities. The results of this review will be then applied in later sections of this chapter, where analyses are undertaken of the potential future hazards along the Hawke's Bay shore.

9.2.1 Field Investigations of Gravel Barrier-Beach Ridges

The significance of the ocean processes and resulting changes in morphologies of coarse-grained barrier-beach ridges are recognized based on the discoveries by past investigations, it having been concluded that the primary controls are the volumes of sediments supplied to that shore (its sediment budget), the basement over which the beach ridge has accumulated, the rate of change in the relative sea level, and the wave climate (Carter and Orford, 1993; Orford et al., 1996). In view of the results from our analyses in previous chapters of the processes important along the Hawke's Bay coast, we can expand this list by including details for the range of astronomical tides, the enhanced measured tides produced by storm surges, and the wave swash runup levels at the shore related to the deep-water climate of wave heights and periods. From this list it is again apparent that the sediment budget is of particular importance, with its net balance governing the volumes and elevations of the gravel beach ridge, determining its stability in response to combinations of ocean processes that determine the total water levels, ranging from episodic storms to the long-term rise in sea levels.

An important research topic for gravel beaches has been occurrences of overtopping or overwash events on barrier beaches or ridges, at times of high tides and storm waves, a process that is expected to occur with greater frequency in the future as the level of the sea rises. Figure 9-1 from the investigation by Orford and Carter (1982) illustrates the continuum of processes and responses as a function of progressively increasing volumes of water that pass over the ridge crest during storms, transporting and redistributing in the landward direction greater quantities of gravel during the more extreme events. The top-most diagram represents an "overtopping" event, when the wave swash is just sufficient to reach and flow over the crest, the water then percolating into the porous gravel, resulting in the deposition of its transported pebbles atop and immediately landward from the ridge crest, raising its elevations. The following pair of diagrams represents progressively more intense "overwash" occurrences, storm events when greater volumes of water passes over the crest of the barrier ridge and continue to flow down its landward slope, commonly ponding inland the ridge. With the greater intensity of overwash during a major storm, gravel is transported from the ocean beach to the landward side of the ridge as depicted in Figure 9-1, and in contrast to the rise in

the level of the crest during a mild overtopping event, the intense flow of an overwash event acts to erode the crest, reducing its elevation, and in the extreme can catastrophically lead to breaching and washing away a portion of the ridge-crest length.
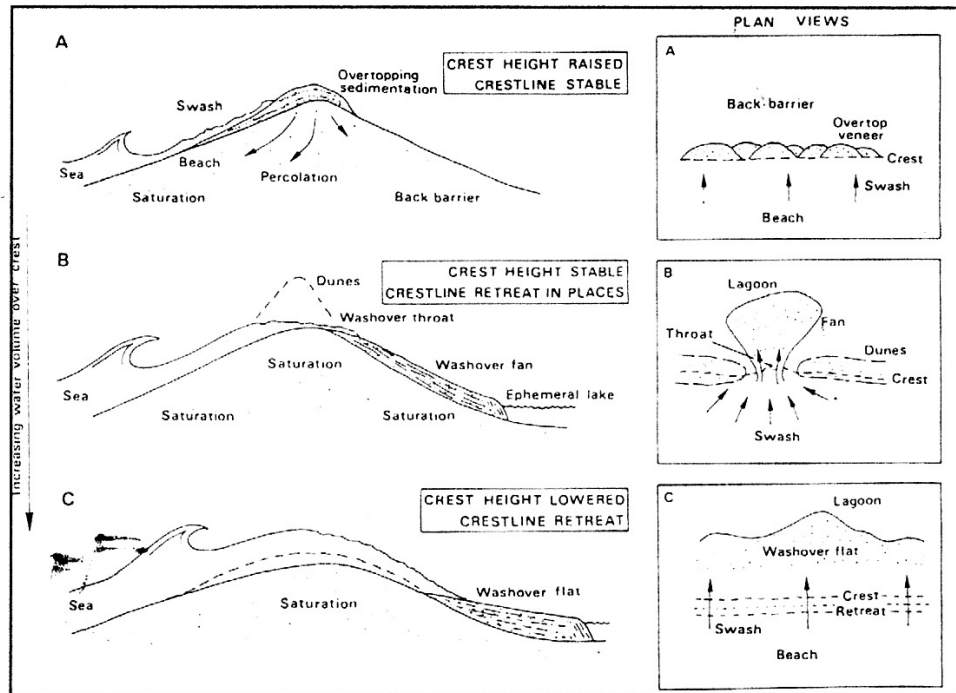
Figure 9-1: The range of overtopping and overwash occurrences on a barrier gravel beach ridge, representing progressively increasing volumes of water and transported sediments passing over its crest during a storm. [*From* Orford and Carter (1982)]

The net consequence of an overwash event during a major storm is a net landward transport of a portion of the ridge's gravel, having been eroded from the ocean beach and thereby contributing to the retreat of its shoreline. Following that extreme event, however, during the years to decades until another major storm occurs, producing a repeat of overwash and erosion, the more normal range of total water levels of tides plus the swash runup of moderate waves can be expected to lead to the development of a new ridge crest, its elevation progressively being raised by the weaker overtopping events. This new crest would tend to form landward from its prior position, considering that the beach had experienced a net loss of gravel during the previous major overwash event, and also in response to a trend of sea-level rise during those decades of crest reformation. The overall consequence is a "rollover" of the barrier beach ridge, having shifted landward with the rise in sea level. The rate of this rollover migration and the distance of the landward shift in the position of the barrier ridge is therefore dependent on the rate of sea-level rise, with the period of time between extreme storms and overwash occurrences determining the episodic nature of this migration and cycle of morphologic changes (Orford et al., 1996).

The investigations undertaken by Orford et al. (1991, 1995) have been directed toward correlating the long-term net rates of landward migrations of gravel beach ridges to the local rate of rise in relative sea level. In their 1991 study the analyses were based on the retreat of

the Story Head barrier beach on the eastern shore of Nova Scotia, Canada, its measured rates of retreat having been derived from nine sets of aerial photographs from 1942 to 1982. The retreat rates between successive sets of photos ranged from 2 m/year to as much as 30 m/year, the latter extreme however having resulted from a severe storm during a short period between successive aerial-photo coverage. Recombining the photographs to represent more uniform intervals of time, 6 to 9 years, the maximum rate was reduced to about 12 m/year. Analyses were then undertaken by Orford et al. (1991) to correlate the retreat rates of the gravel ridge to the changing relative sea levels during those time periods, measured by the nearby tide gauge in Halifax; those rates of change in sea levels ranged from -0.5 to +5 mm/year for the subdecadal intervals. A linear regression between the gravel-ridge migrations and corresponding changes in sea levels yielded an annual retreat of 0.84 metre for every millimetre increase in the annual mean sea level.

Orford et al. (1995) expanded their analyses to include retreat rates measured for the gravel barrier beaches at Westward Ho! on the North Devon coast of England facing the Irish Sea, and at Sillon de Talbert on the north Brittany coast of France (the English Channel), having also included the earlier data from Story Head, Nova Scotia, in their comparisons. The century long rates of increasing relative sea levels for these three sites provided a large range of magnitudes: 0.9 mm/year for Brest, France; 1.5 mm/year for Newlyn on the English coast; and 3.8 mm/year for Halifax, Nova Scotia. In each case the analyses showed the expected increase in barrier retreat rates in response to increasing rates of rise in relative sea levels, but with differences having been found between these three sites. Whereas the data from Sillon de Talbert and Westward Ho! yielded similar correlations, respectively 0.32 and 0.23 metre retreat per millimetre increase in sea level, the increase at Story Head was substantially greater, 0.84 metre retreat per millimetre rise in sea level. The interpretation by Orford et al. (1995) to account for this difference involved the contrasting heights and sediment volumes of these barrier beach ridges, with that at Story Head being substantially smaller having a height of only 3.5 metres and a volume of 130 cubic metres, whereas the heights of the Sillon de Talbert and Westward Ho! beach ridges were respectively 6.5 and 8.0 metres, their volumes being 325 and 340 cubic metres. The conclusion by Orford et al. (1995) was that the larger barrier ridges have a greater "inertia", resisting the rollover movement under the waves and accordingly migrate more slowly for a given rate of rise in sea level.

In summary based on the field investigations of barrier-ridge migrations undertaken by Orford et al. (1991, 1995), with Story Head having a measured migration distance of 0.84 metre per millimeter rise sea-level, if that rate were sustained on average through the 20th century when the global rise in sea level amounted to about 0.17 metre (170 mm), the landward retreat of that gravel barrier ridge would have amounted to nearly 150 metres. The corresponding retreat distances for Sillon de Talbert and Westward Ho! would have been substantially less due to their lower rates of migrations (0.32 and 0.23 metre/mm), respectively having been about 50 and 40 metres. This contrast between their estimated retreat distances resulting from the global rise in sea level is greatly magnified when the calculations are based on their local relative rates of change in sea levels; for Story Head having a local rate of sea-level rise 3.8 mm/year, the ridge migration would have doubled to about 320 metres, while those for Sillon de Talbert and Westward Ho! are reduced to 28 and 34 metres due to their relative rates of sea-level rise being lower than the global average. Projecting such estimates into the future with the prospects for a 1-metre rise in global sea levels during the 21st century, these ranges of migrations would increase to on the order of

800 to 300 metres. While these estimated rates and total extent of inland migrations of barrier gravel ridges might not necessarily be applicable to those on the Hawke's Bay coast, the results make the point that low-lying coasts that are susceptible to overwash events in response to rising sea levels and increasing storm intensities, may potentially experience extreme erosion and flooding of their beaches and backshore properties, significantly more extreme than experienced where land elevations are sufficient to prevent occurrences of overwash in the face of rising sea levels and more severe storms.

### 9.2.2 Models of Beach Retreat under Rising Seas

With the concern being the retreat of shorelines and the erosion of shore-front properties in response to rising sea levels, analyses by coastal scientists and engineers have been directed toward the development and testing of models that could be applied to quantitatively predict the future hazards. Reviews of those models have been undertaken elsewhere [Komar et al. (1991) and Komar (1998, p. 121-129)]. Best known is the simple model formulated by Bruun (1962), one that has seen wide use in coastal management applications, while having been criticized by other investigators. As depicted in Figure 9-2A, Bruun's model involves the upward and landward translation of the beach profile to match the rise in sea level, while conserving the sediment volume during its transport offshore. The analysis is two-dimensional and assumes: (1) the upper beach is eroded due to the landward translation of the profile; (2) the material eroded from the upper beach is transported directly offshore where it is deposited, such that the volume eroded is equal to the volume deposited; and (3) the rise in the nearshore bottom as a result of this deposition is equal to the rise in sea level, thereby maintaining a constant water depth in the shallow offshore. Following these assumptions, Bruun (1962) derived a relationship for the shoreline retreat rate, R, due to an increase in sea level, S; a simplified version of the relationship is

$$R = \frac{1}{tan\theta} S \qquad\qquad (9\text{-}1)$$

where $tan\theta$ is the average slope over which the beach migrates landward, generally taken to include the backshore, the beach itself, and the shallow offshore where the eroded sediment is assumed to accumulate. The ratio $1/tan\theta$ in effect represents an "amplification factor" between R and S, used to estimate the order-of-magnitude shoreline recession that results from a rise in sea level. In that $tan\theta \approx 0.01$ to 0.02 is the range of average slopes for many coastal sites having sand beaches, this relationship yields $R = 50S$ to $100S$, commonly used as a "rule of thumb" to calculate expected shoreline retreat rates or distances R from a rise in sea level S. As an example, for the 1-metre rise in sea level that has been projected by climatologists for the 21st century, the response of coastal sand beaches would be expected to be on the order of 50 to 100 metres of shoreline retreat and property erosion.

Tests of the predictive capability of equation (9-1) derived by Bruun (1962) have included both laboratory experiments in wave channels, and field data from ocean and lake shores (Komar et al., 1991; Komar, 1998), generally having compared the calculated erosion rates to the measured values of shoreline changes derived from aerial photos or repeated beach surveys. Some studies concluded that the Bruun equation yields highly inaccurate predictions; however, those investigations often failed to account for the effects of the sediment budget,

that its negative balance had been the primary cause of the measured erosion, in some cases with jetties or other structures being responsible, only a small portion of the measured erosion having been due to the rise in sea level. When the field studies adequately accounted for the site's sediment budget, reasonable agreement was found between the measured rates of shoreline retreat and those calculated with the Bruun equation, although there continues to be complicating factors such as time delays between the shoreline retreat and the rising elevations of the water levels, the retreat of the beach also being dependent on occurrences of storms and their waves, required to erode the upper beach and carry the sand into the offshore. This simple geometry-based model of Bruun (1962) can be expected to at least provide an order-of-magnitude estimate of the shoreline retreat from a rise in sea level, although its tests have made it evident that the gains or losses of sand and gravel in the budget of sediments must be accounted for if future projections of shoreline erosion and coastal retreat are to be meaningful.
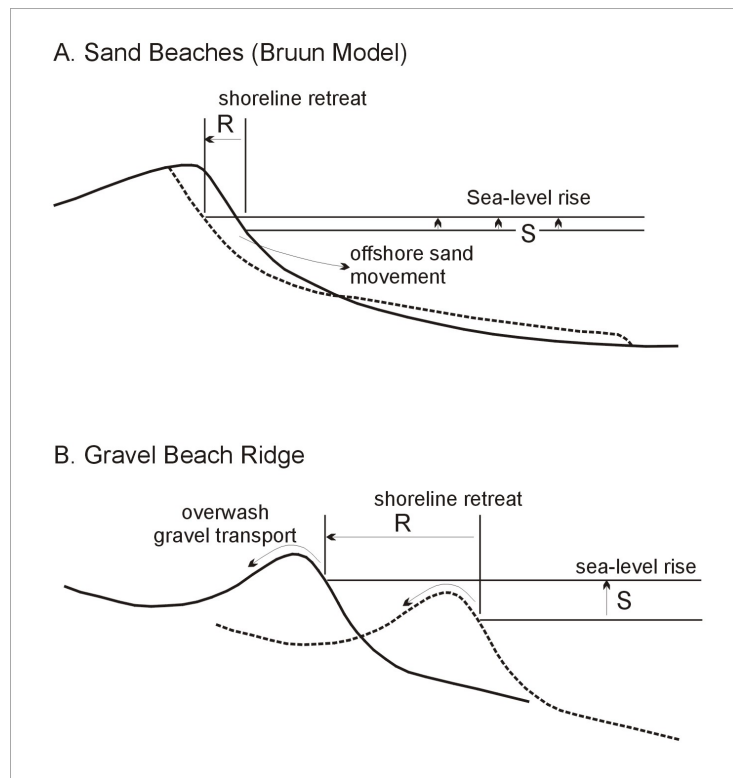
Figure 9-2: A. The model of Bruun (1962) for the retreat of a sand beach due to a rise in sea level, involving the erosion of the beach face and transport of sediment to the offshore where it is deposited; B. The landward migration of a gravel beach ridge in response to a rise in sea level, the gravel being carried landward by overwash events, with the ridge migrating up the regional slope. [*From* Komar (2005)]

While Bruun's (1962) model for sand beaches, involving the erosion of the beach face and the offshore transport of the sand, could in some instances apply to coarse-grained gravel beaches, it was found in the investigations by Orford and Carter (1982) that the more common response of gravel barrier ridges is their inland migration due to overtopping and

overwash events during storms. This response to a rise in sea levels is depicted in Figure 9-2B, serving as the basis for a similar derivation of a geometric model, with the gravel ridge migrating up a regional slope, produced by the landward transport of the gravel during storm events. This diagram is simplified in showing the ridge migration accomplished by gravel being carried landward during mild overtopping events, raising the elevation of the crest at the same rate as the rise in sea level, the ridge migrating landward at a rate that maintains this balance between the crest elevation and the rise in sea level. However, this depiction does not preclude the possibility of there being episodic occurrences of stronger overwash events during major storms, when much of the landward transport of gravel actually occurs. As diagramed, the model in Figure 2B recognizes that there may episodic occurrences of overwash that cut down the elevation of the ridge crest, but followed by decades of reformation of the ridge when this quasi-equilibrium between the crest elevation and level of the sea is restored. Although the responses of sand beaches and gravel barrier ridges are fundamentally different, represented respectively by the pair of diagrams in Figure 9-2, the underlying geometry turns out to be essentially the same, with the model derivation for the gravel ridge migration again yielding equation (9-1), indicating that this simple relationship might also be applied to obtain order-of-magnitude assessments of the rates or distances of inland retreat of gravel barrier ridges in response to a rise in sea level (Komar, 2005). However, in this application to gravel-ridge migration $tan\theta$ represents the regional slope over which the barrier ridge migrates, differing from the Bruun (1962) model developed for sand beaches where this slope is the nearshore zone of active beach migration.

A tentative order-of-magnitude test of this model applied to the migration of barrier gravel-beach ridges is possible using the field data collected by Orford et al. (1991, 1995), their measured rates of ridge migration versus the local rates of increasing relative sea levels. Of interest again are the magnitudes of the "amplification" coefficient between R and S, but also the corresponding values of $tan\theta$ that should approximately correspond to the regional slope over which the gravel ridges have migrated. As such, it would be expected that the $tan\theta$ slopes found here would be much lower than those for Bruun's (1962) application to sand beaches, given the differences in the geomorphology involved in these respective applications. For Sillon de Taibert and Westward Ho! the results of the ridge-migration analysis based on the Orford et al. (1995) data respectively yield 320 and 230 metres of ridge migration for each metre rise in sea levels, in turn yielding $tan\theta = 0.0031$ and 0.0043 for their respective regional slopes. In contrast, the smaller barrier ridge at Story Head in Nova Scotia yields an amplification factor of 840 and $tan\theta = 0.0012$, the former being much higher while the model implies that this results from its migration across a lower regional slope. Values for the actual regional slopes for these three sites were not reported by Orford et al. (1995), so the analysis here cannot represent an actual test of the model derivation, although the magnitudes of the calculated slopes appear to be reasonable for a coastal margin.

It is of interest that the $tan\theta$ regional slopes for barrier ridge migrations are much lower than the slopes in applications of the Bruun (1962) model for the erosional retreat of sand beaches, the result being that the amplification factors for gravel ridges are systematically much greater than those for the erosion of sand beaches, evident in the original measurements by Orford et al. (1991, 1995). The implication is that if both models are basically correct, then for a given rise in sea level, say 1 metre by the end of the 21st century, the erosional migration of barrier gravel ridges would be significantly greater than sand beaches, that is if the ridges are able to maintain their existence under such high rates of

migration. An important question is therefore whether the gravel ridges would be able to remain stable and conform with this model of rapid retreat in response to rising sea levels. The lower the regional slope and the faster the required migration, the more likely the ridge would be unable to maintain a semblance of stability, with it potentially instead ceasing to exist as a barrier that provides protection to inland properties. The consequences of this migration on the morphology of a barrier ridge have been considered by Orford et al. (1996) based on their field observations, noting that if the ridge has a fixed volume of gravel in its cross-shore profile, its width would have to decrease in order for it to maintain its crest elevation while crossing a nearly horizontal inland region as the ocean rises. This narrowing would likely lead to a steeper landward slope and an asymmetrical profile, with the ocean beach maintaining its slope depending on the gravel sizes. The lower the regional slope, the greater the demanded modifications in the cross-shore profile, and the faster the required rollover to meet the necessary high rate of migration. Under such circumstances, the increased demands would likely lead to the catastrophic failure of the ridge as an agent providing protection to inland coastal properties.

There are obvious over simplifications and omissions of factors in this model for barrier gravel-ridge migration in response to rising sea levels, some of which have the possibility of mitigating the trend toward failure, but equally possible they could exacerbate the conditions leading to an earlier loss of the gravel ridge and its protection to properties. Most important again is the sediment budget, discussed above in the context of applications of the Bruun (1962) model to the erosion of sand beaches. It is apparent that if there are significant sources of gravel being added to the barrier beach ridge, yielding a positive balance in its sediment budget, it could have the capacity to survive even a 1-metre rise in sea level within 100 years. But a negative balance in its budget would of course hasten its demise, within years or decades leading to the loss of its protection to inland properties. Sediment budgets and other complicating factors need to be evaluated in applications; applying only the Bruun model or that for gravel-ridge migration to account for the consequences of rising sea levels, would generally be insufficient.

While the simplicity of these geometric models permits relatively direct calculations in applications to assess coastal recession rates in response to a rise in sea level, they can be expected to generally provide only approximate estimates, even when having accounted for sediment budgets and other factors. Furthermore, their applications ignore the details of the processes that actually bring about the erosion and migration of the shoreline, those associated with episodic extreme storm events. More detailed analyses that include the processes are possible in applications of the Ruggiero et al. (2001) model that evaluates the total water levels ($TWLs$) at the shore, the summation of the measured tidal elevations, enhanced by a storm surge or other processes, plus the swash runup of waves on the beach, this combination being depicted here in Figure 9-3 (*Upper*). This model saw application in Chapter 7 where $TWLs$ were calculated from the Port's tide gauge and wave buoy, with their extremes in elevations having been compared with the surveyed elevations of the Hawke's Bay beaches, most important being the beach/backshore junction elevations where the ridge had been uplifted during the 1931 Hawke's Bay earthquake, but also of interest being the crest elevations of the gravel ridges at sites where overtopping occurs during storms. Later in this chapter the model will again be applied to analyze future erosion within the Hawke's Bay littoral cells, accomplished by adding the projected increases in sea levels to determine the elevated total water levels through the 21st century, and also accounting for potential

increases in swash runup levels on the beaches due to greater storm intensities and their higher generated wave heights.
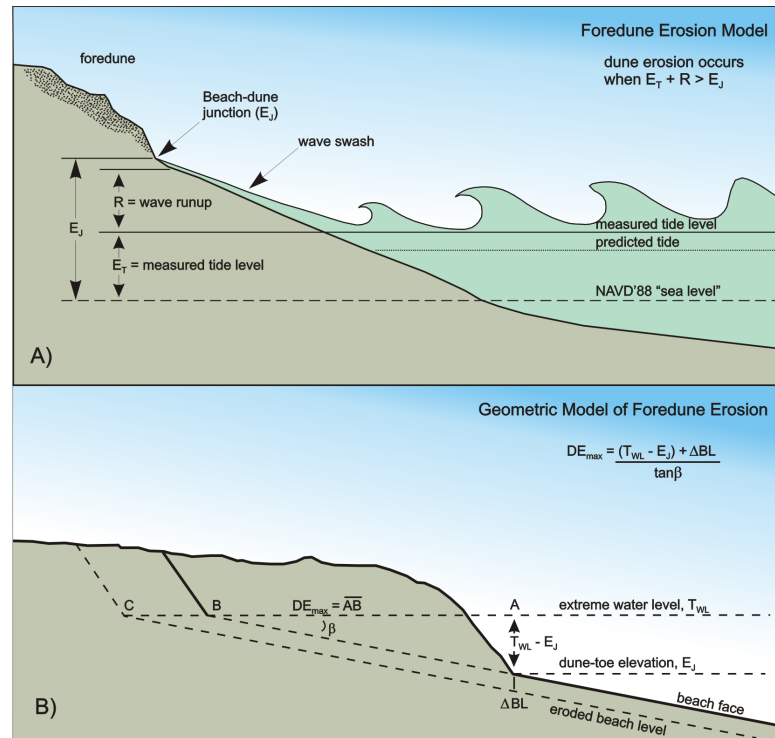
Figure 9-3: (*Upper*) The model of Ruggiero et al. (2001) to calculate the total water levels on a beach as the sum of its hourly measured tides and wave swash runup, which is then compared with the elevation of the toe of a foredune or sea cliff. (*Lower*) The geometric model of Komar et al. (2002) applied to project the maximum extent of potential dune erosion, depending on the total water level.

Having calculated the future $TWLs$ by applying the Ruggiero et al. (2001) model, the next step in the hazard assessments for Hawke's Bay involves an analysis of the resulting extent of the erosional retreat of its gravel beaches and backshore properties. This assessment involves a model we have employed in our applications to the coast of the U.S. Pacific Northwest, for calculations of the erosion during episodic storms of foredunes backing the beaches. This model is shown schematically in Figure 9-3 (*Lower*), it again being geometric with similarities to Bruun's (1962) beach erosion model, the difference being that the measured tides plus the wave swash runup levels are the erosion processes, although multidecadal increases in sea levels and swash runup can be included. As illustrated in the diagram, the erosion of the dune (or gravel ridge) is modeled by the projection of the beach slope up to the elevation reached by the $TWLs$ during major storms (Komar et al., 2002). The result is expected to be an assessment of the potential maximum erosion during the storm, a maximum in that the model does not account for a significant delay in the progress of the erosion. This has been acceptable in most management applications on the U.S. Pacific Northwest coast, since the result is a conservative hazard zone, inherently providing a worst-case margin of safety for homes constructed in vulnerable foredunes. There has been some field verification of the magnitudes of dune erosion derived from this model, through comparisons with episodes of dune erosion experienced along the Oregon coast (Komar et al., 2013). While models are also

available for estimating the erosional retreat of sea cliffs, based on the annual frequencies of wave impacts on the toe of the cliff, that application requires assessments of the resistance of the cliff depending on the compositions of its rocks and the presence of weaknesses such as joints and faults.

Application to an assessment the erosional retreat of a back-shore gravel ridge, as found along the shores of the Bay View and Haumoana Littoral Cells, is conceptually similar to a foredune composed of sand, but with its retreat expected to follow a longer-term course of geometric projections. The extent of retreat of the gravel ridges during individual storms would of course be expected to lag significantly behind the erosion processes, but in the application to Hawke's Bay of interest is the long-term, progressive erosional retreat in response to the slow rise in sea level, during which there would be countless storms over the decades; in that case, it is expected that there would be a minimal degree of lag for the largely unconsolidated gravel-ridge deposits along that shore, in view of the century-long time frames being considered.

9.3 ENHANCED HAZARDS DURING THE 21st CENTURY

The objective of this study has been to analyze the potential future erosion and flooding along the Hawke's Bay coast, enhanced by global warming. This has required examinations of the ocean processes that are responsible for those property impacts, including the degrees to which the changing climate could strengthen those processes. The goal here is to bring together the results of those analyses completed in earlier chapters, of the tides, waves, and increasing sea levels, achieving the goal of this study by providing assessments of the hazards and potential property losses during the 21st century.

Our examinations of the Hawke Bay ocean processes began in Chapter 4 with analyses of the tides that have been measured hourly by the Port of Napier's gauge, the primary interest to erosion and flooding having been their extreme elevations when the predicted levels were increased by storm surges or other processes. Chapter 5 focused on the wave climate of Hawke Bay, with the analyses having been directed toward the wave heights, periods and directions measured by the Port's buoy since August 2000. The chief product of that analysis was a deep-water wave climate that defined the present-day ranges of significant wave heights and periods, but with the analyses also having yielded evidence for there being a trend of progressively increasing wave heights, introducing the possibility of this being a factor in causing the enhanced erosion and flooding along the Hawke's Bay coast during this century.

Chapters 6 and 7 included analyses that transformed the deep-water waves into the processes that operate on the Hawke's Bay beaches, those that are directly responsible for the erosion and flooding of coastal properties. This involved calculations of the wave breaker heights and swash runup levels at the shore, both being dependent on the deep-water wave climate but affected by refraction and shoaling transformations as the waves traveled from deep water to the beaches. Important was the summation of the measured tides and wave runup levels, yielding the total water levels at the shore that were then compared with the elevations of the beaches and backshore properties, yielding correlations between the morphologic evidence of past erosion and flooding events with the extremes in the causative ocean processes. In Chapter 8 we analyzed the present-day rate of rise in sea level on this

coast based on the Port's tide-gauge record, and projected its accelerated rates and elevations through the 21st century based on analyses by climatologists, its increase expected to have the dominant role in determining this coast's future hazards.

Remaining to be accomplished here is to combine the projected rising sea levels with the measured tides and wave swash runup levels, providing assessments of future total water levels at the shore that would result in greater impacts to coastal properties than experienced in the past. Considerations also have to be given to the possibility that changes in the climate will continue to produce increasing storm intensities and the heights of their generated waves, such that superimposed atop the rising sea will be still higher runup levels and swash intensities during major storms, it being this combination that produces the most extreme erosion and flooding occurrences. As reviewed earlier in this chapter, the expected impacts to the Bay View and Haumoana Littoral Cells include higher rates of erosion of the barrier gravel ridges that had been uplifted during the 1931 Hawke's Bay earthquake, with the waves cutting escarpments into the ridges at the backs of the beaches. Of concern is whether the elevations of the barrier ridges will be sufficient to protect homes that have been constructed atop those ridges, preventing overwash events that could flood low-lying inland properties during the potentially most extreme storm events. These concerns are greatest along the southern shore of the Haumoana Littoral Cell, with portions of it having subsided by up to 1 metre during the 1931 earthquake. In view of its low elevations and having a sediment budget that is well into the red, its properties are already experiencing significant hazards so the expectation is that this fragile shore could face inundated by future rising sea levels and intensified storms.

Based on recent research by climatologists, it is accepted that the rates of rising sea levels will accelerate during the next 100 years in response to global warming, but the total increase by the year 2100 remains uncertain, although the consensus of their analyses is that it could be on the order of 1 metre, possibly even greater. That projected global increase will of course occur along the coast of Hawke's Bay, although with some modification due to its changing land elevations (likely increasing the relative change in sea level, due to the subsidence of this shore). In addition, while there is evidence from satellite data and the Port's wave buoy measurements that a trend of increasing wave heights has been occurring along this coast, we are less certain that this region's storms will continue to intensify and generate still higher waves during this century, and if they do what will be of the rates of increase and the resulting swash runup levels on the Hawke's Bay beaches. In light of these respective levels of uncertainty in the analyses presented here, the initial consideration will include only the projected rise in sea levels along this coast, it being assumed in this initial stage of the analyses that the wave climate remains essentially the same as at present. A subsequent analysis will then include a potential increase in wave heights and their swash runup levels on the Hawke's Bay beaches, elevating still further the future total water levels and their resulting impacts. Having derived projections of these processes and their resulting enhanced degrees of erosion and flooding, consideration will then be directed toward the potentially altered sediment budgets for the Bay View and Haumoana Littoral Cells, their modifications representing a feedback response to the increased erosion caused by the rising sea levels and swash runup, wherein some changes in the sediment budget could be expected to moderate the degrees of erosion impacts, while others could locally cause them to be still greater.

The analyses completed in Chapter 7 were based on the present-day wave climate and measured tides, yielding the range of total water levels (TWLs) and their extremes, which were then compared with the surveyed beach profiles; the mean level of the sea was held constant. The extended analyses here include the projected rise in sea level by the end of this century, its analysis in Chapter 8 having yielded a net increase of 0.9 metre by the year 2100 for the Average projection, and 1.3 metre for the High projection derived by climatologists. In the analyses presented here an increase of 1.1 metre has been adopted for future assessments of the TWLs, the result being that the Hawke Bay mean sea level would be raised from its present-day elevation of 10.0 metres RL to 11.1 metres RL. As noted above, the initial assumption is that the deep-water wave climate and calculated swash runup levels will not change during this century; a trend of increase will be added later. With a progressive rise in the sea level spanning this century, the magnitudes of the TWLs analyzed in Chapter 7 for the present-day conditions simply shift upward to higher elevations, occurring at a slow rate but experiencing a total displacement of 1.1 metre by the year 2100. The effects of this extent of sea-level rise relative to the beach and property elevations can be envisioned in Figures 7-7 and 7-8, respectively for the Bay View and Haumoana Littoral Cells, simply by raising the TWL lines in those graphs by 1.1 metre. As expected, the most dramatic consequence would be experienced on the low-elevation profile of survey site HB06 on the shore of South Haumoana, the rise in the Max TWL line relative to the crest elevation of the beach ridge in Figure 7-8 clearly expected to produce more frequent and intense overwash events than occur at present, likely resulting in a landward migration of the barrier ridge by 10s of metres. For the survey sites having higher backshore elevations (e.g., the Bay View Littoral Cell), with a fronting beach having the typical slope of 0.1 (1-in-10) applications of the geometric model (Figure 9-3) to evaluate the extent of erosional retreat of the wave-eroded escarpment (the beach/backshore junction) predict property losses on the order of 10 metres, significant but not catastrophic so long as homes had been constructed well back from the active beach.

This predicted 10-metre erosional retreat of the Hawke's Bay beach ridges produced solely by rising sea levels should be viewed as a minimum estimate for the potential future impacts, since the probability remains that there will be additional losses due to increasing wave heights and swash runup levels. As reviewed in Chapter 2, there is evidence from wave-buoy data and more recently from satellites that storm-generated wave heights have been increasing over much of the world's oceans, although the rates of increase are not well established since those records of data collection are typically short, at maximum being on the order of 25 years. This problem of having only limited wave records is also true for Hawke's Bay, with hourly measurements having been collected by the Port's buoy only since the year 2000, while satellite measurements analyzed by Young et al. (2011) include the 23 years from 1985 though 2008. According to our analyses of the Port's wave record (Figure 5-11), the 13-year annual average deep-water significant wave heights show a trend of increase at a rate of about 0.008 m/year, which if maintained until 2100 would amount to an increase of about 0.7 metre for the annual average. According to the analyses by Young et al. (2011) of the satellite data, the trend of change in the 99th-percentile significant wave height shows a net increase on the order of 1% per year over most of the South Pacific, including along the eastern shore of New Zealand. If that result is applied to Hawke's Bay, the rate would be an increase of 0.0176 m/year, amounting to an increase of 1.6-metres by the end of this century, roughly double that based on the Port's buoy data. Both results are uncertain due to their short records, and at least another 1 or 2 decades of data collection would be required before more confident results are forthcoming, defining the trends of increasing wave heights.

In addition to this uncertainty in the rate of increase of the deep-water wave heights, as seen in Chapter 6 there are also problems in calculating swash runup levels on the Hawke's Bay beaches from the deep-water wave parameters, the analysis not having yielded a definite trend of increasing runup in spite of the increase in wave heights. This result was attributed to the formula used in the calculations, it having a reduced dependence on the wave heights, more important being the wave periods that show only a small range of variations. In spite of that analysis having been inconclusive, there is the distinct possibility that there will be an increase in the Hawke's Bay wave heights (and periods) during this century, producing higher swash runup levels by the year 2100, superimposed atop the rising sea levels already considered. Accordingly, order-of-magnitude estimates have been made, assuming that there will be a 10% trend of increasing wave swash runup levels, a rate that approximately corresponds to the increase in the wave heights measured by the Port's buoy, and confirmed by the satellite data. This could actually be a rather modest projection, in that for example an analysis of swash runup levels on beaches along the U.S. Pacific Northwest, based on its well documented increasing wave heights, concluded that the TWL increase due to the wave runup would actually exceed the rate of rise in the relative sea levels along that coast, expected therefore to have a significant role in future impacts to that coast (Ruggiero, 2013).

One additional complication is that while the rates and magnitudes of sea-level rise are expected to be essentially uniform along the shores of the Bay View and Haumoana Littoral Cells, the magnitudes of the increased swash runup will depend on the site, varying due to the extent of refraction and transformation of the waves from deep water to the shore, the significance of this variation having been shown in Chapter 6.

The results of the analyses that combine rising sea levels and increasing wave heights are given in Table 9-2 for the Bay View Littoral Cell (profile sites HB17 and HB20) and the Haumoana Cell (HB06 and HB10), the same survey sites that were analyzed for the present-day conditions in Chapter 7. For each cell comparisons are made between 2010 and 2100, the changes in mean sea-level elevations (SL), the swash runup (SRU) representing the levels of the highest combinations of tides and wave swash, and the resulting total water levels (TWL) that are the summation of the sea-level elevation SL and SRU for the waves and tides. It is seen for both cells that the difference in SL between 2010 and 2100 amounts to a water-level increase of 1.1 metre, their elevations being relative to the RL datum. The TWLs listed for 2010 are those determined in Chapter 7 based on applications of the Ruggiero et al. (2001) model, which computes the hourly water levels as the summation of the measured tides and swash runup computed from the measured deep-water wave heights. The values listed in Table 9-2 are those for the maximum total water levels (MAX-TWLs) for each of the profile survey sites, based on the frequency distributions in Figure 7-5 that accounted for the degrees of wave refraction experienced by those profile sites.

The SRU values listed in Table 9-2 for the present-day (2010) are based on the MAX-TWL values determined from the wave and tide measurements, having subtracted the 10.0-metre RL value of the mean sea level that is now separately accounted for in the SL column. As discussed above, the determination of the increased SRU values for the end of this century are the most uncertain component in this analysis in that it represents the potential increase in the deep-water wave heights and the resulting increases in computed wave swash runup levels. There is an additional unknown, the possible increase in the extreme storm-surge

magnitudes, which could also raise elevations of the measured tides still further than occur at present. With both the increases in deep-water wave heights and surge magnitudes being dependent on future storm intensities, the 2100 magnitudes listed in Table 9-2 for SRU represent a combined 10% increase, which is carried over into the 2100 values for the MAX TWLs that also include the 1.1-metre increase in mean sea level.

Table 9-2: Analyses of sea levels (SL), wave swash runup (SRU), total water levels (TWLs) based on wave and tide measurements, and an Extreme Scenario for the worst-case storm event.

Year	Sea Level (SL) (metres RL)	Swash Runup (SRU) (metres)	Max- TWL (SL + TWL)	Extreme Scenario TWL (metres RL)
BAY VIEW LITTORAL CELL (HB 17 and HB 20)				
2010	10.0	5.1	15	18
2100	11.1	6.0	17	19
HAUMOANA LITTORAL CELL (HB06 and HB10)				
2010	10.0	3.5	13.5	16
2100	11.1	4.0	15	17

The results of this analysis are graphed in Figures 9-7 and 9-8, respectively comparing the water levels with the beach profiles within the Bay View and Haumoana Littoral Cells, representing the future projections of the present-day conditions that were analyzed in Chapter 7. The 1.1-metre increase in the sea level is reflected in the pair of graphed Mean Sea Level (2010) and (2100) lines, while the increases in the total water levels MAX-TWL from 2010 and 2100 are seen to show greater differences since they include estimates of the increased wave heights and swash runup levels on the beaches.

Having experienced some 2-metres of uplift during the 1931 Hawke's Bay earthquake, the elevations of the barrier ridge crests within the Bay View Cell range from about 18 metres RL at HB17 to 20 metres further to the north at HB20. Based on the MAX-TWL = 17-metre RL projected 2100 level for this cell's beach profiles, graphed in Figure 9-7, the extent of overwash and flooding during storms would continue to be rare to absent, but with the erosional losses of the ocean-front portions of the properties expected to be on the order to 15 to 20 metres according to the geometric erosion model (Figure 9-3). In terms of increased hazards, the change is again most dramatic in the Haumoana Littoral Cell, Figure 9-8, where the projected MAX-TWL = 15 metres RL would completely overtop the beach ridge at profile site HB06, exceeding it by an estimated 1.5 metres, an expected result in that even now this is susceptible to periodic overflow occurrences during storms. Based on the field observations of Orford et al. (1995, 1996) of present-day major overwash events, and in view of the low elevations inland from the HB06 profile site, it is doubtful whether this stretch of the gravel barrier ridge within the Haumoana Cell would remain stable and continue to protect the inland properties and infrastructure. In contrast, with the higher elevations of the uplifted ridge at profile site HB10 on the Napier shore, the analysis results graphed in Figure 9-8 indicate that ridge flooding would extend inland some 30 metres from the present-day beach/backshore junction position, this potentially also approximately being the extent of

erosion loss according to the geometric model, a degree of impact that is comparable to that in the Bay View Cell.
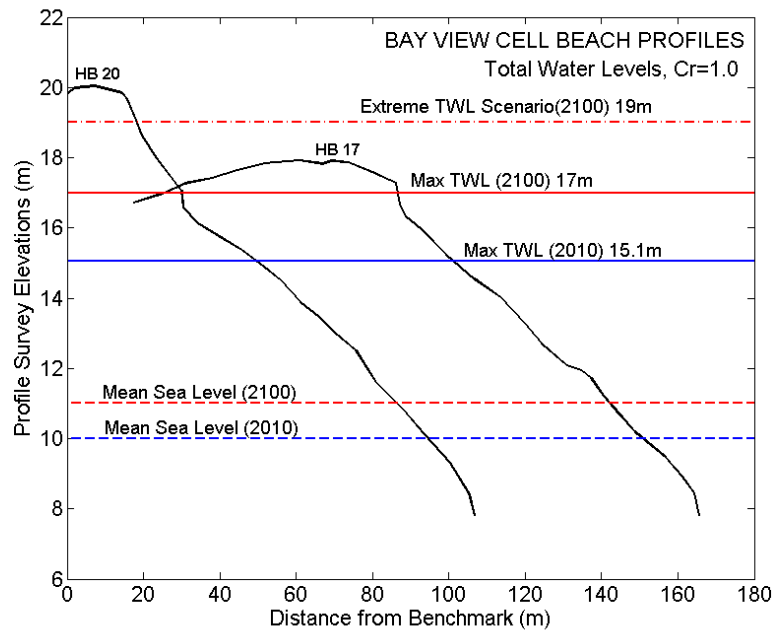
Figure 9-7: Analysis results of $TWLs$ in the Bay View Littoral Cell, contrasting the present-day (2010 in blue) and the end of century (2100 in red) mean sea levels and maximum water levels produced by a 1.1-metre rise in sea level and an increase in wave swash runup levels. Also shown is an Extreme Scenario TWL that attempts to assess the occurrence of a future major storm that produces extremes in both the surge and wave runup levels.
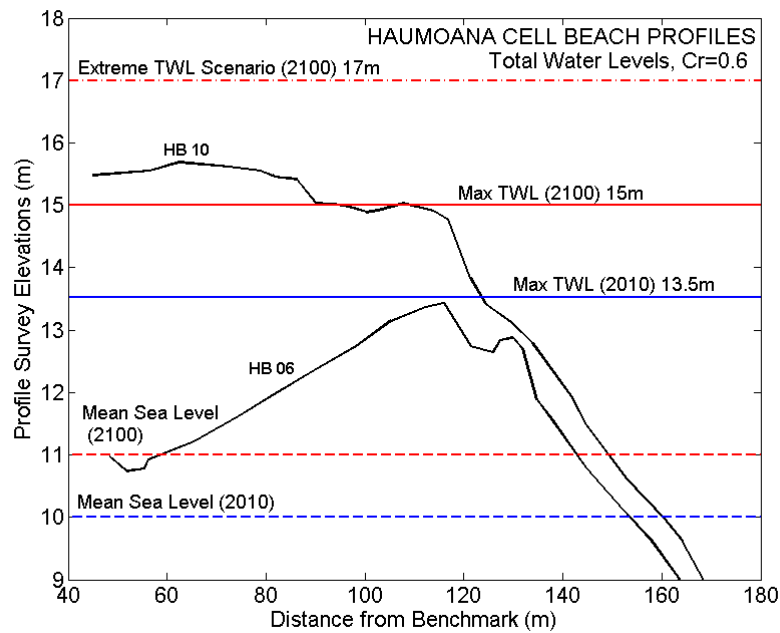
Figure 9-8: Analysis for the year 2100 water levels due to rising sea levels and storm wave runup, compared with the existing morphologies of beach profiles within the Haumoana Littoral Cell.

9 - 15

As discussed in Chapter 7 in the context of analyses of the present-day erosion and flooding hazards, with the total records of the waves and tides for Hawke's Bay being little more than a decade in length, the evaluated maximum TWLs based on their distributions are undoubtedly too low to fully represent the most extreme rare storm events that have only a 1% probability of occurrence (the "100-year event"). This is also true here for the future projections graphed in Figures 9-7 and 9-8, the MAX-TWL magnitudes based on actual measurements of the waves and tides but now including estimates of future increases in sea levels and wave heights. In view of this likely under prediction of the future extreme water levels and potential hazards, as presented in Chapter 7 it is relevant to develop a "scenario" for the conditions representing the extremes of measured tides that have been enhanced by storm surges, together with extremes in swash runup levels, representing the rare but most severe storm event that potentially could impact the Hawke's Bay coast. With this scenario representing combinations of processes and their respective extremes, it is not possible to precisely assess the probability of such an event; it might approximate the 100-year storm occurrence, but it is more likely that the combination represents a still more extreme event, in that it combines the processes of a 100-year storm with a Spring tide. However, of interest in having developed this scenario is that although it represents a rare event, its occurrence is still possible, posing the potentially greatest dangers from erosion and flooding to developments and infrastructure along the coast of Hawke's Bay.

The pair of extreme scenarios in Chapter 7 were developed to be representative of Exposed Shores and Sheltered Shores within Hawke's Bay, depending on the site's degree of exposure to the waves arriving from deep water, affected by the extent of refraction and energy dissipation. Based on the magnitudes projected from the distributions of measured tides and swash runup levels, the estimated potential extreme TWLs obtained in Chapter 7 were 18 metres RL and 14 metres RL (Table 7-2), respectively for the most exposed and sheltered shores. The values used in the present analyses for the actual profile sites in the littoral cells are listed in Table 9-2, given as the MAX-TWL magnitudes in the last column for the Extreme Scenarios. The 18-metre value derived for Exposed Shores is accepted here as being the present-day (2010) water level for both the HB17 and HB20 profile sites within the Bay View Littoral Cell, in that the orientation of this shore faces directly into the dominant waves arriving from the southeast, and the profile sites are not sheltered by the cell's bounding headlands. For the end of the 21st century (2100) the extreme water level has been increased to 19 metres RL, accounting for the rise in sea level but not having included an increase in the storm intensities since these scenarios for surges and wave runup already exceed the 100-year projection, the time frame of this analysis. For the profile sites within the Haumoana Littoral Cell, the Extreme Scenario is taken to be 16 metres RL, lower than that in the Bay View Cell since this shore is oriented obliquely to the direction of the dominant waves so that more refraction and dissipation occurs, although being well north of the sheltering effects of Cape Kidnappers they do not qualifying for the fully Sheltered Shore scenario with a lower 14-metre projected extreme water level. For the end of the century, the level is again increased to account for the rise in sea level, the total water level being 17 metres RL.

These 19-metre and 17-metre extreme water levels respectively for the Bay View and Haumoana Littoral Cells by the end of the century are graphed in Figures 9-7 and 9-8, being compared with the surveyed beach profiles. According to the intent of these projections, this comparison amounts to the potentially most catastrophic storm event that could generate

both extreme surge levels and swash runup from waves, superimposed on the 1.1-metre rise in sea level by the year 2100. Within the Bay View Cell (Figure 9-7), profile HB17 midway along its shore would be expected to experience some degree of ridge overtopping and flooding, at present and increasing during this century due to the rising sea level, accompanied by extensive erosion of the seaward portions of the properties. With a ridge elevation of 20 metres, profile HB20 toward the northern end of the cell's shoreline would not be overtopped by the surge and waves even during such an extreme event, but the erosional retreat of the properties could amount to on the order of 25 to 50 metres, depending on the duration of the storm. Within the Haumoana Cell (Figure 9-8), the lower elevations of the crests of both the HB06 and HB20 ridges (13.5 and 15.5 metres RL) would be overtopped by the 16 to 17 metre projections of this Extreme Scenario storm, but most catastrophic would be the impacts to the low-elevation ridge of profile HB06. According to the field studies of the responses of barrier gravel ridges to major storms (Carter and Orford, 1993; Orford et al., 1991, 1995), reviewed earlier, such an extreme overwash event would generate a high-velocity flow of water that could be expected cut away the HB06 ridge crest, almost certainly leading to its breaching and the extensive flooding of inland areas.

9.4 COASTAL RESPONSES AND CHANGES IN SEDIMENT BUDGETS

The previous section provided assessments of the potential increased rates of erosion and flooding expected during the 21st century along the barrier gravel ridges of the Bay View and Haumoana Littoral Cells, projected from increasing sea levels and greater storm intensities. There is, however, an additional aspect in these hazard assessments that needs to be considered, one that is difficult to evaluate and is largely speculative — the resulting changes in the sediment budgets for these littoral cells, most obvious being that the enhanced erosion of the gravel ridges will provide additional credits in their sediment budgets. It is therefore possible that the erosion of the gravel ridges will have a positive consequence in supplying sufficient volumes of gravel to the beaches that they have an increased capacity to provide buffer protection to the backshore properties; this would thereby represent a feed-back mechanism, reducing the projected property losses derived above, based only on considerations of the impacts of rising sea levels and storm-wave runup.

An estimate of the possible changes in the sediment budget for the Haumoana Littoral Cell is presented in Table 9-3. The left column of values for the credits and debits represents the present-day budget (2010), considered in Chapter 1. Although the volumes of sediment gains and losses are uncertain, these 2010 estimates are at least based on direct observations and measurements, including assessments of contributions by the rivers and surveys of beach profiles over the years that permitted direct calculations of the net balance in the budget. In contrast, the sediment volumes given in the column for the end of this century (2100) are speculative, in some cases representing "guesstimates", the interest however being the directions of change in the net balances, not necessarily their actual magnitudes. For example, in the case of the sediment supplied by the Tukituki River, whereas the present rate is assessed to be about 28,000 m^3/year (Tonkin and Taylor, 2005), the projection for the future (2100) is that it could be reduced to effectively zero, the rationale being that with a rise in sea level of about 1 metre, the lower reaches of the river's channel and estuary might "flood out", deepened to the extent that gravel derived from the inland mountains will be trapped within the river, unable to reach the ocean beaches. There is the

possibility that some sediment would still reach the ocean, particularly the sand component transported by the river, but there is the equal possibility that flood tides will carry greater amounts of sand and gravel from the ocean beach into the estuary, in which case there would be a net loss in the beach sediment budget by the end of this century. While this is highly speculative, with no attempt to estimate the volumes of future gravel exchanges between the Tukituki River and the ocean beaches, the processes themselves suggest an expected reduction in this river being an important source of gravel to the Haumoana Cell's sediment budget, a consequence of rising sea levels.

The other volume estimates in Table 9-3 for the 2100 sediment budget are similarly approximate, the increase in the gravel yield from Cape Kidnappers reflecting its expected increase in erosion due to rising sea levels and greater storm intensities, but with those processes also producing an increase in the debit associated with gravel abrasion. The 10,000-m^3/year credit for the erosion of the gravel ridge along this cell's backshore is based on the extent of retreat assessed in the above model analyses, and the approximate average relief (elevations) of those eroded areas. However, there are again high uncertainties in these estimates, including there being a probable increased loss of beach gravel due to overwash events carrying it inland, its volumes being difficult to predict but expected to be comparatively small compared with the volumes eroded from the ridges and added to the fronting beach.

Table 9-3: An estimate of changes in the Sediment Budget for the Haumoana Littoral Cell during the 21st century, comparing those in 2010 and 2100.

Budget Components	Estimated Annual Rates (m^3/year)	
	2010	2100
Sources ("Credits")		
Tukituki River	28,000	0
Cape Kidnappers Erosion	18,000	25,000
Gravel Ridge Erosion	0	10,000
Total	46,000	35,000
Losses ("Debits")		
Awatoto Extraction	-47,800	0
Pacific Beach Extraction	-12,800	0
Gravel Abrasion	-30,400	-35,000
Total	-91,000	-35,000
Net Balance of Beach Sediments	-45,000	0

Considering the "guestimate" nature of these future projected credits and debits in the 2100 budget, the reality is that the net balance of 0 could be either somewhat in the red or in the black, but in either case the balance would be a considerable improvement in the present-day balance of -45,000 m^3/year that is significantly in the red. But this improved balance for the Haumoana Cell is almost entirely a result of the presumed cessation of the commercial beach-sediment mining operation at Awatoto, which over the decades has annually removed an average of 47,800 m^3/year (Tonkin and Taylor, 2005). The projection in Table 9-3 also assumes the cessation of the 12,800 m^3/year sediment removal at Pacific Beach in Napier,

extracted to provide gravel and sand for the nourishment at Westshore within the Bay View Cell. If both operations were to continue into the future at the present-day rates, the budget for 2100 would have a net balance of approximately -60,600 m³/year, a substantial increase into the red beyond the present-day balance. It is apparent the cessation of these sand mining operations is imperative, such that the overall budget of sediments for the Haumoana Littoral Cell would be vastly improved, at present and in the future, enhancing the stability of the barrier gravel ridge to resist the impacts of rising sea levels and increased storm-wave energies.

As reviewed in Chapter 1 in the context of the present-day sediment budget for the Haumoana Littoral Cell, while the overall budgets as analyzed in Table 9-3 are meaningful reflections of the average health and stability of this embayed shore, the details are far more complex in that at present the primary sources of additional sediment (the Tukituki River and Cape Kidnappers) are located toward the south end of the cell's shore, resulting in a net northward longshore transport and with sediment accumulation along its northern shore. According to our speculations here as to potential changes during the 21st century due to rising sea levels, there could be a loss of that contribution from the river on the southern shore of the cell, but with that loss in part being replaced by the erosion of the barrier ridge, a contribution of gravel to the beach that however would occur mainly along the northern half of this cell's shoreline. Both of these changes would be gradual, with there expected to be a delayed response in the overall orientation of this cell's shoreline, such that the storm waves would continue to arrive primarily from the southeast, producing a northward longshore transport of what little gravel and sand continues to be contributed to the beaches at the south end of the cell. The expectation therefore is that there would then be still greater impacts from erosion and flooding of properties along the southern shore, than are already occurring at South Haumoana, Te Awanga and Clifton. With time, some of the gravel contributed to the beach by barrier ridge erosion along the cell's northern shore might be expected to be transported by waves to the south, eventually acting to partially offset the loss of the contributions by the Tukituki River.

With rising sea levels and increased storm intensities projected to possibly result in dramatic shifts in where sediments are contributed to this cell's shores, and with the resulting changes in the patterns and rates of longshore transport by the waves, the projected responses of this cell's shorelines offered above have extended beyond the capability of our speculations. One avenue to an improved resolution of these complex future changes in shorelines could come from numerical model analyses such as those undertaken by Tonkin and Taylor (2005), which had examined the impacts of beach sediment mining at Awatoto on the patterns of beach erosion versus accumulation, reviewed in Chapter 1. Meaningful quantitative results could similarly be expected in analyses of the future changes to this shore through the 21st century, replacing the speculation that has been offered here.

At present the Bay View Littoral Cell has essentially no natural sources supplying gravel and sand to its beaches, the only river reaching its shore being the Esk that supplies only small quantities of sediments (Chapter 1). In recent decades the dominant sediment source to the beach has been the annual nourishment at Westshore. The one significant debit in the sediment budget is that produced by gravel abrasion. Based on a summary of results from various investigations (Komar, 2005), a sediment budget for the gravel (excluding the sand fraction) placed the total credits in the Bay View Cell at 12,000 m³/year, with the loss to

abrasion having been estimated as -27,000 m^3/year, leaving a balance of -15,000 m^3/year, the budget being in the red but not to the same degree as the net loss at present in the Haumoana Cell. However, considering the uncertainties in evaluating these credits and debits for the Bay View Cell, it was found that the balance could range from being in the black with a net of 3,000 m^3/year, to being further into the red at about -17,000 m^3/year (Komar, 2005).

With the Bay View Cell having an 18-kilometre stretch of shore backed by an uplifted erodible gravel ridge, its erosion resulting from rising sea levels during the 21st century could significantly alter its sediment budget, possibly shifting it into the black. With this shoreline already oriented such that it faces into the dominant waves arriving from the southeast, it is in effect a pocket beach such that while there is a seasonal reversal in the longshore sediment movements, there is little if any net long-term longshore transport of the beach's gravel and sand. It would be expected, therefore, that the extent of erosion of the barrier ridge would in the long term be fairly uniform along this length of shore, maintaining its present quasi-equilibrium orientation. Taking 3 metres to be the approximate average for the height of the escarpment that would be cut into this uplifted gravel ridge, and with the 15 to 20-metre extent of erosion retreat projected earlier, the total volume of gravel added to the active beach between the present and the end of the 21st century could amount to on the order of 0.8 to 1 million cubic metres, on average representing an annual contribution of 9,000 to 12,000 m^3/year. As significant as this potential credit is to the beach, it is still well below the -27,000 m^3/year estimated debit produced by gravel abrasion. Prospects therefore are that in the absence of continued nourishment at Westshore, the sediment budget for the Bay View Littoral Cell would be in the red, that there would be insufficient feed-back reduction of the erosion and flooding as a result of the gravel being contributed to the beach by the recession of the eroding ridge along this shore.

9.6 REFERENCES

Bruun, P. (1962) Sea level rise as a cause of shore erosion: *Journal of Waterways and Harbors Division*, Amer. Soc. Civil Engrs., v. 88, p. 117-130.

Carter, R.W.G., and J.D. Orford (1993) The morphodynamics of coarse-clastic beaches and barriers: a short- and long-term perspective: Journal of Coastal Research, Special Issue 15, p. 158-179.

Komar, P. D. (1973) Computer models of delta growth due to sediment input from rivers and longshore transport: *Geological Society of America Bulletin*, v. 84, p. 2217-2226.

Komar, P.D. (1998) *Beach Processes and Sedimentation*: Prentice-Hall, Inc., Upper Saddle River, N.J., 2nd edition.

Komar, P. D. (2005) *Hawke's Bay, New Zealand: Environmental Change, Shoreline Erosion and Management Issues*: Report for the Hawke's Bay Regional Council, 244 pp.

Komar, P.D., and others (1991) The response of beaches to sea-level changes: A review of predictive models: *Journal of Coastal Research*, v. 7, n. 3, p. 895-921. [Scientific Committee on Ocean Research Working Group 89]

Komar, P.D., J.J. Marra, and J.C. Allan (2002) Coastal erosion processes and assessments of setback distances: *Proc., Solutions to Coastal Disasters Conference*, Amer. Soc. Civil Engrs., p. 808-822.

Komar, P.D., J.C. Allan and P. Ruggiero (2013) U.S. Pacific Northwest coastal hazards: tectonic and climate controls: *Coastal Hazards*, edited by C.W. Finkl, Springer, p. 587-674.

Orford, J.D., and R.W.G. Carter (1982) Crestal overtop and washover sedimentation on a fringing sandy gravel barrier coast, Carnsore Point, SE Ireland: *Journal of Sedimentary Petrology*, v. 52, p. 265-278.

Orford, J.D., R.W.G. Carter, and D.L. Forbes (1991) Gravel barrier migration and sea level rise; some observations from Story Head, Nova Scotia, Canada: *Journal of Coastal Research*, v. 7, p. 477-488.

Orford, J.D., R.W.G. Carter, J. McKenna and S.C. Jennings (1995) The relationship between the rate of mesoscale sea-level rise and the rate of retreat of swash-aligned gravel-dominated barriers: *Marine Geology*, v. 124, p. 177-186.

Orford, J.D., R.W.G. Carter, and S.C. Jennings (1996) Control domains and morphological phases in gravel-dominated coastal barriers: *Journal of Coastal Research*, v. 12, p. 589-605.

Ruggiero, P., P.D. Komar, W.G. McDougal, J.J. Marra, and R.A. Beach (2001) Wave runup, extreme water levels and the erosion of properties backing beaches: *Journal of Coastal Research*, v. 17, no. 2, p. 407-419.

Ruggiero, P. (2013) Is the intensifying wave climate of the U.S. Pacific Northwest increasing flooding and erosion risk faster that sea-level rise?: *Journal of Waterway, Port, Coastal, and Ocean Engineering*. Amer. Society of Civil Engineers, v. 139, p. 88-97.

Tonkin and Taylor (2005) *Shoreline Modelling Report*: Unpublished report to the Hawke's Bay Regional Council.

Young, I. R., S. Zieger and A.V. Babanin (2011) Global trends in wind speed and wave height: *Science*, v. 332, p. 451- 455.

10 Summary and Discussion

The objective of this study has been to undertake analyses of the Hawke's Bay ocean processes that are important to its erosion and flooding hazards — its waves, tides and changing sea levels. The concern is that the magnitudes of these processes and the resulting hazards to shorefront properties will significantly increase during the 21st century, a result of continued global warming. Such concerns are warranted in that the shores of the Bay View and Haumoana Littoral Cells are composed of mixed sand-and-gravel beaches, backed by barrier gravel ridges on which homes have been constructed, while the areas inland from the ridges have elevations that are barely above the present level of the sea. The stabilities of these protective ridges under rising sea levels and increased storm intensities are therefore of paramount importance in preventing future erosion and flooding of these shores.

Contributing to the existing effectiveness of these gravel beaches and backshore ridges as protective barriers is that most of this shore was tectonically raised by 1 to 2 metres at the time of the 1931 Hawke's Bay earthquake. Prior to that event, these ocean shores could not have been developed with homes and infrastructure, since the beaches and backshore experienced frequent overwash flooding during storms, with flooding even occasionally inundating downtown Napier. In contrast, the southern-most stretch of this shore subsided by about 1 metre at the time of the earthquake, the result being that over the decades it has experienced extensive erosion, threatening a number of homes in the communities of Haumoana, Te Awanga and Clifton.

The tectonic setting of Hawke's Bay is an extremely important factor in the natural hazards faced along its shores, foremost being the potential future occurrences of extreme though infrequent major earthquakes and accompanying tsunami, events that prehistorically had impacted this coast. Such extreme tectonic events are the consequence of the collision of two of Earth's major tectonic plates, the ocean crust colliding with and being subducted beneath the continental plate, a tectonic setting that is identical to those along the coasts of Sumatra and Japan, which provide recent examples of the hazards of subduction earthquakes and tsunami. Recent investigations by geologists and seismologists along the Hawke's Bay coast have found evidence for past occurrences of major earthquakes and tsunami, the records of those events having been preserved in sediments deposited hundreds to thousands of years ago along this coast. The sediment records demonstrate that such seismic events were accompanied by an abrupt subsidence of the Bay View and Haumoana Littoral Cells, immediately followed by major tsunami that inundated this shore. Although rare in their occurrence, the repeat of such an extreme earthquake and tsunami represents the ultimate the greatest future hazard to the Hawke's Bay coast.

In terms of this coast's present-day hazards from erosion and flooding, important is that plate subduction is causing this shore to slowly subside, combining with the global rise in the ocean's water levels to produce a "relative" trend of rising annually-averaged sea levels. This

net rise on the Hawke's Bay coast has been analyzed based on the Port of Napier's tide-gauge record, yielding a net trend of increase at a rate of about 2.0 millimetres per year, which would amount to a rise of 20 centimetres over a century; close to the 17-centimetre globally average rise in sea level during the 20th century. If that 2.0 mm/year rate were to continue for the next 100 years, model estimates are that the Hawke's Bay barrier gravel ridges could on average erode landward by about 2 metres, although in fact the local extent of erosion (or accretion) would depend on the budget of beach sediments, its net gains or losses. Projections by climatologists are, however, that with continued global warming there will be an acceleration in the rate of rising sea levels, the consensus amongst climatologists being that it will amount to a rise of about 1 metre by the end of this century. Our projection based on several studies by climatologists place the net rise in sea level for the Hawke's Bay coast at 0.9 to 1.3 metres by the year 2100, in which case the potential erosional retreat of its gravel ridges would on average amount to 10 to 15 metres. While the tectonically elevated stretches of the barrier ridges along this coast should remain reasonably stable even under that extent of rising sea levels, along the southern shore of the Haumoana Cell that had subsided, the enhanced erosion and flooding impacts would be dramatically greater due to the low elevations of its gravel ridge and with its sediment budget being "in the red"; future overwash occurrences on that shore can be expected to be frequent, resulting in significantly greater property damage than is occurring at present.

While an increase in sea levels alone would undoubtedly bring about greater erosion and flooding impacts along the shores of Hawke's Bay, still greater impacts would occur if the changing climate also produces more intense storms, which in turn generate more extreme waves and surge elevations, combining with the rising sea levels to yield still higher total water levels ($TWLs$) at the shore. There is evidence from buoys and satellites that storm-generated wave heights have been increasing over most of the world's oceans, with analyses of measurements derived from the Port of Napier's wave buoy indicating a similar trend of increase along the Hawke's Bay coast. The increased wave heights would in turn result in greater wave breaker heights and swash runup levels on its beaches, with the enhanced runup combining with the increasing sea levels to produce elevated $TWLs$ that are projected to be about 2 metres above the present-day levels on the shores of the Bay View Cell, with a 1.5-metre increase on the Haumoana Cell's shore, essentially doubling the increase contributed by the rise in sea levels acting alone.

Comparisons between these enhanced $TWLs$ projected for the end of this century and surveyed beach profiles demonstrated that the resulting erosion and flooding by overwash of the gravel ridges will become much greater than occurs at present; the resulting erosional retreat of the barrier gravel ridge along the Bay View Cell's shoreline is estimated to be about 15 to 20 metres, while within the Haumoana Cell the erosion along its northern stretch of shore would be on the order of 30 metres. Most destructive would be overwash events during major storms, with the total water levels predicted to significantly exceed the low elevations of the gravel ridges along the southern shores of the Haumoana Cell, potentially resulting in catastrophic impacts from erosion and flooding, leading to the breaching of the barrier ridge and flooding of low-lying inland properties and infrastructure.

Although the above assessments of future erosion and flooding impacts along the Hawke's Bay coast have a sound foundation by having been based on actual data for the wave heights measured by the Port's buoy, and of hourly tides and sea-level trends derived from its tide

gauge, those records of process measurements have been collected only for little more than a decade. Although they supported analyses that yielded reasonable distributions for the measured significant waves heights and tides elevated by storm surges, providing guidance as to their potential extremes during major storms, those results and the corresponding evaluated maximum TWLs are unlikely to represent the most-extreme rare storms that have only a 1% probability of occurrence (the "100-year event"). In view of those analyses having likely under predicted future water levels and hazards representing the most extreme events along this coast, our analyses also included the development of an Extreme Scenario. In its analysis the most severe storm was based on a combination of the extreme measured tide that had been elevated by a 100-year surge, together with extremes in swash runup levels from the waves generated by severe storms, the result representing a rare occurrence that is extreme in its process components but one that is still possible, posing the potentially greatest dangers from erosion and flooding. With this Scenario having combined the extremes in the storm-generated processes, the result could be expected to approximately represent a 100-year storm event, but since it also includes the simultaneous occurrence of a high predicted astronomical tide that is independent of the storm itself, the Scenario more likely represents an event having a recurrence interval that is longer than 100 years (that is, it has a still smaller probability of occurrence), possibly significantly so. It was found in the analysis that this Extreme Scenario produces TWL elevations that are some 2 metres higher than the TWLs extremes for the year 2100 based on the limited wave and tide measurements. Having this magnitude, such an extreme event would result in overwash of the barrier gravel ridges along the entire length of the Haumoana Cell's shore, and at least the southern half of the Bay View Cell's shore. Our motivation in developing this Extreme Scenario was not meant to be alarmist, its objective instead having been to provide an assessment of what might be the worst-case storm event faced on this coast, one that is extreme but is still possible, posing the potentially greatest danger from erosion and flooding to the Hawke's Bay coast — the most extreme hazard, short of the repeat occurrence of a subduction earthquake and tsunami, like those that have occurred in the distant past.

Considerations have also been directed toward potential future changes in the sediment budgets of the Haumoana and Bay View Littoral Cells, altered by the erosion of their barrier ridges that became sources of gravel to the beaches, on average enhancing their buffer protection to backshore properties. While estimates were derived for that credit in the sediment budgets based on the projected future erosional retreat of the ridges, there are other consequences that are more speculative and difficult to evaluate. For example, the rise in sea levels could act to flood the channel and estuary of the Tukituki River, diminishing and possibly cutting off entirely its supply of gravel to the coast, representing a loss of the most significant present-day credit in the Haumoana Cell's sediment budget. Based on a comparison between the existing sediment budget and what might be expected in the future with rising sea levels and more intense storms, it immediately becomes apparent that phasing out the commercial mining of beach sediments at Awatoto is absolutely necessary, the projection being that its continuation would place the net balance significantly more into the red than it is at present, hastening the potential breaching of this cell's barrier ridge. In contrast, by halting the extraction at Awatoto, the sediment budget would become nearly balanced in the future, enhancing the stability of this shore's barrier gravel ridge and its capacity to protect coastal properties.

With the possible future loss of sediment contributions by the Tukituki River to the southern shore of the Haumoana Cell, in part replaced by the erosion of the barrier ridge that would supply gravel mainly to the beach along the northern half of this embayed shore, it can be expected that there would be significant changes in the patterns of longshore transport of the beach sediments by the waves, in turn affecting the beach widths and rates of erosion of the backshore properties. With such "feed-back" responses of the coast to rising sea levels and increased storms, involving dramatic shifts in where sediments are contributed to the shore and in the patterns of their longshore transport, our assessments of the resulting changes in the erosion rates became largely speculative. It was proposed that a better understanding of those future changes along the Hawke's Bay coast could come from numerical model analyses such as those undertaken by Tonkin and Taylor that examined the impacts of beach sediment mining at Awatoto, its effects on the patterns and extent of beach erosion within the Haumoana Cell; a similar analysis directed toward the future changes that result from rising sea levels could replace the speculation we have offered in this report, such analyses providing quantitative assessments of the future changes and yielding details of the expected impacts to shore-front properties.

In conclusion, with the goal of this study having been to investigate the ocean processes and their climate controls, to assess the degrees to which they might intensify during the 21st century, the analyses were hindered by the limited availability of measured waves and tides for Hawke's Bay. However, there was reasonable conformity in the derived wave climate with previous investigations based on wave hindcast analyses, and in the elevations of the measured tides with past occurrences of storm surges along the coasts of New Zealand. Therefore, reasonable confidence can be placed on our analysis results for the present-day hazards, also in view that reasonable conformity was found between the results for the present-day extreme total water levels of tides plus the wave runup, compared with the morphologies of surveyed beach profiles. Our projections into the future to assess erosion and flooding hazards spanning the 21st century are of course more uncertain, having been based on a "consensus" projection by climatologists of there being approximately a 1-metre rise in global-average sea levels by the year 2100, and with our having attempted to account for a potential increase in storm intensities and their generated waves but with the magnitudes of that increase being uncertain. Accordingly, our projections of the future erosion and flooding impacts have comparable levels of uncertainty. Improvements in these projections should be forthcoming in the near future with additional research and data collection, investigations by climatologists that better define the future sea levels, and in particular as additional years of measurements of the Hawke's Bay waves and tides become available, permitting improved projections of their extremes and more confident assessments of the trends of increase in the storm-generated wave heights and sea levels along this shore.

The projected increases derived for future sea levels, storm-wave heights, their combined total water levels, and the resulting enhanced hazards from erosion and flooding, will all take place gradually such that their consequences might not become particularly evident for another 25 years or longer, although each year there is the possibility for the occurrence of a 100-year storm event that would seriously impact this shore. However, while there may be time to wait for the research advances and data collection that provide improved projections of rising sea levels and future storm-wave extremes, there are measures that should be undertaken immediately to enhance the stability of this coast, the integrity of its barrier gravel ridges. As discussed in this chapter, important to the stability is the "health" of its

beach that provides buffer protection to the barrier gravel ridge, with the present and future conditions depending in large part on the sediment budgets of the Haumoana and Bay View Littoral Cells. Efforts therefore need to be directed toward shifting their balances into the "black" with more sediment being contributed to the beaches than lost. Most problematic is the Haumoana Cell where according to the present-day budget each year the losses of sediment significantly exceed its gains, the expectation being that the balance could become worse in the future with rising sea levels. This improvement in the beach sediment budget requires that the primary loss of gravel and sand to commercial mining be phased out as soon as possible. Considerations should also be directed toward the rivers, where measures should be implemented that could enhance their delivery of sediments to the beaches, particularly important being the Tukituki River that might otherwise in the future cease to be a credit in the Haumoana sediment budget. Special consideration needs to be directed toward the fates of coastal properties such as those in the south Haumoana Cell, which are already experiencing problems with erosion, it being evident from the analyses in this study that with rising sea levels and increased storm intensities, the danger to homes along those shores will be significantly greater in the future.